SISSA ISAS
SCUOLA INTERNAZIONALE SUPERIORE DI STUDI AVANZATI
INTERNATIONAL SCHOOL FOR ADVANCED STUDIES

GAMMA-RAY PRODUCTION IN COSMIC DISCRETE SOURCES

Thesis submitted to the
International School for Advanced Studies
– Astrophysics Sector –
in partial fulfillment of the requirements for the degree of

Doctor of Philosophy

CANDIDATE
Włodzimierz Bednarek

SUPERVISOR
Prof. Aldo Treves

Academic Year 1991/92

To my Family

Acknowledgements

I am greatly indebted to my PhD. thesis advisor, Prof. A. Treves, for encouragement, suggestions and scientific supervision. The same thanks are due to Prof. M. Calvani who was my Magister Philosophiae thesis advisor during my first year in SISSA.

I am very grateful also to Prof. D.W. Sciama for the creation of an excellent scientific atmosphere and support.

My interest in high energy astrophysics was initiated by Dr. S. Karakuła and Dr. W. Tkaczyk, at the University of Łódź (Poland). I am extremely grateful to them for the supervision during the years of my work at the Institute of Physics, University of Łódź.

I would like to thank also Dr. J.H. Beall, Prof. M. Calvani, Dr. O. Cremonesi, Dr. F. Giovannelli, Dr. S. Karakuła, Dr. W. Tkaczyk and Prof. A. Treves for collaborations in which part of the results presented in this thesis were obtained and Prof. M. Abramowicz for discussions.

Special thanks are addressed to Joe Pesce and Paul Haines for reading of the manuscript, comments and English corrections.

Table of Contents

Abstract

In this thesis we discuss the theory of γ-ray production in discrete cosmic sources. We concentrate on the specific aspects of the γ-ray production in selected sources, which are, however, representative for bigger classes of objects emitting γ-rays. In chapter 2 we briefly review the mechanisms of γ-ray production and absorption. Since a number of γ-ray sources show anisotropic structure, in chapter 3 we emphasize the theoretical models in which anisotropic production of γ-rays may play an important role. We calculate, moreover, the energy and angular dependent γ-ray spectra from the interaction of relativistic electron and proton beam with background radiation and matter. Possible applications of these calculations in astrophysical scenarios are also considered.

In chapter 4, the production of γ-rays by isolated neutron stars (pulsars) is discussed. In particular, the scenario is proposed in which the redshifted e^+e^- annihilation line observed in pulsed spectrum of the Crab Nebula pulsar can be envisaged. The model discussed by us also predicts the simultaneous appearance of a broad feature at $\sim$ 150 keV at the level $10^{-5} - 10^{-4}$ $phot/cm^2/s$, due to the Compton backscattering of 0.511 MeV photons.

In chapter 5, the very high energy γ-ray emission from the X-ray binary systems is discussed. Taking into consideration the recent reports of neutral emission from Cyg X-3 above 5×10^{17} eV and the earlier reports of observations in TeV (10^{12} eV) and PeV (10^{15} eV) energy ranges, we calculate the γ-ray and neutron spectra according to different production mechanisms. The results of calculations are compared with observations and the final conclusion is reached that only two types of mechanisms can be consistent with the observations of Cyg X-3 between $\sim 10^{12} - 10^{18}$ eV.

Chapter 6 concerns the γ-ray emission from the Active Galactic Nuclei (AGNs). Several objects of this type have been recently reported by the EGRET telescope on the board of the Compton GRO. It is almost certain that the anisotropic effects of γ-ray production in these sources are very important, because most of these AGNs show jet-like features inclined at small angles to the observer's line of sight. We apply hadronic collisions as a main process of γ-ray production in these sources and propose two different physical scenarios. In the first one, the γ-ray production occurs in the extended radio–optical–X-ray jet of the quasar 3C 273. The observed photon flux and X- and γ-ray spectrum from this source may originate in the interaction of relativistic proton

beam with ambient matter (via π° decay), bremsstrahlung of secondary electrons (from decay of $\pi^\pm$), and as a result of comptonization of the microwave background radiation by secondary electrons. In the second scenario, applied to the quasar 3C 279, the γ-ray spectrum arises from the interaction of the conical proton beam with matter of the radiation supported tori. The γ-rays are produced via π° decay and as a result of comptonization of the thermal radiation from the tori (UV bump) by secondary electrons from $\pi^\pm$ decay. We note that, in principle, both scenarios may work simultaneously in AGNs.

1 Introduction

γ-ray photons are produced in the most energetic processes occurring in the Universe and they are excellent signatures of the presence of a high temperature plasma or relativistic particles. Their advantages, they travel in a straight line, and the high penetrability of energetic γ-ray photons through interstellar space, allow us to obtain the direct information about the entire structure of the sources.

The possibilities of investigation of extraterrestrial objects by studying their γ-ray emission has been discussed since 1950s (see, e.g., Morrison 1958). However, there are serious problems with detection of γ-ray photons which mainly concerns the opacity of the Earth's atmosphere (detectors have to be moved to high altitudes or into space), the small cross sections for the interactions of γ-ray photons, and the low fluxes of photons from the cosmic sources.

The first γ-ray observations, carried out in the 1960s (see review by Fazio 1967), did not report positive detections above $\sim$ 100 keV[1]. The first positive result was obtained by the OSO III satellite (launched in 1968) which detected the excess of γ-ray photons from the general direction of the Galactic Center (Kraushaar et al. 1972). However, the most important results, before the GRO era, in high energy γ-rays ($\sim$30 MeV – 5 GeV) were obtained by the SAS 2 and COS B satellites collecting data in the 1970s. The analysis of these observations shows at least 24 point-like sources in the region close to the Galactic plane (Swannenburg et al. 1981) and the diffuse emission with two Galactic and extragalactic components (see review by Bloemen 1989). During the 1970-80s, the observations in soft γ-ray energies were mainly carried out using the detectors on balloons and, in spite of a very poor angular resolution, a few sources were reported as positively detected in soft γ-rays (e.g., the annihilation line source in the Galactic Center, Cyg X-1, Cen A, NGC 4151). The turning-point in this branch of astronomy occurred with the launch of the GRANAT spacecraft (in 1989) and the Compton GRO (in April 1990). The GRANAT has two coded-mask telescopes ART-P (4-30 keV) and SIGMA (35-1300 keV) with the angular resolutions 5' and 15' respectively,

[1]The γ-ray photon energy range usually refers to photons with energies above 0.5 MeV. This energy range is divided on a few bands, Low Energy: 0.5-10 MeV, Medium Energy: 10-30 MeV, High Energy: 30 MeV - 10^{10} eV, Very High Energy (VHE): $10^{10} - 10^{14}$ eV (called also TeV energy range), Ultra High Energy (UHE): $10^{14} - 10^{17}$ eV (PeV energy range), and Extremely High Energy (EHE); $> 10^{17}$ eV (EeV energy range).

which is an order of magnitude better than previous telescopes. The Compton GRO covers the photon energy range from about 20 keV up to 30 GeV, with sensitivity and angular resolution about an order of magnitude better than COS B experiment[2].

The preliminary results of observations by the SIGMA and GRO detectors are revolutionary for γ-ray astronomy. Now, it is certain that the γ-ray sky is highly variable and many objects emit most of their power in this energy range. For instance, the SIGMA telescope discovered a transient, broad e^+e^- annihilation line from the source 1E 1740.7-2942, which is located close to the Galactic Center. The EGRET telescope detected several AGNs above 100 MeV as extremely powerful and variable sources of γ-rays. The number of radio pulsars reported in the γ-ray energy range was enlarged to 5. The most important results, mentioned above, are reviewed in more detail in the subsequent chapters of this thesis.

The detection of γ-ray photons with energies above 10^{11} eV is possible indirectly, from the ground, by the analysis of the secondary products (particles, Cherenkov radiation) of the electromagnetic cascade induced by such energetic photons in the Earth's atmosphere. However, this method is not able to give precise information about the photon fluxes since it is difficult to distinguish between the showers initiated by photons from those one initiated by charged particles[3]. For reviews of the observational techniques and presently operating experiments we refer to e.g., Weekes (1988,1992), Nagle et al. (1988). The positive detection of several sources was claimed in this energy range, e.g. radio pulsars, X-ray binary systems, supernova remnant, AGNs. At present, the best established very high energy source is the Crab Nebula, which was detected at a level $\sim 34\sigma$ by the Whipple Observatory, applying a new technique of selection of γ-ray initiated showers. Other results are discussed in more detail in the following chapters of this thesis.

The recently reported observational results and the progress made in detection techniques of γ-ray photons forecast the excellent future for this branch of astronomy. New experiments are under study and construction. For instance, INTEGRAL and NAE (Nuclear Astrophysics Explorer) are devoted to high and low energy γ-rays. In the energy range 10 GeV – 100 TeV a detector, ASTROMAG, is planned for the Space Station Freedom. Above 10^{11} eV photon energies a few ground based telescopes started to operate or are under construction (e.g., HERCULES, TEMISTOCLE, GREX, PEGGASAS, SINGAO). For a brief summary of the observational perspectives of γ-ray astronomy we refer to e.g. Bednarek (1990) and details of the specific experiments to e.g.

[2]The Compton GRO contains four detectors BATSE, OSSE, COMPTEL and EGRET. For details of their construction and parameters we refer the interested reader to e.g. Kniffen et al. (1989), Bertsch et al. (1988), Kanbach et al. (1988), Diehl (1988), Cameron et al. (1992). For a review of the coded aperture imaging technique (applied in GRANAT telescopes) we recommend the review article by Carioli et al. (1987).

[3]Some criteria are argued to be useful in distinguishing between photon and hadronic particle initiated showers, such as: age parameter, muon content, lateral distribution, ultraviolet excess, the image of the shower (for discussion see Lamb 1989).

Courvoisier et al. (1991), Gehrels & Candey (1989), Eichler & Adams (1987).

In spite of nearly thirty years of observational efforts, γ-ray astronomy is still in its early stage of development. Many claimed detections of sources are unique and not confirmed by independent observations. The situation is, moreover, complicated by the probable significant variability of the γ-ray sources. From the beginning of this branch of astronomy the reported results inspired a group of theoreticians to construct possible models in which γ-ray production can be envisaged. In the next chapter, we summarize the basic mechanisms of γ-ray production in discrete sources and the possible mechanisms of γ-ray absorption. The physical scenarios in which the anisotropic production of γ-rays may be important are discussed separately in chapter 3. In the subsequent chapters (4,5,6), we discuss the γ-ray production in the following types of sources: isolated neutron stars (pulsars), X-ray binary systems, and AGNs. However, some important types of γ-ray sources (for instance, our Sun, γ-ray bursts, supernovae explosions) are not discussed in this work.

The original contribution to the discussed topic is included in section 2.2 in which we calculate the optical depth for the high energy γ-ray photons in the thermal radiation of the accretion disk; in chapter 3, the angular and energy dependent spectra of γ-ray photons from the comptonization of an arbitrary background radiation by the monoenergetic electron beam (section 3.1) and from the interaction of proton beam with background matter (section 3.2) are calculated. Possible applications of these results in astrophysical scenarios are discussed in section 3.3; in chapter 4, we propose the physical scenario in which the redshifted e^+e^- annihilation line, observed in the pulsed photon spectrum of the Crab Nebula pulsar, can be envisaged. Our model predicts moreover the simultaneous appearance of the Compton backscattering feature at $\sim$ 150 keV, whose intensity is estimated in section 4.3.2; In section 5.3.1, we calculate the γ-ray and neutron spectra in the energy range $\sim 10^{12} - 10^{18}$ eV, according to different mechanisms which may potentially work in the VHE γ-ray sources. The results of calculations are compared with the observations of Cyg X-3; In sections 6.3 and 6.4, the relativistic proton beam models of γ-ray production in the quasar 3C 273 and 3C 279 are proposed.

References

Bednarek, W. 1990, *Gamma-Ray Emission from Cosmic Point-Like Sources*, Magister Philosophiae thesis, SISSA

Bersch, D.L., Fichtel, C.E. & Trombka, J.I. 1988, Sp.Sci.Rev. 48, 113

Bloemen, H. 1989, ARAA 27, 469

Cameron, R.A. et al. 1992, *OSSE Contributions to the Second GRO Science Workshop*, OSSE preprint no. 1

Carioli, E. et al. 1987, Sp.Sci.Rev. 45, 349

Courvoisier, T.J.-L. et al. 1991, *International Gamma-Ray Astrophysics Laboratory*, ESA – NASA report, Sci(91)1

Diehl, R. 1988, Sp.Sci.Rev. 49, 85

Eichler, D. & Adams, J.H. 1987, ApJ 317, 551

Fazio, G.G. 1967, ARAA 5, 481
Gehrels, N. & Candey, R.M. 1989, NASA preprint 90-003
Kanbach, G. et al. 1988, Sp.Sci.Rev. 49, 69
Kniffen, D. et al. 1989 *The Gamma-Ray Observatory Science Plan.*
Kraushaar, W.L. et al. 1972, ApJ 177, 341
Lamb, R.C. 1989, *Frontier Objects in Astrophysics and Particle Physics*, eds. F. Giovannelli & G. Mannocchi, v.19, p.421
Morrison, P. 1958, IL Nuovo Cimento 7, 858
Nagle, D.E., Gaisser, T.K. & Protheroe, R.J. 1988, Ann.Rev.Nucl.Part.Sci. 38, 609
Swannenburg, B.N. et al. 1981, ApJL 243, L69
Weekes, T.C. 1988, Phys.Rep. 160, 1
Weekes, T.C. 1992, Sp.Sci.Rev. 59, 314

2 Production and absorption mechanisms of γ-ray photons

2.1 Production of γ-ray photons in isotropic scenarios

The most frequently discussed mechanisms of γ-ray production in astrophysical sources are the following: e^+e^- annihilation, synchrotron and curvature radiation, bremsstrahlung, inverse Compton scattering of low energy radiation, and interactions of hadrons with matter and radiation (π° production and decay, nuclear excitations). We will not discuss the general features of these processes since they are described in an astrophysical context in several reviews. Among them, we refer to Ginzburg & Syrovatskii (1965), Fazio (1967), Stecker (1971), Blumenthal & Gould (1970), Rybicki & Lightman (1979), Ramana Murthy & Wolfendale (1986), Dogiel & Ginzburg (1989), Bednarek (1990). We concentrate here on the main physical scenarios in which the above mechanisms of γ-ray production have been applied.

In general, we can distinguish between thermal and nonthermal mechanisms of γ-ray production. They may occur in isotropic and anisotropic scenarios. Here we discuss only the isotropic scenarios. The anisotropic ones are described in more detail in chapter 3.

The existence of a high temperature thermal plasma in discrete sources is postulated in several models (e.g., spherically-symmetric accretion onto a compact object, high temperature ion supported disks, thermonuclear explosions on the surface of compact objects). Depending on the presence of magnetic field, low energy photons or matter, different production mechanisms of γ-rays may dominate. If there is no essential magnetic field and/or additional low energy photons in the high temperature plasma, the main mechanisms of γ-ray production are bremsstrahlung and decay of π°'s, produced in hadronic collisions and eventually e^+e^- pair annihilation if the plasma is dominated by pairs. The simple formula for photon spectra of thermal bremsstrahlung in the limits of $\Theta_e << 1$ and $\Theta_e >> 1$ ($\Theta_e = kT/mc^2$) were obtained by Quigg (1968) and Gould (1980, 1982). The detailed numerical calculations of the photon spectra for a broad range of plasma temperatures ($0.1 < \Theta_e < 10$) were calculated by Górecki & Kluźniak (1981) for e-p bremsstrahlung and by Dermer (1986) for e-p, e-e, e^+-e^- bremsstrahlung. The results for e-p bremsstrahlung obtained in these two papers are in good agreement. However, the existence of a high temperature thermal

electron plasma is questionable, because, at such energies, the Coulomb collision rate is lower than the bremsstrahlung energy losses (Gould 1982). It has been shown that the thermal electron distribution becomes truncated at $\Theta_e > 10$ (Stepney 1983, Dermer & Liang 1989). The spectra of γ-rays from π° decay, produced in the thermal plasma, have been calculated by Dahlbacka et al. (1974), Kolykhalov & Sunyaev (1979), Marscher et al. (1980), Giovannelli et al. (1982) and Dermer (1986). The spectra calculated by Dermer (1986) are flatter near the peak than the spectra of Kolykhalov & Sunyaev (1979). The spectra calculated by Giovannelli et al. (1982) are much broader at all plasma temperatures than the spectra of Dermer (1986), which is caused by the assumption of separability in angle and energy of these spectra in the center of mass of the colliding protons.

The soft γ-rays can be produced in the process of comptonization of the low energy photons by electrons. This process can be solved analytically in the case of an optically thick non-relativistic thermal plasma (see, e.g., Sunyaev & Titarchuk 1980). The Monte Carlo calculations of the general case (relativistic electrons with thermal or power law distributions) have been performed by Pozdnyakov et al. (1977). The method was next significantly improved by Górecki & Wilczewski (1984) who included the dependence of the probability of photon – electron collisions on the electron energy and scattering angle.

The e^+e^- pair processes become important in a hot thermal plasma if the compactness parameter[1] is $l > 10$. Under such conditions, e^+e^- pairs can be copiously produced in the $\gamma - \gamma$ collisions which in turn originates in bremsstrahlung, π° decay or inverse Compton scattering of lower energy photons (e.g. of synchrotron origin). The thermal equilibrium of such a e^+e^- pair dominated plasma has beeen discussed in several papers (see for instance, Svensson (1990) and references therein).

The single integral formulas for γ-ray photon spectra from the e^+e^- pair annihilation with a thermal distribution were obtained by Svensson (1983) and Dermer (1984). They agree with previous Monte Carlo calculations by e.g., Zdziarski (1980), Ramaty & Meszaros (1984). At non-relativistic temperatures the e^+e^- annihilation line is narrow with the relative width,

$$\frac{\Delta\epsilon}{\epsilon} \sim (\frac{kT}{m_e c^2})^{1/2}, \qquad T_e << 5 \times 10^9\ K, \tag{2.1}$$

and is centered on the rest mass energy of the electron. At relativistic temperatures the line mimics the distribution of thermal particles with line width,

$$\frac{\Delta\epsilon}{\epsilon} \sim 1, \qquad T_e >> 5 \times 10^9\ K, \tag{2.2}$$

and is centered at kT. However, in a realistic case, the e^+e^- annihilation line is expected to be invisible, because of the dominance of the bremsstrahlung emission over the annihilation emission at temperatures $T > 10^{10}$ K.

[1]The compactness parameter is described by $l = \frac{L}{R} \cdot \frac{\sigma_T}{m_e c^3}$, where L is the luminosity of the source and R is the size of the emitting volume.

The photon spectra originated in the annihilation of e^+e^- plasma with different temperatures of electrons and positrons have been calculated by Tkaczyk & Karakuła (1985). These spectra have close to power law shape with spectral index ~ 1 between $\sim m_e c^2$ and kT_{max} (T_{max} is the temperature of the hotter component of plasma). The spectra are very different than those in the case of equal e^+ and e^- temperatures. However, it is difficult to envisage the existence of such a two-temperature plasma in astrophysical sources, avoiding quick thermalization of separate components.

The production of γ-ray photons in thermal magnetized plasma have been discussed with application to accretion processes by Meszaros (1975) and Maraschi et al. (1982). The photon spectrum in these mechanisms is formed by thermal cyclo-synchrotron, bremsstrahlung and multiple Compton scattering processes. The photon spectra according to similar mechanisms (thermal synchrotron-self-Compton) have been also recently calculated by Atoyan & Nahapetian (1989). A simple expression for the thermal synchrotron spectrum in strong magnetic field (but $B << B_{cr}$) and transrelativistic Maxwellian plasma was derived by Petrosian (1981). The quantum synchrotron spectra ($B \sim B_{cr}$, relativistic temperatures) for thermal electron distributions were obtained by Pavlov & Golenetskii (1986), Brainerd & Petrosian (1987) and Baring (1988). These spectra show the high energy cut-off at significantly lower energies than their classical approximations.

The thermal processes, discussed above, are able to produce γ-ray photons with rather low energies (below a few GeV). The mechanisms of production of the higher energy photons must involve nonthermal processes. Two general groups of such mechanisms may be distinguished, interactions of electrons or hadrons with matter and radiation. Recently, models involving both mechanisms have received more peoples attention. The interactions of electrons probably cannot be responsible for the production of γ-rays with energies above $\sim 10^{12}$ eV, although, in principle, such a possibility exists if the extremely relativistic electrons are secondary products of hadronic interactions (e.g., Sikora et al. 1987).

The most popular nonthermal scenario of high energy γ-ray production by electrons engages the process of Compton scattering of synchrotron radiation caused by this same population of electrons (Synchrotron self-Compton (SSC) mechanism). The simplest model of this type, a homogenous spherical source, was studied in detail by Jones et al. (1974). The isotropic filled-sphere and shell-sphere expanding SSC models, proposed by Rees (1967), were considered in detail by Vittello & Salvati (1976), Vitello & Pacini (1978) and Salvati (1979). The more complicated SSC picture, involving different populations of electrons and their creation in hadronic collisions has been recently discussed by Jones & Stein (1990). The comptonization of external origin background photons by relativistic electrons has also been calculated in many papers (see e.g. Jones 1968, Blumenthal & Gould 1970). More recently, Schlickeiser (1989) proposed the comptonization of X-ray photons by

monoenergetic electrons (in the extreme Klein-Nishina limit) as a source of PeV γ-rays, avoiding copious production of lower energy photons.

Another general scenario of γ-ray production was proposed by Guilbert et al. (1983). The authors studied the cascade process which involves the mechanism of γ-ray production in the Compton scattering of background photons by relativistic electrons. The γ-rays converse then on the low energy photons to e^+e^- pairs which again produce additional γ-ray photons. The photon spectra emerging from such cascade process were calculated in several papers (see, e.g., Fabian et al. 1986, Lightman & Zdziarski 1987, Svensson 1987, Done & Fabian 1989).

The possibility of γ-ray production in hadronic collisions with matter and radiation was studied in several early papers (see, e.g., Stecker 1968, Blumenthal 1970). More recently, in the context of compact sources, the cooling time scales of hadrons were calculated for relativistic protons (Sikora et al 1987) and nuclei (Chodorowski et al. 1992). The γ-ray spectra from cascades initiated by protons through secondary production of e^+e^- pairs (from $\pi^\pm$ decay or γ-γ interactions) were calculated by Sikora & Shloshman (1989) and Begelman et al. (1990) and in the interaction of hadrons with soft X-ray photons and magnetic field by Rudak & Meszaros (1991). In hadronic collisions, relativistic neutrons are also efficiently produced. They can transfer energy from the optically thick object to the regions from which the γ-ray photons may freely escape (see Kazanas & Ellison 1986, Sikora et al. 1989, Kirk & Mastichiadis 1989, Mastichiadis & Protheroe 1990). Another type of mechanism was discussed by Mannheim et al (1991). The authors assumed that electrons and protons are both accelerated in the source. The relativistic protons interact with synchrotron radiation of relativistic electrons and produce energetic γ-rays via π^o decay. The γ-ray photons interact with synchrotron radiation supplying a new generation of secondary e^+e^- pairs.

The application of the above mentioned mechanisms in the models of specific sources will be discussed in the subsequent chapters of this thesis.

2.2 Absorption of γ-ray photons

As we mentioned above, one of the most attractive features of γ-ray astronomy is that the Universe is largely transparent to γ-ray photons. Only γ-rays with PeV energies ($\sim 10^{15}$ eV) can be efficiently absorbed by the microwave background radiation, if they are coming from distances $\sim$ 10 kpc (which is a typical dimension of our Galaxy). It was argued that the γ-ray photons with energies $< 5 \times 10^{13}$ eV can arrive even from the most distant objects with small absorption (see e.g. Wdowczyk et al. 1972). However, recent calculations by Stecker et al (1992) show that the absorption of γ-ray photons in the TeV energies ($> 10^{11}$ eV), coming from cosmological distances, is significant. The situation in compact γ-ray sources may be different and specific models of γ-ray production have to take into account possible absorption processes for practically the whole γ-ray photon energy

range.

In general, the absorption processes of γ-rays can be divided into three basic categories:

- Absorption in matter;
- Absorption through interactions with radiation;
- Absorption in a very strong magnetic field.

The first possibility may occur through the interactions of γ-ray photons with hadrons (processes of e^+e^- pair production in the field of nuclei, π°, $\pi^\pm$ production, and excitations of nuclei) and through the interactions with electrons (Compton scattering, e^+e^- pair production in the field of electron). The importance of these processes depends on the values of the cross sections and, in many cases, on the values of the threshold energy above which the particular process operates. For instance, the production of pairs and pions have thresholds at $\sim$ 1 MeV and $\sim$ 145 MeV, respectively. The cross section for photoexcitation of nuclei shows giant resonances between 15-35 MeV and then a plateau. The location of the resonance and value of the cross section depends in a more complicated way on A and Z of the nuclei (see Bishop & Wilson 1957). The cross section for the Compton scattering of γ-rays (described by Klein-Nishina formula) is close to the classical Thomson value for low energies and is inversely proportional to photon energy above a few 10 MeV. The detailed dependence of cross sections for the Compton scattering and e^+e^- pair in the field of a proton is shown in Fig. 2.1. Note that in the ionized plasma the Compton cross section is proportional to number of electrons Z and the cross section for pair production in the field of nuclei is proportional to Z^2. At energies above $\sim$ 140 MeV, the Compton scattering process is dominated by direct production of e^+e^- pairs in the field of an electron (triplet pair production, see Mastichiadis et al. 1986). The absorption of γ-ray photon with energy E_γ in collision with another photon of energy ϵ_{ph} may occur if the energy of photons in the center of mass is greater than $2m_ec^2$ ($E_\gamma \cdot \epsilon_{ph}(1 - cos\theta) > 2m_ec^2$). The cross section for this process reaches a maximum value close to the Thomson cross section at a few MeV and then decreases proportionally to the square of the photon energy (see Jauch & Röhrlich 1980).

A single high energy γ-ray photon can be converted directly into a e^+e^- pair in the presence of a strong magnetic field (magnetopair production process). Because of the quantum nature of this process, the detailed cross section is very complicated, showing a sequence of resonance peaks. The approximate mean free path l of such a γ-ray photon rises exponentially with parameter χ (Erber 1966):

$$l = \frac{4.4}{2\pi/hc} \cdot \frac{h}{2\pi m_e c} \cdot \frac{B_{cr}}{B \cdot sin\beta} \cdot e^{4/3\chi} \cong 10^6 \cdot \frac{e^{4/3\chi}}{B \cdot sin\beta}[cm] \qquad \chi \ll 1$$

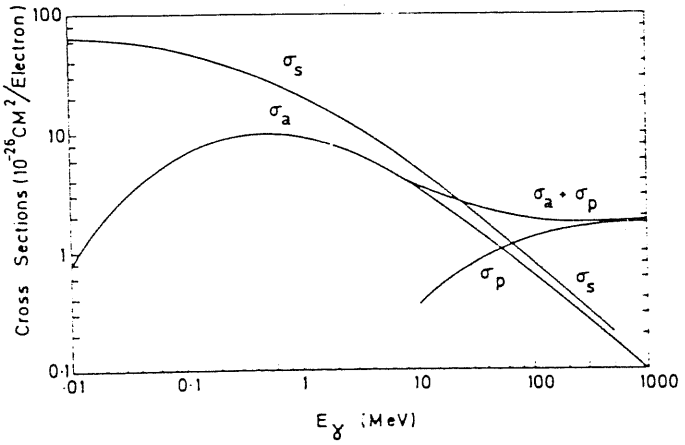

Figure 2.1: Compton scattering (σ_s), Compton absorption (σ_a), and pair production (σ_p cross sections as a function of γ-ray energy for absorption in hydrogen gas (from Stecker 1971).

$$\chi = \frac{E_\gamma}{2m_e c^2} \cdot \frac{B \cdot sin\beta}{B_{cr}} \tag{2.3}$$

where B_{cr} is equal to $4.4 \cdot 10^{13} Gs$ and β is the angle between the directions of the photon and the magnetic field lines. So then, the process is important e.g., for MeV photons in the magnetic field typical for the neutron star surface ($10^{12} - 10^{13}$ Gs), for TeV γ-rays originated in the magnetosphere of a rapidly rotating neutron star ($\sim 10^5$ Gs), and for PeV γ-rays in the magnetic field typical for the binary system ($\sim 10^2 - 10^3$ Gs).

2.2.1 Absorption of γ-rays in the radiation field of the accretion disk

We would like to discuss here the absorption of high energy γ-rays produced in the models of the accretion disk around a neutron star (see Cheng & Ruderman 1989, 1991; Hillas & Johnson 1991). The basic idea of these models is that a very high energy narrow particle beam ($E_p \sim 10^{15}$ eV), accelerated in the inner or outer gap of a neutron star, impinges at a fixed angle on the surface of the accretion disk. The VHE γ-rays are produced in the disk in hadronic cascade. A similar scenario of γ-ray production was also proposed to work in the picture of an accretion disk around a rotating black hole (Slane & Wagh 1990).

However, the high energy γ-rays can escape from the disk surface if the optical depth on the e^+e^- pair production in collisions of γ-ray photons with thermal photons from the disk, is not too high. Otherwise, secondary pairs will be driven by the local magnetic field or lose energy via the Inverse Compton scattering and the primary narrow cone of γ-ray emission may be spread out.

In order to find out if the high energy γ-rays can escape from the thermal radiation field of the disk, we have calculated the optical depth for γ-rays in a simple disk model. Since, in the real case, many different processes can contribute to the soft background radiation in the place of γ-ray

generation, the thermal emission of the disk may be treated as a lower limit of the background photon field. We want to obtain some constraints on the observability of γ-ray emission at different photon energies and inclination angles of the disk plane to the observer's line of sight, and the possibility of developing an electromagnetic cascade initiated by VHE γ-ray photon in the field of thermal radiation of the disk.

The following assumptions were made:

- The accretion disk extends from r_{in} (inner radius) to r_{out} (outer radius) and has half opening angle Δ;
- A simplified temperature profile for the disk surface was assumed to be $T = T_{max} \cdot (r/r_{in})^{-3/4}$, which is reasonable at least for some accretion rates and some values of the viscosity parameter (Pringle & Rees 1972; Shakura & Sunyaev 1973);
- The local black body approximation of disk emission was assumed.

The relativistic particles impinge on the disk surface following magnetic field lines of the magnetosphere of the compact object. However it is difficult to evaluate the structure of the magnetosphere threaded by the accretion disk and a variety of different models were developed with different final conclusions (see, e.g., review by Aly 1985; and references therein). So, in principle, there are no explicit indications concerning the geometry of the interaction between relativistic particles and the disk. For this reason, we assume that γ-ray photons can emerge from the disk surface at an arbitrary distance r_γ from the disk center and in an arbitrary direction characterised by the vertical angle to the disk plane α ($\alpha > \Delta$) and horizontal angle φ_γ measured from the disk radius (see Fig. 2.2). We would like to note here that a such scenario (γ-rays absorbed in the anisotropic radiation field) is more general than previous treatments of γ-ray absorption which usually simplified the problem to isotropic distribution of photons (see, e.g., Gould & Schreder, 1967; Bassani & Dean, 1981).

The optical depth for high energy γ-rays is expressed by the general formula:

$$\tau_\gamma = \int\int\int\int \frac{n(\epsilon, \Omega')}{d\epsilon d\Omega' dV} \cdot \sigma_{tot}(cos\Theta', \epsilon, E_\gamma) \cdot (1. - cos\Theta') d\epsilon d\Omega' dx \qquad (2.4)$$

where $\frac{n(\epsilon,\Omega')}{d\epsilon d\Omega' dV}$ is the differential density of photons emitted by the disk observed at the distance x along the γ-ray photon path; $\sigma_{tot}(cos\Theta', \epsilon, E_\gamma)$ is the total cross section for photon - photon pair production (Jauch & Rörlich, 1980) and Θ' is the angle between the direction of motion of the background photon (with energy ϵ) and the direction of γ-ray photon (with energy E_γ).

In spite of the simplicity of this scenario, it still has a few free parameters (α, φ_α, Δ, r_{in}, r_{out}, r_γ, T_{max},) for which we performed numerical calculations of the optical depth versus the energy of the γ-ray photon emerging from the disk. Some preliminary results of these calculations are

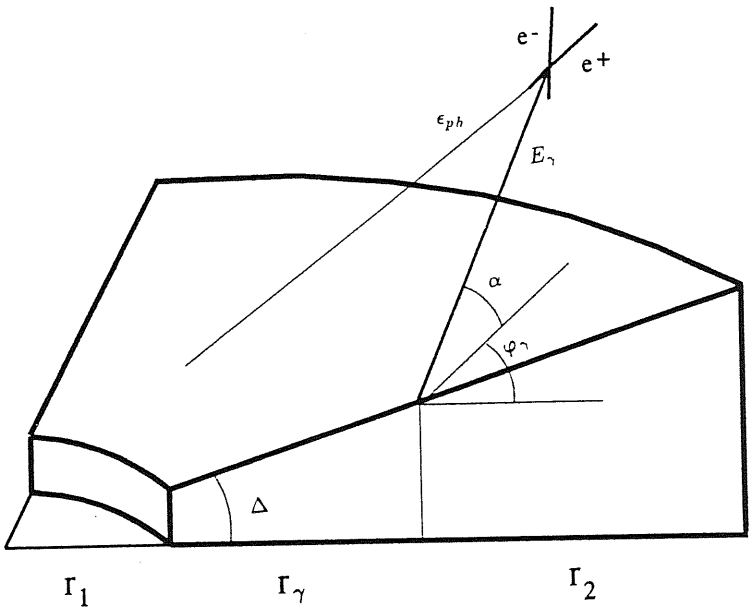

Figure 2.2: Schematic picture of a part of the accretion disk, with inner radius r_1, outer radius r_2 and half opening angle Δ. The γ-ray photon with energy E_γ emerges from the disk at the distance r_γ and angles α and φ_γ. The thermal photon ϵ_{ph}, emitted by the disk, interacts with γ-ray photon and produces e^+e^- pair.

presented in Fig. 2.3. The optical depth for γ-ray photons is large in the range of photon energies, determined by the temperature of the accretion disk (see Fig. 2.3). The absorption of γ-ray photons strongly depends on the distance r_γ (compare values for curves 1 ($T_{bb} = 3 \times 10^7$ K) and curves 2 ($T_{bb} = 10^7$ K) in Fig. 2.3b), and on the angle α (see Fig. 2.3a). It is interesting, that smallest value of the optical depth for γ-ray photons corresponds to the angle α which is between Δ and the normal to the disk plane (for the specific parameters showed in Fig. 2.3a, α is between 30^o and 60^o). More detailed discussion of these calculations, including the dependence of the optical depth on Δ, φ_α, r_{in} and r_{out}, will be performed in Bednarek (1992c).

For the case of large optical depth for γ-ray photons, the secondary pairs are copiously produced. They can lose energy in inverse Compton scattering of thermal photons from the disk, synchrotron and curvature processes. A few different scenarios can occur in this case, depending on the energy of the primary VHE γ-ray photon (E_γ), the radiation field, and the strength of the magnetic field:

i). If the energy losses of secondary e^+e^- pairs are low, the high energy pairs escape from the disk region;

ii). If the Compton energy losses are significant (but comptonization occurs in the Thomson limit) and the magnetic field is weak, most of the energy of primary VHE γ-ray photon (E_γ) will be converted into the low energy photons;

iii). If the Compton energy losses are significant (and comptonization occurs in the Klein-Nishina limit) and the magnetic field is strong, the VHE γ-ray photon may induce an electromagnetic

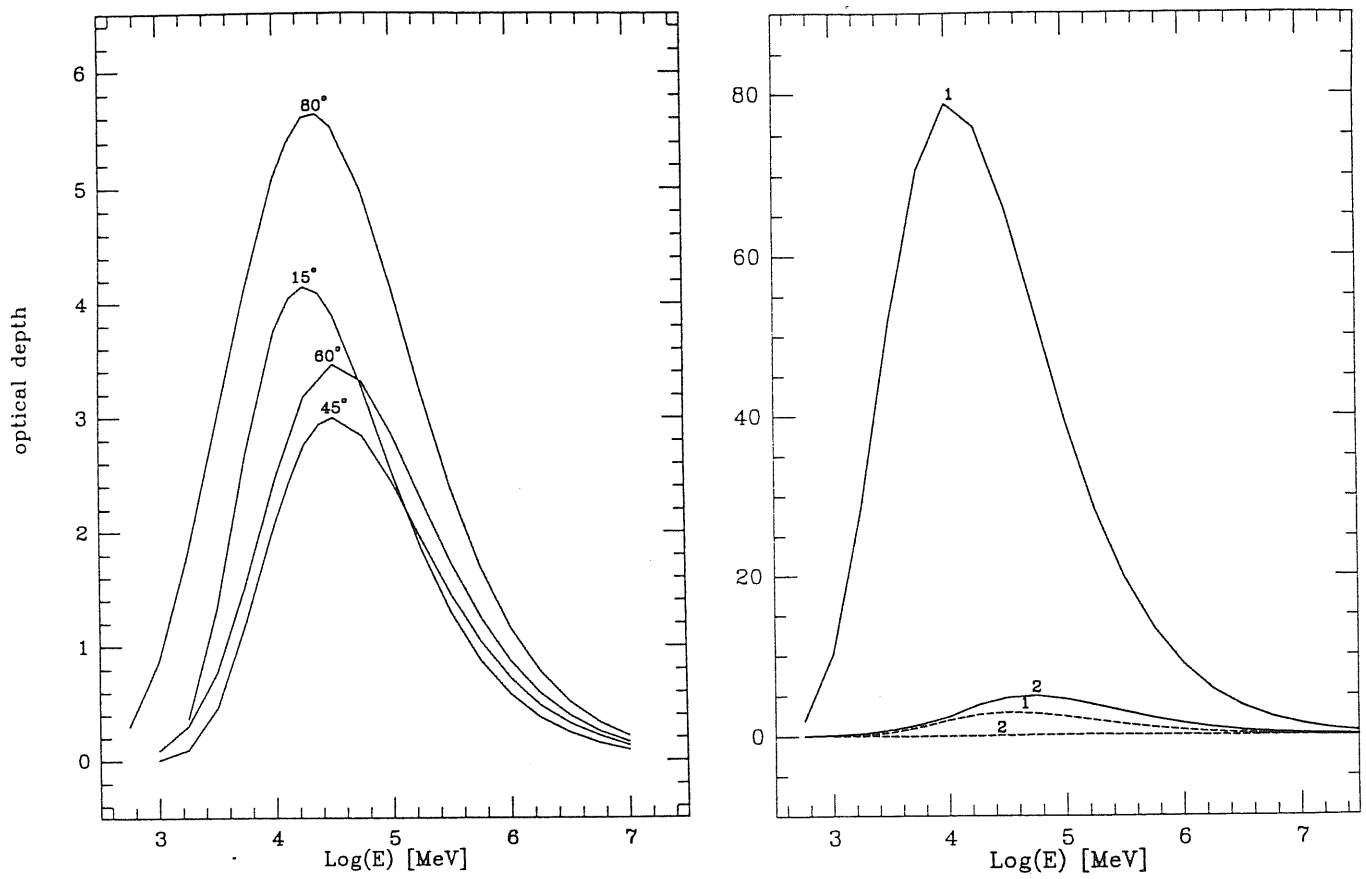

Figure 2.3: (a) The optical depth for γ-ray photons in the thermal radiation field of the accretion disk around Solar mass central object (with $r_1 = 10^6$ cm, $r_2 = 3 \times 10^9$ cm, $\Delta = 10°$, $T_0 = 10^7$ K) versus the energy of the γ-ray photon. The γ-ray photon is emerging from the disk at $r_\gamma = 3 \times 10^7$ cm, in the direction defined by $\varphi_\alpha = 0°$ and angles α= 15°, 45°, 60°, 80°; (b) As in (a) but for: $T_0 = 3 \times 10^7$ K (solid line) and $T_0 = 10^7$ K (dashed line), $\alpha = 45°$, and 1 - $r_\gamma = 3 \times 10^7$ cm, 2 - $r_\gamma = 3 \times 10^8$ cm.

cascade. A significant part of the energy of the primary VHE γ-ray photon may be transferred to the γ-rays with MeV–GeV energies.

Below, we shortly summarize the main features of the above mentioned processes and then, as an example, we discuss in more detail one case for fixed parameters of the disk.

a) Inverse Compton energy losses.

In order to find out if the comptonization of the thermal photons is important, we have calculated the relative energy losses of relativistic electrons on the Inverse Compton scattering of background thermal radiation emitted by the disk, according to the general formula:

$$\frac{d\gamma_e}{\gamma_e} = \frac{1}{\gamma_e^2} \int dx \int d\Omega' \int d\epsilon \int d\Omega'' n(\Omega', \epsilon) \cdot \frac{\epsilon'}{\epsilon} \cdot \sigma_{K-N}(\Omega'', \epsilon') \cdot (\epsilon_1 - \epsilon) \qquad (2.5)$$

where $\sigma_{K-N}(\Omega'', \epsilon')$ is the Klein-Nishina cross section (Jauch & Rörlich, 1980); the solid angle Ω'' and the incident photon energy ϵ' are measured in the electron rest frame; ϵ and ϵ_1 are the energies

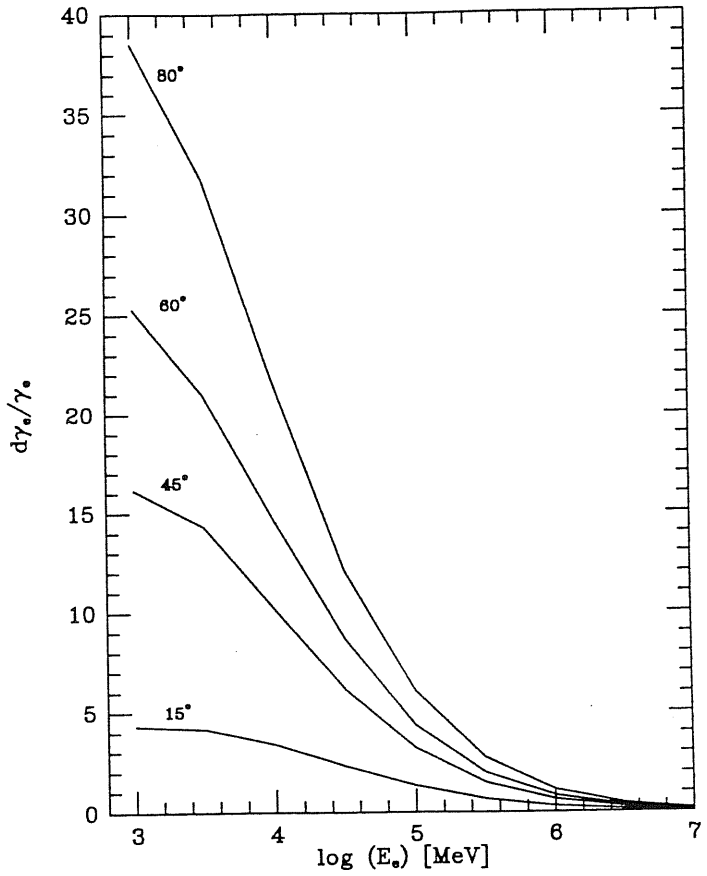

Figure 2.4: The relative energy losses of relativistic electrons, vs. electron Lorentz factor, on the inverse Compton scattering of thermal radiation emitted by the accretion disk. The disk parameters are the following: $r_1 = 10^6$ cm, $r_2 = 3 \times 10^9$ cm, $\Delta = 10°$, $T_0 = 10^7$ K. The electron is emerging from the disk at $r_\gamma = 3 \times 10^7$ cm, in the direction defined by $\varphi_\alpha = 0^o$ and $\alpha = 15°$.

of the incident and scattered photon in the observer's frame, respectively; Ω' is defined as in formula (2.4).

In Fig. 2.4 we present the results of calculations of the relative energy losses of electrons for selected parameters of the disk. The energy losses are very high which means that the energy of electrons will be quickly transformed to lower energy photons.

b) Energy losses in the strong magnetic field.

The characteristic energy of a synchrotron photon emitted by the electron with Lorentz factor γ_e is

$$E_{syn}[MeV] \cong 1.7 \cdot 10^{-14} \cdot \gamma_e^2 \cdot B[Gs] \cdot \sin\alpha \tag{2.6}$$

The time scale of synchrotron losses is described by

$$\tau_{syn} \cong 5.2 \cdot 10^8/(B^2[Gs] \cdot \gamma_e \cdot \sin^2\alpha)[s] \tag{2.7}$$

If the electrons are extremely relativistic and the magnetic field is strong and curved, curvature

radiation may be another important process of electron energy losses. The characteristic energy of curvature photons is described by

$$E_{cur}[MeV] = 3ch\gamma_e^3/4\pi\rho_c \cong 3 \times 10^{-11}\gamma_e^3/\rho_c[cm] \tag{2.8}$$

where ρ_c is the local curvature radius of the magnetic field.

The time scale of energy losses for this process is

$$\tau_{cur}[s] \approx 3m_e\rho_c^2/2e^2c\gamma_e^3 \approx 170 \cdot \gamma_e^{-3} \cdot \rho_c^2[cm] \tag{2.9}$$

As an example, we would like to discuss the VHE γ-ray propagation in the radiation field of the accretion disk (around a Solar mass compact object) for following parameters: $r_1 = 10^6$ cm, $r_2 = 3 \times 10^9$ cm, $r_\gamma = 3 \times 10^7$ cm, $\Delta = 10^o$, $\varphi = 0^o$ and $\alpha = 15^o$. For this case, the absorption of the primary γ-ray photons with energies between $\sim 10^3 - 10^5$ MeV is significant (Fig. 2.3). The energy of secondary e^+e^- pairs, created by γ-ray photons, will be of this same order ($\gamma_e < 10^5$). We have to distinguish two cases depending on the type of energy losses which dominate: Compton or synchrotron. From their comparison (eq. 2.7 and 2.9 with calculations according to eq. 2.5), we can obtain that for, i). neutron stars with strong surface magnetic field ($B_s \cong 10^{12}$ Gs) the synchrotron losses dominates; ii). neutron stars with weak surface magnetic field ($B_s \cong 10^8$ Gs) and black holes, the Compton losses dominates.

i). The typical energy of the synchrotron radiation, emitted by secondary electrons, will be of the order $E_{syn}[MeV] < 2 \times 10^{-4} \cdot B[Gs]$ (eq. 2.6), which for a reasonable value of the magnetic field in the magnetosphere ($B \sim 10^6$ Gs), yields the γ-ray photons with energy ~ 100 MeV. Such γ-ray photons cannot continue the electromagnetic cascade in the radiation field of the accretion disk. If the magnetic field is curved and strong enough (typical curvature radius of the neutron star magnetic field, $\rho_c \sim 10^6$ cm), the energy of the curvature photon is $E_{cur}[MeV] \sim 3 \times 10^{-2}$, for $\gamma_e < 10^5$ (see, eq. 2.8), which is in X-ray photon energies. Therefore, the electromagnetic cascade cannot develop through the interaction of secondary electrons with the magnetic field. The emerged photon spectrum may extend up to ~ 100 MeV, however most of the power will concentrate in low energy photons.

ii). For electrons with Lorentz factors $< 10^5$ most of the comptonization events of thermal photons occurs in the Thomson limit. This means that the energy of the primary VHE γ-ray photons will be converted into photons with energy below ~ 1 GeV.

The final conclusion is , that in analyzed case, the optical depth for energetic photons and the energy losses of secondary electrons, created in photon - photon collisions, will prevent the free escape of γ-rays with energy $\sim 10^3 - 10^5$ Mev from the region of the accretion disk.

The section 2.2.1 is partially based on the paper *"Can very high energy γ-rays escape from the radiation field of the accretion disk"* by W. Bednarek 1992 (in preparation).

References

Aly, J.J. 1985, *Plasma Penetration into Magnetosphere*, eds. N. Kylafis, J. Papamastorakis & J. Ventura, (Crete University Press), p. 125

Atoyan, A.M. & Nahapetian, A. 1989, A&A 219, 53

Baring, M.G. 1988, MNRAS 235, 79

Bassani, L. & Dean, A.J., 1981, Nat 294, 332

Bednarek, W. 1990, *Gamma-Ray Emission form Cosmic Point-Like Sources*, Magister Philosophiae thesis, SISSA

Bednarek, W. 1992c, in preparation

Begelman, M.C., Rudak, B. & Sikora, M. 1990, ApJ 362, 38

Bishop, G.R. & Wilson, R. 1957, *Handbuch der Physik*, ed. S. Flügge, Springer-Verlag (Berlin), v.42, p.309

Blumenthal, G.R. 1970, Phys.Rev. D 1, 1596

Blumenthal, G.R. & Gould, R.J. 1970, Rev.Mod.Phys. 42, 237

Brainerd, J.J.& Petrosian, V. 1987, ApJ 320, 703

Cheng, K. S. & Ruderman, M. 1989, ApJL 337, L77

Cheng, K. S. & Ruderman, M. 1991, ApJ 373, 187

Chodorowski, M.J., Zdziarski, A.A. & Sikora, M. 1992, ApJ submitted, preprint

Dahlbacka, G.H., Chapline, G.F. & Weaver, T.A. 1974, Nat 250, 36

Dermer, C.D. 1984, ApJ 280, 328

Dermer, C.D. 1986, ApJ 307, 47

Dermer, C.D. & Liang, E.P. 1989, ApJ 339, 512

Dogiel, V.A. & Ginzburg, V.L. 1989, Sp.Sci.Rev. 49, 311

Done, C. & Fabian, A.C. 1989, MNRAS 240, 81

Erber, T. 1966, Rev. Mod. Phys. 38, 626

Fabian, A.C. et al. 1986, MNRAS 221, 931

Fazio, G.G. 1967, ARAA 5, 481

Ginzburg, V.L. & Syrovatskii, S.I. 1965, ARAA 3, 297

Giovannelli, F., Karakuła, S. & Tkaczyk, W. 1982, A&A 107, 377

Gould, R.J. & Schreder, G.P. 1967, Phys. Rev. 155, 1408

Gould, R.J. 1980, ApJ 238, 1026

Gould, R.J. 1982, ApJ 254, 755

Górecki, A. & Kluźniak, W. 1981 Acta Astr. 31, 457;34, 494

Górecki, A. & Wilczewski, W. 1984, Acta Astr. 34, 141

Guilbert, P.W., Fabian, A.C. & Rees, M.J. 1983, MNRAS 205, 593

Hillas, A. M. & Johnson, P. A. 1991, 22nd ICRC (Dublin) v. 2, p. 452

Jauch, J.M. & Röhrlich, F. 1980, *The Theory of Photons and Electrons*, (Springer-Verlag; New York, second edition)

Jones, F.C. 1968, Phys.Rev. 167, 1159

Jones, T.W., O'Dell, S.L. & Stein, W.A. 1974, ApJ 188, 353

Jones, T.W. & Stein, W.A. 1990, ApJ 349, 443

Kazanas, D. & Ellison, D.C. 1986, Nat 319, 380

Kirk, J.G. & Mastichiadis, A. 1989, A&A 213, 75

Kolykhalov, P.I. & Sunyaev, R.A. 1979, Sov. Astron. 23, 189

Lightman, A.P. & Zdziarski, A.A. 1987, ApJ 319, 643

Mannheim, K., Krülls, W.M. & Biermann, P.L. 1991, A&A 251, 723

Maraschi, L., Roasio, R. & Treves, A. 1982, ApJ 253, 312

Marsher, A.P., Vestrand, W.T. & Scott, J.S. 1980, ApJ 241, 1166

Mastichiadis, A., Marscher, A.P. & Brecher, K. 1986, ApJ 300, 178

Mastichiadis, A. & Protheroe, R.J. 1990, MNRAS 246, 279

Meszaros, P. 1975, A&A 44, 59

Pavlov, G.G. & Golenetskii, S.V. 1986, Ap&SS 128, 341

Petrosian, V. 1981, ApJ 251, 727

Pozdnyakov, L.A., Sobol, J.M. & Sunyaev, R.A. 1977, Sov. Astr. 21, 708

Pringle, J.E. & Rees, M.J. 1972, A&A 21, 1

Quigg, C. 1968, ApJ 151, 1187

Ramana Murthy, P.V. & Wolfendale, A.W. 1986, *Gamma-Ray Astronomy*, Cambridge University Press (Cambridge)

Ramaty, R. & Meszaros, P. 1981, ApJ 250, 384
Rees, M.J. 1967, MNRAS 135, 345
Rudak, B. & Meszaros, P. 1991, ApJ 383, 269
Rybicki, G.B. & Lightman, A.P. 1979, *Radiative Processes in Astrophysics*, A Wiley-Interscience Publication
Salvati, M. 1979, ApJ 233, 11
Schlikeiser, R. 1989, A&AL 213, L23
Shakura, N.I. & Sunyaev, R.A. 1973, A&A 24, 337
Sikora, M. et al. 1987, ApJL 320, L81
Sikora, M., Begelman, M.C. & Rudak, B. 1989, ApJL 341, L33
Sikora, M. & Shloshman, I. 1989 ApJ 336, 593
Slane, P. & Wagh, S.M. 1990, ApJ 364, 198
Stecker, F.W. 1968, Phys.Rev.Lett. 21, 1016
Stecker, F.W. 1971, *Gamma Ray Astrophysics*, Mono Book Corp., Baltimore, Md.
Stecker, F.W., De Jager, O.C. & Salamon, M.H. 1992, ApJL 390, L49
Stepney, S. 1983, MNRAS 202, 467
Sunyaev, R.A. & Titarchuk, L.G. 1980, A&A 86, 121
Svensson, R. 1983, ApJ 270, 300
Svensson, R. 1987, MNRAS 227, 403
Svensson, R. 1990, *Physical Processes in Hot Cosmic Plasmas*, eds. W. Brinkman, A.C. Fabian & F. Giovannelli, Kluwer Academic Publishers (Dordrecht)
Tkaczyk, W. & Karakuła, S. 1985, 19th ICRC (La Jolla) 1, 15
Vitello, P. & Pacini, F. 1978, ApJ 220, 756
Vitello, P. & Salvati, M. 1976, Phys.Fluids 19, 1523
Wdowczyk, J., Tkaczyk, W. & Walfendale, A.W. 1972, J.Phys. A5, 1419
Zdziarski, A.A. 1980, Acta Astron. 30, 371

3 Anisotropic mechanisms of γ-ray production

There is a great deal of observational evidence at lower photon energies for highly anisotropic emission and non–spherical structure in the case of many astronomical objects. For instance, jet–like features have been detected in more than 100 extragalactic sources (Bridle & Perley 1984) and for a number of sources within our own Galaxy e.g. SS 433, Sco X-1, Cyg X-3 (see review paper by Rees 1985). Superluminal motion has been discovered in the central regions of about 20 extragalactic sources (Zensus & Pearson 1988), which suggest that particles are moving anisotropically with Lorentz factors much greater than 1, at small angles towards the observer's line of sight. In fact, several AGNs (with transparent jet-like features) were recently discovered by the Compton GRO detectors in high energy γ-rays.

The anisotropic mechanisms of γ-ray production are probably also very important in the case of Solar γ-ray flares. A statistical tendency is observed that more energetic flares originate close to the Solar limb (e.g. Vestrand et al. 1991) which is probably a consequence of directional acceleration of particles towards the Solar photosphere. The source geometry (e.g., binary system, presence of accretion disk, strong magnetic field of pulsars) may also be of importance because of the selective absorption of γ-rays in a favored direction or by the creation of anisotropic background matter and radiation fields for energetic particles.

In this chapter we concentrate on calculations of the angular and energy dependent γ-ray spectra produced in two processes: inverse Compton scattering and inelastic hadronic collisions. In the next section, we derive the formula for γ-ray photon spectra from comptonization of an arbitrary background radiation by a relativistic, one–dimensional electron beam, applying the Klein–Nishina cross section. As an example, we calculate such spectra numerically for the isotropic black body and bremsstrahlung background photon spectra. In section 3.2, we derive formulas for the angular and energy dependent spectra of γ-rays and electrons (positrons) , from the interaction of a one–dimensional proton beam with background matter. The differential photon spectra (from decay of neutral and charged pions) are calculated numerically for different proton beam Lorentz factors and angles of photon emission in respect to the beam axis. Possible applications of these calculations

in astrophysical scenarios are discussed in section 3.3. In the paper by Bednarek et al. (1990b), we suggested that γ-ray emission from Cyg X-1 may be explained in terms of such anisotropic scenario in which the γ-ray emission is produced in comptonization of the thermal radiation of a companion star by relativistic electrons emitted by the compact object. Although, it seems, at present, that in the Cyg X-1 system, e^+e^- pair dominated plasma may play important role, we still suppose that the physical scenarios discussed by us may be realized in nature. Another scenario in which our calculations may be valid is the interaction of proton beam emitted by nearly aligned neutron star with an accreting matter.

3.1 Inverse Compton scattering of low energy photons

The production of γ-ray photons in the Compton scattering of low energy radiation (of thermal or synchrotron origin) by relativistic electrons has been investigated in different astrophysical scenarios. However, the efforts concentrated mainly on the isotropic models, because of the smaller number of free parameters involved and the higher degree of symmetry which allows one simplify the problem or even to solve some special cases analytically (see chapter 2).

The anisotropic scenarios seem to be more realistic, although their analysis is much more complicated. There are two main approaches to study them. The first assumes that the electrons are distributed isotropically in the rest frame of the blob moving relativistically. In principle, this idealized approach assumes the unique distribution of electrons and photons in the observer's frame which can sometimes be a good approximation. For instance, the calculations of the angular dependent γ-ray photon spectra from the comptonization of synchrotron radiation by relativistic electrons have been performed by Maraschi et al. (1992), based on the inhomogeneous jet model (proposed originally by Ghisellini et al. 1985). The photon spectra, calculated in such a model, may describe the general shape of γ-ray spectrum observed from the quasar 3C 279.

The second approach is more general. In principle, it assumes an arbitrary angular and energy distribution of the relativistic electrons and low energy photons. However, because of the complexity, such calculations were performed only in the simplest cases, e.g., assuming the Thomson limit, monoenergetic distribution of electrons or background photons. For instance, Melia & Königl (1989) calculated the angular dependent X- and γ-ray spectra from comptonization of the thermal radiation, emitted by the accretion disk, by the relativistic electrons moving along the axis of the disk. The Monte Carlo calculations were performed in the Thomson limit, which limits the validity of resulting photon spectra to rather soft γ-rays. The photon spectra from the comptonization of the radiation emitted by accretion disk (a very simplified model of radiation field was assumed) by relativistic electrons moving at an arbitrary angle to the disk surface were also derived by Ghisellini et al. (1991). Dermer et al. (1992) calculated the photon spectra from comptonization of monoen-

ergetic, one–dimensional background radiation (produced by the disk) by electrons distributed isotropically in the blob moving outwards from the disk surface.

The anisotropic processes are also important when the anisotropic distribution of particles is forced by a strong magnetic field. Canfield et al. (1987) calculated the angular dependent γ-ray spectra (Thomson limit) from comptonization of synchrotron radiation by one–dimensional relativistic electrons moving in strong magnetic field ($B < 10^{11}Gs$). The extension of such calculations in the case of a strong magnetic field ($B > 10^{11}Gs$, when the resonant scattering of photons becomes important) has been done by Dermer (1990).

In Bednarek et al. (1990a), we performed the calculations of angular and energy dependent γ-ray spectra resulting in comptonization of arbitrary background photons by relativistic monoenergetic electrons, applying the *Klein-Nishina cross section.* The comptonized photon spectra were derived for given Lorentz factor of the electron beam (γ) and fixed angle α_1 between the direction of the photon emission and beam axis. They are described by the formula

$$\frac{dN}{d\epsilon_1 d\Omega_1 dt dV} = \int\int\int \frac{c \cdot n_e \cdot n'(\epsilon', \alpha')}{\gamma^2(1 - \beta cos\alpha_1)} \cdot \frac{d^2\sigma}{d\Omega_1' d\epsilon_1'} \cdot \frac{d\Omega_1'}{d\Omega^*} \cdot \frac{d\Omega'}{d\Omega_\mu} \cdot d\Omega_\mu d\epsilon', \tag{3.1}$$

where $d\Omega_1'/d\Omega^* = 1$, $d\Omega'/d\Omega_\mu = 1$ are the Jacobians, $1/\gamma^2(1 - \beta cos\alpha_1)$ is the Jacobian of the transformation of the photon spectrum from the electron rest frame to the observer's rest frame, $n'(\epsilon', \alpha')$ is the distribution of the background photons in the electron rest frame, $d^2\sigma/d\Omega_1' d\epsilon_1'$ is the Klein-Nishina cross-section, and n_e is the electron density of the beam. For more details of these calculations, definitions of angles, and the limits of integration we refer to Appendix A in Bednarek et al. (1990a).

As an example, formula 3.1 was integrated numerically for the two isotropic spectra of background photon fields: black body and bremsstrahlung. In Fig. 3.1 are shown the results of these calculations for a black body photon spectrum (for $T_{bb} = 10^4$K and 10^7 K), different Lorentz factors of the electron beam, and two values of the angle $\alpha_1 = 0°$ and $10°$. Fig. 3.1a concerns the comptonization in the Thomson limit and Fig. 3.1b in the Klein-Nishina limit (cases for $\gamma = 10^3$ and 10^4). The dependence of the comptonized photon spectrum on the angle of photon emission α_1 (for fixed Lorentz factor of electrons $\gamma = 10^3$) is shown in Fig. 3.2. The shape and intensity of the comptonized photon spectra strongly depends on the parameters γ and α_1. For small angles α_1 (in respect to $1/\gamma$), the photon spectra show a broad plateau whose width is proportional to γ^2 (in the Thomson limit) and to γ (the Klein-Nishina limit). In the Klein-Nishina limit, the spectra shows the characteristic Compton peak just before the sharp cut-off. The intensities of the photon spectra are inversely proportional to the electron beam Lorentz factor. For large angles (with respect to $1/\gamma$) and in the relativistic limit ($\gamma >> 1$), the cut-offs in the photon spectra are mainly determined

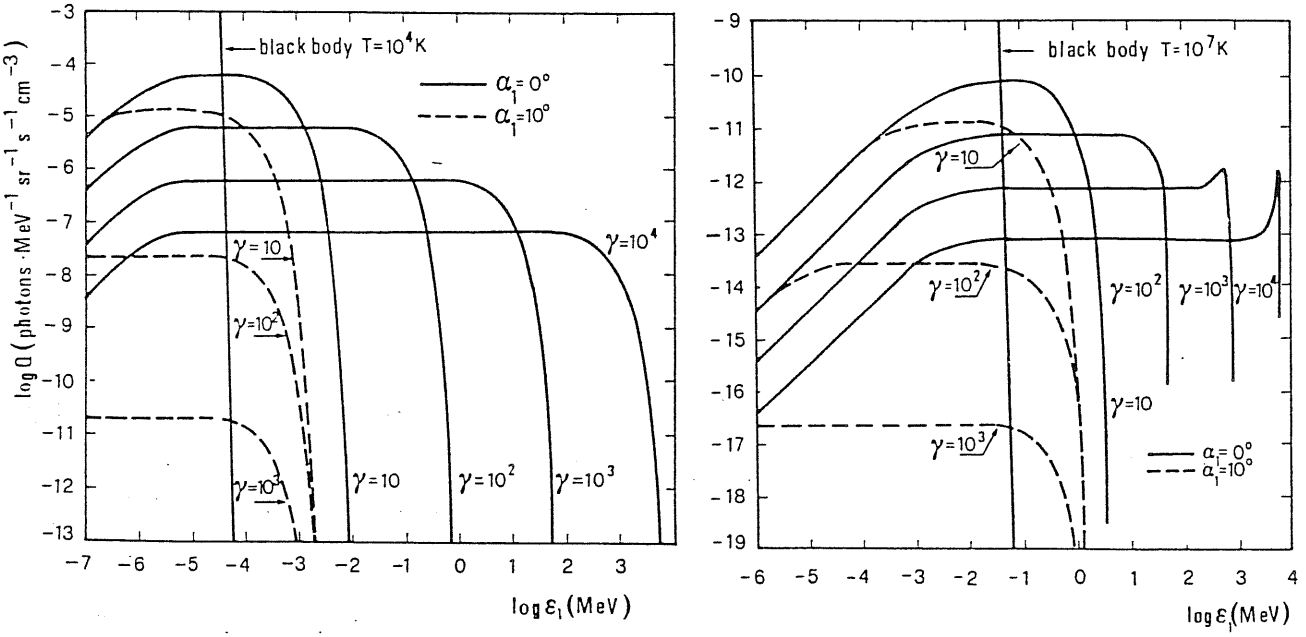

Figure 3.1: The comptonized black body photon spectra, $T_{bb} = 10^4$ K (a) $T_{bb} = 10^7$ K (b), for the Lorentz factors of electrons $\gamma = 10$, 10^2, 10^3, 10^4 and two values of the angles between the direction of the emitted photons and the beam axis: $\alpha_1 = 0°$ (solid line), and 10° (dashed line). The photon energy density of black body spectra are normalized to 1 MeV/cm^3, and the density of electron beam was assumed to be $n_e = 1$ electron/cm^3. (from Bednarek et al. 1990a).

by the value of α_1 (Fig. 3.2), but they are almost independent on the Lorentz factor of electrons γ. The intensities are inversely proportional to γ^3. These general features can be easily obtained in analysis of the formula 3.1 in the Thomson limit (see, Bednarek et al. 1990a).

Fig. 3.3 shows the comptonized thermal bremsstrahlung photon spectra ($T = 10^6$ K) for $\gamma = 10$, 10^2, 10^3, 10^4, and two angles $\alpha_1 = 0°$ and 10°. The general shapes of comptonized bremsstrahlung spectra are similar to the background spectrum. The cut-offs in the spectra are determined by Lorentz factor of electrons (for small angles) and mainly by the value of α_1 (for large angles). The intensities of the comptonized bremsstrahlung spectra are proportional to the Lorentz factor of electrons in the case of small angles (note that this is opposite behaviour than for comptonized black body spectra), and inversely proportional to γ^3 in the case of large angles (similar to comptonized black body spectra).

We would like to note also that the comptonized bremsstrahlung spectra do not show the transparent peak features just before the sharp cut-off (see the curve for $\gamma = 10^4$ and $\alpha_1 = 0°$ in Fig. 3.3), while they are present in the comptonized black body spectra (curves for $\gamma = 10^3$ and 10^4, and $\alpha_1 = 0°$ in Fig. 3.1). Possible application of these calculations in the astrophysical scenario is discussed in section 3.3.

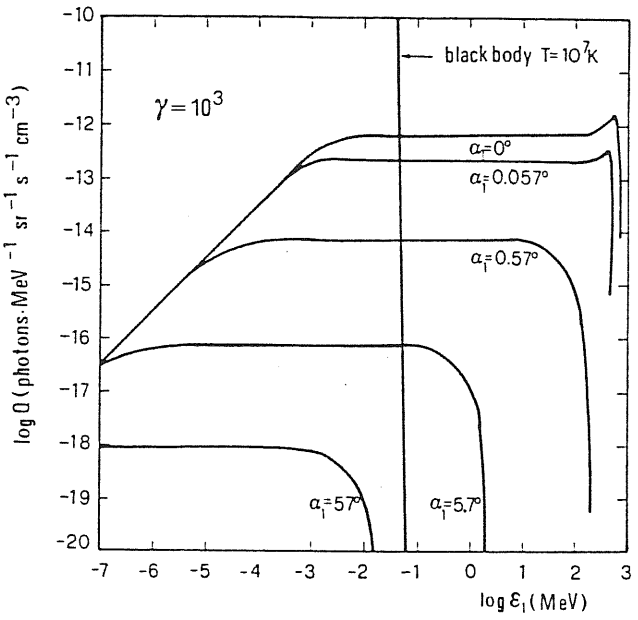

Figure 3.2: The comptonized black body photon spectra ($T_{bb} = 10^7$ K) for the Lorentz factor of electron beam $\gamma = 10^3$, and selected angles α_1 (from Bednarek et al. 1990a).

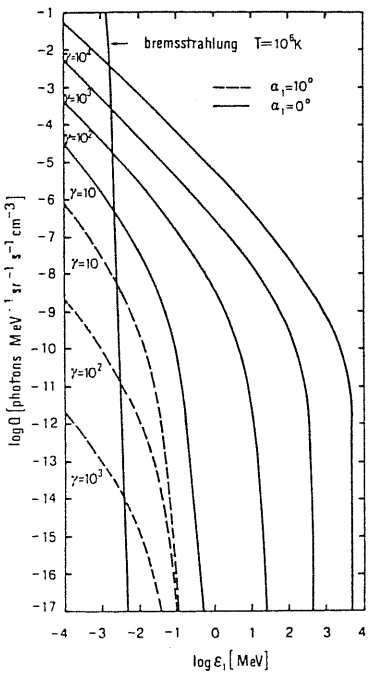

Figure 3.3: The comptonized thermal bremsstrahlung photon spectra, $T_{bb} = 10^6$ K for the Lorentz factors of electrons $\gamma = 10$, 10^2, 10^3, 10^4 and two values of the angles between the direction of the emitted photons and the beam axis: $\alpha_1 = 0°$ (solid line), and 10° (dashed line). The photon energy density of the bremsstrahlung spectra are normalized to 1 MeV/cm^3, and the density of electron beam was assumed to be $n_e = 1$ electron/cm^3 (from Bednarek et al. 1990a).

3.2 Radiation produced in hadronic interactions

In the inelastic interaction of relativistic protons with background matter, the γ-ray photons and electrons (positrons) are produced in a sequence of decays:

$$p + p \rightarrow \pi^{\circ} + \pi^{\pm}; \quad \pi^{\circ} \rightarrow 2\gamma; \quad \pi^{\pm} \rightarrow \mu^{\pm} + \nu_{\mu}; \quad \mu^{\pm} \rightarrow e^{\pm} + \nu_{e} + \nu_{\mu}. \tag{3.2}$$

The calculations of γ-ray and electron spectra, produced in the above reactions, were studied in the case of isotropic high temperature thermal plasma in several papers (see section 2.2 for a short review). The angular and energy dependent γ-ray spectra, from the above process, were recently discussed in the context of two physical scenarios. In the case of Solar γ-ray flares, the spectra of γ-rays from π° decay and the spectra of secondary positrons were calculated by Mandzavidze & Ramaty (1992). The angular and energy dependent spectra of γ-rays from bremsstrahlung for an arbitrary distribution of electrons were calculated by Dermer & Ramaty (1986).

The approximate angular and energy dependent γ-ray spectra from inelastic one-dimensional p + p collisions in a strong magnetic field were calculated by Dermer (1990). The propagation effects of γ-rays in strong magnetic field were included but a rather crude estimate of p + p cross section in isobar model was employed. The physical realization of such a scenario may occur in the accretion column close to the surface of a neutron star.

The basic role in all these calculations takes place the correct description of p + p interaction process. This processes was studied in detail in accelerator experiments, and in order to describe the observed results, a few different semi–empirical models of p + p interaction were proposed. At energies below $\sim$ 3 GeV, the p + p interaction process is best described by the isobar model (Stecker 1970). At energies above $\sim$ 10 GeV, the experimental results are well described by a scaling model (Feynman 1969). Between these energies ($\sim$ 3 – 10 GeV) a two component model, isobar + scaling, was applied in calculations by Dermer (1986). In the energy range $> 10^{12}$ eV there is some evidence that the scaling model breaks and the experimental results are better described in the model proposed by Wdowczyk & Wolfendale (1987).

In this section we want is to present the formulas for the angular and energy dependent spectra of γ-rays and electrons (originated in processes described by 3.2), in the model of a one-dimensional, monoenergetic proton beam interacting with background matter. Since we are interested in the high energy spectra, we applied the scaling model for p + p interaction, described in detail by Stephens & Badwar (1981) for the production of neutral pions, and Tan & Ng (1983) for the production of charged pions. The applications of these calculations in specific astrophysical scenarios are discussed in the next section.

3.2.1 Spectra of γ-ray photons from π^0 decay

Here we are interested in the energy and angular dependent γ-ray spectra produced in the interaction of a monoenergetic, relativistic proton beam with hydrogen cloud. The photon spectra from the decay of π° (see 3.2) are described by the formula

$$\frac{dN_\gamma}{dE_\gamma d\Omega dt dV} = D \int\int\int \frac{d^3\sigma(p_{\pi^\circ}, cos\theta_{\pi^\circ}, \phi_{\pi^\circ})}{dp_{\pi^\circ} d(cos\theta_{\pi^\circ}) d\phi_{\pi^\circ}} \cdot P(E_\gamma, cos\theta, \phi) dp_{\pi^\circ} d(cos\theta_{\pi^\circ}) d\phi_{\pi^\circ}, \qquad (3.3)$$

where $D = \beta \cdot c \cdot n_b \cdot n_H$, n_H is the hydrogen density in the cloud, n_b is the proton density in the beam, $\beta \cdot c$ is the proton velocity, p_{π° is the π° momentum in the observer's frame, and $\theta_{\pi^\circ}, \phi_{\pi^\circ}$ are the angles between the direction of the motion of π° and the beam axis in the observer's frame. The cross section in polar coordinates is related to the invariant cross section $E_{\pi^\circ} d^3\sigma/dp^3$ (Stephens & Badhwar 1981) by

$$\frac{d^3\sigma(p_{\pi^\circ}, cos\theta_{\pi^\circ}, \phi_{\pi^\circ}}{dp_{\pi^\circ} d(cos\theta_{\pi^\circ}) d\phi_{\pi^\circ}} = \frac{p_{\pi^\circ}^2}{E_{\pi^\circ}} \cdot (E_{\pi^\circ} \cdot \frac{d^3\sigma}{dp^3}), \qquad (3.4)$$

$P(E_\gamma, cos\theta, \phi)$ is the energy and angular distribution of photons from π° decay in the observer's frame, and E_γ, θ, ϕ are the energy and angles of the emitted photons in the observer's frame (in polar coordinates). For details of these calculations and the limits of integration we refer to Appendix B in Bednarek et al. (1990a).

The differential photon spectra were calculated numerically according to formula (3.2). Some results of these calculations are shown in Fig. 3.4. The shapes and intensities of these spectra are very sensitive to γ and α_1. For small angles α_1 (defined as above), the intensities, the widths, and the positions of maximum in the spectra grow proportionally with γ. For large angles α_1, the shapes and intensities of the photon spectra are almost independent of the γ. We would like to note that for a certain range of angles, the intensities of the spectra are comparable in the energy range 100 MeV – 1 GeV (see, e.g., Fig 3.4a). Therefore, if we observe two identical relativistic proton beams interacting with background matter, at small and large angles, the γ-ray intensity is comparable in the 100 MeV – 1GeV energy range but, e.g., the TeV γ-rays are observed only by an observer located on the beam axis. Such effects should appear in the interaction of relativistic proton beams with interstellar cloud (scenario discussed by e.g., Rose et al. 1984, 1987).

3.2.2 Spectra of secondary electrons from $\pi^\pm$ decay

The interaction of the relativistic protons in a jet with the ambient matter gives rise to charged pions which then decay via muons into secondary electrons (see 3.2). As in the case of γ-ray spectra,

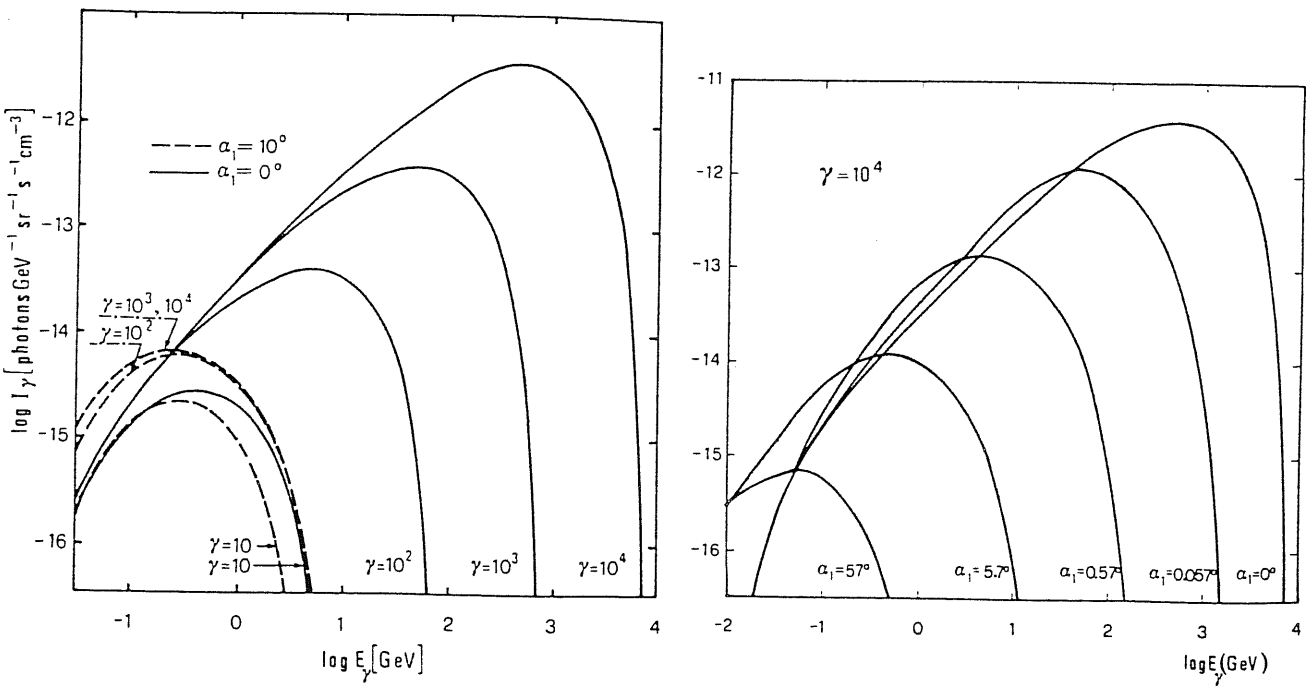

Figure 3.4: a). The differential photon spectra from π^0 decay from the monoenergetic proton beam with Lorentz factors $\gamma = 10, 10^2, 10^3, 10^4$, and two values of the angles between the direction to the observer and the beam axis $\alpha_1 = 0°$ (solid line) and 10° (dashed line). b). As in a) but for fixed proton beam Lorentz factor $\gamma = 10^4$ and selected angles α_1. The densities n_b and n_H are normalized to $1 particle/cm^3$ (from Bednarek et al. 1990a).

we are mainly interested in the angular dependence of the spectrum of the secondary electrons with respect to the axis of the proton beam.

We consider a monoenergetic, one–dimensional proton beam with Lorentz factor γ. The beam propagates at an angle α to the line of sight. The spectrum of muons from the decay of charged pions is then described by the formula

$$\frac{dR_\mu}{dE_\mu d\Omega_\mu dt dV} = D \int\int\int \frac{d\sigma(p_\pi, \cos\theta_\pi, \phi_\pi)}{dp_\pi d(\cos\theta_\pi) d\phi_\pi} P(\gamma_\pi, E_\mu, \Omega_\mu) dp_\pi d\Omega_\pi, \tag{3.5}$$

where

$$\frac{d\sigma(p_\pi, \cos\theta_\pi, \phi_\pi)}{dp_\pi d(\cos\theta_\pi) d\phi_\pi} = \frac{{p_\pi}^2}{E_\pi} \left(E_\pi \frac{d^3\sigma}{dp_\pi^3} \right), \tag{3.6}$$

and: $E_\pi \times d^3\sigma/dp_\pi^3$ is the invariant cross–section for the production of charged pions, taken from Tan and Ng (1983), $P(\gamma_\pi, E_\mu, \Omega_\mu)$ describes the energy and angular distribution of muons, in the observer's frame, from the decay of pions with momentum p_π and Lorentz factor γ_π. For details of the calculations we refer to Appendix A of Bednarek & Calvani (1991).

Assuming then that muons decay instantaneously, the angular dependent spectrum of secondary electrons is given by:

$$\frac{dN_e}{dE_e d\Omega_e dt dV} = \int\int\int \frac{dR_\mu}{dE_\mu d\Omega_\mu dt dV} J n^*(E_e^*, \Omega_e^*) dE_\mu d\Omega_\mu, \tag{3.7}$$

where $dR_\mu/(dE_\mu d\Omega_\mu dt dV)$ is the angular dependent spectrum of muons from decay of pions expressed by (eq. 3.5), $J = dE_e^* d\Omega_e^*/dE_e d\Omega_e = \gamma_\mu^{-1}(1 - \beta_\mu \cos\theta_e)^{-1}$ is the Jacobian of the transformation of the angular and energy dependent spectrum of electrons from the muon rest frame to the observer's frame, neglecting the electron rest mass with respect to electron's energy. The energy and angular distribution of electrons in the rest frame of polarized muons is (Lee & Young 1957)

$$n^*(E_e^*, \Omega_e^*) = 2x^2[(3 - 2x) - (1 - 2x) \cdot cos\theta_e^*], \tag{3.8}$$

where $x = 2E_e^*/m_\mu$. For details of the calculations we refer to Appendix B of Bednarek & Calvani (1991).

The numerical results for the spectrum of secondary electrons are presented in Fig. 3.5, for Lorentz factors $\Gamma = 10$, 10^2, 10^3, 10^4 of the monoenergetic proton beam and for angles $\alpha = 0°$, $10°$. The general behaviour of the spectra of secondary electrons is very similar to the spectra of photons from π^0 decay (see section 3.2.1). The shape and maximum intensity of the spectra strongly depend on γ and α. For small α and in the relativistic limit $\gamma >> 1$, the value and the position of the maxima grow proportionally to γ (Fig. 3.5). The spectra of secondary electrons have smaller intensities and are shifted to lower energies than the spectra of secondary positrons because of the difference in the cross sections for π^- and π^+ production in p + p collisions. For large α, the shape of the spectra and the position of the maxima are practically determined only by the value of α, the intensities for different γ's in relativistic limit being comparable (Fig. 3.5).

The secondary electrons produced in hadronic collisions via decay of charged pions can be important in discrete γ-ray sources from two reasons. First, the secondary electrons take a significant part of the power released in the inelastic p + p collision. Second, in such a process, the secondary electrons can be produced with extremely high energies. A direct acceleration of electrons to comparable energies can be impossible because of the huge energy losses suffered by electrons in magnetic and radiation fields. The interaction of the secondary electrons with matter (bremsstrahlung) and radiation (inverse Compton scattering) will result in production of X- and γ-ray photons. However, the detailed calculations involving the angular and energy distribution of electrons are very complicated, particularly, if the structure of the magnetic field is important. Some simple applications in astrophysical scenarios (neglecting the possible importance of the magnetic field) are discussed in chapter 6 of this thesis.

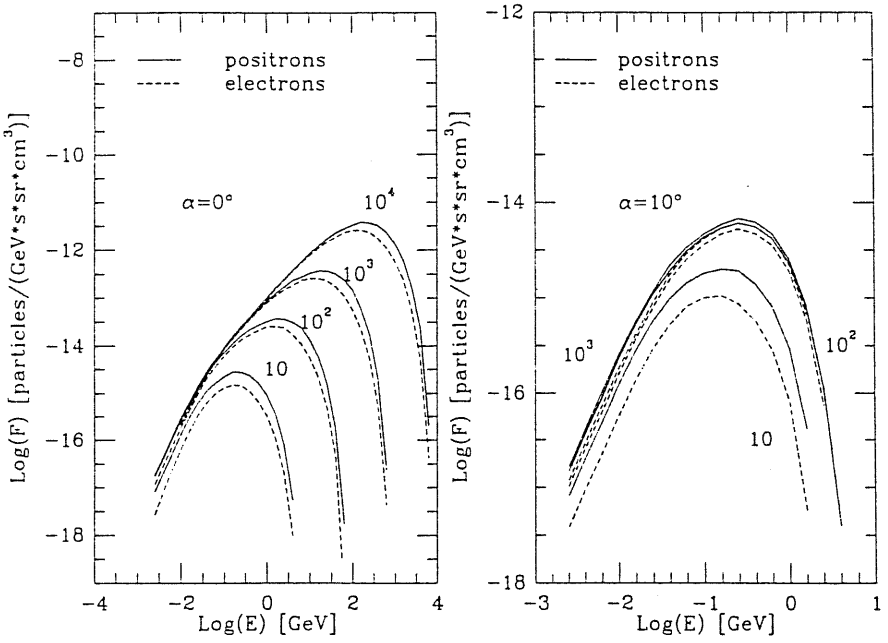

Figure 3.5: a) The spectra of secondary electrons arising from proton–proton interactions (p + p $\rightarrow \pi^{\pm} \rightarrow \mu^{\pm} \rightarrow e^{\pm}$) are shown. The different lines correspond to different values of the Lorentz factors and $\alpha = 0°$. b) As in a), for $\alpha = 10°$ (from Bednarek & Calvani 1991).

3.3 Possible applications to astrophysical scenarios

The observations in low photon energies clearly show the anisotropic structure of many astrophysical sources (e.g. AGNs, pulsars, binary systems), suggesting the importance of physical scenarios in which production of radiation depends on the viewing angle of the source. A similar structure of sources is also expected in the γ-ray energies, and, in fact, such anisotropic effects are observed in the case of γ-ray emitting radio pulsars. It is also almost certain, that γ-ray emission from several recently discovered AGNs is anisotropic. Most of these AGNs (if not all ?) are sources with jet-like features, showing superluminal motion in their central parts.

Based on our calculations (described in section 3.1 and 3.2), we suggest here possible scenarios of γ-ray production in two types of galactic sources: Cyg X-1 (binary system) and in a model of an old, accreting neutron star. The application of our calculations to AGNs (3C 273 and 3C 279) will be discussed in detail in chapter 6.

Cyg X-1

It is a binary system with orbital period $\cong$ 5.6d, separation of the components $\cong 3 \cdot 10^{12}$cm, orbital inclination $\cong$ 30°, mass function $\cong 0.22 M_{\odot}$, and distance $\cong$ 2.5 kpc (Ninkov et al. 1987a). For general information concerning this source we refer to the papers by Oda (1977) and by Liang & Nolan (1984). Cyg X-1 is a source of non–thermal radio emission which suggests the existence of relativistic electrons (Woodsworth 1980). The hard X-ray and soft γ-ray emission is highly

variable, showing a few different states. In the MeV photon energy range, the spectrum becomes transiently very flat up to $\sim$ 10 MeV (see recent review by McConnell & Owens 1992). Based on the observational high energy properties of this source we proposed a model (Bednarek et al. 1990b), in which the transient MeV emission can originate in comptonization of the thermal black body radiation ($T_{bb} = 3 \cdot 10^4$ K), emitted by the supergiant companion HDE 226868, by relativistic electron beam with a Lorentz factor $\sim$ 600 (see Fig. 3.6 for the geometry of the source)[1]. We calculated the soft γ-ray spectra according to the above scenario, following the general formula (3.1). The results of these calculations were compared in Fig. 3.7 with the observed Cyg X-1 spectrum at energies above 1 MeV, and with photon spectrum predicted by the single–temperature inverse Compton model (Sunyaev & Titarchuk 1980) at energies below 1 MeV.

In our model, the observed photon spectrum of Cyg X-1 can be expressed by

$$I_{obs} = I_{theor} \cdot \rho_{ph} \cdot \frac{1}{d^2} \cdot \frac{R}{c} \cdot N_e, \tag{3.9}$$

where I_{obs} is the observed photon spectrum measured by McConnell et al. (1989), I_{theor} is the comptonized photon spectrum calculated for the Lorentz factor of electrons $\sim$ 600 and a black body temperature $T_{bb} = 3 \cdot 10^4$ K; ρ_{ph} is the average photon density ($\cong 5 \cdot 10^7 MeV/cm^3$) along the line of propagation R, calculated from the absolute magnitude of HDE 226868 ($M_v = -6.5$); R - is the range in which comptonization of background photons into the MeV energy range is important, obtained from our computations for the reported orbital inclination of the system, and the separation of the components; N_e is the emissivity in the relativistic electrons.

From the observed intensity of photons above 1 MeV, we have estimated the lower limit on the emissivity of relativistic electrons in Cyg X-1 (following formula 3.9), which is $\sim 1.5 \cdot 10^{38} electrons/s$, corresponding to an electron luminosity $\sim 7 \cdot 10^{34} erg/s$. We note that the attenuation length λ of the background photons ($T_{bb} = 3 \cdot 10^4$ K) for 0.3 GeV electrons is equal to $\sim 10^{13}$ cm (Karakuła & Tkaczyk 1987). Therefore, the electron's Lorentz factor does not change drastically during the propagation through the binary system, since $R/\lambda \cong 0.36$. The background low energy radiation in this system is probably dominated by HDE 226868, since there is no evidence of a large accretion disk around the compact object of Cyg X-1 (Beall 1984, Ninkov et al. 1987b). The bremsstrahlung of relativistic electrons, from the interaction with the stellar wind of the massive companion, is negligible in comparison to the discussed comptonization process. In Bednarek et al. (1990c), we discussed a possible mechanism for the observed variability of the MeV flux and suggested its connection with the orbital period 5.6d and observed 294d long term X-ray periodicity

[1] A similar general scenario, the comptonization of the optical photons of the primary by relativistic electrons emitted by the compact object, as a mechanism of γ-ray production was suggested previously by Maraschi & Treves (1981) for the γ-ray source LSI 61° 303 (Wills et al. 1980; Perotti et al. 1980).

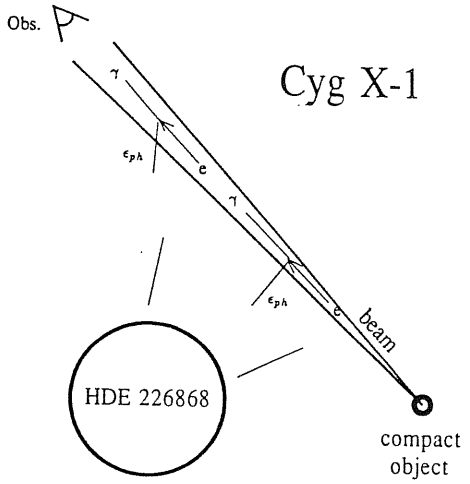

Figure 3.6: The schematic picture of possible scenario of soft γ-ray production in Cyg X-1 (not to scale). The relativistic electron beam emitted by the compact object comptonizes the low energy thermal photons (ϵ_{ph}), emitted by the supergiant companion HDE 226868, to the soft γ-ray energy range. The observer is located on the axis of the beam.

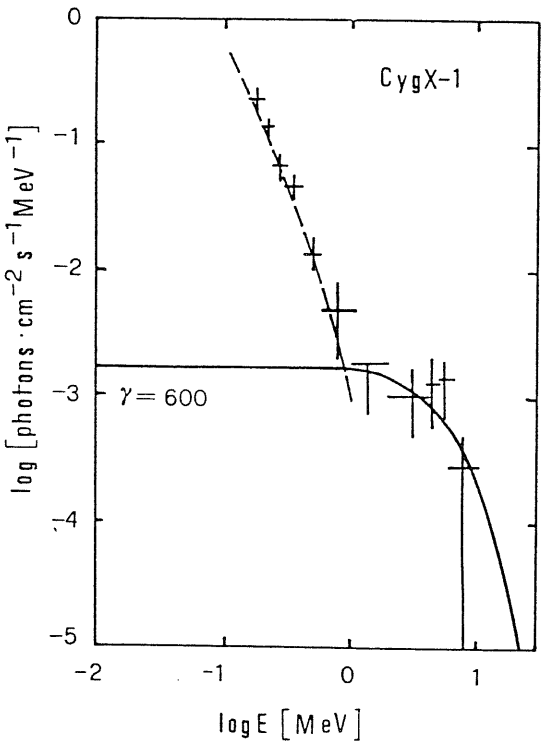

Figure 3.7: The differential photon spectrum of Cyg X-1 (McConnell et al. 1987) and the best fit by calculated photon spectra: the solid line refer to the comptonized black body spectrum ($T_{bb} = 3 \cdot 10^4$ K), for the electron beam Lorentz factor $\gamma = 600$; the dashed line refers to the single–temperature inverse Compton model (Sunyaev & Titarchuk 1980) (from Bednarek et al. 1990b).

(Priedhorsky & Terrell 1983).

It seems, at present, that Cyg X-1 shows some features common to a small group of objects[2] in which e^+e^- pair dominated plasma may play an important role. However a final conclusion was not reached on this matter and our scenario may be valid especially if the appearance of the MeV feature is correlated with observed periodicities at 5.6d and 294d.

An old nearly aligned neutron star

We suggest that the old neutron stars can be a weak sources of the high energy γ-ray emission. Such emission can originate in the interaction of beamed relativistic particles with accreted matter. Above mechanism may be realized in the model of an old neutron star whose magnetic axis is close to rotational axis (see Fig. 3.8). The protons accelerated close to the magnetic pole of the neutron star can interact with matter accreting from interstellar cloud. As a result, the production of γ-rays is collimated in a hollow cone between the angles α_{in} and α_{out}. The observer is located at the angle β to the direction of rotational axis.

In the paper by Bednarek et al. (1990b), we discuss such scenario as a possible model for 2CG 195+04 (Geminga). However, at present it is certain that such application is irrelevant, since Geminga is a relatively young pulsar with period 237ms (Halpern & Holdt 1992).

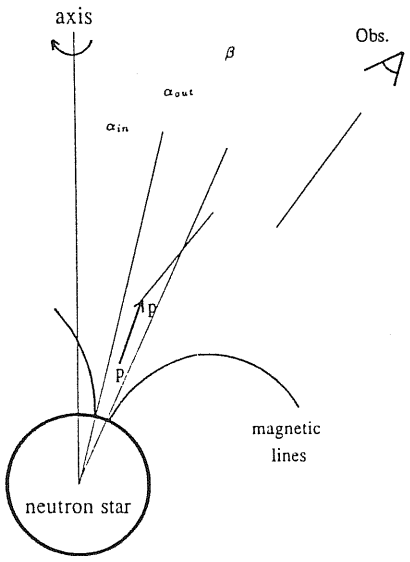

Figure 3.8: The schematic picture of possible scenario of γ-ray production in the model of old, nearly aligned neutron star (not to scale). The proton beam propagating along the magnetic axis of the neutron star interacts with accreting matter. Because of rotation of neutron star, the protons are accelerated into the hollow cone (between angles α_{in} and α_{out}). The observer is located at the angle $\beta > \alpha_{out}$.

[2]They are black hole candidates (e.g. 1E 1740.7-2942, Nova Musca), and show a bump in the MeV energy range of the photon spectrum. The weak evidence (1.9σ) for a tentative, narrow annihilation line at $\sim$ 511 keV in the Cyg X-1 photon spectrum was reported by Ling & Wheaton (1990).

This chapter is partially based on the papers: *"The photon spectra from beam interactions with matter and radiation"* 1990a, A&A 236, 268, and *"Origin of the γ-ray spectra of Cyg X-1 and Geminga"* 1990b, A&A 236, 175 by Bednarek, W., Giovannelli, F., Karakuła, S., Tkaczyk, W.; and *"X- and γ-ray emission from 3C 273"* by Bednarek, W. & Calvani, M 1991, A&A 245, 41 (included in an Appendix).

References

Beall, J.H. et al. 1984, ApJ 284, 745
Bednarek, W. & Calvani, M. 1991, A&A 245, 41
Bednarek, W., Giovannelli, F., Karakuła, S.& Tkaczyk, W. 1990a, A&A 236, 268
Bednarek, W., Giovannelli, F., Karakuła, S. & Tkaczyk, W. 1990b, A&A 236, 175
Bednarek, W., Giovannelli, F., Karakuła, S. & Tkaczyk, W. 1990c, 21st ICRC (Adelaide), 1, 204
Bridle, A.H. & Perley, R.A. 1984, ARAA 22, 319
Canfield, E., Howard, W.M. & Liang, E.P. 1987, ApJ 323, 565
Dermer, C.D. 1986, A&A 157, 223
Dermer, C.D. 1990, ApJ 360, 197
Dermer, C.D. & Ramaty, R. 1986, ApJ 301, 962
Dermer, C.D, Schlickeiser, R. & Mastichiadis, A. 1992, A&A 256, L27
Feynman, R.P. 1969, Phys.Rev.Lett. 13, 145
Ghisellini, G., Maraschi, L. & Treves, A. 1985, A&A 146, 204
Ghisellini, G. et al. 1991, MNRAS 248, 14
Halpern, J.P. & Holt, S.S. 1992, Nat 357, 222
Karakuła, S. & Tkaczyk, W. 1987, Acta Universitatis Lodziensis, Folia Physica, 10, 127
Lee, T.P. & Young, C.N. 1957, Phys.Rev. 105, 1674
Liang, E.P. & Nolan, P.L. 1984, Sp.Sci.Rev. 38, 353
Ling, J.C. & Wheaton, W.A. 1990, ApJL 343, L57
Mandzavidze, N. & Ramaty, R. 1992, ApJ 389, 739
Maraschi, L., Ghisellini, G. & Celotti, A. 1992, ApJL in press
Maraschi, L. & Treves, A. 1981, MNRAS 194, 1p
McConnell, M.L. et al. 1989, ApJ 343, 317
McConnell, M.L. & Owens, P.P. 1992, Comm. on Astrophys., to be published
Melia, F. & Königl, A. 1989, ApJ 340, 162
Ninkov, Z., Walker, G.A.H. & Yang, S. 1987a, ApJ 321, 425
Ninkov, Z., Walker, G.A.H. & Yang, S. 1987b, ApJ 321, 438
Oda, M. 1977, Sp.Sci.Rev. 20, 757
Perotti, F. et al. 1980, ApJL 239, L49
Priedhorsky, W.C. & Terrell, J. 1983, ApJ 270, 233
Rees, M. 1985, 19th ICRC (La Jolla) 9, 1
Stecker, F.W. 1970, Ap&SS 6, 377
Rose, W.K. et al. 1984, ApJ 280, 550
Rose, W.K. et al. 1987, ApJ 314, 95
Stephens, S.A. & Badhwar, G.D. 1981, Ap&SS 76, 213
Sunyaev, R.A. & Titarchuk, L.G. 1980, A&A 86, 121
Tan, L.C. & Ng, L.K. 1983, J.Phys. G 9, 1289
Vestrand, W.T., Forrest, D.J. & Riegler, E. 1991, 22nd ICRC (Dublin) 3, 69
Wdowczyk, J. & Wolfendale, A.W. 1987, J.Phys. G: Nucl.Phys. 13, 411
Wills, R.D. et al. 1980, Adv. in Space Exploration v.7
Woodsworth, A.W., Higgs, L.A. & Gregory, P.C. 1980, A&A 84, 379
Zensus, J.A. & Pearson, T.J. 1988, *The Impact of VLBI on Astrophysics and Geophysics*, eds. M.J. Reid & J.M. Moran, (Kluwer: Dordrecht), p.7

4 γ-ray emission from isolated neutron stars

Neutron stars are mainly composed of an extremely high density, degenerate neutron fluid. The existence of matter in such a state was suspected by Landau (1932) and its possible origin in supernova explosions was suggested by Baade & Zwicky (1934). Pacini (1967) was the first who showed that a rapidly rotating neutron star, with a strong dipolar magnetic field (magnetic axis oblique to rotational axis), would act as a very energetic electric generator providing a source of energy for a surrounding nebula.

The confirmation of these theoretical analyses arrived unexpectedly from radio astronomers. A few months after Pacini's paper appeared, Hewish et al. (1968) announced the discovery of a source (present symbol PSR 1919+21) emitting very regular radio pulses and suggested that a model should contain very compact object (e.g. white dwarf or neutron star). Since then about 500 pulsars with periods of rotation in the range $1.6ms$ to $4.3s$ have been discovered and investigated. For reviews of different aspects of pulsar observations we refer to books by Manchester & Taylor (1977) and Smith (1977), and the review article by Taylor & Stinebring (1986).

The link between the theoretical work of Pacini and newly discovered pulsating objects was at first envisaged by Gold (1968) and next this proposition was developed by Pacini (1968) and Ostriker & Gunn (1969). In this last paper, a more detailed model of the pulsar was proposed in which the authors discussed the pulsar's evolution and possible mechanisms of particle acceleration to very high energies in the wind zone[1].

The structure of the inner part of a pulsar magnetosphere was studied in the simple case of aligned magnetic rotator by Goldreich & Julian (1969). The authors argued that a neutron star should possess a dense charge separated magnetosphere, corotating with the star up to the light cylinder. The charged particles can escape from such magnetosphere through the light cylinder radius being accelerated to very high energies. However, it is very difficult to envisage how such a magnetosphere may be filled with charge (one sign of charge should cross to the oppositely charged part of the magnetosphere on its way from the pulsar surface). In spite of many further efforts,

[1] For recent studies of particle acceleration in terms of this model, see Thielheim (1991).

there is no self-consistent pulsar model (see for review Michel 1982). Some progress in this topic, related to high energy radiation from pulsars, will be discussed in section 4.2 of this chapter.

In the next section of this chapter we briefly review the main results of γ-ray observations of pulsars and in section 4.2 the theoretical models of γ-ray production in the radio pulsars . Our original contribution to this topic is included in section 3.3. We review in more detail the high energy emission from the Crab Nebula pulsar which is, at present, the best established source of γ-rays. Then we concentrate on theoretical analysis of the results of γ-ray line emission from the Crab pulsar. Based on the present pulsar model elaboratored by Ruderman and collaborators and analysis of pulsar electrodynamics, we propose a picture in which the production of the $\sim$ 440 keV line, observed in Crab pulsar photon spectrum, can be envisaged. As a result of our model we predict the possible appearance of a transient feature at $\sim$150 keV in the Crab pulsar spectrum, resulting from Compton backscattering of 511 keV e^+e^- annihilation photons in the neutron star crust.

4.1 Observations

Because of nonthermal spectra, radio pulsars were suspected as favorable targets for high energy observations. However, for more than 20 years, only two of them were well established as γ-ray emitters. The Crab pulsar (PSR 0531+21) and the Vela pulsar (PSR 0833-45). Since the Crab pulsar is the best investigated and our original contribution to this topic concerns also this specific object, we will review this source in more detail in a separate section. Here we start with a short description of the γ-ray observations of Vela pulsar and then we mention the results collected for other pulsars including preliminary observations by the Comptel GRO.

Vela pulsar

The Vela pulsar is a $\sim 89ms$, relatively young, radio pulsar discovered by Large et al. (1968), with characteristic age $P/2\dot{P}\sim 12000yr$ and at a distance $\sim 450pc$. Its common origin with the Vela supernova remnant, which is a source of soft X-ray emission (Seward et al. 1971), is usually postulated. The light curve of the Vela pulsar, compared in different wavelengths, is very unusual (see Fig. 4.1). The radio emission is strong and radio light curve shows a single peak. Its optical emission is extremely faint, $\sim$ 24 magnitude (Wallace et al. 1977). The optical light curve shows double peak structure (separated by about 35ms) and shifted for about 13ms after the radio peak. Such a configuration suggests different emission mechanism in these two photon energies and/or different geometrical locations.

At high energies, the Vela pulsar was observed in γ-rays at 35-200 MeV by SAS 2 (Thompson et al. 1975; Thompson et al. 1977a) and in the 50–5000 MeV energy range by COS B (Bennett

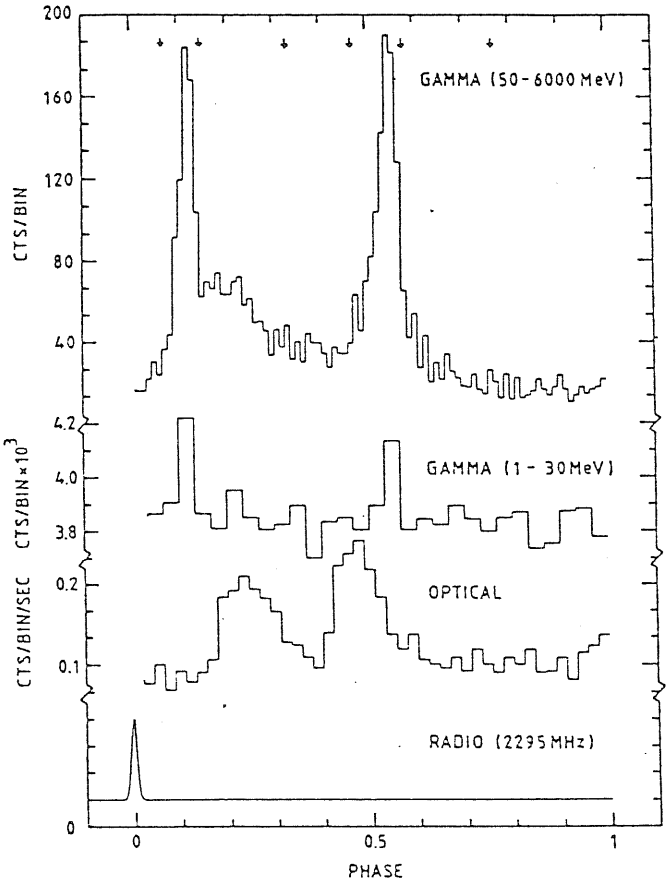

Figure 4.1: The light curve from PSR 0833-45 at radio, optical, soft energy γ-rays and high energy γ-rays (for references see Grenier et al. 1988).

et al. 1977) as the strongest source in the sky. The γ-ray light curve shows two sharp peaks separated by 0.42 in phase and bracketing the optical pulses (see Fig. 4.1). Significant emission is also observed from the interpeak region and the trailer after the secondary peak (Kanbach et al. 1980). The detailed studies of spectral characteristics of the Vela pulsar, based on the final COS B data (Grenier et al. 1988), shows that the time integrated differential photon spectrum is better described by two power laws (spectral index 1.72 ± 0.07 below 300 MeV and 2.12 ± 0.07 above) than by single power law in all COS B energy range[2]. The spectrum also shows long time variability specially in the softer part ($< 300 MeV$) and in the interpulse region just after the first main peak. The spectrum in the second peak is much harder than in the first peak, while the trailer seems to exhibit an extremely soft spectrum. The main spectral features of the Vela pulsar light curve were recently confirmed by observations of the GAMMA-1 telescope above 100 MeV (Akimov et al. 1991). The general light curve of the Vela pulsar observed by GAMMA-1 presents the same shape but significant morphological differences exist in the interpeak region. The observation in autumn 1990 shows a transparent gap in the interpeak region which is not seen in spring 1991.

[2]In fact, COS B data and observations in other energy bands suggest that the total Vela pulsar γ-ray spectrum can be fit by a smooth curve, continuously steepening with increasing energy.

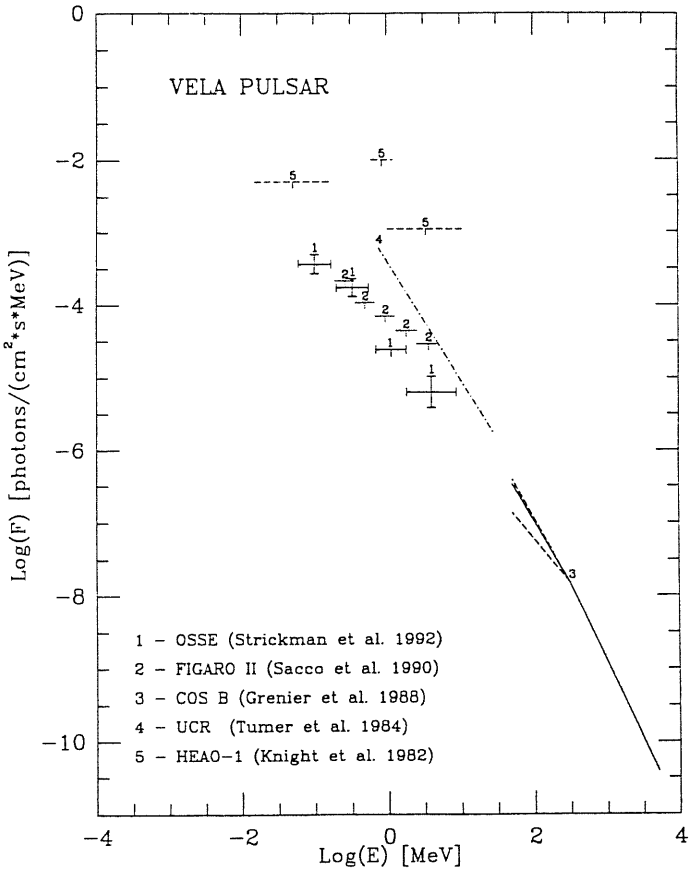

Figure 4.2: The Vela pulsar γ-ray spectrum collected from different experiments in the low and high energy range. The dashed lines in the spectrum measured by COS B (Grenier et al. 1988) refer to lower and upper spectral indexes of the γ-ray spectrum (between 50–300 MeV), observed in different periods.

Another important piece of information concerning the mechanism and geometry of γ-ray production in the Vela pulsar may be obtained from studies of radiation polarization. In fact, possible linear polarization of γ-ray photons from the Vela pulsar was found by Caraveo et al. (1988). However Mattox et al. (1990) concluded that even 100% γ-ray polarization would not be detected by the COS B telescope so this result is in serious doubt [3].

For a long time, the pulsed emission from the Vela pulsar was not detected in X-ray energy band. In soft γ-rays, the Vela pulsar was detected between 0.3–30 MeV (Tümer et al. 1984), 31 days after a large glitch in the pulsar period. The soft γ-ray light curve is exactly the same as observed at energies above 35 MeV but the energy spectrum appears to bend away from SAS 2 and COS B power law. However, that result was not confirmed by the FIGARO II group (Sacco et al. 1990) who observed the Vela pulsar on 1988 November 25. Two sigma upper limits for the pulsar flux, in the γ-ray energy range 0.2–6. MeV, were significantly lower than the flux measured by Tümer et al. (1984), see Fig 4.2. Recently, the OSSE team (Strickman et al. 1992) announced the positive detection of the Vela pulsar in hard X-rays and low energy γ-rays with spectrum consistent with

[3] A Monte Carlo simulation shows that the EGRET telescope on board of Compton GRO does not have sufficient sensitivity to detect linear polarization even for 100% polarized γ-ray sources (Mattox 1991).

upper limits obtained by Sacco et al. (1990). Also the Comptel detector on board the GRO detected the Vela pulsar between 10-30 MeV with the flux lower than ever seen before[4], but results of these observations are not yet published.

The clear break seen in the Vela pulsar spectrum between low and high energy γ-rays (Fig. 4.2) was predicted, based on theoretical grounds, by Salvati (1983) and its relation to the Vela pulsar spectrum was discussed by Salvati (1986).

The Narrabri and Ooty groups reported their results of observations of the Vela pulsar in TeV photon energies. The Narrabri group claimed the observation of a 4σ effect above 0.3 TeV with photon flux 1.0×10^{-11} $phot./cm^2/s$ (Grindlay et al. 1975), although regarded by the authors as an upper limit. The reported light curve showed only a single narrow peak, 3ms before the radio peak. The Ooty group reported detection of a double peak structure with significance 4.4σ (first peak) and 2.2σ (second peak) above $\sim$10 TeV with flux 5×10^{-13} $phot./cm^2/s$ (Bhat et al. 1980). The peaks are separated by about 0.42 in phase, which is exactly the same as observed in the COS B γ-ray energy range. Although these results are not consistent, both of them are three orders of magnitudes below the extrapolation of γ-ray spectrum measured by COS B and suggest the high energy break in the γ-ray photon spectrum.

The γ-ray emission from a few other radio pulsars has been indicated in the SAS 2 and COS B data (see e.g. Thompson et al. 1976; Ögelman et al. 1976; Buccheri et al. 1978; Pinkau et al. 1979) but these reports were never confirmed. A few sources were claimed at photon energies above 0.1 TeV: PSR 0355+54, PSR 1509-58, PSR 1953+29, PSR 1937+21, PSR 1957+20, PSR 1855+09, although they were not confirmed independently (see for review Weekes 1988). The best potential candidates of the steady TeV emission seems to be plerions[5]. A few such sources are recommended for deeper studies by Weekes (1992): CTB80 (PSR 1951+32), LMC 0540-69 (PSR 0540-69), MSH 15-52 (PSR 1509-58), 201.2+8.2 (PSR 0656+14) and 3C58 (?). The detection of TeV γ-ray photons from two milisecond pulsars (PSR 1953+26 – Chadwick et al. 1985; PSR 1937+214 – Chadwick et al. 1989) was announced by the Durham group. These results were not confirmed independently.

The significant progress in detection of γ-rays from pulsars is expected with the analysis of data from the Compton GRO detectors. Preliminary results are very promising. Two more radio pulsars have been discovered in γ-rays. The first one, PSR1706-44 with period 102ms, reported by the EGRET team above 100 MeV (Kniffen et al. 1992), identified also in COS B data with the source 2CG342-02, shows a single broad pulse in the γ-ray light curve. Recently the pulsed emission from this source has been also detected in soft X-rays by ROSAT satellite (Becker et al.

[4]The information taken from Compton Observatory Newsletter, 1992, v.2, no.1.

[5]The plerions are Crab-like supernova remnants with X-ray emitting filled centers. The X-ray emission from their interior indicates the presence of a pulsar which continues to pump relativistic particles into the volume of the Nebula. For a review of observations of plerions we refer to, e.g. Seward (1989) and theory to, e.g. Bandiera 1990.

1992). The second one, PSR1509-58 with period 150ms, was reported by OSSE team in soft γ-rays (Wilson et al. 1992) and also shows single peak in the light curve. Simultaneous observations of this pulsar in radio and X-ray bands (Kawai et al. 1991) show that the radio peak leads the X-ray peak by $37 \pm 3ms$. In this context, the absolute localization of γ-ray peak in pulsar light curve is very important for detailed studies of radiation mechanism of pulsars[6].

The most recent identification of a pulsar emitting γ-rays concerns the object, Geminga (2CG195+04). Geminga was first detected in γ-rays above 35 MeV by SAS 2 (Fichtel et al. 1975), and tentatively identified with the X-ray source 1E0630+178 (Bignami et al. 1983; Halpern & Tytler 1988). The analysis of ROSAT data by Halpern & Holt (1992), collected for 1E0630+178, shows pulsations of X-ray emission at a period of $\sim 0.237s$. This X-ray period was confirmed by analysis of γ-ray data from the EGRET (GRO) detector (Bertsch et al. 1992) and old data from COS B (Bignami & Caraveo 1992; Hermsen et al. 1992). The Geminga light curve shows two narrow peaks separated in phase by ~ 0.5 and emission from the interpeak region (similar to Crab and Vela pulsar). The period derivative, $\dot{P} = 1.099 \pm 0.001 \times 10^{-14} s \cdot s^{-1}$, suggests that Geminga is a nearby (upper limit on distance $\sim 380pc$), isolated neutron star with a surface magnetic field of $1.6 \times 10^{12} Gs$ and characteristic age $\cong 3.2 \times 10^5 yr$. The soft γ-ray emission was not detected from this source by the SIGMA (Lebrun et al. 1991) and COMPTEL (GRO) detectors. There is also no observed periodic radio signal (Seiradakis 1992). These two facts place strong limits on the radiation mechanism and/or geometry of the emitting region.

Summing up, the picture of the pulsar emission arising from these observations seems to be quite complicated. Even with such small number of investigated cases, the general light curves show a large variety of behaviour (two peaks, one peak, different separation between two peaks, differences in the peak phases observed in different energy ranges, variability of peaks intensities). The fine structure of the light curve shows time variable interpeak components, trails, dependence of the light curve on the photon energy range. The time integrated photon spectra also show big differences between specific cases, e.g. Crab pulsar clearly seen in soft γ-rays, Vela pulsar emission is much less evident but Geminga was not detected at all; Crab pulsar observed in TeV photon energies but significant break in Vela pulsar photon spectrum between GeV and TeV photon energies.

4.2 Models

Up to now there is no widely accepted model of photon emission by pulsars. However, a few interesting propositions appeared which are usually based on the idea of γ-ray production in electromagnetic processes in pulsar magnetosphere. Most of these scenarios accept, as a starting point,

[6]There are some problems with absolute time measurements on the board of the Compton GRO and at present such analysis is not possible.

the model of pulsar magnetosphere proposed by Goldreich & Julian (1969) known to be not completely self–consistent. It is believed that rotation of the pulsar may create, in the magnetosphere, regions of charge separation in which high electric potentials are induced. Following these ideas, Sturrock (1971) assumed that electrons (positrons) can be accelerated close to the polar cap of the pulsar up to the Lorentz factors of the order 10^7. He showed that electrons, flowing out of the surface may develop electromagnetic cascade in the strong, dipole magnetic field of the magnetosphere via curvature radiation and magnetopair production. Some aspects of this general proposition (e.g. optical depth for γ-rays in pulsar magnetosphere, pulse shapes and difference between pulses in different energy ranges) were investigated by, e.g., Hardee (1977), Harding et al. (1978).

The Sturrock proposition was studied in detail by Salvati & Massaro (1978). These authors derived approximate analytic transfer equations of relativistic electrons moving in a detailed model of the pulsar magnetosphere. The processes of curvature radiation, pair production in magnetic and induced electric fields, and synchrotron radiation emitted by first generation of pairs were taken into consideration. The γ-ray spectrum and light curve resulting from this model are in good agreement with observational data of the Vela pulsar. In the paper by Massaro & Salvati (1979), calculations of γ-ray spectra were performed for a wide range of pulsar parameters. The detailed numerical simulations according to the above scenario was performed by Harding (1981). These simulations also took into account multiple generation of e^+e^- pairs since their synchrotron radiation make important contributions to the final γ-ray spectrum $> 25MeV$. Estimated γ-ray luminosity of the pulsar in the model analyzed by Harding (1981) is given by formula:

$$L_\gamma \cong 1.2 \times 10^{35} \cdot B_{12}^{0.95} \cdot P^{-1.7}\ phot./s,$$

and efficiency of rotational energy conversion of the pulsar into γ-ray photons is:

$$n_\gamma \cong \frac{2 \times 10^{31}}{4\pi^2 \cdot I} \cdot B_{12}^{0.95} \cdot \frac{P^{1.3}}{P_{dot}},$$

where P is pulsar period, P_{dot} period derivative and I is the moment of inertia of the pulsar.

The detailed studies of an acceleration process in a polar gap region were carried out by Ruderman & Sutherland (1975). In their model, the polar gap over the polar cap region of a neutron star may be caused by the outflow of charged particles along field lines induced by the neutron star rotation. The discharge of the gap occurs through 'sparks' initiated by positrons with Lorentz factors $\sim 3 \times 10^6$. However, the growth of electric potential is limited to a value on the order of $10^{12-13}eV$, as a result of multiple e^+e^- pair production in electromagnetic cascade via curvature radiation and magnetopair production processes (see Fig 4.3). The escape of very high energy γ-rays from regions close to the surface seems to be impossible because of γ-ray absorption in the magnetopair production process[7].

[7]The effect of capture of photons by a curved, strong magnetic field (see Shabad & Usov 1982), resulting in bending

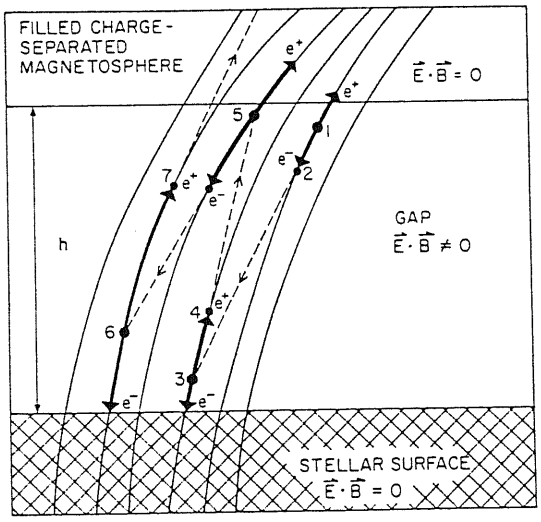

Figure 4.3: Nature of the pair-production discharge. A photon (of energy $> 2mc^2$) produces an e^+e^- pair at '1'. The electric field of the gap accelerates the positron out of the gap and accelerates the electron toward the stellar surface. The electron moves along a curved field line and radiates an energetic photon at '2' which goes on to produce a pair at '3' once the component of its momentum perpendicular to the magnetic field is sufficiently large. This cascade of pair production – acceleration of electrons and positrons – curvature radiation – pair production results in a 'spark' breakdown of the gap (from Ruderman & Sutherland 1975).

The above calculations of γ-ray spectra (Salvati & Massaro 1978; Harding 1981) do not include the part of the cascade which develops during the acceleration of electrons. It was done analytically by Ayasli (1981) who concluded that this part of the cascade does not influence the final γ-ray spectrum. However, its importance on the formation of γ-ray spectrum was envisaged in detailed numerical simulations performed by Daugherty & Harding (1982).

The problem, which should also be mentioned here, is the possibility of huge energy losses suffered by relativistic electrons close to the surface of a young neutron star (e.g. Crab type). If the temperature of the polar cap is greater than $\sim 10^6 K$[8] and the surface magnetic field is of the order $\sim 10^{12} Gs$, the resonant Compton scattering of thermal radiation[9], emitted by the neutron star, may be an important mechanism of electron energy losses (Xia et al. 1985; Daugherty & Harding 1989). Consequently, the electrons cannot be accelerated to very high energies in the polar gap and the cascade via curvature radiation and magnetopair production proposed by the Ruderman & Sutherland model will not develop. However, this process by itself can produce γ-ray photons near the polar cap surface and its possible relation to γ-ray bursts was discussed in several papers

of the photon trajectory is important for rather low energy γ-ray photons ($< 30 MeV$), assuming typical magnetic field strength of the pulsar of a few $10^{12} Gs$ and curvature radius $\sim 10^6 cm$.

[8]The upper limit on the temperature of the Crab pulsar surface was estimated on $\sim 2.6 \cdot 10^6 K$ (Harnden & Seward 1984). However the temperature of the polar cap region may be significantly higher (see Helfand et al. 1980).

[9]The cross section for the inverse Compton scattering in strong magnetic fields shows resonance behaviour when incident photon energy in the electron rest frame is close to the cyclotron frequency. The total cross section can even be three orders of magnitude higher than the classical Thomson cross section.

(see, e.g., Dermer 1989, 1990; Vittelo & Dermer 1991; Preece & Harding 1992).

The Compton scattering of synchrotron radiation, emitted by relativistic electrons in the magnetic field of the outer magnetosphere, was studied in detail by, e.g., Treves (1971), Cheng & Ruderman (1977), Schlickeiser (1980) as a mechanism responsible for γ-ray emission from pulsars. In terms of this radiation mechanism, the general photon spectrum of pulsars can be described. A more ambitious model of pulsar emission, applying the above discussed mechanism, was constructed by Morini (1983). The author proposed that two peaks of the Vela pulsar light curve are produced by this same population of electrons following these same magnetic field lines but in two different places. In the first, the γ-ray pulse is produced near the light cylinder by ICS of synchrotron photons. In the second, the γ-ray pulse is produced near the surface by ICS of synchrotron photons and thermal black body photons from the surface. The big advantage of this model is that it can naturally explain the morphological and spectral differences between two γ peaks, different location of the peaks observed in different photon energies and fine structure of the light curve like: interpeak emission, trail. The total γ-ray photon spectrum of the Vela pulsar is also reasonably well fit in terms of this model.

Another model of photon emission by pulsars involving a sequence of possible radiation mechanisms in the pulsar magnetosphere was proposed by Cheng et al. (1986a). The authors argue that between the null surfaces in the pulsar magnetosphere and light cylinder, vacuum gaps can be centrifugally induced in which particles are accelerated to very high energies. Three regions in the magnetosphere may be distinguished in which occur interdependent radiation processes (see Fig. 4.4). In the 'first region' primary electrons (positrons) are accelerated to ultrarelativistic energies. They produce energetic γ-rays (via curvature radiation and/or ICS) which next partly convert to e^+e^- pairs within the gap. A part of the secondary pairs escape to the 'second region' in which only a small electric field component exists along magnetic field lines, although it is high enough to partly separate electrons and positrons. In this region, secondary γ- and X-ray photons originate via curvature and ICS processes. Since the primary electrons and positrons move in the gap in opposite directions, the secondary γ-rays create tertiary pairs in $\gamma - \gamma$ collisions in the 'third region'. The tertiary pairs have relatively low energies so then they can emit mainly soft synchrotron radiation at a broad angle. These soft photons illuminate other regions of the magnetosphere, supplying a low energy photon target for energetic processes in regions 'first' and 'second'. A part of the photons which escaped from all regions create the main peaks in the pulsar light curve. The model is able to describe the total spectrum of the Crab and Vela pulsars (see Cheng et al. 1986b) and can explain general features of the pulsar light curve (e.g. double peak structure). However, it is difficult to envisage the mechanism of interpeak emission and time variability of the light curve.

All the models, discussed above, concern the pulsed γ-ray emission from pulsars. However, there

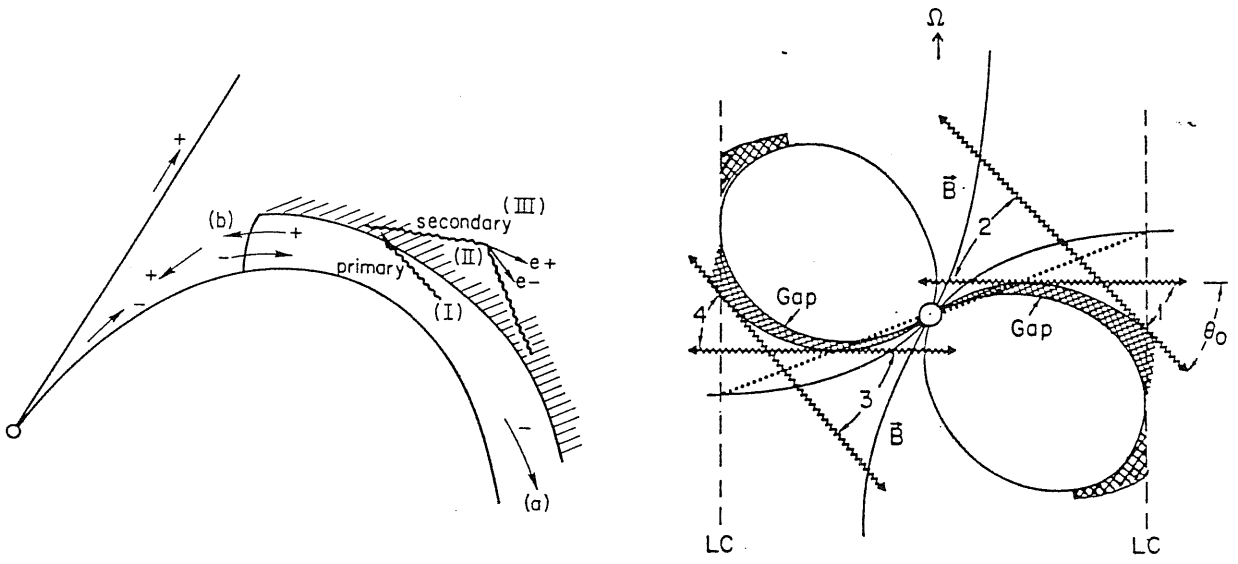

Figure 4.4: On the left, schematic representation of positions of primary (I), secondary (II) and tertiary (III) regions associated with an outer gap. Acceleration of electrons to ultrarelativistic energies occurs only in region I (from Cheng et al. 1986b). On the right, Model of the outer magnetosphere with indicated regions of the gaps. The pulsar radiation is observed if an observer is located inside the cone θ_0 (from Cheng et al. 1986a).

are positive reports of steady γ-ray flux at least from the direction of Crab Nebula or pulsar (for review of these observations see section 4.3). The steady photon emission, from optical to soft γ-rays, was explained in terms of the MHD model for the Crab nebula (see Kennel & Coroniti 1984a, and also Pacini & Salvati 1973; Rees & Gunn 1974) as due to synchrotron radiation of relativistic electrons produced in the pulsar magnetosphere (Kennel & Coroniti 1984b). The steady TeV γ-ray emission from the Nebula is usually interpreted as the Compton scattering of synchrotron radiation of relativistic electrons; starting from the oldest and simplest models by Gould (1965), Rieke & Weekes (1969), Grindlay & Hoffman (1971) and finishing on the recent ones by Stepanian (1991) and De Jager & Harding (1991). However, it is difficult to describe simultaneously the steady γ-ray spectrum observed by COS B and that in TeV energies. The TeV flux, calculated by Stepanian, is lower than observed from the Crab Nebula. The calculations by De Jager & Harding fits the reported flux at TeV energies well but in order to describe simultaneously the COS B results, electrons with extremely high energies $\sim 10^{16} eV$ are required.

Another explanation for steady γ-ray emission was proposed by Kwok et al. (1991) who argue that unpulsed TeV γ-rays may originate inside the region of several light cylinder radii from the pulsar. According to the authors, such emission is produced in collisions of ultrarelativistic e^+e^- pairs, which escaped from the outer gap of the magnetosphere (Cheng et al. model). Following a toroidal magnetic field outside the light cylinder, they interact with low energy photons produced in the opposite gap.

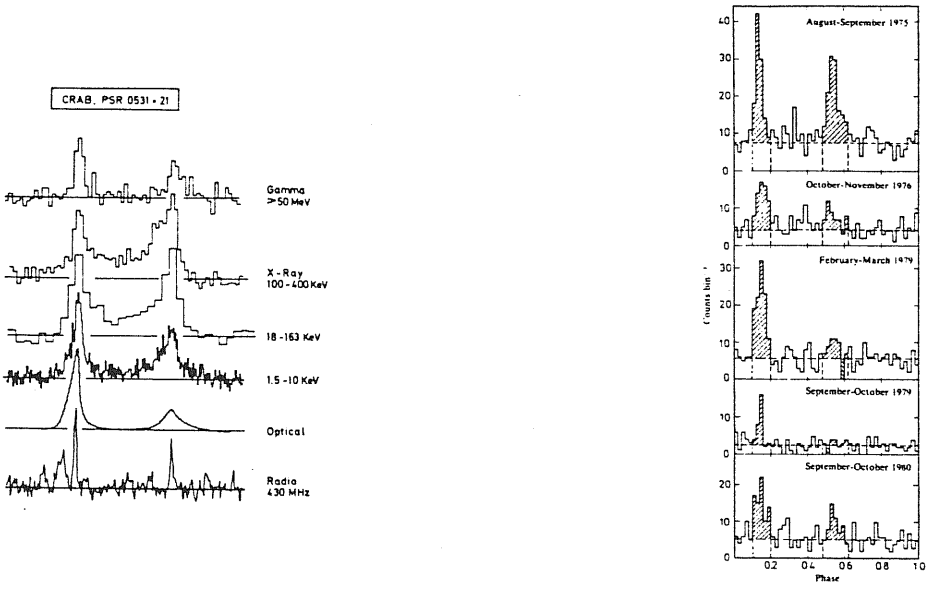

Figure 4.5: On the left, light curves for the Crab pulsar at different photon energies (from Kanbach 1983). On the right, γ-ray light curves at different epochs (from Wills et al. 1982)

4.3 Crab Nebula pulsar

The Crab Nebula is a remnant of supernova explosion in the year 1054, observed by ancient Chinese astronomers. The distance to this source is estimated to be $\sim 2kpc$ and the dimension of the Nebula to be $\sim 1.4 \times 2.1pc$. For a long time it was a puzzle as to what is the origin of the huge amount of energy ($\sim 10^{38} erg/s$) generated inside the Nebula. The situation became much clearer since the discovery of a young radio pulsar with period 33ms in the Crab Nebula by Staelin & Reifenstein (1968) and its optical counterpart by Cocke et al. (1969). The pulsar is losing rotational energy at the rate of $\sim 4.5 \times 10^{38} erg/s$, amazingly similar to the Nebula luminosity. Now, it is widely believed that connection between these two objects is caused by magnetic fields and relativistic particles emitted by pulsar.

The Crab Nebula pulsar is clearly seen in all photon energies, from radio to γ-rays. The emission is modulated according to pulsar period. The light curves, obtained in the X-rays, agree remarkably well with observations in other wavelengths (see Fig. 4.5). They show double peak structure with narrow peaks separated by $\sim 13.2 \pm 0.3$ msec with significant emission from the interpeak region. The phase averaged spectrum of the Crab pulsar from soft X-rays up to GeV γ-rays can be described by a simple power law with spectral index ~ 2.2 (see Fig. 4.6). However, the detailed studies shows that the spectrum from the interpulse region is flatter than in the peak regions which suggests two different components of X-ray emission. These features were recently confirmed by preliminary analysis of OSSE (GRO) data in hard X-rays (Ulmer et al. 1991).

The detailed studies of the hard X-ray spectrum of the Crab nebula pulsar indicate the existence

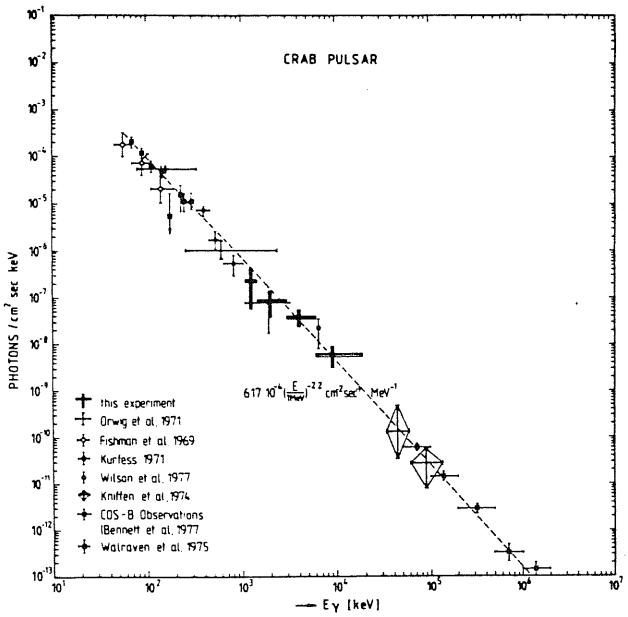

Figure 4.6: The energy spectrum of the Crab pulsar between 10 keV and 2 GeV (for references see Graser & Schönfelder 1982).

of possible line features. Ling et al. (1979) and Manchanda et al. (1982) reported the emission line at $\sim 73keV$ with consistent intensities, although only unpulsed data were analyzed. Strickman et al. (1979) initially reported no line feature in the pulsed signal from the Crab pulsar, however further analysis of these same data indicated a line at $76.6 \pm 2.5keV$ (Strickman et al. 1982) during the first 25 minutes of a 3hr observation. On the other hand, there have been several observations of the Crab Nebula during which no line emission near 73 keV was detected (see, e.g., Hameury et al. 1983; Knight 1982; Mahoney et al. 1984). A similar situation is in the case of second line reported close to $\sim 400keV$, which can be interpreted as a redshifted annihilation line on the surface of the Crab pulsar. More detailed discussion of this line and its possible physical interpretation will be carried out in the next section.

The first clear identification of Crab Nebula pulsar in γ-rays have been done by the SAS 2 experiment in the energy range 30–200 MeV (Kniffen et al. 1974; Thompson et al. 1977b), although early claims of positive detections appeared starting from the early seventies. The Crab pulsar light curve showed structure similar to that in lower energies (see Fig. 4.5) and the total photon spectrum was in good agreement with extrapolation from lower energies. These results were generally confirmed by the COS B experiment which observed the Crab pulsar in 5 periods (Wills et al. 1982). Moreover their measurements found a decrease in the strength of the second peak relative to the first. No change was observed in the 2–12 keV X-ray light curve simultaneously measured by COS B. The total data also contain the first evidence of interpulse emission between the two peaks in the energy range 50–3000 MeV which was earlier reported in X-rays (see above). The reanalysis

of COS B data (Clear et al. 1987) confirmed the statistical significance of the fluctuations of emission from the secondary peak (3σ), and reported no systematic variations of the spectral index with pulsar phase (contrary to observations in X-rays). There was also measured unpulsed γ-ray emission from the Crab region for energies up to 500 MeV, but the spectrum of this emission may be described by a power law with spectral index 2.7 ± 0.3 which is steeper than the pulsed spectrum (spectral index $\sim$2). The situation with observations of soft γ-ray emission from the Crab is similar to observations of line features in the Crab pulsar spectrum. There are reports of an excess at MeV energies relative to the simple power law extrapolation between X-ray and high energy γ-ray observations (Hillier et al. 1970; Baker et al. 1973; Gruber & Ling 1977). Most recent results based on HEAO-3 data (Ling et al. 1991) report an appearance of a broadened Gaussian bump (with significance of 10σ). It was not observed by Graser & Schönfelder (1982) whose spectrum in the 1–10 MeV range is consistent with simple power law between hard X-rays and 2GeV. However, observations of White et al (1985) suggest two different production mechanisms (components) for low- and high-energy γ-rays.

The Crab Nebula was observed by a number of Cherenkov experiments in TeV energies starting from the sixties and the first positive result was reported by Fazio et al. (1972). Before 1988, many reports of positive detections (although with poor significance) and upper limits (sometimes in conflict with positive claims) appeared. They were, altogether, not very convincing (for a review of the field see Weekes 1988). All these results can be divided in three kinds: steady emission, pulsed according to Crab pulsar period and transient emission. The steady TeV emission was recently reported with a very high significance level by Whipple Observatory (9σ – Weekes et al. 1989; 20σ – Vacanti et al. 1991) based on the optimization technique of selection of γ-ray showers. The spectrum of γ-rays derived by Vacanti et al. (1991) has the form $N(E) = 2.5 \times (E/0.4TeV)^{-2.4\pm0.3}\ photons/cm^2/s/TeV$ between 0.4 – 4 TeV and its extension to lower energies was confirmed by Akerlof et al. (1990), see Fig. 4.7a. The periodic TeV emission was claimed in a few experiments[10] but it is not confirmed by recent, much more sensitive, observations (see Fig. 4.7b for a review of these observations). Recent observations postulate abrupt changes in the pulsed spectrum of the Crab pulsar between 10 – 100 GeV because, as we mentioned above, the pulsed γ-ray flux measured by COS B is four times higher than steady emission (Fig. 4.7a). The outbursts in TeV emission on time scale of 15 min were reported in two experiments (see Fig. 4.7b). The bursts appeared in the pulsar light curve as a single pulse, although their phases are unknown.

The detection of the Crab Nebula (pulsar) at PeV energies have been reported in a number of air shower area experiments (we refer to reviews by Weekes 1988, 1992). The significance of these results is weak and collection area of showers is, in the best cases, a few degrees which makes

[10] However, the localization of pulses in the Crab pulsar light curve was conflicting.

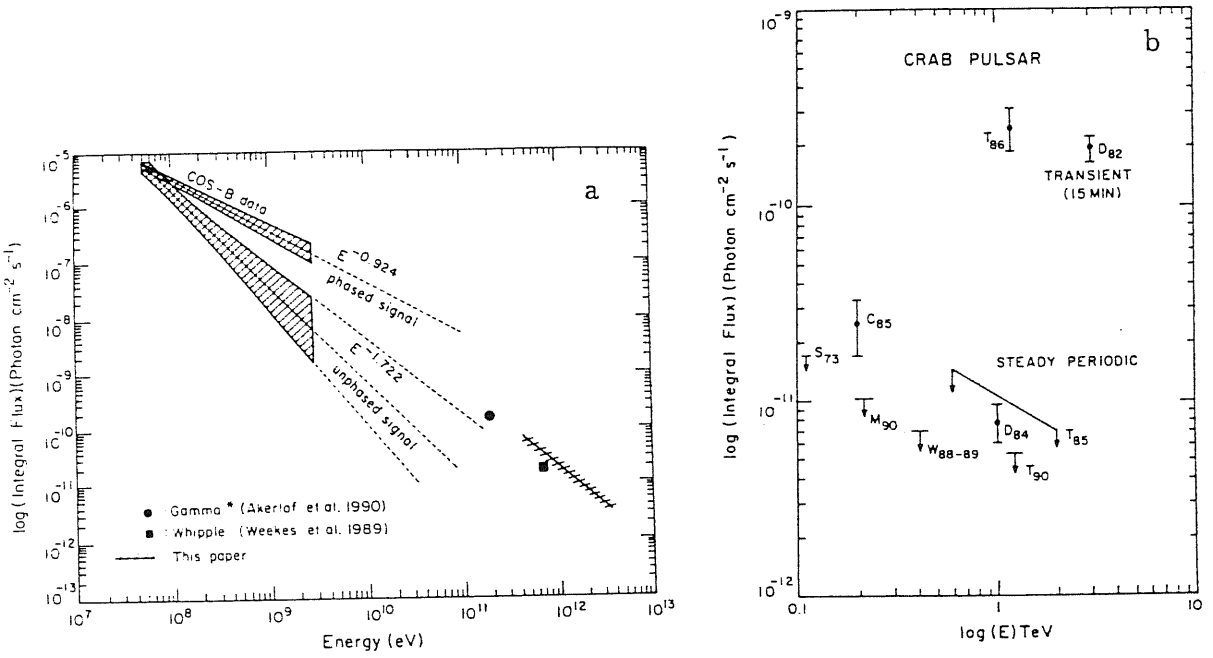

Figure 4.7: (a) Measured integral photon flux from the Crab Nebula. (b) Upper limits and detections reported for the Crab pulsar by different observations:W_{88-89} - Vacanti et al. 1991; S_{73} - Helmken et al. 1973; C_{85} - Tumer et al. 1985; M_{90} - Akerlof et al. 1989; D_{84} - Dowthwaite et al. 1984; T_{90} - Bhat et al. 1990; T_{85} - Vishwanath et al. 1985; T_{86} - Bhat et al. 1986; D_{82} - Gibson et al. 1982, (from Vacanti et al. 1991, for references see this paper).

clear identification with any source emitting steady photon flux problematic. However, recently, the possibility of an outburst on 23 February 1989 at energies of 0.1 to 1 PeV from the Crab pulsar have been reported in three separate experiments (Alexeenko et al. 1992; Acharya et al. 1990; Aglietta et al. 1991). There also appeared a report of the pulsed flux $> 2 \cdot 10^{14} eV$ which is nearly constant with time over the three years of observations (Gupta et al. 1991). However, this claim is evident in conflict with recent observations in TeV energies unless a very atypical shape of high energy photon spectrum is accepted.

Summing up, the spectrum of the Crab Nebula (pulsar) is quite well established up to TeV photon energies. However, the pulsar emission is probably not so stable as previously has been expected from an isolated point source. There are some reports of variability of pulsar light curve in high energy γ-rays, transient emission features in soft γ-rays (cyclotron, annihilation line, MeV bump) and sporadic TeV – PeV photon bursts. We suggest a possibility that all these transient features may be related to each other. In the next section we concentrate on theoretical analysis of the annihilation line feature reported from the Crab pulsar and propose its possible physical explanation in terms of present pulsar models.

4.3.1 Annihilation line from the pulsar

The observation of the 511 keV positron annihilation line in astrophysical sources has long been considered as a key feature for the interpretation of the emission mechanism. In fact, the feature is expected in models where the electron energies are ultrarelativistic and the volume is small. Conversely, the line appears to be an effective diagnostic of the high energy part of the electron spectrum.

For many years the only source for which there was convincing evidence of the presence of the narrow annihilation line ($FWHM < 3keV$) was the Galactic Center, see in particular the seminal paper of Leventhal et al. (1978). At present it seems to be certain that there are at least two components of emission. One is the very narrow, long–time variable line observed by many balloon flights (see, for a review, Lingenfelter & Ramaty 1989 and recent observations by OSSE GRO reported by Purcell et al. 1991) and the second is a strongly variable, broad annihilation line feature which arrives from 1E 1740.7-2942, a hard X-ray variable, located 0.4° from the Galactic Center (Sunyaev et al. 1991; Bouchet et al. 1991). Other sources, Cyg X-1 (Ling & Wheaton 1990), Nova Muscae (Sunyaev et al. 1992; Goldwurm et al. 1992), the source at $l^{II} = 3.1^0, b^{II} = -13.9^0$ – V1223 Sgr (Briggs et al. 1991), emit also at least sporadically the 511 keV line. The annihilation line observed from the direction of Galactic Center is sometimes accompanied by a weaker emission feature at 170 keV (Leventhal et al. 1978; Leventhal and MacCallum 1980; Matteson et al. 1991; Slassi et al. 1991), which is considered to be a Compton backscattering 0.511 MeV line (Lingenfelter & Hua 1991). A similar feature at $\sim$ 170 keV is also observed in Nova Muscae (Sunyaev et al. 1992; Goldwurm et al. 1992).

The existence of an emission feature at 440 keV associated with the Crab Nebula was suspected since the observations of Leventhal et al. (1977). The feature was confirmed by Ayre et al. (1983) and disproved by other groups (see, e.g., upper limits by Hameury et al. (1983) and Mahoney et al. (1984)), so that the possibility of an intrinsic variability is seriously considered. For a detailed review on the subject we refer to Owens (1991). Among the most recent and significant observations we quote the ones from the FIGARO II team. The feature was observed in two balloon flights, one in 1986 (Agrinier et al. 1990), and one in 1990 (Massaro et al. 1991a), see Fig. 4.8, and it appears only in correspondence with the secondary pulsar peak. Its significance, as from the addition of the data from the two flights, is about 3σ. The line is located between 0.43 and 0.46 MeV, its width is consistent with the energy resolution of the detector, its intensity is $I \cong 0.86 \pm 0.33 \cdot 10^{-4} ph/cm^2 s$. Recent observations by the OSSE detector on Compton GRO (Ulmer et al. 1991) cannot conclusively exclude the existence of the 440 keV line and 2σ upper limit equal to 0.8×10^{-4} $phot/cm^2/s$ reported in this work is consistent with observations by Massaro et al. (1991a).

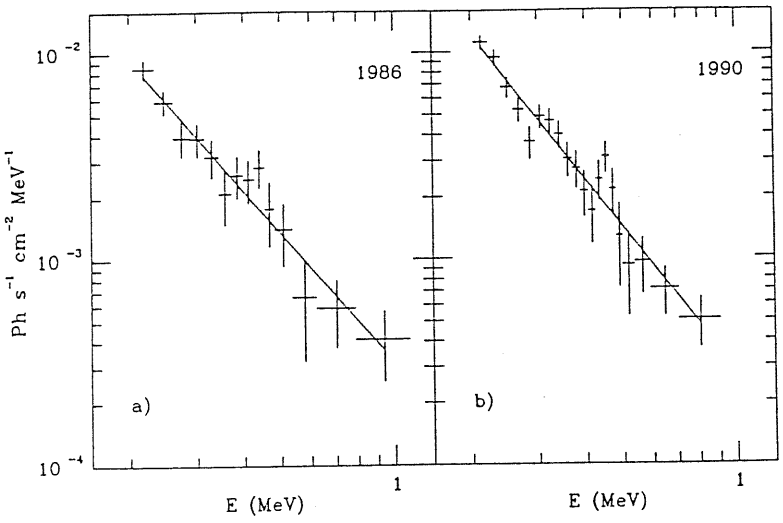

Figure 4.8: The spectra of the secondary peak photon emission of the Crab pulsar after subtraction of the off–pulse signal, for the two FIGARO II flights of (a) 1986 July 11 and (b) 1990 July 9 (from Massaro et al. 1991a).

An obvious interpretation of the feature is that it is due to the 511 keV e^+e^- annihilation line redshifted by the gravitational field of the neutron star. Although far from being uncontroversial, we accept this interpretation as a valuable working hypothesis.

4.3.2 Constraints on pulsar parameters

Assuming a distance of 2 Kpc to the Crab Nebula and a beaming factor k, the observed flux of line at 440 keV corresponds to a rate of release of annihilation photons

$$R \cong 4 \cdot 10^{38} \times k_{100}\ ph/s, \tag{4.1}$$

where k_{100} is k/0.01.
This corresponds to a line luminosity

$$L_{511} \cong 3 \cdot 10^{32} \times k_{100}\ erg/s \tag{4.2}$$

which is a small fraction of the total pulsar luminosity

$$L_{tot} \cong 10^{35} \times k_{100}\ erg/s. \tag{4.3}$$

The 511 keV photons are produced by annihilation of positrons, which in turn will be a product of an electromagnetic shower. We now consider that the showers are produced by a flow of particles accelerated towards the neutron star. The picture will be specified in the following text. It seems difficult to us to consider an atmosphere of pairs, since, due to the huge fields, it would immediately expand, and the annihilation process, if occurring at all, would take place in a region of low gravitational redshift.

The flow of particles responsible for the generation of the showers, and therefore ultimately for the annihilation photons, can be expressed as

$$P_{Sh} \cong 4 \cdot 10^{38} \times \xi^{-1} \times k_{100}\ s^{-1}, \tag{4.4}$$

where ξ is the number of annihilation photons outgoing from the star for the infalling primary particle.

The current associated to the particle flux is

$$I_e = e \cdot P_{Sh} \cong 2 \cdot 10^{29} \times \xi^{-1} \times k_{100}\ esu/s. \tag{4.5}$$

The associated magnetic field can be estimated from the Ampére law, if a relevant space dimension l is chosen. Assuming, as a scale, the radius of the neutron star $l_6 = l/10^6$ cm, we get

$$B_e = 2 \cdot I_e/(c \cdot l) \cong 1.3 \times 10^{13} \times l_6^{-1} \times \xi^{-1} \times k_{100}\ G. \tag{4.6}$$

If $l = 10^5 cm$, the dimension of the active polar cap, and $k_{100} \approx 1$, one would have

$$B_{pc} \sim 10^{14}/\xi\ G. \tag{4.7}$$

The magnetic field on the Crab pulsar's surface is estimated at $\sim 6 \times 10^{12} Gs$. Therefore, in order not to destroy the neutron star's magnetic field, the number of annihilation photons ξ produced in cascade which is initiated by single relativistic particle should be

$$\xi \gg 100. \tag{4.8}$$

A further constraint to energy E_{prim} of the particle impinging the star's crust can be set by the upper limit on the thermal emission from the neutron star which is known to be $L_{th} \sim 5.8 \cdot 10^{34} erg/s$ (Toor, & Seward 1977; Harnden & Seward 1984). The shower developing in the crust will heat up the crust at a rate

$$L_{Sh} = E_{prim.} \cdot P_{Sh} \cong 4 \cdot 10^{38} \times E_{prim.} \times k_{100} \times \xi^{-1}\ erg/s. \tag{4.9}$$

From $L_{sh} < L_{th}$ and assuming $k_{100} = 1$ and ξ independent of the energy of the primary electron, we get

$$E_{prim.}[MeV] < 900 \times \xi. \tag{4.10}$$

In order to have an estimate of a realistic value ξ, we consider relativistic positrons hitting the neutron star's surface.

In particular we have considered a Monte Carlo simulation of showers produced by positrons impinging perpendicularly onto an iron slab, based on the EGS4 (Electron Gamma Shower simulation program, Nelson, Hirayama and Rogers 1985). The code simulates showers in three dimensions

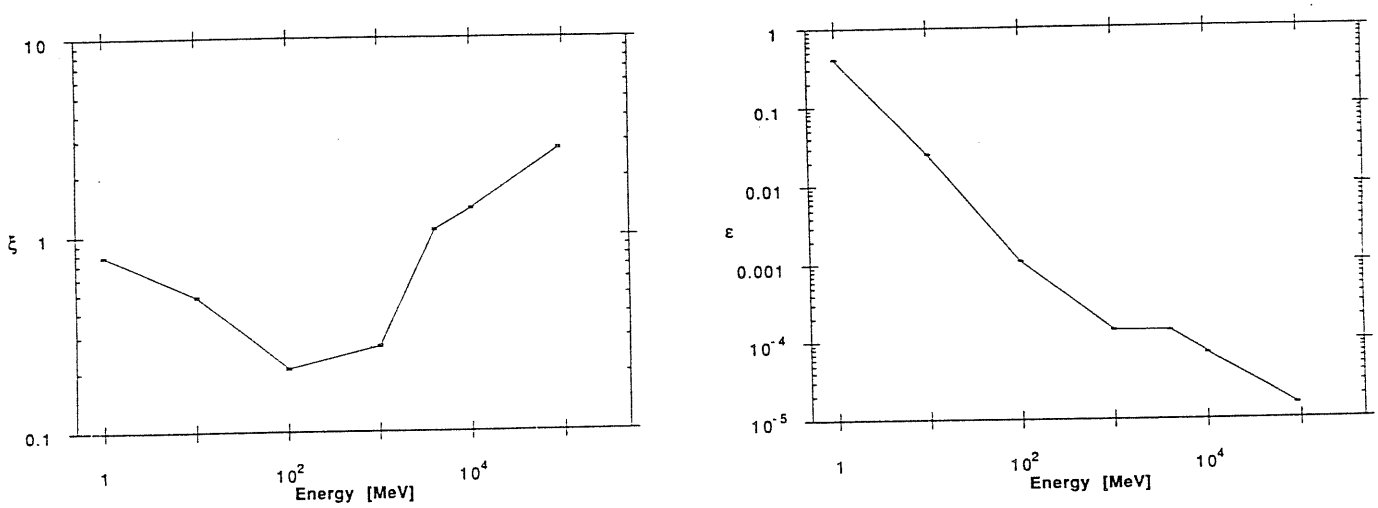

Figure 4.9: (a) Number of outgoing annihilation photons vs the energy of the positron producing an electromagnetic shower impinging on an iron slab. (b) The fraction of energy outgoing in the form of annihilation photons vs. the energy of the positron producing the electromagnetic shower (from Bednarek et al. 1992a).

following electrons and photons down to ~20 keV. Several interaction mechanisms (Photoelectric effect, Compton scattering, pair production, Bremsstrahlung, continuous energy loss, multiple scattering, Moller, Raleigh and Babha scattering, positron annihilation) are accounted for according to Heitler (1954) and Messel & Crawford (1970). Possible effects due to strong magnetic fields are not taken into account. We have disregarded the temperature of the Iron slab, consistently with the fact that we are interested in hard X ray $\sim$ 20 keV, and the upper limits on the temperature of the Crab pulsar are $< 2.5 \cdot 10^6$ K (Harnden & Seward 1984). A plot of ξ as a function of positron energy is given in Fig. 4.9a, while in Fig. 4.9b the fractional energy which is released in the form of an outgoing annihilation line is given versus the positron energy. Independent of the energy of the impinging positron, the photon yield is $\sim$ 3, which means that, energetically it is much more favourable to hit the surface with low energy positrons (photons). Even taking into account effects typical of neutron star matter (see calculations of cascade in the Iron crust by Jones 1978; Bogovalov & Kotov 1989), it seems difficult to consider much higher values of ξ. Therefore, it appears that condition (4.8) cannot be fulfilled.

The limitations derived in these sections from consistency with pulsar electrodynamics put strong constraints of the possible models. It seems to us that a remaining possibility is that the current is indeed transported by primary relativistic particles, but the shower starts to develop above the crust, because of the interaction of electrons and photons with the magnetic and photon field. The particles will arrive at the crust with low energy (satisfying condition 4.10) and the yield of annihilation photons may be reasonably high. If such a situation can be established, the

limitations due to the conditions of not overcoming the neutron star magnetic field (eq. 4.6) and not overheating the neutron star surface (eq. 4.10), may be fulfilled, and the yield of annihilation photons may be still compatible with the observations. In the next subsection we present a picture which attempts to satisfy these constraints.

4.3.3 Description of the model

We refer to the model of Ruderman and collaborators where particles are accelerated in an outer gap (far away in the magnetosphere, Cheng et al. 1986a,b) and in a second gap close to the polar cap (see Ruderman & Sutherland 1975). The surface of the polar cap is heated to much higher temperature than the temperature of the neutron star because of the flux of high energy particles on it. Typical temperatures are supposed to be $10^6 - 10^7 K$ (Helfand et al. 1980). According to Cheng et al. (1986b) for a young pulsar, one would have production of $3 \cdot 10^{32}$ *electrons/s* with energy $\sim 10^{12} eV$ in the outer gap, moving towards the star surface (in fact, in the paper, the case of the Vela pulsar was exemplified). The associated magnetic field is negligible (see eq. 4.6). Primary *electrons*[11] with energy $\sim 10^{12} eV$ will produce an electromagnetic cascade: via curvature radiation (CR) in the strong magnetic field, Inverse Compton Scattering (ICS) of thermal photons emitted by neutron star, and pair production in the strong magnetic field by photons which in turn were produced in CR and ICS (see Fig. 4.10). Such a cascade, although in the opposite direction, was calculated by Daugherty & Harding (1982). From such calculations it is possible to derive that the amplification of the number of particles will be on the order of 10^3, yielding a flux moving downwards $\sim 10^{35}$ *electrons/s*. We suppose that a fraction of particles will enter the inner gap.

The energy of these particles will be strongly influenced by the resonant ICS in strong magnetic field, which, in the vicinity of the neutron star, is regulated by the surface temperature and strength of the magnetic field. We calculated energy losses of relativistic electrons on the ICS of thermal photons in a strong magnetic field following analytical formulas derived by Dermer, 1990 (see also numerical calculations by Xia et al., 1985 and Daugherty & Harding 1989). However contrary to Dermer (1990) we again assumed that electrons are moving towards the surface of the neutron star. In Fig. 4.11a we report the results of our calculations of the energy loss versus the electron energy for various temperatures and magnetic field $6 \cdot 10^{12} G$. From Fig. 4.11a it is apparent that for temperatures larger than $10^6 K$, energy losses are so large that one can assume that the final Lorentz factor of electrons will be small and therefore its energy just above the polar cap will be of the order of a few MeV. The cascade process in the pulsar magnetosphere will not be modified by the electric field since $\bar{E} \cdot \bar{B} = 0$.

The situation is different when electrons are propagating in the polar gap because now $\bar{E} \cdot \bar{B}$

[11] We call here *electrons* on e^+ and e^-.

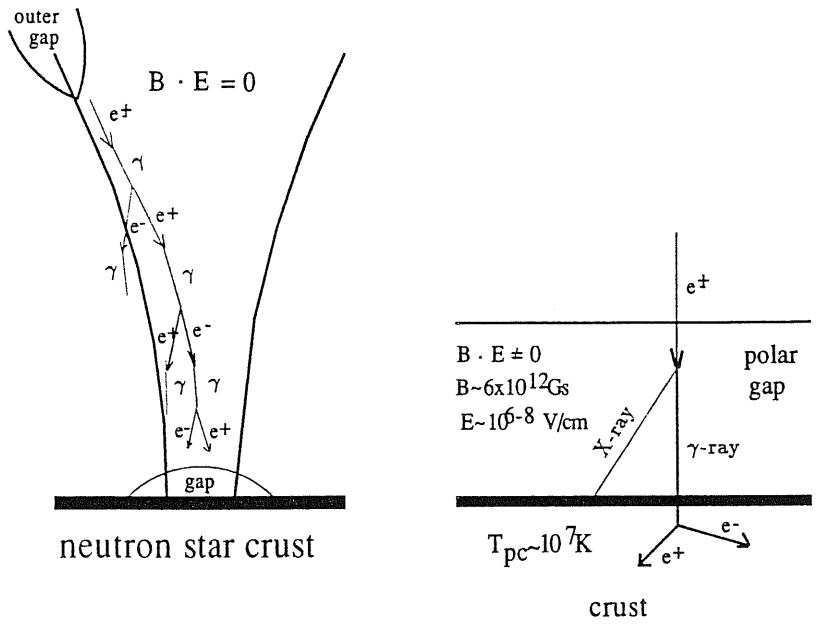

Figure 4.10: Schematic drawing of a cascade developing in the neutron star magnetosphere (left side) and polar gap (right side). There is no acceleration of electrons (positrons) in the magnetosphere ($B \cdot E = 0$) and processes of curvature, ICS and pair production are important. In the polar gap, there is acceleration of electrons (or positrons) because $B \cdot E \neq 0$. and ICS dominates.

$\neq 0$, see model by Ruderman & Sutherland (1975). In the polar gap, there is a competition between electron energy losses on ICS and energy gains from the electric field (see Fig. 4.10b). In Fig. 4.11b we have calculated such losses and gains versus the energy of electron entering the polar gap for a magnetic field $B_{pc} = 6 \cdot 10^{12} G$, temperature of the polar cap $T_{pc} = 10^7 K$ and a few strengths of the electric field in the gap which we assumed in the first approximation as a homogeneous through the gap. The interesting property is that there are two Lorentz factors for electrons (γ_e) for which energy losses are equal to energy gains γ_1 and γ_2. If

- $\gamma_e > \gamma_2$, electrons will be accelerated reaching very high energy.
- $\gamma_1 < \gamma_e < \gamma_2$, electrons will be quickly decelerated and achieve Lorentz factor γ_1.
- $\gamma_e < \gamma_1$, electrons will be quickly accelerated also to the Lorentz factor γ_1.

This means that for certain parameters of the neutron star polar gap, the electron energy distribution during their propagation in the polar gap will be strongly peaked in the γ_1.

The characteristic energy of comptonized photons by electrons crossing the polar gap will be determined by γ_1 and the temperature of the polar cap,

$$\epsilon_{ph} \sim \epsilon_{therm.} \cdot \gamma_1^2 \tag{4.11}$$

where we assumed $\epsilon_{therm.} \simeq 3kT_{pc}$, and T_{pc} is surface temperature of the polar cap.

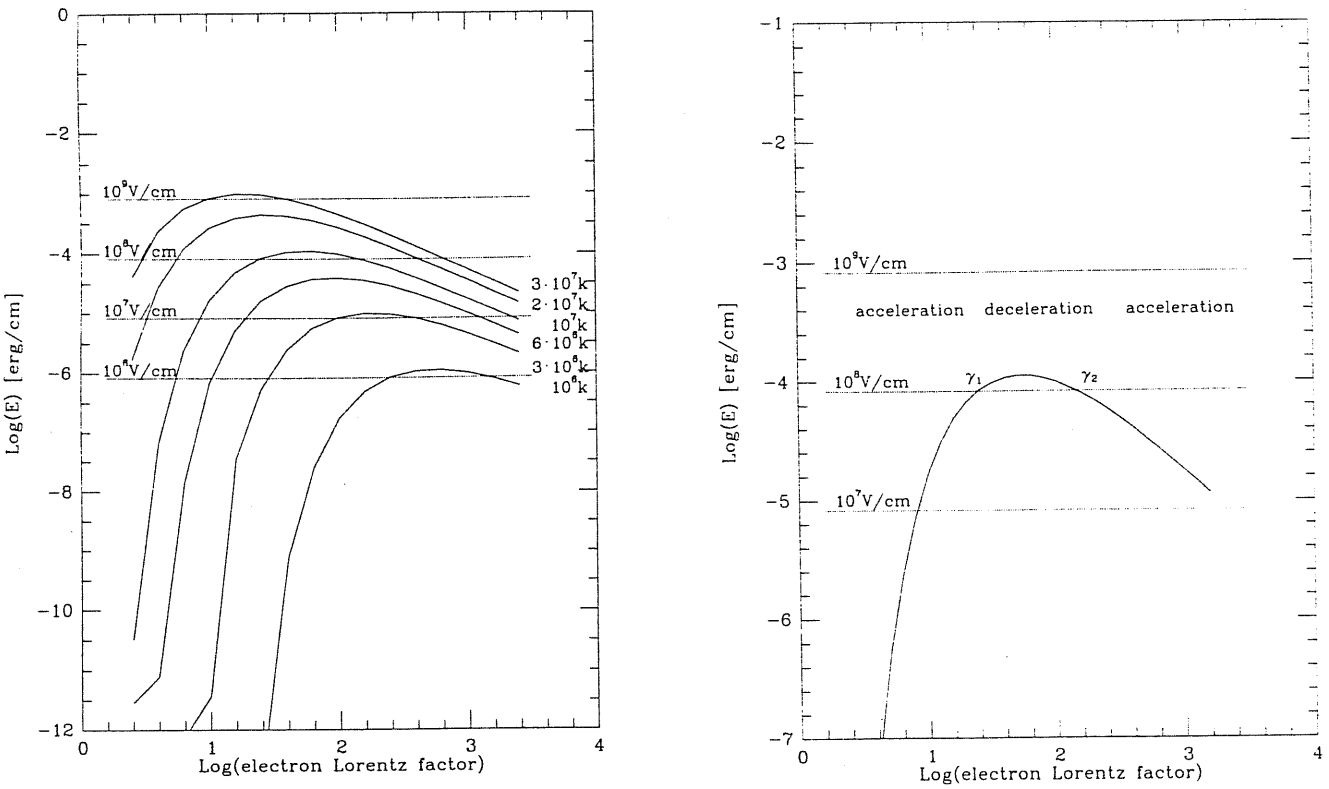

Figure 4.11: a). The energy losses of electrons by ICS in a strong magnetic field versus Lorentz factor for a magnetic field strength $6 \cdot 10^{12}$ G and different temperatures of blackbody radiation emitted by the polar cap. The dotted lines represent the electron energy gain for various homogenous electric fields. b). The γ_1 and γ_2 points are indicated for a particular value of energy gain $10^8 V/cm$, and $T = 10^7 k$, and $B = 6 \cdot 10^{12} G$. They define regions of acceleration and deceleration of electrons in the inner gap (from Bednarek et al. 1992a).

For some parameters of γ_1 and T_{pc}, the energy of comptonized photons is peaked at about a few MeV. Most of these MeV photons is conversed in the iron slab into the e^+e^- pairs with energies comparable to the energy of primary photon. If the potential drop in the polar gap is of the order of $\sim 10^{11} \div 10^{12} eV$, which is suggested in the original paper by Ruderman & Sutherland (1975), one obtains that each electron crossing the polar gap will produce about 10^5 photons with energy close to a few MeV. So, the total number of MeV photons entering the surface of the polar cap per second is of the order $3 \cdot 10^{32}$ (from the outer gap)$\times 10^3$ (multiplication in the magnetosphere)$\times 10^5$ (multiplication in the polar cap in ICS)$= 3 \cdot 10^{40}$. From comparison of this value with P_{ph} (eq. 4.4), we obtain, for $k_{100} = 1$, that $\xi \sim 10^{-2}$. This value is consistent with the expectations from the Monte Carlo simulations of positron initiated cascade in the iron slab (see Fig. 4.9) and calculations by Bogovalov & Kotov (1989). The total energy of MeV photons falling onto the polar cap in the above picture is consistent with the condition of not overheating of the neutron star (eq. 4.9). The high collimation of produced annihilation photons along the magnetic field lines, which is inferred from the observed pulsation of the annihilation line, is consistent with calculations of photon spectra from e^+e^- pair annihilation at rest in a strong magnetic field (Kaminker et al. 1991).

4.3.4 Estimates of the backscattering feature at ~ 150 keV in the Crab pulsar

As we described above in detail our proposal for the origin of the annihilation line is that it is due to MeV photons hitting the pulsar surface which develops an electromagnetic cascade in the crust. However, the appearance of the backscattering feature at ~ 170 keV in the presence of annihilation line in the source at the Galactic Center and Nova Musca inspired us to search for such a feature in Monte Carlo simulations (see subsection 4.3.2). In the case of the Crab pulsar, because of the gravitational redshift, the feature should appear at ~ 150 keV.

We extended Monte Carlo simulations in order to calculate the photon spectra at energies below 0.511 MeV. The primary particles are supposed to hit the iron slab perpendicularly. The free parameters are the energy of the primary positron and viewing angle, which is represented by Θ, the cosine from the normal (Θ=1 if the observer is in the normal direction). Each simulation corresponds to $5 \cdot 10^4$ primary positrons. Results of some simulations are reported in Figs. 4.12 and 4.13. The backscattering feature at ~ 170 keV is visible in all cases but is less apparent for higher energies of the primary positron, because the optical depth for the outgoing photons in this case becomes much larger than 1. The stronger annihilation feature at 511 keV is present in all cases.

The Monte Carlo simulations also yield the angular distribution of the backscattered photons. As illustration in Fig. 4.14, we give the angular dependence of the photon spectra integrated over three ranges of angles Θ for two energies of impinging particles 5 MeV and 50 MeV. The backscattering feature is narrower and more transparent for smaller values of Θ. The angular dependence of the intensity in two energy bands for two energies of the impinging positrons is shown in Fig. 4.15. While for 50 MeV positrons the distributions are similar, for 5 MeV the emission around the backscattering feature at ~170 keV is more zenithal than for the annihilation line.

Since the emission feature due to Compton backscattering is not a line, in order to give a qualitative description of its intensity one should specify the frequency where the intensity is calculated and the chosen continuum. We take as extremes of the feature 100-300 keV and we evaluate the continuum with a linear interpolation of the fluxes averaged in the 20-90 keV and 310-490 keV intervals (see Figs. 4.13). The intensity of the backscattering feature was normalized to that of the 511 keV line, which is assumed to be $0.86 \cdot 10^{-4} ph/cm^2/s$ (Massaro et al. 1991a). The resulting values are given in Table 4.1. The continuum flux in the same energy interval and in the same units is also reported. The statistical errors are on the order of a few percent (see Table 4.1).

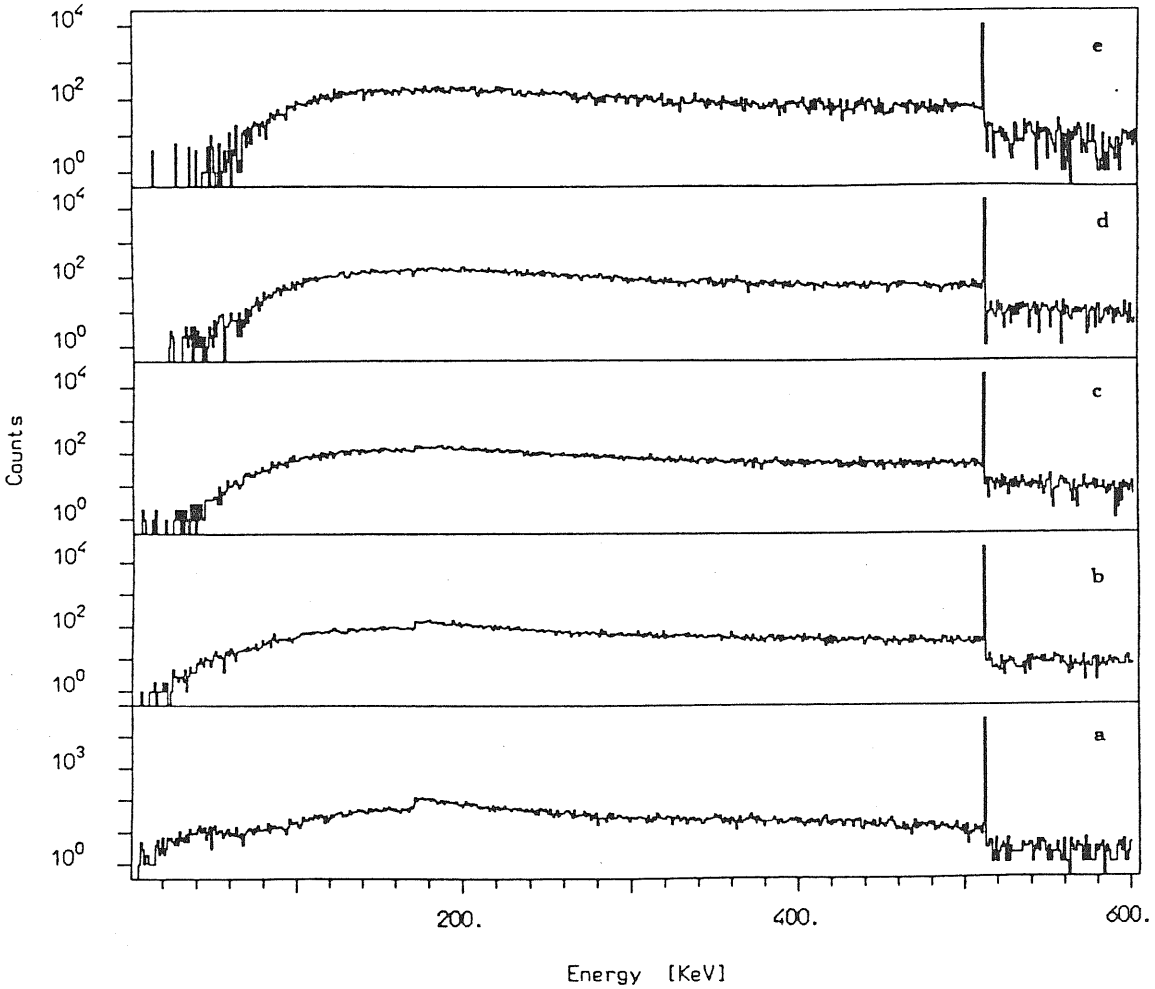

Figure 4.12: The Compton backscattered photon spectrum obtained by Monte Carlo simulations of a cascade initiated in an Iron slab by positrons with different primary energy: 1 MeV (a), 5 MeV (b), 10 MeV (c), 20 MeV (d), 50 MeV (e). (from Bednarek et al. 1992b).

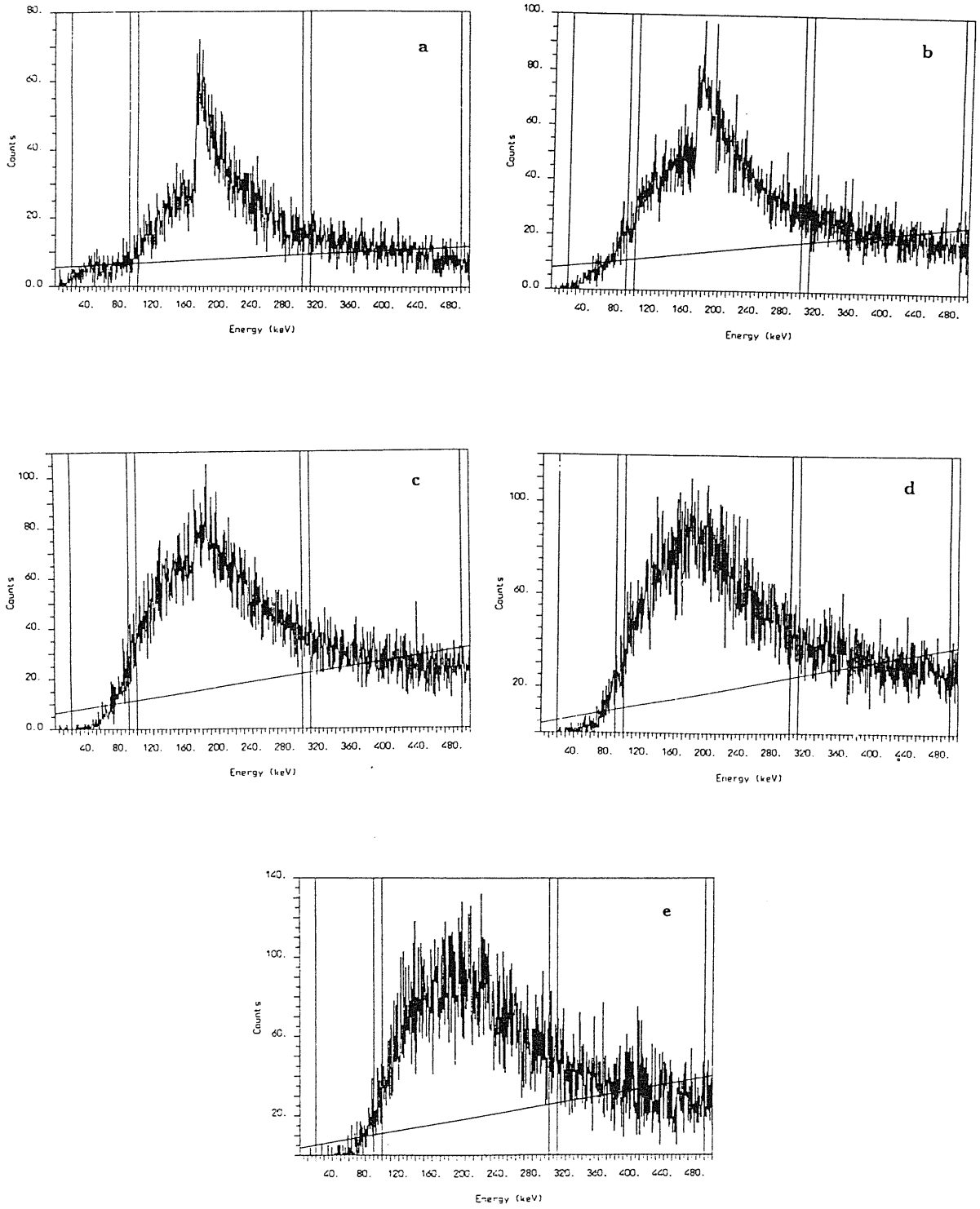

Figure 4.13: Amplification of Fig. 1.12 in the region containing the 170 keV feature. The straight line represents the adopted continuum and is described in text (from Bednarek et al. 1992b).

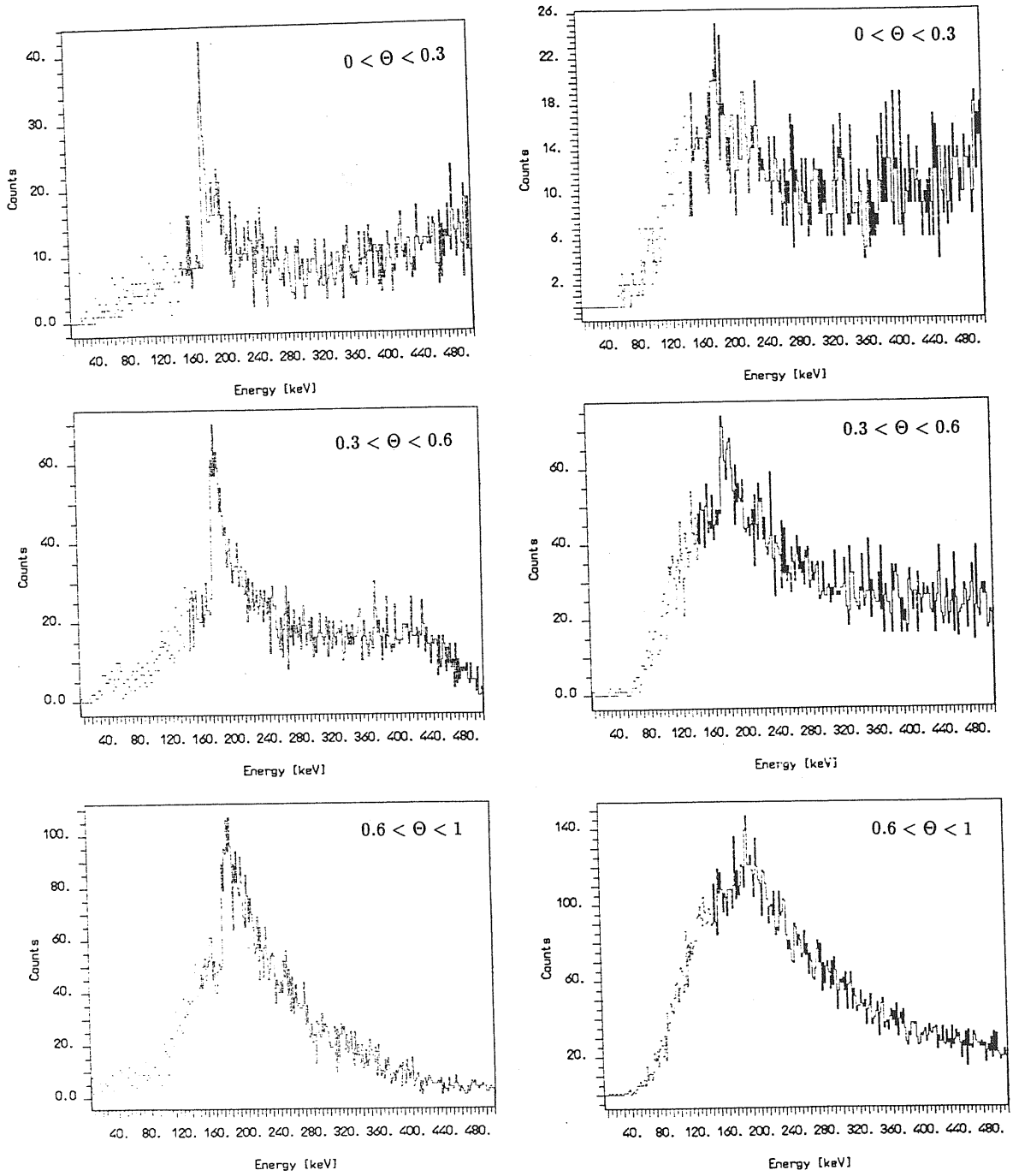

Figure 4.14: Angular dependence of the photon spectra integrated for three different ranges of Θ and two energies of impinging positrons 5 MeV – left side; 50 MeV – right side (from Bednarek et al. 1992b).

Energy[a] MeV	Feature[b] $[ph/cm^2/s]$	Error $[ph/cm^2/s]$	Continuum[c] $[ph/cm^2/s]$	Error $[ph/cm^2/s]$
1	$1.78 \cdot 10^{-5}$	$3.0 \cdot 10^{-7}$	$7.71 \cdot 10^{-6}$	$1.4 \cdot 10^{-7}$
5	$3.53 \cdot 10^{-5}$	$4.9 \cdot 10^{-7}$	$1.66 \cdot 10^{-5}$	$2.4 \cdot 10^{-7}$
10	$5.89 \cdot 10^{-5}$	$7.3 \cdot 10^{-7}$	$2.43 \cdot 10^{-5}$	$3.4 \cdot 10^{-7}$
20	$1.00 \cdot 10^{-4}$	$1.2 \cdot 10^{-6}$	$3.65 \cdot 10^{-5}$	$5.2 \cdot 10^{-7}$
50	$1.71 \cdot 10^{-4}$	$2.2 \cdot 10^{-6}$	$5.83 \cdot 10^{-5}$	$8.8 \cdot 10^{-7}$

Table 4.1: The estimates of photon flux in the backscattering feature from the Crab Nebula pulsar. [a]Energy of impinging positrons. [b]Intensity of the feature normalized to the 440 keV line. [c]Continuum in the 100-300 keV energy region (from Bednarek et al. 1992b).

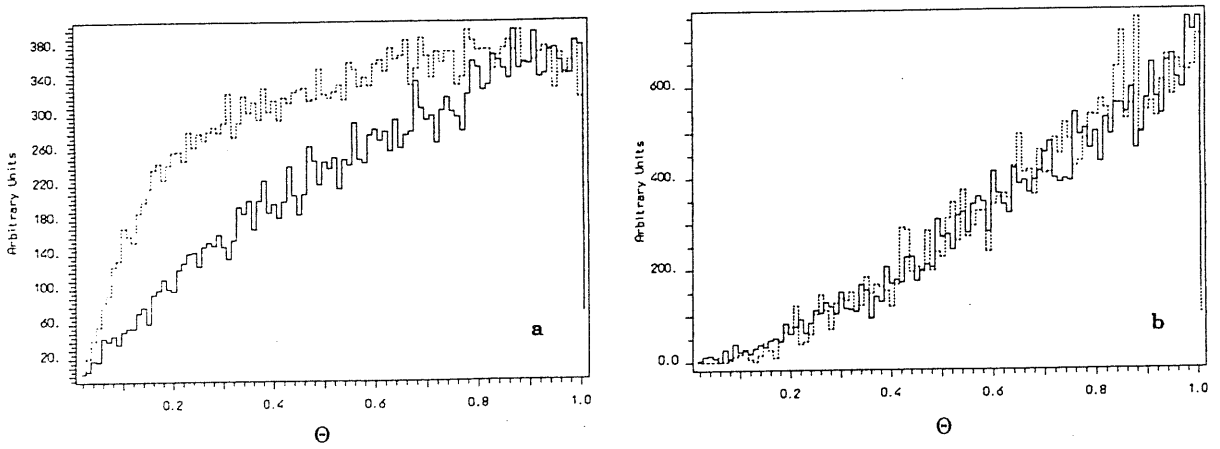

Figure 4.15: Angular dependence of the photon intensity in two energy bands for impinging positrons of energy 5 MeV (a) and 50 MeV (b), Θ is the cosine from the normal. The dotted line shows the distribution of photons of energy including the e^+e^- annihilation line (506 - 516 keV). The solid line refers to photon energy including the backscattering feature between 100 - 300 keV (from Bednarek et al. 1992b).

4.3.5 Discussion

We considered a picture where the annihilation line is created by positrons interacting with the neutron star surface. The first result is that the required positron current has an associated magnetic field which exceeds the pulsar's field, therefore the positrons must hit the neutron star in the form of pairs or showers. However, it is not possible to consider very energetic electrons hitting the surface because in that case the neutron star will be overheated by impinging particles in contradicting the observed limits of the thermal luminosity of the Crab pulsar.

Thus, the particles hitting the surface must be of energy of a few MeV.

We have then shown that within the model of Ruderman and collaborators such a situation

can be envisaged. The outer gap is used as a source of particles moving downwards. They are multiplied and slowed down by the interaction with the magnetic field and the photon atmosphere. In the inner gap the electrons acquire a fixed energy such as to radiate γ-rays downward which then interact with the surface and produce positrons.

Depending on the photon atmosphere (i.e., on the temperature of the polar cap), the magnetic field, and the electric field in the inner gap, one may have a situation where the gamma rays produced by the comptonization are too energetic in the sense that the showers enter too deeply into the crust contrary, it is possible that the photons are below the threshold of pair production. Such possible situations can be clearly distinguished in Fig. 4.16 in which we illustrate the parameter space, obtained from the calculations, for three different scenarios:

(I) – Comptonized thermal photons have energy less than $2m_ec^2$ – no pair production in the NS crust;

(II) – Comptonized photons have energy greater than $2m_ec^2$ – pair production – the annihilation line feature will emerge;

(III) – electrons will be accelerated continuously in the polar gap – production of γ-ray photons not efficient – no transparent annihilation line will appear.

For a magnetic field of the Crab nebula pulsar of $\sim 6 \cdot 10^{12}G$ and the electric field of the inner gap $10^7 V/cm$ we obtained from the Fig. 4.16 that the efficient comptonization of photons into the MeV energy range occurs for a polar cap temperature $\sim 3.5 - 6 \times 10^6 K$.

Our picture also predicts that the annihilation line at $\sim$ 440 keV from the Crab pulsar should be accompanied by a feature at $\sim$150 keV caused by Compton backscattering of the 511 keV photons. In Table 4.1, we calculated that the expected flux of the backscattering feature is in the range $10^{-5} - 10^{-4}$ ph/cm^2/s.

To our knowledge there is no clear indication of a $\sim$ 150 keV feature in the data published so far. Mahoney et al. (1984) on the basis of HEAO 3 data, gave a 3σ upper limit for line emission between 50 keV and 10 MeV of $\sim 2 \cdot 10^{-4} ph/cm^2/s$, which is somewhat above the expected intensity. An improvement of the sensitivity by a factor 10 is expected with OSSE (e.g. Cameron et al. 1991), and this should allow detection of the feature.

If the backscattering feature were beamed, as suggested by the simulations, and therefore modulated with the pulsar period, the possibility of detection would be enhanced. The FIGARO team (Massaro et al. 1991b) reports that the annihilation line has a rather large emission in the interpulse phase. It may be worth noting that Knight (1982), on the basis of MED HEAO 1 data, showed that at 100 keV the interpulse spectrum is harder than that of the two pulses, but the energy resolution was too poor to allow detection of a feature of the kind considered here.

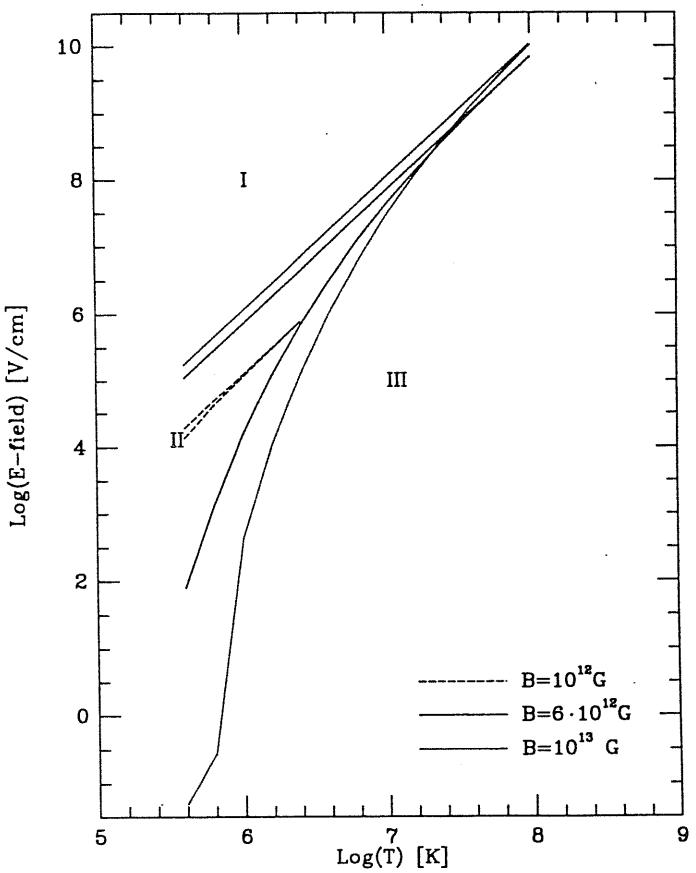

Figure 4.16: The gap electric field – cap temperature plane is divided in three parts depending on the strength of NS surface magnetic field. In part I, the electrons are accelerated, in part II they reach steady energy γ_1 which yields Compton photons with an energy above 1MeV, in part III the Compton photons have energy below 1 MeV (from Bednarek et al. 1992a).

Another consideration which should be taken into account is that the feature at $\sim$ 150 keV is probably variable, since such variability is suspected for the 440 keV feature. This possibility is in agreement with our picture because of the tuning required to produce photons in the correct energy interval. It is possible that the annihilation line occurs only in one polar cap in correspondence with the secondary pulsar peak, as suggested by the observation of line emission. The same argument may also justify the variability of the line intensity which is suggested by some observational data.

Obviously the observation of a backscattering feature at $\sim$ 150 keV in conjunction with the $\sim$ 440 keV line one would favour our picture, while its absence at the level described would be considered a disproof of the model.

These two lines may be also physically related to other transient features observed in the Crab pulsar γ-ray emission. For instance we suggest that the instability may be induced in the pulsar outer gap (by e.g. miniglich or passing meteorite ?). As a results, a part of 100 MeV – GeV γ-ray emission produced in the outer gap may be converted to e^+e^- (*decrease of 100 MeV – GeV flux*). Enhanced flux of pairs will impinge on the polar cap region of neutron star and the surface

temperature will increase. Higher flux of thermal photons emitted by the polar cap can swith on the process of efficient energy losses of pairs by resonant Compton scattering (*our picture will start to work and e^+e^- annihilation feature may appear in the pulsar spectrum*). If the temperature of the polar cap is high enough, the process of thermoemission of ions will start. They will be next accelerated in the polar and/or outer gap. The interaction of ions with extremely high energy ($\sim 10^{15}$ eV) with low energy radiation will result in production of PeV γ-ray burst. Suggested above scheme is very speculative, however our purpose is to draw peoples attention on the importance of correlative searches of transient features in all range of γ-ray spectrum observed from the Crab Nebula pulsar.

This chapter is partially based on two papers: *"On the 440 keV Line in the Crab Nebula Pulsar"* by W. Bednarek, O. Cremonesi & A. Treves, 1992a, ApJ 390, 489 (included in an Appendix) and *"Estimates of the Compton Backscattering Feature at $\sim$ 150 keV in the Crab Nebula Pulsar"* by W. Bednarek, O. Cremonesi & A. Treves, 1992b, ApJ (submitted).

References

Acharya, B.S. et al. 1990, Nat 347, 364
Aglietta, M. et al. 1991, Europhys. Lett. 15, 81
Agrinier, B. et al. 1990, ApJ 355, 645
Akerlof, C.W. et al. 1990, Nuclear Physics B 14A, 237
Akimov, V.V. et al. 1991, 22nd ICRC (Dublin) 1, 153
Alexeenko, V.V. et al. 1992, J. Phys. G: Nucl. Phys. 18, L83
Ayasli, S. 1981, ApJ 249, 698
Ayre, C.A. et al. 1983, MNRAS 205, 285
Baade, W. & Zwicky, F. 1934, Phys.Rev. 45, 138
Baker, R.E. et al. 1973, Nat.Phys.Sci. 245, 18
Bandiera, R. 1990, *Physical Processes in Hot Cosmic Plasmas*, eds. W. Brinkmann, A.C. Fabian & F. Giovannelli, Kluwer Academic Publishers, Dordrecht, NATO ASI v. 305, p. 325
Becker, W. et al. 1992, IAU Circ. No. 5555
Bednarek, W., Cremonesi, O. & Treves, A. 1992a, ApJ 390, 489
Bednarek, W., Cremonesi, O. & Treves, A. 1992b, ApJ submitted
Bennett, K. et al. 1977, A&A 61, 279
Bertsch, D.L. et al. 1992, Nat 357, 306
Bhat, P.N. et al. 1980, A&AL 81, L3
Bignami, G.F. & Caraveo, P.A. 1992, Nat 357, 287
Bignami, G.F., Caraveo, P.A. & Lamb, R.C. 1983, ApJL 272, L9
Bogovalov, S.V. & Kotov, Yu.D. 1990, Astrophys. 31, 490
Bouchet, L. et al. 1991, ApJL 383, L45
Briggs, M.S. et al. 1991, 22ICRC (Dublin), v.2, p.153
Buccheri, R. et al. 1978, Nat 274, 572
Cameron, R. A. et al. 1991, *The Second GRO Science Workshop*, OSSE preprint no. 1
Caraveo, P.A. et al. 1988, ApJ 327, 203
Chadwick, P.M. et al. 1985, Nat 317, 236
Chadwick, P.M. et al. 1989, *High Energy Gamma Ray Astronomy*, ed. K.E. Turver, p. 159
Cheng, A.F. & Ruderman, M.A. 1977, ApJ 216, 865
Cheng, K.S., Ho, C., Ruderman, M. 1986a, ApJ 300, 500
Cheng, K.S., Ho, C., Ruderman, M. 1986b, ApJ 300, 522
Clear, J. et al. 1987, A&A 174, 85

Cocke, W.J., Disney, M.J. & Taylor, D.J. 1969, Nat 221, 525
Daugherty, J.K. & Harding, A.K. 1982, ApJ 252, 337
Daugherty, J.K. & Harding, A.K. 1989, ApJ 336, 861
De Jager, O.C. & Harding, A.K. 1991, 22ICRC (Dublin), 1, 572
Dermer, C.D. 1989, ApJL 347, L13
Dermer, C.D. 1990, ApJ 360, 197
Fazio, D.J. 1972, ApJL 175, L117
Fichtel, C.E. et al. 1975, ApJ 198, 163
Gold, T. 1968, Nat 218, 731
Goldreich, P. & Julian, W.H. 1969, ApJ 157, 869
Goldwurm , A. et al. 1992, ApJL, 389, L79
Gould, R.J. 1965, Phys.Rev. Lett. 15, 577
Graser, U. & Schönfelder, V. 1982, ApJ 263, 677
Grenier, I.A., Hermsen, W. & Clear, J. 1988, A&A 204, 117
Grindlay, J.E. & Hoffman, J.A. 1971, Astrophys.Lett. 8, 209
Grindlay, J.E. et al. 1975, ApJ 201, 82
Gruber , D.E. & Ling, J.C. 1977, ApJ 213, 802
Gupta, S.K. et al. 1991, A&A 245, 141
Halpern, J.P. & Holt, S.S. 1992, Nat 357, 222
Halpern, J.P. & Tytler, D. 1988, ApJ 330, 201
Hameury, J.M. et al. 1983, ApJ 270, 144
Hardee, P.E. 1977, ApJ 216, 873
Harding, A.K., Tademaru, E. & Esposito, L.W. 1978, ApJ 225, 226
Harding, A.K. 1981, ApJ 245, 267
Harding, A.K. 1991, Phys. Rep. 206, 328
Harnden, F. R. & Seward, F. D. 1984, ApJ 283, 279
Heitler, W. 1954, *The Quantum Theory of Radiation*, (Clarendon Press, Oxford)
Helfand, D.J., Chanan, G.A., Novick, R. 1980, Nat 283, 337
Hermsen, W. et al. 1992, IAU Circ. No. 5541
Hewish, A.S.J., Bell, J.D.H et al. 1968, Nat 217, 709
Hillier, R.R. et al. 1970, ApJL 162, L177
Jones, P.B. 1978, MNRAS 184, 807
Kaminker, A.D, Pavlov, G.G., Mamradze, P.G. 1987, Ap&SS 138, 1
Kanbach, G. et al. 1980, A&A 90, 163
Kanbach, G. 1983, *Positron–Electron Pairs in Astrophysics*, AIP No. 101, eds. M.L. Burns, A.K. Harding & R. Ramaty, p. 129
Kawai, N. et al. 1991, ApJL 383, L65
Kennel, C.F. & Coronitti, F.V. 1984a, ApJ 283, 694
Kennel, C.F. & Coronitti, F.V. 1984b, ApJ 283, 710
Kniffen, D.A. et al. 1974, Nat 251, 397
Kniffen, D.A. et al. 1992, IAU Circ. No. 5485
Knight, F. K. 1982, ApJ 260, 538
Kwok, P.W., Cheng, K.S. & Lau, M.M. 1991, ApJ 379, 653
Landau, L. 1932, Physik Zeits. Soviet Union, 1, 285
Large, M.I., Vaugham, A.E. & Mills, B.Y. 1968, Nat 220, 340
Lebrun, F. et al. 1991, 22ICRC (Dublin), v.1, p.165
Leventhal, M., MacCallum, C. J. 1980, Ann NY Acad. Sci. 336, 248
Leventhal, M., MacCallum, C. J. & Stang, P. D. 1978, ApJ 225, L11
Leventhal, M., MacCallum, C. & Watts, A. 1977, ApJ 216, 491
Ling, J.C. et al. 1979, ApJ 231, 896
Ling, J.C. et al. 1991, *Gamma-Ray Line Astrophysics*, ed. Ph. Durouchoux & N. Prantzos (New York: AIP)
Ling, J.C. & Wheaton, W.A. 1990, ApJL 343, L57
Lingenfelter, R. E. & Hua, X.M. 1991, ApJ 381, 426
Lingenfelter, R. E. & Ramaty, R. 1989, ApJ 343, 686
Mahoney, W. A., Ling, J. C., & Jacobson, A. S. 1984, ApJ 278, 784
Manchanda, R.K. et al. 1982, ApJ 252, 172
Manchester, R.N. & Taylor, J.H. 1977, *Pulsars*, (San Francisco: Freeman)
Massaro, E. & Salvati, M. 1979, A&A 71, 51

Massaro, E. et al. 1991a, ApJL 376, L11
Massaro, E. et al. 1991b, 22nd ICRC v. 1, p. 18
Matteson, J. L. et al. 1991, *Gamma-Ray Line Astrophysics*, ed. Ph. Durouchoux & N. Prantzos (New York: AIP), p. 45
Mattox, J.R. 1991, Exp. Astron. 2, 75
Mattox, J.R., Mayer–Hasselwander, H.A. & Strong, A.W. 1990, ApJ 363, 270
Messel, H. & Crawford, D. F. 1970, *Electron–Photon Shower Distribution Function*, (Pergamon Press, Oxford)
Michel, F.C. 1982, Rev.Mod.Phys. 54, 1
Morini, M. 1983, MNRAS 202, 495
Nelson, W. R., Hirayama, H., Rogers, D. W. O. 1985, SLAC Report N. 265
Ostriker, J.P. & Gunn, J.E. 1969, ApJ 157, 1395
Owens, A. 1991, *Gamma-Ray Line Astrophysics*, ed. Ph. Durouchoux & N. Prantzos (New York: AIP), p. 341
Ögelman, H.B. et al. 1976, ApJ 209, 584
Pacini, F. 1967, Nat 216, 567
Pacini, F. 1968, Nat 219, 145
Pacini, F. & Salvati, M. 1973, ApJ 186, 249
Pinkau, K. 1979, Nat 277, 17
Preece, R.D. & Harding, A.K. 1992, ApJ 386, 308
Purcell et al. 1991, *The Second GRO Science Workshop*, OSSE preprint no. 1
Rees, M.J. & Gunn, J. 1974, MNRAS 167, 1
Rieke, G.H. & Weekes, T.C. 1969, ApJ 155, 429
Ruderman, M.A. & Sutherland, P.G. 1975, ApJ 196, 51
Sacco, B. et al. 1990, ApJL 349, L21
Salvati, M. 1983, Sp.Sci.Rev. 36, 145
Salvati, M. 1986, A&A 154, 379
Salvati, M. & Massaro, E. 1978, A&A 67, 55
Schlickeiser, R. 1980, ApJ 236, 945
Seiradakis, J.H. 1992, IAU Circ. No. 5532
Seward, F.D. 1989, Sp.Sci.Rev. 49, 385
Seward, F.D. et al. 1971, ApJ 169, 515
Shabad, A.E. & Usov, V.V. 1982, Nat 295, 215
Slassi, S. et al. 1991, 22nd ICRC (Dublin), v. 1, p. 145
Smith, F.G. 1977, *Pulsars*, (Cambridge University Press, Cambridge)
Staelin, D.H. & Reifenstein, E.C. 1968, Science 162, 1481
Stepanian, A.A. 1991, *Proc. Frontier Objects in Astrophysics and Particle Physics*, eds. F. Giovannelli & G. Mannocchi, SIF, v. 28, 377
Strickman, M.S. et al. 1979, ApJL 230, L15
Strickman, M.S., Kurfess, J.D. & Johnson, W.N. 1982, ApJL 253, L23
Strickman, M.S. et al. 1992, IAU Circ. No. 5557
Sturrock, P.A. 1971, ApJ 164, 529
Sunyaev, R. A. et al. 1991, ApJL 383, L49
Sunyaev, R. A. et al. 1992, ApJL 389, L75
Taylor, J.H. & Stinebring, D.R. 1986, ARAA 24, 285
Thielheim, K.O. 1991, Nucl. Phys. B (Proc. Suppl.) 22B, 60
Thompson, D.J. et al. 1975, ApJL 200, L79
Thompson, D.J. et al. 1976, Astrophys. Lett. 17, 173
Thompson, D.J. et al. 1977a, ApJL 214, L17
Thompson, D.J. et al. 1977b, ApJ 213, 252
Toor, A. & Seward, F.D. 1977, ApJ 216, 560
Treves, A. 1971, IL Nuovo Cimento B 4, 88
Tümer, O.T. et al. 1984, Nat 310, 214
Ulmer, M.P. et al. 1991, *The Second GRO Science Workshop*, OSSE preprint no. 1
Vacanti, G. et al. 1991, ApJ 377, 467
Vittelo, P. & Dermer, C.D. 1991, ApJL, 374, 668
Wallace, P.T. et al. 1977, Nat 266, 692
Weekes, T.C. 1988, Phys.Rev. 160, 1

Weekes, T.C. et al. 1989, ApJ 342, 379
Weekes, T.C. et al. 1992, Sp.Sci.Rev. 59, 314
White, R.S. et al. 1985, ApJL 299, L23
Wills, R.D. et al. 1982, Nat 296, 723
Wilson, R.B. et al. 1992, IAU Circ. No. 5429
Xia, X.Y. 1985, A&A 152, 93

5 Very high energy γ-ray emission from X-ray binary systems

The X-ray binary systems distinguish themselves among many different types of binaries by strong X-ray emission. The first source of this type, Cen X-3, discovered by the Uhuru satellite, showed a very short period of pulsations $\sim 4.8s$ (Giacconi et al. 1971; Schreier et al. 1972). Soon after a second, similar, object was found in Uhuru data, Her X-1, with a period $\sim 1.24s$ (Tananbaum et al. 1972). It became clear that X-ray binaries are composed of a 'normal star'[1] and a compact object which is usually a neutron star, white dwarf or black hole[2].

The basic feature of X-ray binary systems is the exchange of mass between a companion and a compact object through stellar wind or Roche lobe overflow. Depending on the parameters of the compact object and surrounding matter, accretion can occur via the formation of a disk, direct accretion onto magnetic poles or a quasi-spherical accretion below the shock which may be formed in the interaction of the stellar wind with the magnetosphere of a compact object. During the accretion process a large amount of gravitational energy of the falling matter is converted into X-ray radiation. For detailed discussions of different accretion modes and energy generation during such processes the reader is referred to books by for example Shapiro & Teukolsky (1983), Frank et al (1985), a review article by Pringle (1981) and to a collection of the most important works on this topic by Treves et al. (1989). Another possibility of energy generation in such systems is the extraction of rotational energy from the magnetized compact object. Such a process may dominate the energy generation with respect to accretion, particularly, for smaller accretion rates (see e.g. Priedhorsky 1986).

Depending on the nature of the compact star and on the mass of the optical companion, the X-ray binary systems can be divided into three general subclasses: High Mass X-Ray Binaries (HMXRB), Low Mass X-Ray Binaries (LMXRB) and Cataclismic Variables (CVs). The first two classes contain neutron stars (or black holes ?) as compact objects and, what is particularly inter-

[1] There are evidences that some companions are more luminous than predicted by stellar evolution models.

[2] A few compact objects were claimed having mass above critical value for a neutron star (e.g. Cyg X-1, AO620-00, LMC X-3, V404 Cyg). However it is practically impossible to prove that the specific compact object is really a black hole since the estimation of its mass is based on some assumptions concerning the mass of 'normal star', a distance to the binary and that there is no other massive objects in these systems.

HMXRB	LMXRB
1. Massive companion ($> 8 - 10 M_\odot$); Optical spectrum: Early type star	1. Low-mass companion ($< 1 - 1.5 M_\odot$); often: no stellar spectrum visible; accretion disk.
2. Hard X-ray spectrum; pulsating	2. Softer X-ray spectrum; non-pulsating (2-3 exceptions)
3. In galactic plane; young stellar population ($< 2 \times 10^7 yr$)	3. Concentrated towards galactic center (old: mostly $5 - 15 \times 10^9 yr$)
4. No X-ray bursts.	4. Often X-ray bursters.

Table 5.1: Characteristics of high mass and low mass X-ray binaries (from van den Heuvel 1985).

esting, some of them were claimed as sources of very high energy γ-rays. The CVs contain a white dwarf as a compact object and only two of them, AE Aqr and AM Her, were reported in TeV photon energies. The energy generation per unit accreting mass in their case is much lower than for HMXRB and LMXRB. For more detailed information concerning the physical properties of CVs, models and classification schemes we refer to recent reviews by for example Szkody & Cropper (1989), Cropper (1990), Giovannelli & Martinez-Pais (1991).

The HMXRB and LMXRB significantly differ in their origin and physical properties. HMXRB belong to extreme stellar population I and contain very luminous optical companions. LMXRB are a mixture of old disk population ($5 - 10 \times 10^9 yr$) and extreme population II (globular cluster sources, age $\sim 1.5 \times 10^{10} yr$) and contain a low mass star whose optical emission is dominated by the compact object. Some of the compact objects (in HMXRB) show evidence of a strong surface magnetic field of the order $\sim 10^{12} Gs$ (value estimated from observations of cyclotron lines at $\sim 58 keV$ in Her X-1 by Trümper et al. 1978 and at $\sim 20 keV$ in 4U0115+63 by Wheaton et al. 1979). In Table 5.1 are listed the important features of these two groups. For detailed review of observational properties of X-ray binaries, their origin and evolution we refer to articles by Joss & Rappaport (1984), Giovannelli & Sabau Graziati (1992) and proceedings from the conferences dedicated to this topic e.g. Lewin & van den Heuvel (1983), Trümper et al. (1985).

In the next section we review shortly the observational results of very high energy γ-rays from HMXRB and LMXRB. In section 5.2 we discuss possible models of γ-ray production in these sources. The original contribution to this topic is included in section 5.3 in which we discuss possible production mechanisms of γ-rays and neutrons above 10^{11} eV. Based on the reported observational parameters of Cyg X-3, we fit the general Cyg X-3 spectrum in TeV–EeV energy range in terms of these mechanisms. From these fits, we calculate the required total luminosity of Cyg X-3 in relativistic particles. We conclude that the description of the EeV emission from Cyg X-3 by neutron flux is favorable from an energetical viewpoint (acceleration of particles to

lower energies is postulated) and avoids difficulties concerning attenuation of VHE photons in the strong magnetic field of the binary system. We show that a model in which relativistic neutrons, emitted by the compact object, interact with the background matter occulting the compact object in the phase of the orbital period observed in TeV and PeV energy ranges, seems to be the most successful in describing the spectrum of Cyg X-3 and gives reasonable values for the required total particle luminosity. Also a model in which the electromagnetic cascade initiated by nuclei (e.g. He) and developing in the matter and magnetic field surrounding the binary system is consistent with observations.

5.1 Observations

The existence of sources emitting high energy γ-rays was suspected for a long time. The searches of such sources were stimulated by the discovery of cosmic rays (Hess 1912). It was natural to postulate that γ-rays should be produced as a secondary products during the acceleration and propagation of relativistic particles inside sources of cosmic rays. At first, the scientists attention was concentrated on the most powerful phenomena in our Galaxy: supernova and radio pulsars. However only two such objects, the Crab Nebula and the Vela pulsar, observed already by satellites in MeV – GeV photon energies, were reported in the very energetic γ-rays above 10^{11} eV (see chapter 4 for details). The new results came unexpectedly from another side. The X-ray binary, Cyg X-3, was detected at TeV energies and, this result was confirmed by several other observations, although many observations also reported negative results (for detailed reviews of these observations we refer to e.g. Weekes 1988 and Stepanian 1989). Up to now, several X-ray binaries were claimed as detected at photon energies $> 10^{11}$ eV (see Table 5.2). We shortly review here the observational results concerning the best documented ones: Her X-1, 4U0115+63, Cen X-3 and Vela X-1. Cyg X-3, which is most frequently observed in this energy range, is reviewed separately in section 5.3. For more complete reviews of recent observations and discussion of these results, the reader is referred to: Chadwick et al. (1990), Ramana Murthy (1990) and Turver (1991) – TeV energy range; Goodman (1990) – PeV energy range; Weekes (1988, 1992) and Fegan (1990) both TeV and PeV energy ranges.

Her X-1 is a close ($\sim 6kpc$) LMXRB which exhibits modulation of the emission on time scales of 1.24s (pulsar period), 1.7d (orbital period) and 35d (probably precession of the neutron star or accretion disk). The burst in the VHE γ-rays from Her X-1 with duration of $\sim$ 3 min was reported by the Durham group (Dowthwaite et al. 1984) showing modulation according to the pulsar period. The appearance of such bursts of emission with duration 3–100 min was later confirmed by several other observations (see Table 5.2), but negative results were also reported (see e.g. Reynolds et al. 1991). However, especially important for the mechanism of γ-ray production in this source, is the

Source	Energy	Result	Group	Principal references
Cyg X-3	TeV	Discovery	Crimea	Vladimirsky *et al.*, 1973
		Confirmation	Crimea	Neshpor *et al.*, 1980
		Confirmation	Tien Shan	Mukanov, 1981
		Confirmation	Whipple	Weekes *et al.*, 1981
		Confirmation	Iowa -	Lamb *et al.*, 1982
		Confirmation	Durham	Dowthwaite *et al.*, 1983
		Upper limit	Whipple	Lamb *et al.*, 1991
	PeV	Discovery	Kiel	Samorski and Stamm, 1983a
		Confirmation	Leeds	Lloyd-Evans *et al.*, 1983
		Upper limit	Cygnus	Lu *et al.*, 1991
		Upper limit	CASA	Krimm *et al.*, 1991
	EeV	Discovery	Fly's Eye	Cassiday *et al.*, 1989
		Confirmation	Akeno	Teshima *et al.*, 1990
		Upper limit	Leeds	Lawrence *et al.*, 1989
Her X-1	TeV	Discovery	Durham	Dowthwaite *et al.*, 1984c
		Confirmation	Whipple	Gorham *et al.*, 1986a, b
		Confirmation	Whipple	Lamb *et al.*, 1988
		Confirmation	Haleakala	Resvanis *et al.*, 1988
		Upper limit	Whipple	Lamb *et al.*, 1991
	PeV	Discovery	Fly's Eye	Baltrusaitis *et al.*, 1985
		Confirmation	Cygnus	Dingus *et al.*, 1988
		Upper limit	Cygnus	Lu *et al.*, 1991
		Upper limit	CASA	Krimm *et al.*, 1991
Cas Gam-1	TeV	Discovery	Crimea	Stepanian *et al.*, 1972
4U0115	TeV	Discovery	Durham	Chadwick *et al.*, 1985
		Confirmation	Durham	Brazier *et al.*, 1990c
		Confirmation?	Haleakala	Resvanis *et al.*, 1987b
		Upper limit	Tata	Acharya *et al.*, 1990b
		Upper limit	Whipple	Macomb *et al.*, 1991
Vel X-1	TeV	Discovery	Potch.	North *et al.*, 1987
		Confirmation	Potch.	Raubenheimer *et al.*, 1989
		Confirmation	Durham	Carraminana *et al.*, 1989a
		Upper limit	JANZOS	Bond *et al.*, 1990b
	PeV	Discovery	Adelaide	Protheroe *et al.*, 1984
		Confirmation	BASJE	Suga, 1985
		Confirmation	Potch.	van der Walt *et al.*, 1987
Cen X-3	TeV	Discovery	Durham	Carraminana *et al.*, 1989b
		Confirmation	Durham	Brazier *et al.*, 1990d
		Confirmation	Potch.	North *et al.*, 1990
1E2259 + 58	TeV	Discovery	Durham	Brazier *et al.*, 1990c
		Upper limit	Whipple	Cawley *et al.*, 1991
Sco X-1	TeV	Discovery	Potch.	de Jager *et al.*, 1985
		Confirmation	Durham	Brazier *et al.*, 1990e
LMC X-4	TeV	Upper limit	Durham	Brazier *et al.*, 1990g
	PeV	Discovery	Adelaide	Protheroe and Clay, 1985
SMC X-1	TeV	Discovery	Durham	Brazier *et al.*, 1990g

Table 5.2: Summary of the best observed X-ray binary systems at energies above 10^{11} eV (for references see Weekes 1992).

modulation of signal with period shorter than observed in X-rays for Her X-1 pulsar. There is also no clear correlation of the γ-ray emission with other periods of the system: 1.7d and 35d. In the PeV energy range, the emission from Her X-1 was detected by the Fly'e Eye group (Baltrusaitis et al. 1985). The burst of PeV emission lasted for about 40 min and exhibited the 1.2377s periodicity, consistent with observations at TeV energies. More recent results in this energy range are confusing. One result shows a slight 2.8σ DC excess from Her X-1 (Acharya et al. 1991), another a 4.2σ excess at the period of 1.236s (Muraki et al. 1991b), but other groups observed no significant excess (e.g. McKay et al. 1991).

4U0115+63 is a HMXRB system containing a neutron star with period 3.6s and a Be companion star with orbital period 24.3d and eccentricity 0.34. TeV radiation was first reported from this source by the Durham group (Chadwick et al. 1985a; confirmed by Brazier et al. 1990a). The emission was pulsed at the 3.6s period without any evidence of modulation with the orbital period. However, an

earlier DC excess in this region of the sky was found by the Crimean group (Stepanian et al. 1972) who reported the existence of a transient VHE source, Cas γ-1, which may concern 4 U0115+63. Other observations reported sporadic burst emission from 4U0115+63 lasting from 15 min up to 3 days or the lack of detection (see Table 5.2). It seems that 4U0115+63 is not a steady periodic source of VHE γ-rays, although it may be a sporadic one, as suggested by observations in X-rays.

Cen X-3 is a HMXRB system containing a 4.82s pulsar in a 2.1d orbit. This source was identified above 0.25 TeV by the Durham group (Brazier et al. 1990b), showing modulation according to the pulsar period. Emission was detected only in the 0.7-0.8 orbital phase interval. These parameters were confirmed independently by the Potchefstroom group (North et al. 1990). However, more recent observations reported during the 22nd ICRC do not confirm these earlier results.

Vela X-1 is a HMXRB system containing a rather slow pulsar with period 283s in a 8.96d orbit. The TeV γ-ray flux from this source has been reported by the Potchefstroom group (North et al. 1987; Raubenheimer et al. 1989) and confirmed by Durham group (Carraminana et al. 1989). The persistent emission observed from this source is modulated according to a period which is shorter by $\sim 0.3s$ than the pulsar period observed in X-rays. This puzzling feature is also reported in the case of Her X-1 (see above). Recent results reported during the 22nd ICRC by these same groups are consistent with previous persistent emission (without modulation according to orbital period) and also claim the detection of a burst at phase 0.91, with respect to eclipse. However, other groups failed to find any evidence of TeV γ-ray emission. There are also claims of the excess of particles at PeV energies corresponding to ~ 0.63 orbital phase of Vela X-1 (Protheroe et al. 1984).

Recently, two cataclismic variables were discovered at TeV energies AE Aqr and AM Her. AE Aqr shows weak pulsed TeV emission according to the white dwarf 33s period, associated with flaring activity of the source (see Bowden et al. 1991; Meintjes et al. 1991). AM Her was also observed in TeV photon energies (Bhat et al. 1991). Its light curve exhibits two broad emission peaks close to 0.1 ± 0.2 and 0.6 ± 0.2.

The above results, claiming the detection of X-ray binaries in VHE and UHE γ-rays, were not the end of this surprising story. Recently, new results have appeared, announcing the discovery of neutral emission above 10^{17} eV from three X-ray binaries. The results concerning Cyg X-3, claimed at these energies by two independent groups, are described in section 5.3. Two others in the southern hemisphere, 2A 1822-37 and LMC X-4, were found in data collected by SUGAR (Sydney University Giant Air shower Recorder) experiment, and reported in papers by Clay et al. (1992) and Meyhandan et al. (1992). The flux of particles estimated for 2A 1822-37 is $2 \times 10^{-15}\ cm^{-2}s^{-1}$ above 1.8×10^{17} eV and for LMC X-4 is $(5.2 \pm 1.5) \times 10^{-16}\ cm^{-2}s^{-1}$ above 2×10^{17} eV. They are

consistent with positive detections of these sources at PeV energies by Ciampa et al. (1989) and Protheroe & Clay (1985). These observations, if real, is very difficult to explain on the theoretical grounds (see discussion of models in the next section).

In conclusion, in spite of several reports of positive detection of X-ray binaries above 10^{11} eV, only a few of them are considered as well established. However, there are big hopes between cosmic ray astrophysicists since these sources may be responsible for production of the cosmic rays in our Galaxy. Recent claims of detection of sources above 10^{17} eV (Cyg X-3, 2A 1822-37 and LMC X-4) seem to support the ideas that high energy particles, filling our Galaxy, originate in compact objects.

There are two main problems connected with detection of the highest energy photons. First, the poor sensitivity of telescopes (most of the observations report the detection of sources with only $3 - 4\sigma$) makes the observations very difficult and results unsure. Second, the possible variability of sources at these energies prevents the confirmation of claimed earlier results. Positive detection of these sources by the detectors on the board of Compton GRO below 10 GeV will have a very important influence on the future development of high energy γ-ray astronomy.

5.2 Models

The evidences of extremely high energy γ-ray emission in X-ray binary systems created a serious theoretical problems which are not solved in spite of many efforts. The three main concerns: *particle acceleration mechanism, energy generation, and mechanisms of γ-ray production.* In this section we will shortly discuss acceleration mechanisms and possible sources of energy generation, in the context of specific models. The possible mechanisms of an extremely high energy γ-ray production will be discussed in more detail in section 5.3 taking into consideration Cyg X-3 as an example.

Acceleration mechanism

The observations of X-ray binary systems postulate the acceleration of particles up to 10^{16} eV or even 10^{18} eV (if recent reports concerning the observations of $\sim 10^{17}$ eV neutral particles are confirmed). It is very difficult to envisage a mechanism for particle acceleration to such huge energies, keeping in mind their possible energy losses during the acceleration process. The TeV γ-ray emission reported from the direction of several sources may be explained by the emission of relativistic electrons. However, production of higher energy γ-rays (PeV, EeV) has to engage hadronic interactions because of the huge energy losses of electrons during the acceleration process in magnetic and radiation fields. The following acceleration mechanism were discussed in the literature:

1. *Dynamo Acceleration.* A large–scale electric field may be induced by the rotation of an ordered magnetic field. If such an object is rotating in vacuum, then a possible potential of $V =$

$e \cdot (v \times B) \cdot R/c$ can be used for particle acceleration up to $\sim 10^{17}$ eV. However, in the realistic case (e.g., the presence of plasma around a pulsar), only a small part of this value is available for electron acceleration because of the development of e^+e^- pair cascade in a strong magnetic field. For more details of particle acceleration by this mechanism in the pulsar model we refer to section 4.2 of this thesis.

2. *Shock Acceleration.* Charged particles can gain energy by scattering back and forth across the shock front from magnetic irregularities which move with the fluid and act as converging walls, or in diffusion process through the shock front (first order Fermi acceleration, Fermi 1954). The spectrum of accelerated particles escaping downstream is a power law with index dependent on the compression ratio of the shock. The maximum acceleration energy of the particles is determined by the balance of energy gain in this process and energy loss which depends on the model. The protons may reach maximal energy $E_p^{max} \cong e \cdot (u_1/c) \cdot B \cdot R_{sh}$ (where u_1 is the upstream velocity of the shock, B is magnetic field and R_{sh} the typical dimension of the shock). The acceleration process also depends on the orientation of the shock propagation to the direction of magnetic field (parallel, perpendicular, or oblique shocks) which result in different efficiencies and maximum energies of particles. More recent studies of acceleration by relativistic shocks, $u_1 \sim c$, (Kirk & Schneider 1987) indicate that they are more efficient in accelerating particles (the energy gains larger per one crossing of the shock, the resulting power law spectrum flatter).

3. *Magnetic Reconnection.* The interaction of plasma flow with magnetic field can distort its structure allowing reconnection along neutral sheets, where oppositely directed field lines are brought together. Along these neutral sheets, the potential drops may be maintained and acceleration of particles can take place. The maximum energy to which protons can be accelerated is $E_p^{max} \approx e/\eta(v_A/c) \cdot B \cdot R$, where $v_A = B/(4\pi\rho)^{1/2}$ is the Alfven velocity and $\eta < 1$ is the efficiency factor. The spectrum of particles accelerated by magnetic reconnection depends on the geometry and boundary conditions and may be monoenergetic or of the power law type.

4. *Plasma Turbulence.* If a magnetic field is present in turbulently moving plasma, the charged particles can gain energy in head–on collisions and lose in head–tail collisions with magnetic blobs, but the net result is a systematic acceleration. This mechanism is often referred as second order Fermi acceleration (Fermi 1949). In the most favourable case (turbulence on all scales, radiative losses not important), energies of the order $\sim 10^{16}$eV may be achieved.

In principle, the above discussed mechanisms may explain the observations of PeV γ-ray emission, however there is no known mechanism in which possible acceleration of particles in discrete

sources may occur up to (or above) $\sim 10^{18}$ eV. From another side, the observations of cosmic ray particles, with energies $\sim 10^{19}$ eV, postulate the existence of such mechanisms.

Another, equally important problem of VHE γ-ray observations concerns the source of energy in X-ray binary sources which can be efficiently transformed to high energy γ-rays. Two sources of power available for particle acceleration in X-ray binaries are accretion and neutron star rotation. In principle, in some special situations, both processes can interplay (see, e.g., Priedhorsky 1986), but usually, they are analyzed separately since most of the models concentrate on only one of these possibilities. The accretion process will take place if the energy density of the relativistic wind produced by the rotating neutron star is lower than the energy density of the plasma at the accretion radius[3]. The observations of some sources require very high luminosities, up to $\sim 10^{39}\ erg/s$ in the case of Cyg X-3, which is above the maximum energy generated in spherical accretion onto a solar mass neutron star (Eddington limit) and above the X-ray luminosity of these sources. Therefore, the possibility of collimated acceleration of particles (and production of high energy γ-rays) in these sources is often considered. We will start a short review of the models from those engaging the accretion scenario. For more detailed reviews we refer to Hillas (1987), Weekes (1988), Chadwick et al. (1990) and Harding (1991).

The possibility of induction of large scale potentials in the disk rotating in a nearly perpendicular magnetic field of the neutron star was adopted for X-ray binaries by Chanmugam & Brecher (1985). In this model, particles can be accelerated by parallel electric fields, above the disk, if the plasma is deficient there. The potential difference may be $V = 1.4 \times 10^{13} \cdot (B(r_A)/10^5\ Gs) \cdot (r_A/10km)^{1/2} \cdot ln(r_{out}/r_A)\ volts \cong 2.8 \times 10^{14} \cdot B_{12}^{-0.43} \cdot L_{38}^{0.71}\ volts$, where B_{12} is the surface magnetic field in units of $10^{12}Gs$, and L_{38} is the accretion power in units of $10^{38}erg/s$. Then, the maximum energies of particles are obtained for the high accretion rates onto a neutron star with a weak surface magnetic field. Such a model is able to explain the reported TeV emission from the Vela X-1 which contains

[3]For instance, in the case of the quasi-spherical scenario, accretion will occur if the kinetic energy density of matter is higher than the energy density of magnetic field at the accretion radius:

$$B^2(r_{acc})/8\pi < m_p n_\infty v_\infty^2,$$

where $B(r_{acc})$ is the magnetic field strength at the accretion radius, m_p is proton mass, n_∞ and v_∞ are the density of particles and their velocities at the accretion radius, respectively.

Then, in the case where the light cylinder of the rotating neutron star is smaller than the accretion radius (which is for $P_{NS} < 560 \cdot v_7^{-2}$, P_{NS} is the period of the neutron star in seconds and v_7 is the velocity of particles in units $10^7 cm/s$), the accretion process will start if

$$B_8 < 8 \cdot n_0^{1/2} \cdot P_{NS}^2/v_7,$$

where B_8 is the magnetic field in units of $10^8 Gs$ and n_0 is the density of matter at the light cylinder in $particles/cm^3$.

If the light cylinder is greater than the accretion radius, the critical value for the strength of the magnetic field for which the accretion of matter will occur is

$$B_8 < 1.2 \times 10^7 \cdot n_0^{1/2} \cdot v_7^{-5}$$

However, in this case, the centrifugal force may prevent accretion if the neutron star is an oblique rotator.

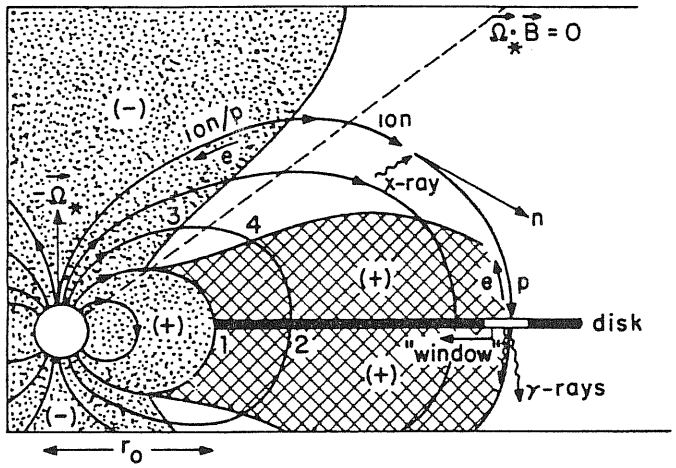

Figure 5.1: The magnetosphere around an aligned neutron star. The dotted region corrotates with the star. The crosshatched region corrotates with that part of the disk to which it is attached by a magnetic field. The gap is between these two regions. The drifting 'window' in the disk, in which production of γ-rays occurs, is also labelled (from Cheng & Ruderman 1989).

a rather old neutron star (period $\sim 283s$), but is not promising in the case of Her X-1 which is thought to have a surface magnetic field of $\sim 10^{12}Gs$.

A model, involving similar scenario (pulsar plus accretion disk), was suggested by Cheng & Ruderman (1989,1991). It is proposed that two parts of the pulsar magnetosphere (the first, rotating rigidly with the pulsar, and the second, rotating with the disk – keplerian rotation) are separated by a vacuum gap in which huge electric potentials are induced (see Fig. 5.1). The maximum potential drop $V \sim 10^{17} \cdot B_8^{-3/7} \cdot L_{38}^{5/7} eV$ is higher than in the previous model since the acceleration takes place closer to the neutron star. The advantage of this model is the possibility of explaining the surprising difference between the periodicity of TeV γ-ray signal and the pulsar period, observed in the case of the Vela X-1. In this model the difference is caused by drifting 'windows' (parts of the disk with smaller or higher surface density than the entire disk) on the surface of the accretion disk which is illuminated by relativistic particles (see Fig. 5.1). The emission of γ-rays is collimated along the trajectories of relativistic protons impinging on the disk surface.

Another type of accretion model applies the acceleration of particles in the shock. For instance, Kazanas & Ellison (1986) postulate the formation of a spherical collisionless shock at a distance $\sim 10 - 50$ neutron star radii. The protons can be accelerated up to $\approx 3 \times 10^{16} eV$. However UHE γ-rays cannot escape from this region freely because of the magnetopair production process. Therefore the authors suggest that the energy is transferred outside through production of energetic neutrons in p + p collisions. Neutrons are not captured by magnetic field and can produce UHE γ-rays in the outer magnetosphere.

Kiraly & Meszaros (1988) proposed a model in which some of material, accreting onto the polar

cap, is expelled in a jet along the axis of the neutron star's magnetic pole. Protons are accelerated in the shock which is formed when the jet encounters matter accumulated farther from the neutron star. The advantage of this model is that it uses the full gravitational potential of the neutron star, however the efficiency of transforming this energy into the jet is very uncertain. This model can not explain the γ-ray signals modulated according to the pulsar period since the shock has a shell shape surrounding the neutron star.

The possibility of plasma turbulence in accretion columns of neutron stars was proposed by Katz & Smith (1988). The energy may be transported along such columns from deeper regions (close to the neutron star surface) by the convective motions of the region close to the light cylinder (Smith et al. 1992; Johnson 1991). Protons can be accelerated in collisions with turbulent cells to energies $\approx 10^{14} - 10^{16} eV$. A narrow beam of protons, accelerated in such a scenario, can interact with the matter of the accretion disk producing γ-rays in hadronic cascade (Hillas & Johnson 1991). The above model postulates the highly collimated production of γ-ray photons (which is favoured from the energetics viewpoint), and can easily explain the periodic and transient emission reported from some sources (e.g. Her X-1).

Second group of models postulates the extraction of rotational energy of fast, nonaccreating pulsars, which may occur inside or outside the light cylinder. The first case is typical for isolated pulsars and was already discussed in section 4.2 of this thesis. Here we shortly review the second possibility which seems much more promising for models of UHE γ-ray production (no magnetopair production by UHE γ-rays). It was proposed that the spin-down energy of the pulsar is transported by a relativistic MHD wind consisting mostly of e^+e^- pairs (Rees & Gunn 1974). The interaction of such a MHD wind of a rapidly spinning pulsar with the wind of a companion star in a binary system could form a shock (see Fig. 5.2), in which an essential part of pulsar energy may be released (Bignami et al. 1977). Protons and electrons may be accelerated by such a shock and their interaction with matter, in the binary system, may produce the observable VHE and UHE γ-rays (Harding & Gaisser 1990). The maximal energy of protons for a strong shock is

$$E_p^{max} = 7 \times 10^{18} \cdot B_{12} \cdot P_{ms}^{-2} \left\{ \begin{array}{ll} 1, & R_s << a - r_* \\ \frac{r_*}{(a-r_*)}, & R_s \approx a - r_* \end{array} \right\} [eV], \qquad 5.1$$

where r_* is the companion radius, a is the orbital separation of the binary, and R_s is the spherical shock radius. The observed UHE γ-ray signal should be modulated according to the orbital period of the system, but no modulation according to the pulsar period is expected.

Another problem which needs to be explained by the model of γ-ray emission from X-ray binaries is the appearance of a signal in special phases of the orbital period. The simple geometrical model proposed by Vestrand & Eichler (1982) postulates that γ-ray pulses should appear in phases close to 0.2 and 0.8. At that time, it was consistent with observations of Cyg X-3 but later results

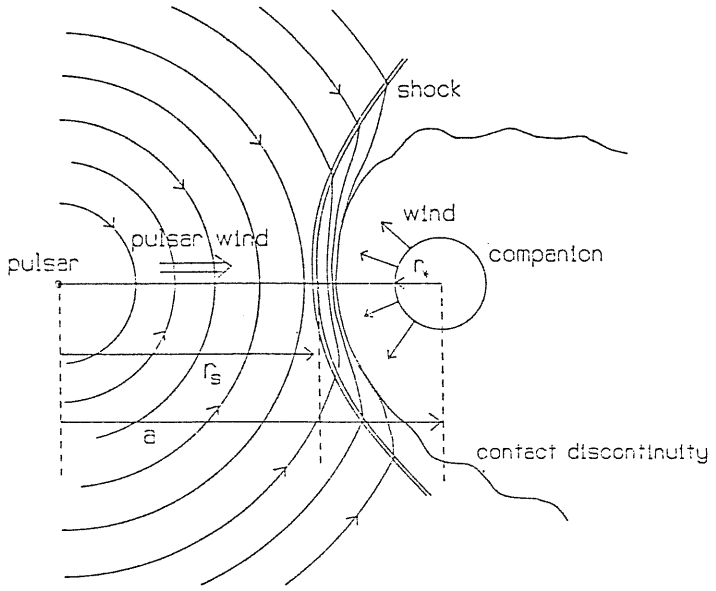

Figure 5.2: Pulsar wind shock acceleration for the case of confinement by the companion star wind (from Harding & Gaisser 1990).

showed evidence of emission only in phase close to ~ 0.6, where the neutron star is supposed to be in front of the companion. These observations can be explained in the model of γ-ray production in the accretion tail formed behind the neutron star or bulge on the accretion disk surface (see Fig. 5.3). Another solution was proposed by Protheroe & Stanev (1987) who studied propagation of relativistic particles emitted isotropically by the neutron star in the dipole magnetic field of the companion. However, no clear mirroring of trajectories close to phase ~ 0.6 is seen in his calculations.

5.3 Cyg X-3

Cyg X-3, one of the earliest sources discovered in X-rays (Giacconi et al. 1967), shows a variety of peculiar behaviour in almost all ranges of the photon spectrum. It is one of the brightest, variable X-ray source in the Galaxy, a bright infrared source and a radio source that undergoes huge radio outbursts. The periodicity of $\sim 4.8hr$, discovered in X-rays (Persignault et al. 1972) and confirmed in infrared observations (Becklin et al. 1972), suggests that Cyg X-3 is a binary system. The recent discovery of broad He I and He II emission lines (but no strong hydrogen lines) indicates that the companion is probably a Wolf-Rayet star producing a dense wind in the Cyg X-3 system (van Kerkwijk et al. 1992). The second companion is probably a neutron star which is suggested by high X-ray luminosity and a 12.6ms periodicity, discovered in TeV photon energies by Chadwick et

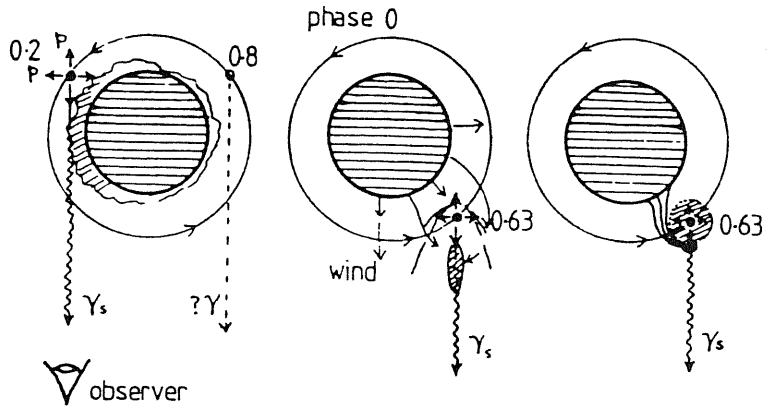

Figure 5.3: Possible gas targets in X-ray binaries. (a) Atmosphere of companion, (b) accretion tail, (c) structure attached to accretion disk (from Hillas 1987)

al. (1985b) (see also Bowden et al. 1992) and independently confirmed by Gregory et al. (1990)[4]. Because of the location of Cyg X-3 close to the Galactic plane and behind the spiral arm at $\sim 8kpc$, this source was not identified up to now in optical range, which is a big inconvenience for the detailed investigation of the system. However, very interesting structure of the source emerged in radio observations. VLBI mapping showed the existence of a double-sided jet expanding with relativistic velocity ($\sim$ 0.48c - Geldzahler et al. 1983; between 0.16–0.31c - Molnar et al. 1988). This structure was also confirmed on arcsecond scales (Strom et al. 1989)[5]. For general information concerning Cyg X-3 the interested reader is referred to Bonnet-Bidaud & Chardin (1988).

The soft X-ray emission, $\sim 1.6 \times 10^{38} erg/s$ for 8.5kpc (Priedhorsky 1985), varies continuously with a $\sim 4.8hr$ period, showing low and high states. However the outbursts observed in radio wavelengths are not seen in this energy range. In contrast, the hard X-ray spectrum ($> 20keV$) is stable during low and high soft X-ray states and it is well described by a power low with spectral index 2.2 up to $\sim 200keV$ (Hermsen et al. 1987). This is consistent with earlier observations (e.g., Ulmer et al. 1974; Reppin et al. 1979; Dolan et al. 1982) except results reported by Meegan et al. (1979), who find a much flatter spectrum up to 1 MeV.

There is no clear agreement between different reports of high energy γ-ray observations Cyg X-3. The results of observations in the 100 MeV – GeV range are collected in Table 5.3. The results obtained by SAS 2 and COS B suggest the variability of γ-ray emission from Cyg X-3 in the high

[4]This period is probably observable close to the huge radio flares only. The observations which were not confined to the specified windows (radio flares) failed to detect this periodicity (e.g. Resvanis et al. 1986; Bhat et al 1988; Fegan et al. 1989).

[5]Such extraordinary features were reported in only a few Galactic sources (SS433, Cir X-1, Sco X-1 (at present in doubt), and 1E1740.7-2942).

Reference	Energy	Flux ($phot./cm^2/s$)	Experiment
Galper et al. (1976)	> 40 MeV	$(2.0 \pm 0.8) \times 10^{-4}$ (3.6σ)	balloon
Mckechnie et al. (1976)	> 70 MeV	$< 6.5 \times 10^{-6}$	balloon
Lamb et al. (1977)	> 100 MeV	$(4.4 \pm 1.1) \times 10^{-6}$ (4.5σ)	SAS 2
Fichtel et al. (1987)	> 100 MeV	confirmation	SAS 2
Hermsen et al. (1987)	> 100 MeV	$< 9.7 \times 10^{-7}$ (2σ)	COS B
Li & Wu (1989)	> 100 MeV	$(1.3 \pm 0.6) \times 10^{-6}$	COS B

Table 5.3: Results of high energy γ-ray observations of Cyg X-3, collected from different experiments.

energy γ-ray range.

One of the most interesting features of this source is the discovery of very high energy emission in the TeV (Vladimirsky et al. 1973) and PeV (Samorsky & Stamm 1983; Lloyd–Evans et al. 1983) energy ranges. These first positive reports were later confirmed by other experiments (more recently see, e.g., Baltrusaitis et al. 1987; Muraki et al. 1991a), although negative reports were also claimed (see for a review Weekes 1988 or Fegan 1990). All the observations of Cyg X-3, are, at present, debated and a part of the scientific community doubt in any positive detection (see, e.g., the discussion by Chardin & Gerbier (1989). However, it is quite natural to suppose that the very high energy (VHE) γ-ray emission from Cyg X-3 is strongly variable (see observations of outbursts in lower photon energies). In fact, some previous observations indicated association of VHE emission with radio flares (e.g., Lambert et al. 1985; Alexeenko et al. 1987) which were recently confirmed by Gregory et al. (1990) and Tonwar et al. (1992). The positive observations of the Cyg X-3 above TeV energies show an excess close to two phases of the 4.8hr orbital period, at ≈ 0.2 and ≈ 0.6 (starting from X-ray minimum). However, recent reports concern only the emission at this second phase.

The surprising detection of Cyg X-3 in the EeV ($10^{18} eV$) energy range was announced by the Fly's Eye group (Cassiday et al. 1989, 1990). The excess of showers with flux $(2 \pm 0.6) \times 10^{-17}$ $particles/cm^2/s$ was reported. At first, it was not confirmed by the Haverah Park group (Lawrence et al. 1989), upper limit 4×10^{-18} $particles/cm^2/s$. But later the consistent excess was reported by the Akeno group (Teshima et al. 1990, Hayashida et al. 1991).

The integral photon spectrum from Cyg X-3 (from hard X-rays up to PeV γ-rays), summed over different periods of the observations, can be described by a power law with spectral index close to –1.1. The results reported by Lloyd–Evans et al. (1983) suggest the presence of a cut–off at energies > 10 PeV. However the neutral emission at energies $> 0.5 EeV$ (Cassiday et al. 1989,1990; Teshima et al. 1990) seems to follow the spectral index –1.1. In Fig. 5.4 are shown some results of

observations of neutral emission from Cyg X-3 in TeV and PeV energies (collected by Watson 1985 plus some most recent) and the fluxes in EeV energies observed by Cassiday et al. (1989,1990) and Teshima et al. (1990).

Cassiday et al. (1989) recently suggested that the excess of the neutral particles from the direction of Cyg X-3 above $0.5EeV$ can be caused by relativistic neutrons. Sommers and Elbert (1990) discussed in detail the consequences of the TeV–EeV emission from the Cyg X-3 and proposed several different mechanisms of EeV neutron production in this source. In the next subsection we discuss possible radiation mechanisms of TeV–EeV γ-ray emission from Cyg X-3.

5.3.1 Production of γ-rays and neutrons in Cyg X-3

The VHE observations of Cyg X-3 postulate the acceleration of particles in the source to extremely high energies (at least $\approx 10^{18}eV$). It is difficult to imagine a model of acceleration of particles up to so high energies if we keep in mind additional radiative processes that take place in strong magnetic and radiation fields (see discussion in section 5.2). It seems unlikely that electrons are responsible for this emission because of the huge synchrotron and inverse Compton losses. Moreover, the small rigidity of electrons will not allow them to propagate linearly through the binary system (magnetic field may be essential) and the observed very high energy emission close to fixed phases of the orbital cycle (e.g. Cyg X-3) should be diluted.

The source of energy, required by the observations, seems to be problematic in the accretion scenario onto a neutron star if we assume isotropic acceleration of particles. Super–Eddington accretion of matter onto a neutron star, extraction of rotational energy of a neutron star, accretion onto a more massive object (e.g. black hole) or highly anisotropic acceleration of particles by the neutron star is recommended. For a recent critical discussion on energy generation and particle acceleration in Cyg X-3, we refer to the paper by Mitra (1991).

The mechanisms of VHE γ-ray production in X-ray binaries can be classified depending on the kind of target encountered by the relativistic particles: matter or radiation. The most promising of those are:

a). Interaction of relativistic nuclei (emitted by the Compact Object – CO) with background photon field. The VHE photons are produced through deexcitation of relativistic nuclei ($A + \gamma_{ph} \rightarrow A_1^* \rightarrow A_1 + \gamma$) and through decay of neutral pions produced in the interaction of nuclei (and their fragments) with low energy photons ($p + \gamma_{ph} \rightarrow \pi^0 + ...; \pi^0 \rightarrow 2\gamma$). The neutrons are produced from fragmentation of nuclei ($A + \gamma_{ph} \rightarrow n + ...$) and in charge exchange of protons during their interactions with photons ($p + \gamma_{ph} \rightarrow n + ...$).;

b). Interaction of relativistic protons (accelerated by CO) with a thin column density of matter. The VHE photons are produced via the decay of neutral pions ($p + p \rightarrow \pi^0 + ...; \pi^0 \rightarrow 2\gamma$)

and the neutrons from charge exchange of proton beam ($p + p \rightarrow n + ...$);

c). Interaction of relativistic neutrons (produced in CO) with a thin column density of matter. The VHE photons and neutrons are produced as in item b) plus neutrons which escape without interaction;

d). Formation of the VHE neutral spectrum observed from Cyg X-3 in a cascade initiated by the monoenergetic particles. TeV and PeV photons are produced in the electromagnetic cascade calculated by Hillas (1984). EeV neutrons are produced in fragmentation of nuclei during their interaction with matter.

e). Interaction of relativistic nuclei (with power law spectrum) with a thin column density of matter (< 1 interaction length). The VHE photons are produced via decay of neutral pions ($A + p \rightarrow \pi^0 + ...; \pi^0 \rightarrow 2\gamma$) and neutrons mainly from fragmentation of nuclei and charge exchange of relativistic protons.

Of course, in reality several – if not all – of these mechanisms can be important. However, for simplicity we will discuss them separately as a unique explanation of possible VHE emission from Cyg X-3.

5.3.1.1 Interaction of nuclei with the photon field

The production of VHE photons in the interaction of relativistic nuclei with radiation field was firstly investigated in the context of cosmic γ –ray sources by Balashov et al. (1990). The authors described the VHE photon spectra from two sources: Cyg X-3 ($10^8 - 10^{16} eV$) and the Crab pulsar ($10^{11} - 10^{16} eV$) by a component model, iron nuclei and protons interacting with radiation field. However, their fit to the Cyg X-3 spectrum is somewhat controversial and within the model it is impossible to describe the recent observations in the EeV energy range and the spectrum below $10^{11} eV$ only by photons from proton – proton or proton – photon interaction. The required amount of energy in relativistic particles would be enormous and EeV photons should be absorbed in magnetic field.

We performed calculations of the photon spectra also including contribution of neutrons from fragmentation of iron nuclei to the total emitted spectrum. It was assumed that the relativistic Fe nuclei (accelerated by e.g. a neutron star), with a power law spectrum and high energy cut–off, interact with black body radiation emitted by the stellar companion and/or accretion disk around compact object in Cyg X-3 system. The spectra of photons from the deexcitation of nuclei were obtained in an approximate way following the calculations of multiplicity and the average energy of photons produced during the decay of nuclear giant resonance (Moskalenko & Fotina 1989). The complete disintegration of Fe nuclei was assumed. The spectra of photons from photoproduction of

neutral pions in particle – photon collisions were calculated according to resonance approximation (see Stecker 1973). This approximation is good enough since the considered energy range is far away from the jet region of the particle – photon interaction where the cross section increases again (for detailed results see Mannheim & Biermann 1989). The spectrum of neutrons from fragmentation of nuclei, and further interaction of products of fragmentation with background photons, were calculated assuming an elasticity coefficient equal to 0.4 and a probability of proton conversion into neutron equal to 0.5 (Kirk & Mastichiadis 1989). The probability of survival of relativistic neutrons against decay on the way from Cyg X-3 to the Earth was included in the calculations by the formula $P = exp(-0.108D[kpc]/E[Eev])$ (Cassiday et al. 1989).

In Fig. 5.4 are shown some results of observations of VHE neutral emission from Cyg X-3 (fluxes reported from a 4.8hr periodicity search) and the calculated spectra of photons and neutrons according to the above prescription. As we can see, it is possible to achieve a reasonable fit for the following parameters: power law spectrum of the iron nuclei with spectral index 2.7 and cut–off at $10^{11}GeV$; temperature of the background photon field $T_{bb} = 10eV$; column density of background photons equal to one interaction length for pion photoproduction in particle– photon collisions.

From the fitting of the observed flux of neutral emission from Cyg X-3 by the calculated photon spectrum (deexcitation in TeV range, photoproduction in PeV range) and neutron spectrum (from fragmentation in EeV range) we obtained the required luminosity of Cyg X-3 in the energy range $10^6 - 10^{11}GeV$ in relativistic Fe nuclei:

$$L_{Fe}[erg/s] = 2.2 \times 10^{38} \cdot \Delta\Omega[sr]/\delta t, \qquad 5.2$$

where $\Delta\Omega$ is the solid angle in which relativistic nuclei are emitted and δt is the duty cycle of photon emission. The distance to Cyg X-3 is taken to be 10kpc.

If we assume $\delta t = 1/20$ and $\Delta\Omega = 1$, the calculated luminosity is much higher than the classical Eddington one ($\approx 1.3 \times 10^{38} M/M_{\odot}[erg/s]$) for a typical mass of the neutron star. This can be acceptable if the particles emitted by Cyg X-3 are strongly collimated or if the mass of the compact object is much greater than $1M_{\odot}$ (however, a black hole would contradict the reported 12.6ms periodicity).

The photon flux in TeV energy range is consistent with observations (Fig. 5.4, see curve b), if we assume that the magnetic field in the source volume does not influence the electromagnetic cascade initiated by VHE photon in the background photon field. In such case, an essential part of TeV photons can emerge from the source region if the mean value of the magnetic field in the source region is $\sqrt{B^2}[Gs] < 10^{12} \times \epsilon_{bb}/E_{ph}$ (see Gould & Rephaeli 1978), which, e.g. for photon energies $\approx 10^{16}eV$, yields $\sqrt{B^2} < 5 \times 10^{-4}Gs$. On the contrary (important magnetic field – electromagnetic cascade do not develop), a much smaller absorption length must be used (see Gould & Schreder

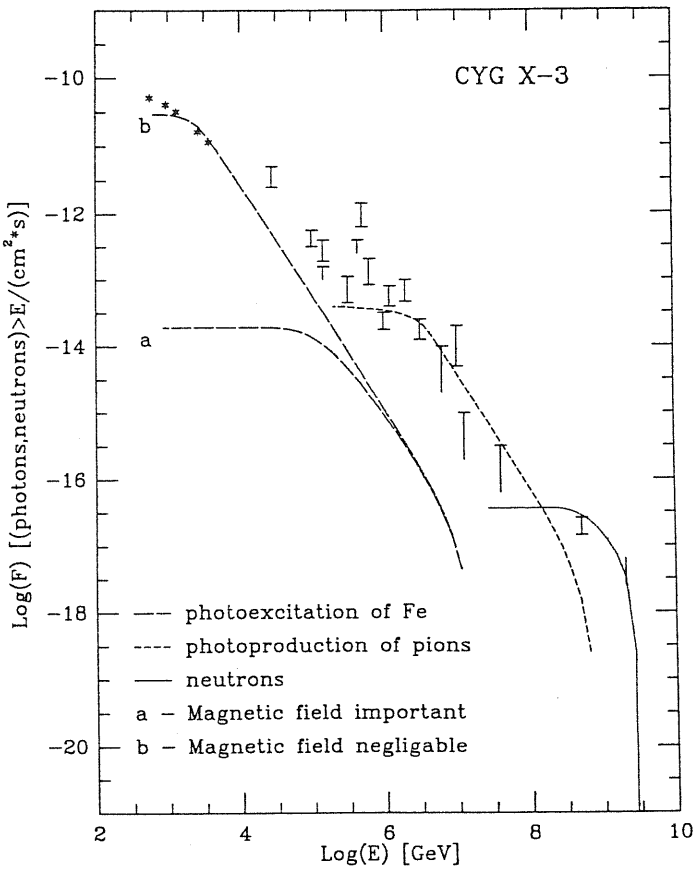

Figure 5.4: The observational results of VHE emission from the direction of Cyg X-3 above $10^{11}eV$ fit by the γ–ray spectrum from: 1) the photoexcitations of relativistic Fe nuclei (power low, spectral index 2.7) by low energy black body photons with $kT = 10eV$ – long dashed line; the photoproduction of neutral pions created in the interactions of nuclei with thermal photons – short dashed line; 2) the neutron spectra from the photodisintegration of Fe nuclei – dotted line (from Bednarek 1992a).

1967) and the VHE photons are strongly attenuated (see Fig 5.4 curve a). Another restriction on the magnetic field in this model is connected with the reported evidence of a periodical emission of photons from Cyg X-3 at certain phases of the 4.8hr orbital period. In order to be self–consistent with this observation, the relativistic particles interacting with the photon field have to propagate almost linearly through the source diameter. This requirement puts an upper limit on the magnetic field of $\approx 1Gs$ for nuclei with energy $10^{16}eV$, Z=26, and source diameter $r = 10^{12}cm$.

To model the quiescent radio emission of Cyg X-3, Vestrand (1984) estimated a magnetic field strength of $B_{\perp}^{0} \approx 1000Gs$ at a distance $r \approx 10^{11}cm$ with a linear decrease for farther regions of the binary system. Stephens & Verma (1984) gave the lower limit $B_{\perp}^{0} \approx 100Gs$, from the consistency of radio observations with the Razin–Tsytovich effect. These lower limits on the magnetic field in Cyg X-3 are much higher than the above mentioned upper limits and therefore make this model inconsistent at TeV energies.

When the optical depth for nuclei in the radiation field is much less than the interaction length

for photoproduction processes, we can neglect the production of photons through the photoproduction of neutral pions. In such cases, it is possible to describe the neutral flux from Cyg X-3 in TeV and PeV energy range by the photon spectrum from deexcitations of nuclei if the spectrum of relativistic nuclei is a power law type with spectral index close to 2. However, the neutron flux in the EeV energy range from the photodisintegration of nuclei (calculated simultaneously) will be much higher than fluxes reported for Cyg X-3 by Cassiday et al. (1989,1990) and Teshima et al. (1990). Moreover, the previous problems concerning the limit on the magnetic field strength are still valid and the required luminosity of Cyg X-3 in relativistic nuclei should be even greater.

5.3.1.2 Interaction of relativistic protons with background matter

The mechanism of VHE photon production in p + p collisions (via π^0 decay) as a possible explanation of TeV and PeV emission from Cyg X-3 was first proposed by Vestrand & Eichler (1982). The fits of the general shape of the Cyg X-3 spectrum by the calculated photon spectra from p + p interaction in the thin target model were discussed by Bednarek et al. (1990) and Piskunova (1990). Here, we developed our previous calculations including self–consistently calculated spectra of neutrons from charge exchange of relativistic protons. In Fig 5.5 we show the observational data from Cyg X-3 above $10^{12}eV$ and the photon and neutron spectra for spectral index of primary proton spectrum equal to 2 and different cut–offs at $E_0 = 10^9 GeV, E_1 = 10^{10} GeV$ and $E_2 = 2.5 \times 10^{10} GeV$. As we can see, the fit to the observational data in the broad energy range by the calculated photon spectrum is quite good (for cut–off in proton spectrum $\approx 10^{10} GeV$), although the contribution of neutrons from charge exchange of protons in the EeV energy range is negligible. From this fit one can compute the proton luminosity in the energy range $10^2 - 10^{10} GeV$ for a distance to Cyg X-3 10kpc:

$$L_p[erg/s] \approx 5 \times 10^{38} \cdot \Delta\Omega[sr]/\delta t/x_H[g/cm^2], \qquad 5.3$$

where x_H is the column density of background matter in g/cm^2.

If we assume $x_H = 30 g/cm^2$, $\delta t = 1/20$ and $\delta\Omega = 1$, the proton luminosity is equal to $L_p \approx 3.2 \times 10^{38}[erg/s]$.

Again, the main problem of this model concerns the value of the average magnetic field which is required in the Cyg X-3 system in order to avoid strong attenuation of EeV photons in the magnetic field through magnetic pair production processes (Erber 1966). To be consistent with the positive detection of Cyg X-3 at about EeV, the average magnetic field strength up to a distance of $10^{13} cm$ from the center of the binary system should be on the order of $\sim 2Gs$. However, the lower limit on the value of the magnetic field ($\approx 100Gs$, see subsection 2.3.1.1) is much higher. The problems concerning requirements of nearly linear propagation of relativistic protons through source volume in order to guarantee photon emission in fixed phase of 4.8hr orbital period are also still valid.

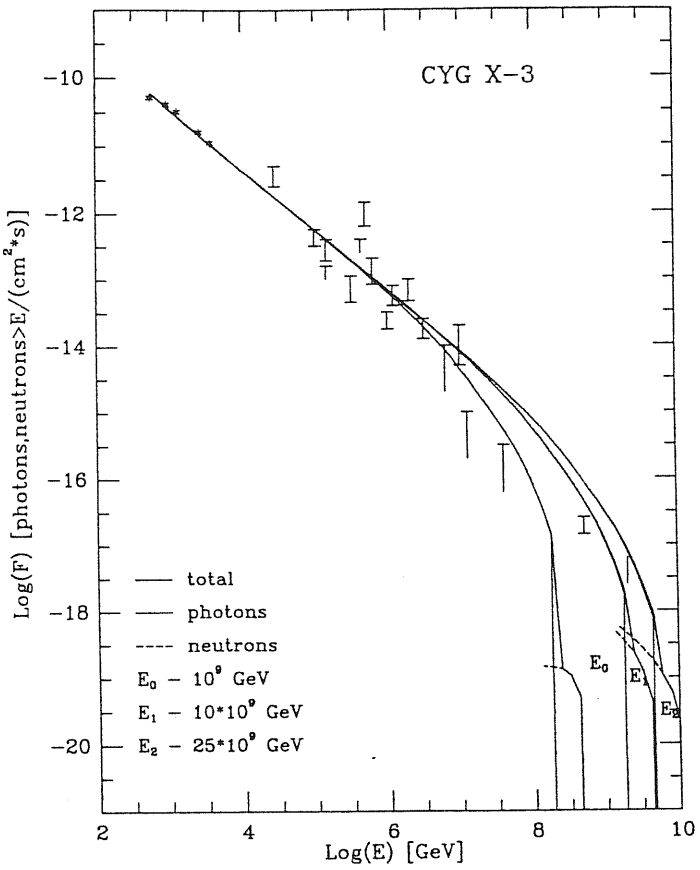

Figure 5.5: The observational results as in Fig. 1 fit by the spectra of photons and neutrons produced in the interaction of relativistic proton beam with background matter: dotted line - γ–ray spectrum from the decay of neutral pions; dashed line - spectrum of neutrons; full line - total spectrum (photons plus neutrons). The spectrum of relativistic protons is a power law with spectral index 2 and different cut–offs at E_0, E_1, E_2 (from bednarek 1992a).

5.3.1.3 Interaction of relativistic neutrons with matter

The emission of VHE neutrons by compact object is quite probable since it is difficult to imagine the escape of charged relativistic particles from very compact source. During propagation through a dense photon field (e.g., from the accretion disk or magnetosphere of neutron star) or through the high column density of matter with strong magnetic field (accretion), neutrons from the discharge of relativistic protons (and neutrinos) can be the only relativistic particles which escape without trouble (see, e.g., the model by Kazanas & Ellison 1986).

Based on such a scenario of neutron production, we have calculated the spectra of photons (from $n + p \rightarrow \pi^0; \pi^0 \rightarrow 2\gamma$) and neutrons (from $n + p \rightarrow n + ...$; plus neutrons which escaped without interaction) for the power law spectrum of neutrons with differential spectral index 2. The cut–off at the neutron spectrum was put at $4 \times 10^9 GeV$ (which is the maximum energy of particles observed from the direction of Cyg X-3; Cassiday et al. 1990). Since we do not know the duty cycle for neutron emission, we made calculations for a few different cases, among which: 0.05 - duty cycle

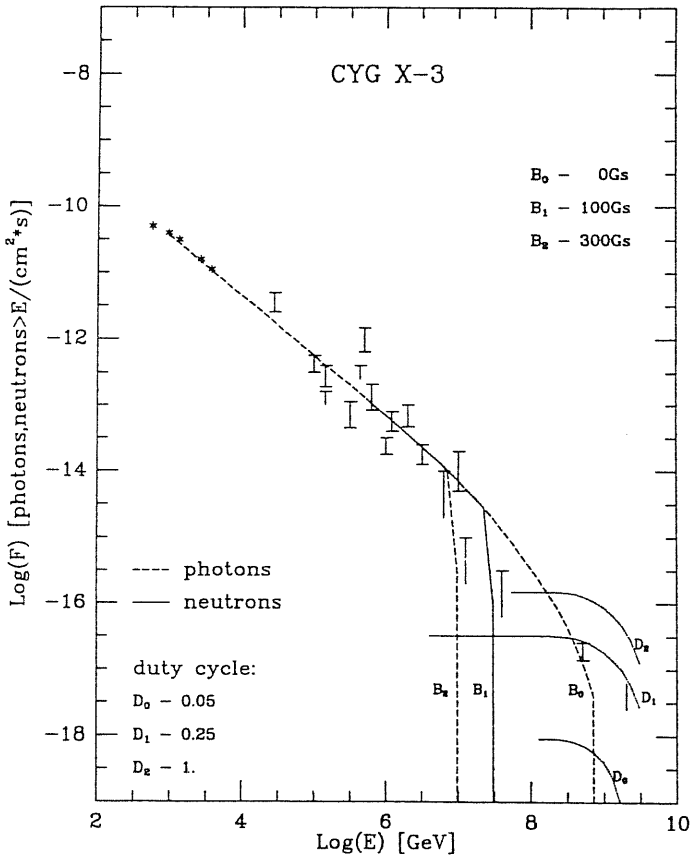

Figure 5.6: The observational results as in Fig.1 fit by the spectra of photons and neutrons produced in the interaction of relativistic neutron beam with background matter: dashed line - spectra of photons calculated for different values of magnetic field in the source region (B_0, B_1 and B_2); dotted line - spectra of neutrons calculated for different duty cycles of neutron emission D_0, D_1 and D_2. The spectrum of relativistic protons is a power law type with spectral index 2. and cut–off at $4 \times 10^9 GeV$ (from Bednarek 1992a).

observed in TeV and PeV photon energies; 0.3 - suggested by Cassiday et al. (1990) in EeV energies and 1. - suggested by Teshima et al. (1990) also in EeV energies.

The results of these calculations with their fit to the observed flux of particles from Cyg X-3 are shown in Fig. 5.6. As we can see, the best fit in EeV energies was obtained for a neutron duty cycle equal to ~ 0.25 (which is close to the value ~ 0.3 suggested by Cassiday et al. 1990). We note here that the obtained duty cycle for neutron emission (EeV energy range) is different from the duty cycle for photon emission (TeV and PeV energy range). This can be understood if only a small part of the broad neutron beam emitted by the compact object is obscured by background matter where photons are produced. Such a picture postulates that the photon emission can appear sporadically (when the observer is inside the broad cone of neutron beam) although the 4.8hr modulation during this active period can be observed.

The estimated neutron luminosity of the compact object in the energy range $10^2 - 4 \times 10^9 GeV$

is equal to:

$$L_n[erg/s] \approx 4.5 \times 10^{38} \cdot \Delta\Omega[sr]/\delta t/x_H[g/cm^2], \quad 5.4$$

where δt is the duty cycle for photon emission.

Corresponding to the above value, the luminosity of charged particles emitted by the compact object is about $2-4$ times higher (see estimations of the conversion of luminosity from protons to neutrons by Kazanas & Ellison 1986).

This model has two big advantages. First, there is no problem with linear propagation of relativistic neutrons in the Cyg X-3 binary system which allows one to observe particle emission concentrated in spatial phases of 4.8hr cycle. Second, the EeV emission is well described by neutrons which, contrary to photons, are not attenuated in the magnetic field of the binary system. The cut–off in the Cyg X-3 photon spectrum (at first calculated by Stephens & Verma 1984; and shown in Fig 5.6.) for average magnetic field $< B >= 100Gs$ and $300Gs$ and for a source radius $R = 10^{13}cm$, is not restrictive for the model. For such values of the magnetic field this model predicts a big dip in the integral spectrum of Cyg X-3 between $10 - 100PeV$.

5.3.1.4 Electromagnetic cascade initiated by monoenergetic particles

The mechanism of production of VHE photons in electromagnetic cascade initiated by monoenergetic protons with energy $\sim 10^{17}eV$ was applied to Cyg X-3 by Hillas (1984) in two scenarios:

- when the column density of background matter is very high ($\sim$ 16 radiation length) and the magnetic field is negligible;
- when the column density of matter is of the order of 1–4 radiation lengths but the magnetic field is of the order $\sim 500Gs$ (which is the value proposed by Vestrand 1983).

Both models can successfully describe the general shape of the Cyg X-3 spectrum in the TeV and PeV energy ranges if the luminosity of monoenergetic protons is $\sim 10^{39}erg/s$.

However, the efficiency of energy conversion of relativistic protons into photons with energy above $10^{12}eV$ is very small in the thick target model (less than 1%) while for the thin target models (e.g., $x_H \approx 30g/cm^2$), this value can be on the order of 10% (see, e.g., Stanev 1990). Therefore from an energetic point of view, the second proposition seems to be more relevant.

In the second proposition, Hillas (1984) showed that if the magnetic field in the matter is $> 10Gs$, an electromagnetic cascade develops through synchrotron emission of VHE photons since bremsstrahlung losses are much lower. However if we want to describe observations of EeV neutral emission from Cyg X-3 by this model, the magnetic field should be less than $\sim 2Gs$ in order not to attenuate EeV photons on magnetopair production process. This seems in contradiction with the assumption of a magnetic field strength $> 10Gs$, required by the model.

Moreover in both propositions, the EeV emission from Cyg X-3 cannot be described by the neutron flux from the discharge of relativistic protons, since it is proportional to the photon flux calculated in subsection 5.3.1.2 (see Fig. 5.5) and is not able to supply the reported flux at EeV energies.

A much more promising scenario able to explain recent observations also in EeV energies is the initialization of the above mentioned cascade by nuclei, e.g. helium (a possibility also suggested by Hillas). The energies of nuclei should be $\geq 10PeV$ in order to explain TeV–PeV emission but significant number of nuclei should have energy close to $\sim 10EeV$ in order to produce enough free neutrons (from fragmentation of He) in the EeV energy range.

For simple estimations we can assume that all He nuclei have energy $\sim 10EeV$ and the luminosity of Cyg X-3 in relativistic particles is $\sim 10^{39}erg/s$ (required to explain the flux in the TeV–PeV energy range). We can roughly calculate the total number of interacting He nuclei equal to $\sim 6 \times 10^{31}He/s$. For a column density of target matter equal to 2 radiation lengths, the number of neutrons produced in fragmentation of He nuclei is equal to $\sim 10^{32}neutr/s$ which corresponds to a neutron luminosity of $L_n \approx 2 \times 10^{38}erg/s$ above 1EeV. This value is the upper limit since, in reality, the nuclei with energy greater than $\sim 10PeV$ take part in the production of the observed flux of photons in the TeV–PeV energy range (but on the Earth we can observe only neutrons with energy $> 0.5EeV$). The derived upper limit is in very good agreement with the estimate of the total luminosity from Cyg X-3 above 0.5EeV equal to $2 \times 10^{35}erg/s$ (Cassiday et al. 1989) and allows one to explain the EeV emission by neutron flux.

The electromagnetic cascade discussed above cannot be initiated by relativistic neutrons because the time of decay of secondary muons (produced in neutron–proton interaction) with Lorentz factor $\sim 10^9$ into electrons is long enough for them to escape from the binary system. In this case an electromagnetic cascade will not develop.

5.3.1.5 Interaction of relativistic nuclei with matter

The interaction of relativistic nuclei (with a power law spectrum) with matter can be an efficient source of photons from π^0 decay and neutrons from fragmentation of nuclei. In the case of Cyg X-3, the nuclei cannot be very heavy since the data reported by the Fly's Eye experiment do not contain cosmic ray background events with energy greater than 80EeV which, for the most energetic particles reported from Cyg X-3, gives an upper limit of $Z \approx 20$ (Sommers & Elbert 1990).

If we take into account the Helium nuclei interacting with background matter, we can assume that very high energy protons and neutrons (bound in helium nuclei) interact with matter as separate particles. So, in rough approximation, the interaction of helium nuclei can be treated as a sum of processes discussed in subsections 5.3.1.2 and 5.3.1.3. Fig. 5.5 and 5.6 clearly show that it is

impossible to describe the flux from Cyg X-3 in the TeV–EeV energy range for a low column density of background matter because of the small flux of neutrons in EeV energy range and attenuation of photons with EeV energy in the magnetic field.

5.3.2 Conclusion

In this section we discussed the probable emission mechanisms of TeV–EeV neutral particles from discrete sources using as an example for detailed discussion Cyg X-3. We showed that, in principle, it is possible to fit the general shape of the spectrum of Cyg X-3 above $10^{11}eV$ by the spectra of photons and neutrons calculated according to different mechanisms (see Fig. 5.4, 5.5, 5.6). However, additional features of Cyg X-3 such as: 1) the required luminosity of relativistic particles derived from the above fits; 2) the value of magnetic field suggested in the Cyg X-3 binary system (Vestrand 1983; Stephens & Verma 1984); and 3) the observations of VHE emission in spatial phases of the 4.8hr orbital period , allow us to reject the mechanisms of:

- interaction of relativistic nuclei with the background radiation field;
- interaction of relativistic protons with matter;
- electromagnetic cascade initiated by monoenergetic protons;
- interaction of relativistic nuclei with matter.

Two mechanisms are able to describe the VHE neutral emission and they are not in contradiction with the above mentioned features of Cyg X-3 system. In the first model, the interaction of relativistic neutrons (emitted by compact object) with low column density background matter is able to describe the TeV and PeV emission from Cyg X-3 by photon spectra produced from the decay of π^0 and EeV emission by neutrons from $n+p \rightarrow n+...$; plus neutrons which escape without interaction (Fig. 5.6). The spectrum of neutrons was assumed as a power law E_n^{-2} with cut–off at $4 \times 10^9 GeV$ (which is the maximum energy of particles from Cyg X-3 reported by Cassiday et al. 1990) and a duty cycle of neutron emission 0.25 (the value ~ 0.3 was suggested by Cassiday et al. 1990 on the basis of observations). The required neutron luminosity $L_n \approx 4.5 \times 10^{38} \cdot \Delta\Omega[sr]/\delta t/x_H[g/cm^2]$ above $10^2 GeV$ is reasonable if $x_H = 20 \div 30 g/cm^2$ and the duty cycle of photon emission $\delta t = 1/20$. We note that only a part of the broad neutron beam (duty cycle ~ 0.25) emitted by the compact object is obscured by background matter where photons are produced. This conclusion suggests the possibility of long term sporadic appearance of VHE photon emission. During this active phase the emission is modulated according to the orbital period of 4.8hr.

In the second model (proposed by Hillas, 1984), the TeV and PeV emission from Cyg X-3 was successfully described by VHE photons produced in electromagnetic cascade initiated by monoenergetic relativistic particles. However, EeV emission cannot be explained in terms of photon

production since photons should be strongly attenuated in magnetic field on magnetopair production process (see, Stephens and Verma 1984 and discussion in subsection 5.3.1.1). We suggest that if nuclei (e.g. helium) are the primary particles initiating the cascade as calculated by Hillas, then the EeV emission can be caused by neutrons from their fragmentation. The $\sim 10^{39} erg/s$ (assuming isotropic emission) needed for the explanation of TeV–PeV emission from Cyg X-3 can also explain the observed luminosity $\sim 2 \times 10^{35} erg/s$ above 0.5EeV, if $\approx 0.5\%$ of luminosity of Cyg X-3 is in the form of relativistic helium nuclei with energy close to $\sim 10 EeV$.

This chapter is partially based on the paper *"The emission mechanism of neutral particles from discrete sources in TeV–EeV energy range"*, 1992a, A&A (in press) by W. Bednarek (included in an Appendix).

References

Acharya, B.S. et al. 1991, 22nd ICRC (Dublin) 1, 237
Alexeenko, V.V. et al. 1987, 20th ICRC (Moscow) 1, 219
Balashov, V.V., Korotkikh, V.L. & Moskalenko I.V. 1990, 21st ICRC (Adelaide) 2, 416
Baltrusaitis, R.M. et al. 1985, ApJL 293, L69
Baltrusaitis, R.M. et al. 1987, ApJ 323, 685
Becklin, E.E. et al. 1972 Nat.Phys.Sci. 239, 130
Bednarek, W. 1992a, A&A in press
Bednarek, W., Karakuła, S. & Tkaczyk, W. 1990, 21st ICRC (Adelaide) 2, 79
Bhat, P.N., Ramana Murthy, P.V. & Visvanath, P.K. 1988, Astrophys.Astron. India 9, 155
Bhat, C.L. et al. 1991, ApJ 369, 475
Bignami, G.F., Maraschi, L. & Treves, A. 1977, A&A 55, 155
Bonnet-Bidaud, J.M., Chardin, D., 1988, Phys.Rep. 170, 326
Bowden, C.C.G. et al. 1991, 22nd ICRC, 1, 356
Bowden, C.C.G. et al. 1992, J. Phys. G: Nucl. Phys. 18, 413
Brazier, K.T.S. et al. 1990a, 21st ICRC (Adelaide), 2, 379
Brazier, K.T.S. et al. 1990b, ApJ 350, 745
Caraminana, A. et al. 1989, ApJ 346, 967
Cassiday, G.L. et al. 1989, Phys.Rev.Lett. 62, 383
Cassiday, G.L. et al. 1990, 21st ICRC (Adelaide) 4, 282
Chadwick, P.M. et al. 1985a, Nat 318, 642
Chadwick, P.M. et al. 1985b, A&AL 151, L1
Chadwick, P.M., McComb, T.J.L. & Turver, K.E. 1990, J.Phys. G: Nucl.Phys. 16, 1773
Chanmugam, G. & Brecher, K. 1985, Nat 313, 767
Chardin, G. & Gerbier G. 1989, A&A 210, 52
Cheng, K.S. & Ruderman, M. 1989, ApJL 337, L77
Cheng, K.S. & Ruderman, M. 1991, ApJ 373, 187
Ciampa, D., Clay, R.W. & Edwards, P.G. 1989, ApJ 346, 151
Clay, R.W. et al. 1992, A&A 255, 167
Cropper, M. 1990, Sp.Sci.Rev. 54, 195
Dolan, J.F. et al. 1982, Astrophys.Lett. 22, 147
Dowthwaite, J.C. et al. 1984, Nat 309, 691
Erber, T. 1966, Rev. Mod. Phys. 38, 626
Fegan, D.J. et al. 1989, A&A 211, L1
Fegan, D.J. 1990, 21st ICRC (Adelaide) 11, 23
Fermi, E. 1949, Phys.Rev. 75, 1169
Fermi, E. 1954, ApJ 119, 1
Fichtel, C.E., Thompson, D.J. & Lamb, R.C. 1987, ApJ 319, 362
Frank, J.F., King, A.R. & Raine, D.J. 1985, *Accretion Power in Astrophysics*, (Cambridge University Press, Cambridge)

Galper, A.M. et al. 1976, Sov.Astr.Lett. 2, 206
Giacconi, R. et al. 1967, ApJL 148, L119
Giacconi, R. et al. 1971, ApJL 167, L67
Giovannelli, F. & Martinez-Pais, I.G. 1991, Sp.Sci.Rev. 56, 313
Giovannelli, F. & Sabau Graziati, L. 1992, Sp.Sci.Rev. 59, 1
Geldzahler, B. et al. 1983, ApJL 273, L65
Goodman, J.A. 1990, Nucl.Phys. B (Proc.Suppl.) 14A, 84
Gould, R.J., Schreder, G.P. 1967, Phys.Rev. 155, 1404
Gould, R.J., Rephaeli, Y. 1978, ApJ 225, 318
Gregory, A.A. et al. 1990, A&AL 237, L5
Harding, A.K. & Gaisser, T.K. 1990, ApJ 358, 561
Harding, A.K. 1991,*Frontier Objects in Astrophysics and Particle Physics*, eds. F.Giovannelli & G. Mannocchi, SIF, v.28, p.243
Hayashida, N. et al. 1991, 22nd ICRC (Dublin) 1, 309
Hermsen, W. et al. 1987, A&A 175, 141
Hess, V.F. 1912, Phys. Z. 13, 1084
Hillas, A.M. 1984, Nat 312, 48
Hillas, A.M. 1987, *VHE Gamma-Ray Astronomy*, ed. K.E. Turver (Dordrecht: Reidel), p. 71
Hillas, A.M & Johnson, P.A. 1991, 22ICRC (Dublin), v.2, p.452
Johnson, P.A. 1991, 22ICRC (Dublin), v.2, p. 440
Joss, P.C. & Rappaport, S.A. 1984, ARAA 22, 537
Katz, J.I. & Smith, I.A. 1988, ApJ 326, 733
Kazanas, D. & Ellison, D.C. 1986, Nat 319, 380
Kiraly, P. & Meszaros, P. 1988, ApJ 333, 719
Kirk, J.G. & Schneider, P. 1987, ApJ 315, 425
Kirk, J.G. & Mastichiadis, A. 1989, A&A 213, 75
Lamb, R.C. et al. 1977, ApJL 212, L63
Lambert, J. et al. 1985, 19th ICRC (La Jolla) 1, 245
Lawrence, M.A., Prosser, D.C. & Watson, A.A. 1989, Phys.Rev.Lett. 63, 1121
Lewin, W.H.G. & van den Heuvel, E.P.J. 1983, *Accretion-driven stellar X-ray sources*, (Cambridge University Press, Cambridge)
Li, T. & Wu, M. 1989, ApJ 246, 391
Lloyd–Evans, J. et al. 1983, Nat 305, 784
Mannheim, K. & Biermann, P.L. 1989, A&A 221, 211
McKay, T.A. et al. 1991, 22nd ICRC (Dublin) 1, 230
McKechnie, S.P. et al., Mount, K.E. & Ramsden, D. 1976, ApJL 207, L151
Meegan, C.A., Fishman, G.J. & Haymes, R.C. 1979, ApJL 234, L123
Meintjes, P.J. et al. 1991, 22nd ICRC, 1, 360
Meyhandan, R. et al. 1992, ApJ 391, 236
Mitra, A. 1991, ApJ 370, 345
Molnar, L.A., Reid, M.J. & Grindlay, J.E. 1988, ApJ 331, 494
Moskalenko, I.V. & Fotina, O.V. 1989, Yad. Fiz. (USSR) 49, 1623
Muraki, Y. et al. 1991a, ApJ 373, 657
Muraki, Y. et al. 1991b, 22nd ICRC (Dublin) 1, 245
North, A.R. et al. 1987, Nat 326, 567
North, A.R. et al. 1990, 21st ICRC (Adelaide), 2, 275
Persignault, D. et al. 1972, Nat. Phys. Sci. 239, 123
Piskunova, O.I. 1990, Sov. J. Nucl. Phys. 51, 846
Priedhorsky, W. 1985, Sp.Sci.Rev. 40, 305
Priedhorsky, W. 1986, ApJL 306, L97
Pringle, J.E. 1981, ARAA 19, 137
Protheroe, R.J., Clay, R.W. & Gerhardy, P.R. 1984, ApJL 280, L47
Protheroe, R.J. & Clay, R.W. 1985, Nat 315, 205
Protheroe, R.J. & Stanev, T. 1987, Nat 328, 136
Ramana Murthy, P.V. 1990, Nucl.Phys. B (Proc.Suppl.) 14A, 73
Raubenheimer, B. et al. 1989, ApJ 336, 394
Rees, M.J. & Gunn, J.E. 1974, MNRAS 167, 1
Reppin, C. et al. 1979, ApJ 234, 329

Resvanis, L. et al. 1986, *Workshop on VHE Gamma Ray Astronomy*, (Durham), Reidel, Holland, p. 105
Reynolds, P.T. et al. 1991, ApJ 382, 640
Samorsky, M. & Stamm, W. 1983, ApJL 268, L17
Schreier, E. et al. 1972, ApJL 172, L79
Shapiro, S.L. & Teukolsky, S.A. 1983, *Black Holes, White Dwarfs and Neutron Stars*, A Wiley-Interscience Publication, New York
Smith, I.A., Katz, J.I. & Diamond, P.H. 1992, ApJ 388, 148
Sommers P. & Elbert J.W. 1990, Astro.Lett. & Commun. 27, 397
Stanev, T. 1990, Nucl.Phys. B (Proc. Suppl.) 14A, 17
Stecker, F.W. 1973, Ap&SS 20, 47
Stepanian, A.A. et al. 1972, Nat.Phys.Sci. 239, 40
Stepanian, A.A. 1989, *Frontier Objects in Astrophysics and Particle Physics*, eds. F.Giovannelli & G. Mannocchi, SIF, v.19, p.251
Stephens, S.A. & Verma, R.P. 1984, Nat 308, 828
Strom, R.G., van Paradijs, J. & van der Klis M. 1989, Nat 337, 234
Szkody, P. & Cropper, M. 1988, *Multiwavelength Astrophysics*, (Cambridge University Press, Cambridge)
Tananbaum, H. et al. 1972, ApJL 174, L143
Teshima, M. et al. 1990, Phys.Rev.Lett. 64, 1628
Tonwar, S.C. et al. 1992, ApJ 390, 273
Treves, A., Maraschi, L. & Abramowicz, M. 1989, *Accretion. A Collection of Influential Papers*, World Scientific, Singapore
Trümper, J. et al. 1978, ApJ 219, 105
Trümer, J., Lewin, W.H.G. & Brinkmann, W. 1985, *The Evolution of Galactic X-Ray Binaries*, Reidel Publishing Company, Dordrecht, NATO ASI, v. 167
Turver, K.E. 1991, Nucl.Phys. B (Proc.Suppl.) 22B, 86
van den Heuvel, E.P.J. 1985, *The Evolution of Galactic X-Ray Binaries*, eds. J. Trümer, W.H.G. Lewin & W. Brinkmann, Reidel Publishing Company, Dordrecht, NATO ASI, v. 167, p.107
van Kerkwijk, M.H. et al. 1992, Nat 355, 703
Vestrand, W.T. 1983, ApJ 271, 304
Vestrand, W.T. & Eichler, D. 1982, ApJ 261, 251
Vladimirsky, B.M., Stepanian, A.A. & Fomin V.P. 1973, 13th ICRC (Denver) 1, 456
Ulmer, M.P. et al 1974, ApJ 192, 691
Watson, A.A. 1985, 19th ICRC (La Jolla) 9, 111
Weekes, T.C. 1988, Phys.Rep. 160, 1
Weekes, T.C. 1992, Sp.Sci.Rev. 59, 314
Wheaton, W.A. et al. 1979, Nat 282, 240

6 γ-ray emission from AGNs

Active Galactic Nuclei (AGN) is a common name of particular types of galaxies (e.g. radio galaxies, Seyfert galaxies, quasars, BL Lac objects etc ...)[1] which show violent activity in their nuclei. The nuclei are very compact[2], emit nonthermal radiation with luminosity in a big range (from $10^8 L_\odot$ up to $10^{15} L_\odot$) and show rapid variability of radiation flux on time scales as short as minutes. Many AGNs show both small and large scale structures (in the range from parsecs up to a few hundred kpc) which are (or are supposed to be) morphologically linked with the central core. The radio maps show extended lobes (usually symmetrically situated on both sides of the central core) and highly collimated jets sometimes seen also in optical and even the X-ray photon energy range. From the central parts of some quasars and BL Lac objects emerge irregularly blobs (observed in radio wavelengths) with apparent speed greater than velocity of light (superluminal motion). Although this was a surprising feature, it can be well understood if we accept that the blobs are moving within a small angle towards us with relativistic velocity. The photon spectra of AGNs are often nonthermal (flat in the central core and steep in the blobs) and extend through all parts of the electromagnetic range, from radio to γ-rays. There are also observed a variety of broad and narrow emission lines, bumps in the spectrum (e.g. the most famous being the UV bump) and even in a few cases, X-ray iron lines. These basic observational facts were discussed in many general reviews (see e.g. Begelman et al. 1984; Wiita 1985) and reviews dedicated to specific problems. For instance, compact radio sources were discussed by Kellerman & Pauliny-Toth (1981); extragalactic radio jets by Bridle & Perley (1984) and Begelman et al. (1984); emission line regions of AGNs by Osterbrock & Mathews (1986); polarization properties of extragalactic sources by Saikia & Salter (1988); variability of extragalactic radio sources by Altschuler (1989); multiwavelength studies of AGNs by Urry (1988); continuum radiation from AGNs by Bregman (1990); superluminal motion in AGNs by Cohen (1986).

It is a big challenge for scientists working in the theory of extragalactic objects to explain the enormous amount of energy generated in the very compact central engine of AGNs. Below we

[1] This is a few percent of the known galaxies.

[2] No information about the structure of the central engine can be obtained by any observational technique. The present angular resolution of the Very long Baseline Interferometry technique $\sim 10^{-3} arcsec$ corresponds to the linear distance of $\sim 10^{17} cm$ in the case of the closest AGNs.

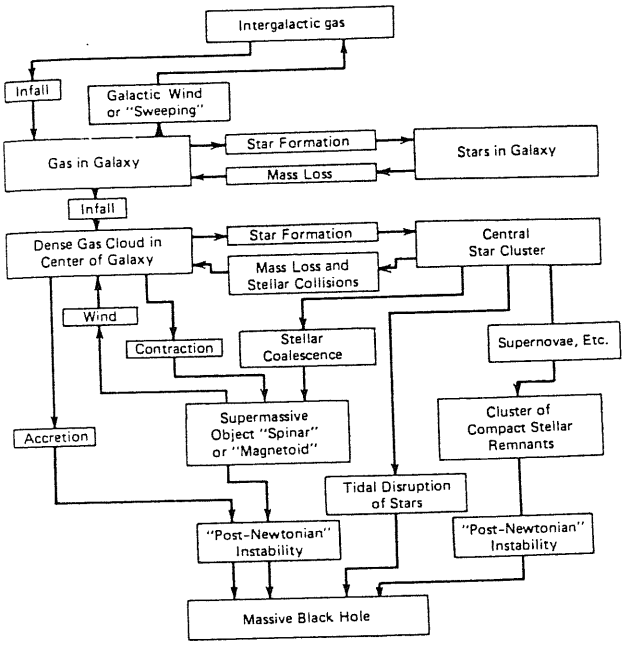

Figure 6.1: The diagram indicating the ways leading to formation of a massive black hole in the galactic center (from Begelman et al. 1984).

will review general theoretical models in more detail, since, in their terms, the production of γ-ray radiation by AGNs should be clearly envisaged. Although a few different propositions appeared (e.g. matter–antimatter annihilation, multiple supernova explosions, 'white holes', explosions initiated by tidal disruption of stars around black holes, multiple neutron star systems), two are the most likely: supermassive stars and accreting black holes.

Supermassive stars (spinars)

The possibility that AGNs may be powered by supermassive stars stabilized by rotation (analogy to the pulsar model) was first proposed by Morrison (1969) and production of radiation by AGNs in such model was discussed by, for example Cavaliere et al. (1970) and Pacini & Salvati (1978). Other mechanisms of stabilization of supermassive stars by magnetic fields (Ozernoi & Chertoprid 1966) or radiation pressure (Hoyle & Fowler 1963) were also suggested. Such models have the advantage that the rotation and/or magnetic field symmetry defines a direction in space along which jets could be generated. However in the spinar model we should expect periodicities with characteristic times corresponding to the spinar period which are not observed[3]. Moreover it is argued that spinars should become dynamically unstable (see, e.g Ozernoy & Usov 1971), and after relatively short time collapse to a black hole.

[3] Accept one case: the Seyfert galaxy NGC 6814 in which long lived period of 12130.39±0.05 seconds was discovered (Kunieda et al. 1991). Can this source be interpreted in terms of spinar model ?

Accretion onto a black hole

The formation of a massive black hole (BH) in galactic nuclei is expected in most of the scenarios of the evolution of matter in a galaxy (see Fig. 6.1). Once a supermassive HB has formed, it will exist in the nucleus for an extremely long time[4] and will continue accretion of galactic matter. The idea that accretion processes onto a BH could produce the enormous amounts of energy observed in AGNs was first postulated by Zeldovich (1964) and Salpeter (1964). However, the detailed studies of spherical accretion onto BH (see, e.g., Shvartsman 1971; Shapiro 1973) show that the efficiency of gravitational energy conversion into radiation is only on the order of few percent (not more than 10% in the best scenarios) and only lower luminosity objects (with $L/L_{Edd} \approx 10^{-2}$)[5] can be fit (Krolik & London 1983). Moreover other arguments (angular momentum of infalling galactic gas or observations of aspherical structure of AGNs) support the accretion scenarios onto BH via formation of a disk or torus. Four general modes of such disk accretion have been distinguished and the choice between them depends on the accretion rate of the matter (Fig. 6.2). They are:

- *An Ion torus* should form if accreting matter is unable to cool efficiently on the infall timescale (see Rees et al. 1982). This may happen if the accretion rate is low ($\dot{m} < 0.1$ [6]). In such a case a two temperature, thick torus may form with high temperature ions ($\sim 100 MeV$) emersed in low temperature electrons ($\sim 10 keV$). The high energy radiation may be produced through hadronic interactions.

- *A thin accretion disk* should form if the accretion rate is increased ($0.1<\dot{m}<10$). The first calculations of the structure and radiation spectrum of such disks were done by Pringle & Rees (1972), Shakura & Sunyaev (1973) and Novikov & Thorne (1973). The expected spectrum is a modified black body with characteristic temperatures on the order of 1 keV.

- *A radiation tori* should form when the accretion rate is high ($10<\dot{m}<100$). In this case radiation pressure dominates the gas pressure and the structure of the torus can be computed if the distribution of angular momentum and entropy is specified (see e.g. Jaroszyński et al. 1980). The interesting feature of such structures is the formation of narrow funnels, along the rotational axis, from which luminosity can exceed L_{Edd} (see Abramowicz et al. 1980). However, the effective temperature of this radiation is low and high energy photons are not produced in the disk.

- *Super-critical Accretion.* At the highest accretion rates ($\dot{m} > 100$) most of the accreted matter will be expelled by energy generated from the small amount of matter which is able to reach

[4] The only known process for the disappearance of a BH, quantum evaporation (Hawking 1974), is very inefficient in the case of massive BH.

[5] $L_{Edd} \cong 1.3 \times 10^{38} \cdot M_{BH}/M_{\odot}$ $erg\ s^{-1}$ is the Eddington limit.

[6] $\dot{m} = \dot{M}_{acc}/\dot{M}_{Edd}$, where $\dot{M}_{acc}$ is the accretion rate in [g/s] and $\dot{M}_{Edd} \equiv L_{Edd}/c^2$.

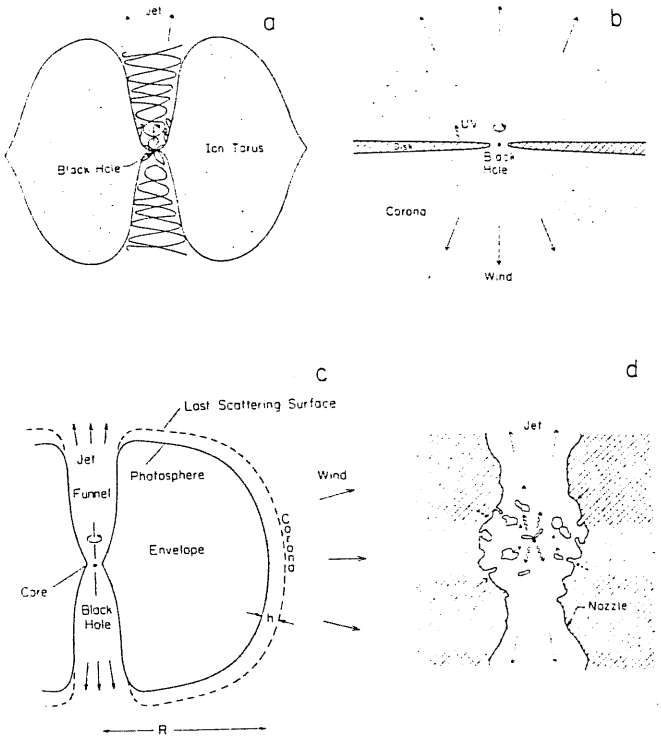

Figure 6.2: Four modes of disk accretion: (a) Ion torus, (b) thin disk and corona, (c) Radiation torus, and (d) Super–critical accretion (from Blandford 1985).

the black hole. The outflowing matter may either take the form of a wind (Meier 1982) or a radiation dominated jets (the "cauldron" model of Begelman & Rees 1984).

Another interesting possibility of energy generation in AGNs is the extraction of rotational energy of the BH. The idea that particles interacting and escaping from the ergosphere[7] may gain energy from the BH was proposed by Penrose (1969) and next developed in the context of inverse Compton scattering by Piran & Shaham (1977) and pair production by Leiter & Kafatos (1978). In principle, it is possible to extract, up to ~29% of BH's rest–mass energy from speedily rotating BH. Other possibility, in which rotating BH hole is coupled with the accretion disk via an anchored magnetic field (dynamo mechanism), were proposed by e.g. Lovelace (1976) and Blandford & Znajek (1976). In these kinds of models (they favour the ion tori scenario around BH), the electric field is induced along the rotational axis, allowing acceleration of particles and creation of highly collimated relativistic jets (see, e.g., Wang et al. 1990).

The above theoretical considerations bring us to a basic question: *What is the interdependence between theoretical models and observations of different types of AGNs ?* The answer is not easy since, in principle, many free parameters may be essential (accretion rate, BH mass, angular momentum of matter, magnetic field and, what is particularly difficult to include, the microphysics

[7]The ergosphere is the region between the event horizon and the static limit for rotating and/or charged BH described by $r(\theta) \equiv M + \sqrt{m^2 - Q^2 - a^2 \cdot cos^2\theta}$ where M,Q and a are mass, charge and angular momentum per unit mass (all in normalized units) respectively and θ is measured from the rotational axis of BH

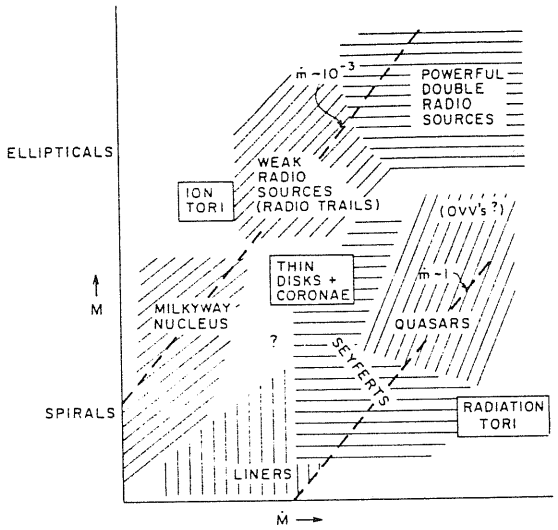

Figure 6.3: A two–dimensional "unified" AGN scheme is displayed schematically in the $\dot{M}$ - M plane (from Begelman 1986).

which determines, viscosity, radiation production and transfer). First efforts of early construction of unified models of all AGNs have been undertaken. For instance, Begelman (1986) proposed that differences between different classes of AGNs are determined by two parameters: accretion rate and mass of the BH, see Fig. 6.3 for results of his analysis. However it is also argued that the viewing angle in the case of axi–symmetric system play a very important role (see recent review by Urry et al 1991). The observed differences between Seyfert I and Seyfert II galaxies (Antonucci & Miller 1985) or between quasars and BL Lac objects can be explained in terms of this parameter.

After these general remarks we concentrate in this chapter on γ-ray emission from AGNs. In the next section (6.1) we review the main observational data collected during the last 20 years and new results (although preliminary and very fragmentary) obtained by the Compton GRO and SIGMA telescopes. Section 6.2 is dedicated to theoretical interpretations of production of high energy radiation in AGNs from the viewpoint of radiation mechanisms. In the two last sections (6.3 and 6.4) we discuss, in more detail, the observational results concerning two specific AGNs: quasar 3C 273 and quasar 3C 279. We propose possible physical scenarios in which γ-ray production in these two sources can be envisaged.

6.1 Observations

The large number of extragalactic sources observed in hard X-rays suggests that an essential part of AGNs energy should be emitted in the γ-ray energy range. In spite of many experiments, technical problems concerning observations of very low γ-ray fluxes and poor angular resolution of detectors

allowed positive identification of only a few AGNs. The situation changed completely after launching Compton GRO whose results concerning γ-ray emission from AGNs are *'revolutionary'* for this topic. Since preliminary analysis of GRO data is in progress and only fragmentary information is available we will start a short review of the observations of AGNs in the γ-ray energy range from the era before Compton GRO. For detailed reviews in which γ-ray emission from extragalactic objects is reported, we refer to for example Ramaty & Lingenfelter (1982); Trombka & Fichtel (1983); Bassani et al. (1985); Fichtel (1986); Weekes (1988) or to the rapporteur talks during International Cosmic Ray Conferences.

Early positive detections of AGNs in γ-rays concern different classes of objects. They are:

- Quasar - 3C 273 (SAS 2 and COS B data)
- Radio galaxy - Centaurus A (MeV and TeV energy range)
- Seyfert galaxies - NGC 4151 and MCG8-11-11 (MeV range, Perotti et al. 1981)

There is also weak evidence of an excess in COS B data from the direction of NGC 1275 reported as by Strong & Bignami (1983). In Fig. 6.4 are shown photon spectra in X- and γ-ray energy range of some of them. Below we will discuss two of the three best investigated (NGC 4151 and Cen A) in more detail in order to show how scarce is our knowledge. A more detailed review of 3C 273 is included in section 6.3.

NGC 4151

Low energy γ–ray emission up to about 19 MeV from the direction of NGC 4151 was detected for the first time in May 1977 by the MISO telescope (Perotti et al. 1979). The measured spectrum follows the spectral index from the X-ray energy range, and after about 3MeV breaks into a very steep spectrum. Observations of the source using this same telescope in September 1979 (Perotti et al. 1981), generally confirmed the shape of the spectrum (spectral index of 1.3 ± 0.3 before the break), however the γ–ray luminosity in the energy range 0.5–5 MeV showed reduction on the order of 4 ± 2. The three positive observations of soft γ–rays up to 2 MeV were also reported by HEAO 1 satellite (Baity et al. 1984). Results of the two observations can be well fit by a power law photon spectrum with index $\approx 1.6 \pm 0.1$ in the 2 keV–2 MeV energy range. The third observation shows a clear break in the spectrum above 50 keV. Moreover, the upper limits in this energy range, reported by other balloon experiments (Meegan and Haymes, 1979), are at a much lower level. We would like to note here that the observations in soft γ-ray energy range are performed with wide field of view detectors and interpretation of an excess as caused by one steady source may be misleading.

From analysis of the above observations, it seems to be evident that the γ–ray intensity from the direction of NGC 4151 is highly variable within a factor of 3–10 over time scales of months

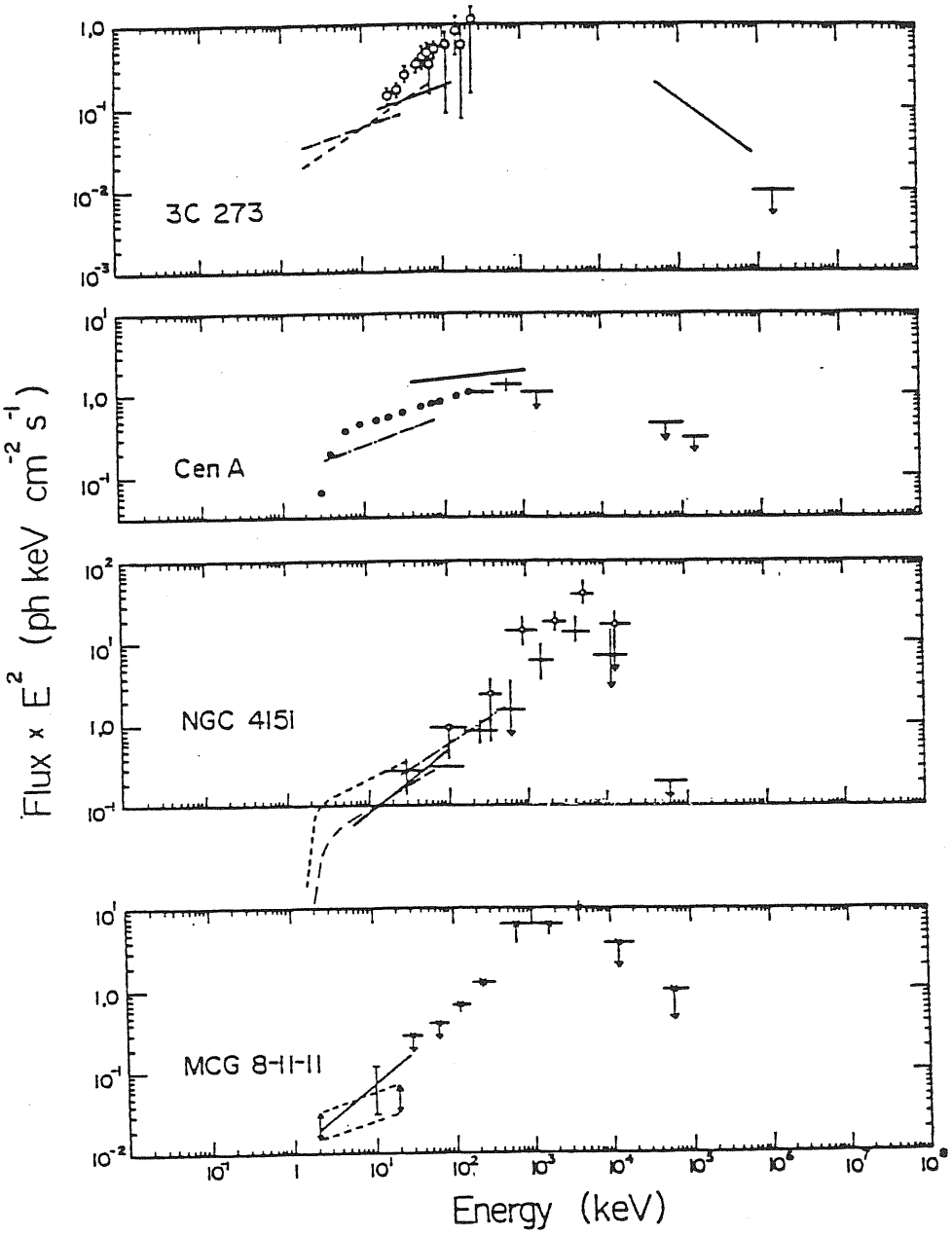

Figure 6.4: The photon emission spectra observed from some AGNs. A major fraction of the emitted power is concentrated in low energy γ-rays which underlines the importance of γ-ray observations (from Bassani & Dean 1983)

(Bassani et al. 1985). There is also some evidence of simultaneous variation of soft γ-rays with the photon emission below 100 keV (Baity et al. 1984). The sharp change in the γ–ray spectrum of NGC 4151 above a few MeV is also postulated by the upper limits reported by SAS 2 and COS B satellites between 35–200MeV (Bignami et al. 1979; Pollock et al. 1981). In the TeV energy range only some upper limits are available (Cawley et al. 1985). The general photon spectrum from the direction of NGC 4151 in X and γ–ray range is shown in Fig 6.4.

Centaurus A (NGC 5128)

The soft γ–ray emission from the direction of Cen A was observed in a few experiments. The continuum emission (from hard X–rays to soft γ–rays) was described by a power law spectrum with spectral index –1.9 between 40–1000 keV by Hall et al. (1976); –1.6 between 10–140 keV and –2. between 140–2300 keV by Baity et al. (1981); –1.59 between 100–500 keV by Gehrels et al. (1984). The above results are consistent in the limits of errors. In the higher energy region, Von Ballomoos et al. (1987) detected this source with 4σ significance level and found that the spectrum between 0.7–20 MeV can be described by a power law with spectral index –1.4. However, extrapolation of this spectrum to higher energies is clearly above the observations of γ–rays by SAS 2 satellite between 35–100 MeV (Bignami et al. 1979) and COS B between 50–200 MeV (Pollock et al. 1981) which yielded the upper limits of $10^{-10}\ photons\ cm^{-2}s^{-1}keV^{-1}$ and $2.5\times10^{-11}\ photons\ cm{-}2s^{-1}keV^{-1}$, respectively. Moreover, the 3σ upper limits derived by O'Neill et al. (1989) are a factor of 2 below the results reported by Von Ballmoos et al. If these observations are true, strong variability of the flux in the MeV range seems to be sure. For the general spectrum of Cen A in X- and γ-ray energy range, see Fig. 6.4. The detection of broad emission lines at 1.6 MeV and 4.5 MeV with 3.3σ significance from the direction of Cen A was reported by Hall et al. (1976). However these lines were not observed by the following experiments and only upper limits were derived.

The only statistically significant detection of Cen A above 0.3 TeV (with 4.6σ) was reported by Grindlay et al. (1975a). The detected flux was $(4.4\pm1.0)\times10^{-11}\ photons\ cm^{-2}\ s^{-1}$ for energies >0.3 TeV. Recently, the derived 3σ upper limit of $7.8\times10^{-11}\ photons\ cm^{-2}\ s^{-1}$ at energies >0.3 TeV (Carraminana et al. 1990) is apparently compatible with the flux reported by Grindlay et al. (1975a). At energies >1 PeV, there exist only an upper limit of $10^{-14}\ photons\ cm^{-2}\ s^{-1}$ derived by Clay et al. (1984), although a slight excess in the error box containing Cen A (2.7σ significance level) was also mentioned. However, one should expect a large attenuation of γ–rays with energies 0.1–10 PeV on 2.7K black–body radiation propagating through the distance of 4–6 Mpc to Cen A.

Summing up, in spite of the small distance to the Cen A, our knowledge about its γ–ray emission is poor. Only soft γ-ray emission seems to be well documented. Sporadic positive observations in higher energies (2-20 MeV; TeV; PeV) are not confirmed and at least strongly suggest variability

of this source.

The re-analysis of SAS 2 data by Young & Yu (1988) shows 15 AGNs at photon energies above 100 MeV, but reliability of these results is poor because of the relatively small number of photons collected by the SAS 2 detector and the big error boxes of data collection. There are also upper limits available in the literature for several AGNs obtained in TeV photon energies (Cawley et al. 1985; Vacanti et al. 1990) and derived from SAS 2 and COS B data close to 100 MeV (Bignami et al. 1979; Pollock et al. 1981). They may be of importance in future studies of the variability of the AGNs recently detected in the γ-ray energy range.

The turning point in γ-ray observations of AGNs started 1-2 years ago when the first results appeared from SIGMA and Compton GRO detectors. It is now clear that high energy photon emission from AGNs is highly variable. For instance, applying imaging facilities of the SIGMA telescope, Jourdain et al. (1991) found a break in the photon spectrum of NGC 4151 close to 50 keV (which is in agreement with older observations by Baity et al. 1984 and Bassani et al. 1986). On the contrary, recent results by Maisack & Yaqoob (1991) and Perotti et al. (1991) indicate the power law photon spectrum extending to at least a few hundred keV. Similar behaviour was discovered in the case of 3C 273 (Bassani et al. 1991). The quasar shows the evidence of variability in intensity by a factor of 2.7 ± 1 on a time scale of a month in hard X-rays.

However the most exciting results have been announced by the team working with EGRET detector on board of Compton GRO. Preliminary results show very intense γ-ray emission from several AGNs at photon energies above 100 MeV. Up to now 14 sources were tentatively identified[8]. They are: 3C 279 (Hartman et al. 1992a; Kanbach et al. 1992), PKS 0202+149, PKS 0420-014, PKS 0235+164 (Hartman et al. 1992b), QSO 0836+710 (Fichtel et al. 1992), 3C 454.3, CTA 102 (Michelson et al. 1992), PKS 208-512, 4C38.41, PKS 0528+134, Mrk 421, QSO 0710-714, 3C 273, PKS 0537-441. It is evident that most of the power emitted by these sources is concentrated in high energy γ-rays (assuming isotropic emission). Moreover some sources (e.g. 3C 279) show significant variability on a time scale of days. These two basic facts (luminosity and variability) are challenging for present theoretical models of radiation production in AGNs.

A very intriguing new result has been obtained recently by the Whipple γ-ray collaboration (Weekes 1992b). TeV γ-rays have been detected from the BL Lac object Mkn 421 between Mar. 24 and May 8. A flux was detected in 409 min of observation at the 5 σ level. The flux was 1.2×10^{-11} $photons/cm^2/s$ above 0.5 TeV with no evidence of variability during the observations. During this same observing interval no TeV flux was detected from 3C 279, PKS 0528+134, QSO 0836+710 and 4C 38.41, all of which have been detected by EGRET (see above).

[8]I base here on the Compton Observatory Newsletter v.2, n.2 (July 1992).

6.2 Physical interpretation

Many radiation mechanisms and scenarios have been suggested as responsible for γ-ray emission from AGNs. In general they can be divided into accretion and jet scenarios and the most frequently studied mechanisms are: synchrotron and inverse Compton scattering by relativistic electrons and interaction of hadrons (protons) with radiation and matter. We will start a short review of these models from accretion scenarios.

One of the oldest (and simplest) scenarios of γ-ray production in AGNs are those which based on spherically symmetric accretion onto BH. During such accretion, matter can be heated by compression. In principle, high temperature plasma may be produced, allowing production of γ-rays via bremsstrahlung and inelastic p + p collisions. First calculations based on very simple model of accretion onto non–rotating BH (adiabatic compression of hadronic component) have shown that significant γ-ray luminosity should be observed (Kolykhalov & Sunyaev 1979; Giovannelli et al. 1982,1984). However more detailed calculations by Maraschi et al. (1982) and Colpi et al. (1984) who took into account e–p coupling and magnetic field (synchrotron and ICS losses) do not predict high γ-ray luminosities in the case of high accretion rates since maximal proton temperatures are lower than assumed in previous simplified scenario. The situation is not improved if the quasi-spherical accretion occurs onto Kerr BH (Colpi et al. 1986). The thermal adiabatic accretion onto a black hole was also recently considered by Park (1990). He finds that a significant fraction of total luminosity is radiated in γ-rays only for accretion rates less than 10^{-3} of Eddington accretion rate ($M_{Edd} = L_{Edd}/c^2$), which corresponds to very weak sources.

In another scenario, discussed by Maraschi & Treves (1977), the particles (protons, electrons) are accelerated in a electric field which is induced by magnetic field during spherical, turbulent accretion onto the BH. The γ-ray photons are produced in this scenario via Compton scattering of synchrotron radiation by relativistic electrons. A similar model was recently discussed by Atoyan & Nahapetian (1990) and X- and γ-ray spectra were calculated. The acceleration of particles to high energies may occur as well in the standing shock which randomizes the infall kinetic energy of spherically accreting matter close to the massive BH (see Protheroe & Kazanas 1983; Kazanas & Ellison 1986). The γ-rays may be produced directly in collisions of relativistic protons with matter ($p + p \rightarrow \pi^0 \rightarrow 2\gamma$) and via ICS of low energy photons (e.g. originated in synchrotron mechanism) by relativistic secondary electrons from decay of charged pions. Such a scenario was applied by Protheroe & Kazanas (1983) to quasar 3C 273 and predicts correlated variability of radio and γ-ray emission. Similar processes of γ-ray production (plus Penrose processes) were also discussed in the model of thick accretion disk supported by high temperature ion plasma (Eilek 1980; Eilek & Kafatos 1983). However, predicted γ-ray spectra, by this model, decline rapidly above 1 GeV which

is not confirmed by recent observations of AGNs by the EGRET detector on Compton GRO.

All the above discussed scenarios produce γ-ray photons isotropically in a compact region close to the BH. It is rather unlikely that they can supply enough power in γ-rays in order to be consistent with γ-ray observations of recently discovered AGNs (e.g. 3C 279). Another basic problem of these models concerns a big compactness parameter which can be estimated from variability time scale and observed luminosity. In the isotropic scenario γ-rays should be absorbed in many AGNs.

However, a very interesting consequence of the Kazanas & Ellison (1986) model (discussed above) is the possibility of acceleration of protons up to extremely high energies $\sim 10^7 - 10^8 GeV$ (see Biermann & Stritmatter 1987). The essential part of protons energy (~10–30%) should be converted to very high energy neutrons, which, contrary to protons, may freely escape from the dense central core of AGN and create a neutron halo between 1–100 pc (Kirk & Mastichiadis 1989; Sikora et al. 1989). In the halo, relativistic neutrons (and protons from decay of neutrons) will produce very high energy γ-rays and secondary electrons which will also contribute to the γ-ray region via electromagnetic cascade. As a consequence of such scenario, high stable fluxes of γ-ray photons with energies up to $\sim 10^{15}$ eV should be observed from AGNs (Begelman et al. 1990; Mastichiadis & Protheroe 1990; Giovanoni & Kazanas 1990). This model fits very well to recently detected TeV γ-ray emission from blazar Mkn 421 (Weekes 1992b). If the structure of magnetic field around central part of AGN is not isotropic, extremely relativistic protons can escape freely in certain directions. They can produce secondary electrons in $p - \gamma$ interactions via decay of pions (Sikora et al. 1987) which may next initiate an electromagnetic cascade by ICS, synchrotron production and direct pair production by $e - \gamma$ interactions.

The high energy γ-ray emission from AGNs can be also interpreted in terms of proton initiated cascade mechanism (PIC) recently proposed by Mannheim et al. (1991) and Mannheim & Biermann (1992). In this model, protons and electrons are continuously accelerated by a shock in blobs or knots of a jet. The protons lose energy in collisions with low energy synchrotron photons produced by accelerated electrons. The cascade process is maintained by proton secondaries which supply additional relativistic electrons.

Another general physical scenario in which γ-ray photon may originate is the production of radiation by relativistic, highly collimated jets (beams) commonly observed in AGNs. The importance of ICS of synchrotron radiation by relativistic electrons (synchrotron self-Compton model – SSC) is often considered in such a scenario because of the high likelihood that continuum radiation in AGNs from radio to optical has a synchrotron origin. The comparisons of calculations according to SSC mechanism in the case of homogeneous, isotropic case (see e.g. Jones et al. 1974) with observations of AGNs showed that predicted photon flux is orders of magnitude larger than observed (Marscher et al. 1979). This contradiction can be solved if the SSC mechanism is working

in the region moving with relativistic speed towards the observer. The calculations along this idea (inhomogeneous models) were performed in the case of jet model by e.g. Marscher (1980), Königl (1981) and Ghisellini et al. (1985). However these kind of models usually predicts a break in the photon spectrum in the X-ray energy range (see e.g. Königl 1981), which is not observed in AGN spectra. In order to fit the γ-ray spectra from AGNs (spectral index close to 2), the high energy break in electron spectrum is also necessary. Such a break can be naturally introduced by limited acceleration of electrons caused by essential energy losses. We should note also that SSC beam models are able to explain naturally the very short term variability observed in X-ray energies from Bl Lac objects.

γ-rays can be produced as well in the comptonization of thermal photons. Such a model in the isotropic scenario was postulated by Jones (1979) as a mechanism of γ-ray production in quasar 3C 273. A similar but much more complicated scenario has been discussed by Melia & Königl (1989) who calculated high energy photon spectra from comptonization of anisotropic, thermal radiation from the accretion disk. However, in this work, the Thomson approximation of cross section was assumed and the high energy γ-ray range was only marginally covered.

Turning back now to hadronic interactions, Morrison et al. (1984) proposed that γ-rays can be produced in the interactions of mildly relativistic proton beam with matter entrained in the extended jets of AGNs. The isotropization of relativistic protons by random magnetic field was postulated. However in such a case, the emission from the jet should be nearly isotropic and also counterjets of AGNs should be clearly seen in X- and γ-ray energy range[9]. The relativistic proton beam model in which γ-ray photon spectra are dependent on the viewing angle of the jet are discussed in chapter 3 of this thesis.

There exist also other classes of models of AGNs in which the main role is played by e^+e^- pair dominated plasma (see for review Zdziarski 1991). Such scenarios are important if the compactness parameter of the source l[10] is greater than 10 (Guilbert et al. 1983). For certain parameters, such plasma can exist in pair equilibrium (see, e.g., Salvati et al. 1983; Svensson 1984; Zdziarski 1985) but its efficient production of high energy radiation is probably limited only to the soft γ-ray energy range (broad e^+e^- annihilation line with steep high energy tail plus narrow 0.511 MeV line from annihilation of escaped and slowed down positrons, see Zdziarski et al. 1990). However these processes may be in strong relation to the observed MeV bump in the photon spectra of some AGNs (e.g. Seyfert galaxies: NGC 4151, MGC8-11-11, see fig 6.4) and diffuse extragalactic γ-ray spectrum.

[9]Up to now, only in a few cases, the soft X-rays has been reported from the AGNs jets. The angular resolution of γ-ray detectors is too poor to distinguish between core and jet emission.

[10]$l \equiv L \cdot \sigma_T / R \cdot m_e \cdot c^3$, where L is the luminosity of source in soft γ-ray range; R is the source size which, in principle, can be estimated from the variability time scale $\Delta t \cong R/c$).

6.3 Quasar 3C 273

The quasar 3C 273 was discovered in the optical as a 13.0 magnitude object (Schmidt 1963). The reported redshift ($z \cong 0.157$) makes it one of the closest objects of this type. The structure of 3C 273 is unusual because of a one–sided optical jet extending about ~ 20" from the nucleus (Greenstein & Schmidt 1964). This optical jet is elongated at least 22° to the direction of the inner jet discovered in the radio range (e.g. Unwin et al. 1985). The discovery of superluminal motion ($\beta \approx 5$) in inner radio jet (Seilstad et al. 1979; Pearson et al. 1981) implies the existence of relativistic particles with Lorentz factor of $\sim 6 \times h^{-1}$ and propagation at an angle $\alpha < 16° \times h^{-1}$ to the line of sight[11] (e.g. Unwin et al. 1985).

The spectrum of the quasar 3C 273 extends over many decades in frequency — from radio to γ–rays — being variable and complex with no strong evidence of correlation between different wavelengths (Courvoisier et al. 1987). Soft X–ray emission was detected during several rocket flights and the shape of the spectrum was approximated by a power law with spectral index of 1.5 (Turner et al. 1990). Hard X–ray emission was first reported by Worrall et al. (1979) and Primini et al. (1979) and subsequently confirmed by balloon flights (e.g. Dean et al. 1990). In this energy range the spectrum is usually described by a power law with index 1.5 (however Bezler et al. 1984 observed a much flatter spectrum with an index of 1.2 up to 200 keV). Recent observations by the SIGMA telescope (Bassani et al. 1991) indicate a strongly variable hard X-ray emission from 3C 273 (increase in intensity by a factor 2.7 ± 1 in 41 days). Evidence was also reported of a possible new transient X-ray source only 15' away from the position of 3C 273 which might contaminate the quasar emission. A small fraction of the soft X–ray emission is connected with the optical part of the jet of 3C 273 (Willingale 1981; Harris & Stern 1987).

The strong evidence of γ–ray emission from 3C 273 comes from measurements on board of SAS 2 and COS B satellites. Swannenburg et al. (1978) found in these data γ–ray excess (CG291+65) which was identified with quasar 3C 273[12]. This result was confirmed by Bignami et al. (1981) who pointed out that the γ–ray spectrum in the energy range 70–600 MeV can be fitted by the lower law: $(3.7 \pm 1.4) \times 10^{-6} \cdot (E/150)^{-2.5 \pm 0.6}$ *photons* cm^{-2} s^{-1} GeV^{-1}, where E is the photon energy in MeV. The total emitted power in this spectrum is $\sim 2 \times 10^{46} erg/s$ (assuming the isotropic case). Very recently, preliminary results of observations of 3C 273 by the Compton GRO were reported by von Montigny et al. (1992) above 100 MeV (EGRET detector) and Hermsen et al. (1992) in the 1–30 MeV energy range (COMPTEL detector). The γ-ray flux above 100 MeV during two observations (June and October 1991) was approximately $(3 \pm 1) \times 10^{-7}$ *photons* cm^{-2} s^{-1}

[11] $h = H_\circ/100 km/s/Mpc$ and $H_\circ$ –Hubble constant

[12] The typical error box of the SAS 2 and COS B detectors was about 1 - 2 degrees so the identification with 3C 273 was not very reliable.

and preliminary spectrum has a photon index of 2.45[13]. This spectrum fits rather well to the COMPTEL measurements in 1–30 MeV energy range, although the extrapolation of the EGRET power law spectrum comes up too high in the COMPTEL energy range. Base on present analysis, it is difficult to find out if the γ-ray emission from 3C 273 is variable. A few upper limits in the very high energy range were derived (for review see Weekes 1988,1992). The most recent one equal to $\sim 10^{-11}$ *photons* cm^{-2} s^{-1} in TeV range was reported by Vacanti et al. (1990).

According to Bassani and Dean (1986), the variability of the X–ray flux implies that X and γ–rays cannot be produced isotropically in the same place because of the large compactness parameter of the X–ray source. They conclude that either X and γ–rays are both beamed or that they are produced in different places. Moreover, Bignami et al. (1981) reported the γ–ray emission to be stable during observations with COS B.

In this section we propose a scenario in which X- and γ-ray emission from 3C 273 can be described. In next subsection we will present the relativistic proton beam model and calculate the expected X- and γ-ray spectra. We compare the observational data from the direction of 3C 273 with these calculations in subsection 6.3.2. The last subsection is dedicated to discussion of the validity of this proposition in context of observations in lower photon energy range.

6.3.1 Relativistic proton beam model

Several models have been suggested in order to explain the X and γ–ray emission from the quasars. However all of them have some difficulties in explaining all current observations of 3C 273 (the compactness of the central source evaluated from X–ray variability (Marshall et al. 1981), lack of correlation between X and γ–rays (Bignami et al. 1981), and do not take into account the existence of the jet in 3C 273).

Our favourite scenario is similar to that one proposed by Morrison et al. (1984), because such a general model naturally avoids problems with compactness of the central core and fits nicely with the observed superluminal motion of blobs emerging from the core of 3C 273.

However some new observational facts encouraged us to modify the Morrison et al. scenario. After all, no deceleration of relativistic blobs in the inner radio jet of 3C 273 (Unwin et al. 1985) was reported and the large scale superluminal motion was recently observed up to at least 120 pc (Davis et al. 1991). Moreover observations of other AGNs with morphological structure similar to 3C 273 (one sided jet) can be easy explained if the relativistic beaming is present also in outer jet. For instance, investigating depolarization asymmetry, Laing (1988) and Garrington et al. (1988) suggest the existence of a relativistic motion in the outer part of the jet of Cygnus A. This same

[13]Note that the COS B observations reported γ-ray flux $\sim 6 \times 10^{-7}$ $phot \cdot cm^{-2} \cdot s^{-1}$ above 100 MeV with no variation within 50% uncertainty and similar spectral index 2.5 ± 0.6 (Bignami et al 1981). However, that result may be also contaminated by 3C 279 which is only $\sim 11^{o}$ away from 3C 273.

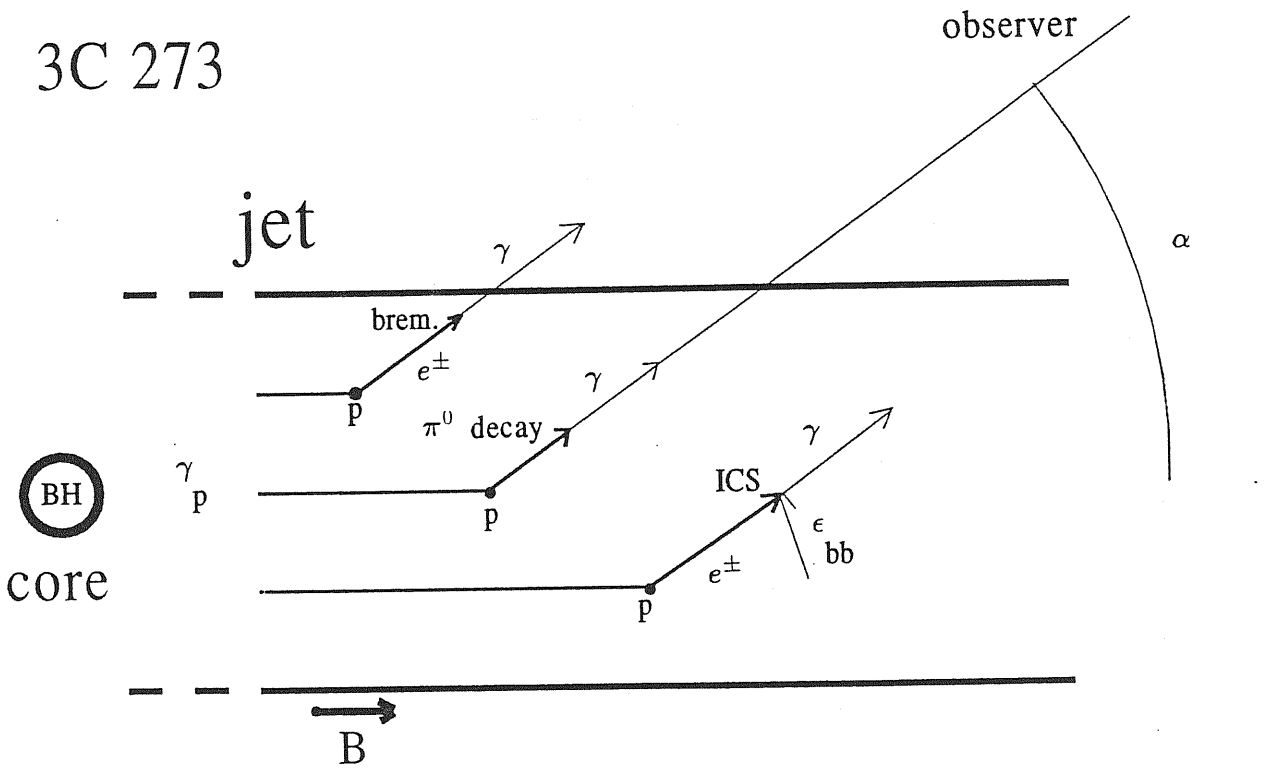

Figure 6.5: Schematic picture of the relativistic jet model applied to 3C 273 (not to scale). Relativistic proton beam emitted by the central core interacts with background matter of the jet ($p + p \rightarrow \pi^0 + \pi^{\pm} + ...$) and produces γ-rays directly from decay of π^0 and as secondary products in the bremsstrahlung process and ICS of microwave photons ϵ_{bb} by secondary electrons from decay of $\pi^{\pm}$.

effect has been discovered in the case of 3C 47 by Fernini et al. (1991). Stiavelli et al. (1992) and Sparks et al. (1992) reported identification of the hotspot in the radio lobe which is on the opposite side of the core than the one sided jet of M 87. Such a hotspot can be provided by an invisible relativistic counterjet.

These new observational results supports our earlier proposition (Bednarek & Calvani 1991) according to which protons emitted by central engine continue to move relativistically along the jet. They interact with matter of the jet and produce γ-ray photons (from π^0 decay) and secondary electrons (from $\pi^{\pm}$ decay). We are interested here in the production spectra which are dependent on the angle to the jet axis since the observer at the Earth is located at the fixed angle to the jet (see Fig. 6.5). For detailed calculations of these spectra we refer to chapter 3 and papers by Bednarek et al. (1990) and Bednarek & Calvani (1991). Since the magnetic field is parallel to the jet axis, the secondary electrons follow a helix path and interact with, matter (via the bremsstrahlung process)

and microwave background radiation (via Inverse Compton scattering). The radiation produced by them will contribute from the soft X-ray up to γ-ray energy range. Such a scenario postulates strong beaming of radiation and may naturally explain one sideness of jets from some AGNs.

6.3.2 X and γ–rays from the jet of 3C 273

In the previous subsection we have proposed a simple model in which a monoenergetic, highly collimated proton beam interacts with matter entrained in the jet volume. Turning now to 3C 273, its extended optical jet (in which we locate the production of X and γ–rays), is elongated at least 22° to the direction of the inner jet observed in radio wavelengths (Unwin et al. 1985). The secondary electrons produced by the decay of charged pions (originated in p–p collisions) can emit observable X and γ–rays via bremsstrahlung processes (if the column density of matter in the jet is high enough) and Inverse Compton scattering of microwave cosmic background radiation. Since secondary electrons are highly relativistic (Lorentz factor up to 10^3, see Fig. 3.5), the produced radiation is strongly collimated along the direction of motion of the electrons (Koch & Motz 1959; Bednarek et al. 1990) and we can assume that significant contribution to the bremsstrahlung spectrum emitted at the angle α is given by the secondary electrons moving very close to α.

Under such assumption the spectrum of the bremsstrahlung radiation produced by secondary electrons is given by:

$$\frac{dN_{brem}}{dE_\gamma d\Omega dt dV} \simeq \lambda \int \frac{dN}{dE_e d\Omega_e dt dV} \frac{dQ(E_e)}{dE_\gamma} dE_e \tag{6.1}$$

where λ is the mean column density traversed by relativistic electrons in particles/cm^2;

$dN/(dE_e d\Omega_e dt dV)$ is the angular dependent spectrum of secondary electrons from decay of polarized muons (see eq. 3.7) and $dQ(E_e)/dE_\gamma$ is the bremsstrahlung spectrum produced by monoenergetic electrons with energy E_e (Blumenthal & Gould 1970).

The spectrum of the Comptonized photons produced by secondary electrons is given by:

$$\frac{dN_{Comp}}{dE_\gamma d\Omega dt dV} \simeq \frac{l}{c} \int \frac{dN}{dE_e d\Omega_e dt dV} \int n(\epsilon) \frac{dP(E_e, \epsilon)}{dE_\gamma dt} d\epsilon dE_e \tag{6.2}$$

where l is the distance on which Comptonization of photons occurs; c is the velocity of light;

$dP(E_e, \epsilon)/dE_\gamma dt$ is the cross section for Inverse Compton scattering of photon with energy ϵ into the energy range $E_\gamma : E_\gamma + dE_\gamma$ by monoenergetic electrons with energy E_e (see, Blumenthal & Gould 1970; formula 2.42) and $n(\epsilon)$ is the differential concentration of background low energy photons.

In order to apply the above results to 3C 273, we have adopted proton beam parameters: Lorentz factor $\Gamma = 6$ and angle $\alpha = 35°$ (which is reasonable if we take into account possible curvature

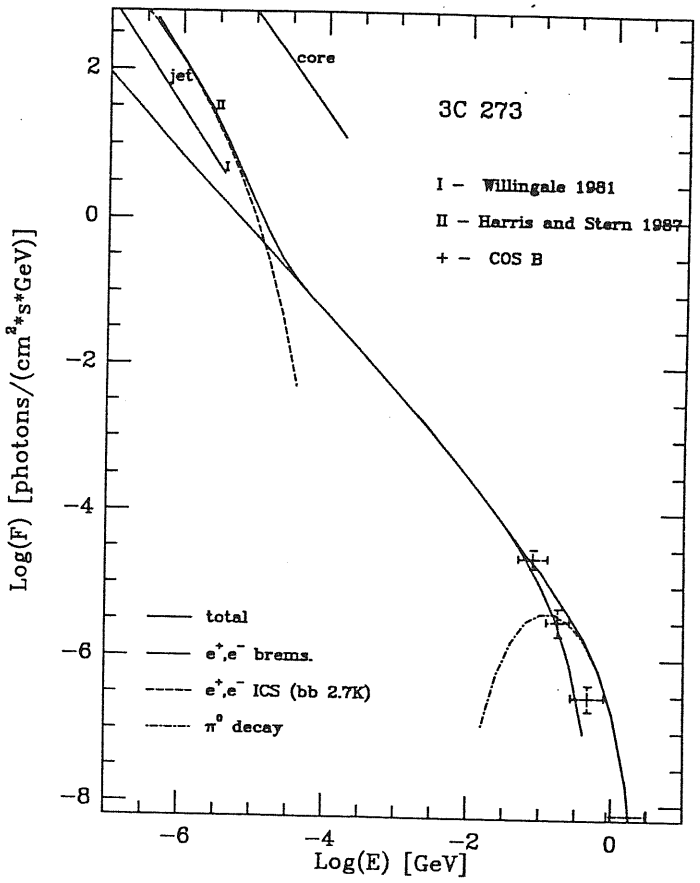

Figure 6.6: The observational data of X and γ–ray emission from 3C 273 are shown. The full line is the fit to the data of the calculated photon spectrum (Lorentz factor $\gamma = 6$ and $\alpha = 35°$). The dot–dashed line describes the spectrum of γ–rays from π^0 decay; the dotted line the spectrum of photons produced by bremsstrahlung of secondary electrons; the dashed line the spectrum of photons from Inverse Compton scattering of cosmic microwave background radiation by secondary electrons (from Bednarek & Calvani 1991).

of the jet, see Unwin et al. 1985). We then compared the photon spectra from bremsstrahlung of secondary electrons (eq. 6.1) from Inverse Compton scattering of background microwave photons by secondary electrons (eq. 6.2) and from π^0 decay ($p + p \rightarrow \pi^0 +$ anything; $\pi^0 \rightarrow 2\gamma$, see Bednarek et al. 1990) with the measurements of X–rays from the jet of 3C 273 and γ–rays observed by COS B from direction of this source (Hermsen et al. 1981). Fits to observational data are presented in Fig. 6.6. From the fits we can estimate the total energy in relativistic protons in the jet of 3C 273 using the relation:

$$E \approx 3 \times 10^{17} \Gamma d^2 \ell / \lambda \; ergs, \tag{6.3}$$

where d is the distance to the quasar in cm, $\ell = d \sin\beta / \sin\alpha$ is the true length of the jet, β is the angular apparent length of the jet.

For $\lambda \approx 70 \; g/cm^2$ (from the fit), $d \approx 860 \; Mpc$ and $\beta \approx 20''$ we find $E \approx 3 \times 10^{60} \; ergs$. The required power emitted in relativistic protons by the core of 3C 273 is equal to $P = Ec/\ell \approx$

2.6×10^{47} $ergs/s$, which corresponds to a mass loss in relativistic protons of $M \approx 0.7 M_{\odot}/yr$ in the jet.

6.3.3 Discussion

We have shown above that the entire spectrum of 3C 273, X–rays from the jet and γ–rays from the direction of this source, can be explained with a simple model in which this radiation are produced by the interaction of the relativistic proton beam with matter entrained in the jet volume. Our model is similar to the one of Morrison et al. (1984), but it differs in that we assume that a relativistic proton beam propagates along the magnetic field which is parallel to the jet axis. We have considered the angular dependence of the spectrum of secondary electrons produced in the interaction of a relativistic proton beam. In such a magnetic field, the trajectory of secondary electrons is a helix along the jet axis. The X-ray (from the jet) and γ–ray spectrum from 3C 273 can be accounted for by bremsstrahlung and Inverse Compton spectra produced by secondary electrons and spectra of photons produced by π^0 decay (assuming a Lorentz factor $\Gamma \approx 6$ for the bulk motion of the proton beam and an angle of $\alpha \approx 35^{\circ}$ between the jet axis and the line of sight), see Fig. 6.6. From the fit of the observed spectrum with the theoretical one (bremsstrahlung radiation calculated according to eq. 6.1, Inverse Compton spectrum according to eq. 6.2 and radiation from π^0 decay calculated in Bednarek et al. (1990), we have found that the total power emitted in relativistic protons by the central core of 3C 273 is equal to $P = 2.6 \times 10^{47}$ $ergs/s$ which corresponds to a mass loss of $\dot{M} = 0.7 M_{\odot}/yr$. However we note that a high column density in the jet of 3C 273 is required: $\lambda \approx 70$ g/cm^2, and accumulation of a large amount of matter in the jet volume is possible (see, e.g., discussion in Morrison et al. 1984). Recent observations of emission lines from the jet of Cen A also supports the hypothesis of an existence of essential amounts of matter in the jet (Morganti et al. 1992). From another side, numerical simulations of propagation of a jet in the extragalactic medium by De Young (1986) show that a jet can entrain a minimum of $\approx 5 M_{\odot}/yr$, which implies a total enrichment as high as $10^9 M_{\odot}$ for some jets.

A few different mechanisms of particle acceleration in active galaxies were proposed (see e.g. Wiita 1985). Relativistic particles with power law spectrum can be produced by shocks close to the central engine (see e.g. Blandford & Eichler 1987). Monoenergetic (or close to monoenergetic) relativistic particles can be accelerated in electromagnetic processes (see e.g. Lovelace 1976; Blandford & Znajek 1977) or by radiation pressure (e.g. Abramowicz & Piran 1980; Sikora & Wilson 1981; Calvani & Nobili 1983). In our model we assume that the jet is monoenergetic and made of relativistic protons. Indeed: a) the existence of relativistic knots far away from the central core of 3C 273 suggests such a distribution of particles (if not, the knots should be diluted and superluminal motion will not be observed); b) such choice allows us to limit the number of free parameters in

the model (in fact we are here mainly interested in investigating the main features of our model to check whether it is in agreement with observations); c) arguments supporting a proton beam are discussed by Roberts (1984).

Our model can work if the energy losses of electrons are not completely dominated by synchrotron processes. This is true if the magnetic field (the perpendicular component to the electron's motion) is $B_\perp[\mu G] \leq 1.1 n_H^{1/2}/E$ (from comparison of synchrotron and bremsstrahlung energy losses) and $B_\perp[\mu G] \leq 14.4 W_{ph}[eV/cm^3]$ (from comparison of synchrotron and Inverse Compton energy losses), where E is the energy of electrons in GeV (see Schlickeiser 1982). From polarization measurements, Röser & Meisenheimer (1986) estimate that the magnetic field in the jet of 3C 273 is of the order of $10\mu G$. If we now compare the synchrotron and bremsstrahlung energy losses, we find that this value is near the acceptable limit for the most energetic secondary electrons (with energy $\approx 1\ GeV$) but is well acceptable for the lower energy ones. Synchrotron and Inverse Compton energy losses for the above parameters are comparable.

The density of photons with power law spectrum below $10^{15} Hz$ in the jet volume of 3C 273 (see Fraix-Burnet & Nieto 1988) is about one order of magnitude lower than the density of the microwave background radiation (for the volume of the optical jet and the observed spectrum of photons below $10^{15} Hz$ from Fraix-Burnet & Nieto 1988). Moreover these photons are probably also collimated along the jet axis of 3C 273 if we keep in mind some observational evidence of their synchrotron origin (Fraix-burnet and Nieto, 1988) and the strong collimation of secondary electrons postulated by our model. Therefore Comptonization of these photons (with power law spectrum) to the X–ray range is negligible in comparison to Comptonization of cosmic background radiation.

Our model moreover predicts a strong angular dependence of the photon spectrum with respect to the jet direction. The emission of radiation from the counter jet (produced by secondary electrons at an angle $\alpha \approx 145°$ to the line of sight) should be much less than the one from the jet pointing towards us because of much smaller Lorentz factors of secondary electrons produced backwards.

One of the advantages of our model is, we think, its simplicity. Of course, a more realistic model for 3C 273 should take into account propagation effects of relativistic protons and secondary electrons and curvature of the jet. In such a case we expect the theoretical photon spectrum to be more steep in the γ–ray range and the deduced parameters of relativistic beam and jet containment less restrictive.

6.4 Quasar 3C 279

The quasar 3C 279 was the first object in which superluminal motion was recognized (Whitney et al. 1971). During early 1970s the motion appeared to the rapid expansion with an apparent separation speed of $\beta_{obs} \approx 9h^{-1}$ (Cotton et al. 1979). However the VLBI data collected between

1981 and 1984 shows much slower motion with speed $\beta_{obs} \approx 2.1h^{-1}$ (Unwin et al. 1989) which is only one quarter of early reports. This dramatic change does not imply a deceleration of the earlier component, but only means that the old relativistic component moved too far to be detected and the next one, with much smaller velocity emerged. The compact core of 3C 279 shows a flat radio spectrum contrary to the steep spectrum of the jet. Its optical emission is highly variable on a time scales of days and strongly polarized (e.g. Webb et al. 1990). 3C 279 is also a relatively strong X-ray source showing variability on the order of a factor 2 (Zamorani et al. 1984). More recent results in the X-ray energy range were collected by the Ginga satellite. Observations carried out on two occasions (June 1987 and July 1988) indicate that the 2-20 keV flux increased by a factor more than 4, within about a year (Makino et al. 1989). During the outburst, the X-ray spectrum became slightly harder than in the quiet period, changing from $\Gamma = 1.70 \pm 0.06$ to 1.58 ± 0.03. This X-ray flare was also accompanied by a dramatic increase in the optical and near-infrared flux (Kidger et al. 1992).

3C 279 is one of the objects best studied by Comptel GRO. Its γ-ray spectrum can be described between 30 MeV to 5 GeV by a simple power law with spectral index 2.02 ± 0.07 and intensity $(2.8 \pm 0.4) \times 10^{-6} ph\ cm^{-2} s^{-1}$ above 100 MeV (Hartman et al. 1992c), which corresponds to isotropic emission of $1.1 \times 10^{48} erg/s$ (for z = 0.538 and $H_0 = 75 km/s/Mpc$). Such extremely high photon luminosity strongly suggests the beaming of γ-ray emission which is consistent with the observations of superluminal motion in the central core of 3C 279. Another strong constraint on the model of γ-ray production in 3C 279 is placed by the significant variability on the order of 3 days observed by GRO in June 1991 (Kanbach et al. 1992).

In this section we propose a physical scenario in which γ-ray production and variability in AGNs can be envisaged. In the following subsections we describe the main points of cone beam model and in terms of this model we calculate: the spectra of γ-rays and secondary electrons produced in p + p interactions via pion decay and the spectra of X- and γ-rays produced by secondary electrons in Inverse Compton Scattering (ICS) of UV photons emitted by the thick accretion disk. As an example, we compare these results with X- and γ-ray emission from 3C 279. Our model has some points in common with previous works (see mechanisms of γ-ray production discussed by e.g. Begelman et al. (1990); Jones & Stein 1990; Bednarek & Calvani 1991), but contrary to them it is also able to explain the reported variability of γ-ray emission from 3C 279.

6.4.1 Physical scenario applied to 3C 279

The basic assumption of the model is the existence of the geometrically thick accretion disk around the central engine of the AGN (see the review by Begelman et al. 1984 and references therein) which is also responsible for production of the UV bump in the AGN spectrum (Shields 1978;

Malkan & Sargent 1982). The structure of such radiation supported disks was studied by e.g. Jaroszyński, Abramowicz & Paczyński (1980), and the emission of radiation from the disk funnels by e.g. Abramowicz, Calvani & Nobili (1980) and Madau (1988).

Moreover, we assume that blobs or shocks containing relativistic particles (e.g. accelerated in one of the mechanisms discussed by Rees 1984) can emerge sporadically from the region close to the central engine. A possible model for the blob (shock) production may be the one proposed by Protheroe & Kazanas (1983) and Kazanas & Ellison (1986) and may be connected with the rapid change in the accretion scenario in the inner part of AGN or with instabilities of the accretion disk (Papaloizou & Pringle 1984). The blobs are moving inside the narrow funnel of the thick accretion disk (see Fig. 6.7). If relativistic particles are emitted by such a blob inside the cone with opening angle α_{out} (which is bigger than the disk funnel angle α_{in}) then some of the relativistic particles will interact with matter in the accretion disk. Although this is an *ad hoc* assumption, it may be supported by the existence of viscous forces in the disk funnel. As a result of these forces, the velocity of the relativistic blob (shock) close to the axis of the funnel should be greater than close to the walls. This effect should cause a bending of the shock and permit emission of relativistic particles inside the limiting angle measured from the axis of the funnel.

We assume moreover, that the disk has a dense corona between angles α_{in} and α_{out}. In the inelastic p + p interactions of relativistic protons with matter of the disk (and matter of the induced wind), the γ-rays and secondary electrons from pion decay are produced. The γ-rays below $\sim$ 100MeV are produced via ICS of thermal UV photons from the disk by secondary electrons inside the disk funnel. For the shake of simplicity, we assume that the funnel of the optically thick accretion disk emits black body radiation with the temperature $T_{bb} \cong 4.5 \times 10^4$ K. A small gradient of temperature in the narrow funnel of the disk is suspected because of multiple scattering of radiation on the funnel's walls. The thermal emission of the funnel is consistent with the upper limit on the disk radiation of 3C 279 equal to $\sim 3 \times 10^{46}\ erg/s$ (Makino et al. 1991). We note that the radiation from such disk is dominated by the emission from the funnel (Madau 1988).

Under energy release of the relativistic particles, the outer part of the thick disk evaporates producing a strong wind which surrounds the relativistic beam (Fig. 6.7). The efficient escape of γ-rays from π^0 decay will be possible only in some region close to the limb of the thick disk (disk corona, Fig. 6.7), where the column density of matter is not extremely high. In the regions where matter is opaque to γ-ray photons ($\alpha > \alpha_{out}$), only high energy neutrinos can escape. We further point out that X- and γ-ray emission from 3C 279 can be described by such a scenario.

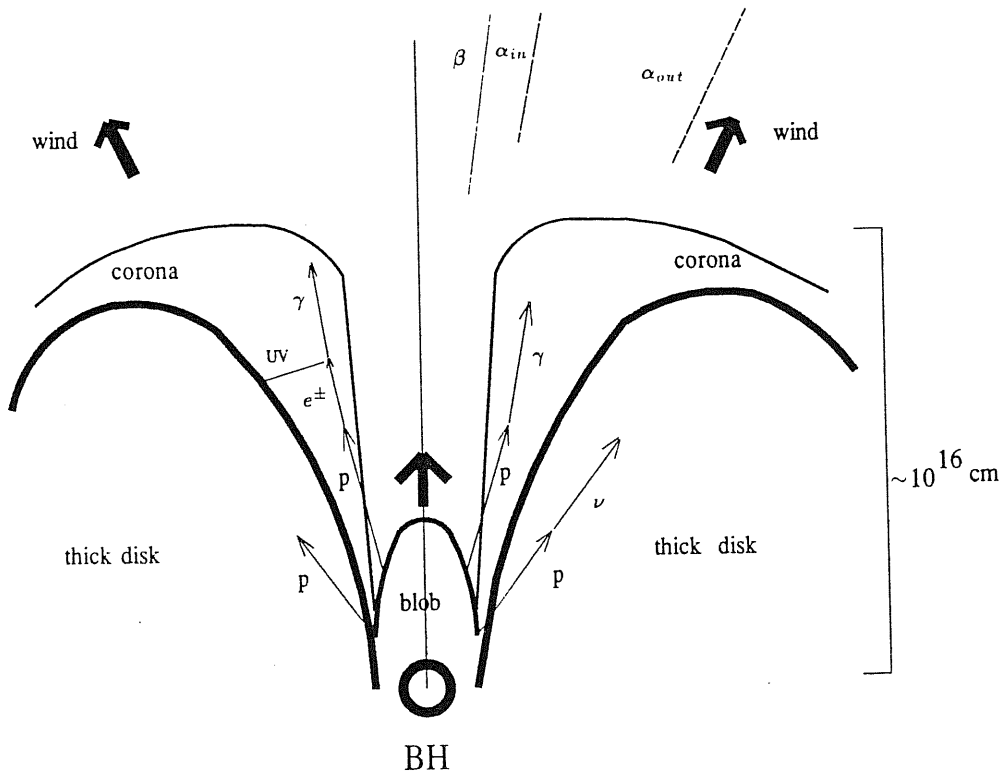

Figure 6.7: Schematic picture of the central part of an AGN (not to scale). The relativistic blob is emerging from the region close to the central black hole and is moving in the funnel. Protons emitted by the blob interact with the dense disk corona (region between angles α_{in} and α_{out}) and produce γ-rays and secondary electrons. The optically thick disk emits UV photons which are comptonized by secondary electrons. The observer is located at the angle β to the disk axis.

6.4.2 Production of γ-ray photons

As we mentioned above, the main mechanism of the high energy γ-ray production in our model is the interaction between relativistic protons and ambient matter accumulated in the thick accretion disk. In such collisions neutral and charged pions are produced which next decay to γ-ray photons, secondary electrons (electrons and positrons) and neutrinos ($p + p \rightarrow \pi^0 + \pi^{\pm} + ...$; $\pi^0 \rightarrow 2\gamma$; $\pi^{\pm} \rightarrow e^{\pm} + \nu_e + \nu_{\mu}$). In order to reduce the number of free parameters, we assume instead a monoenergetic proton beam with Lorentz factor γ_p. The beam propagates inside the cone with half angle α_{out} and interacts with matter accumulated between angles α_{in} and α_{out} (see Fig. 6.7). Since the detailed structure of the thick accretion disk is unknown, we assume for simplicity that the column density of background matter (λ) crossed by relativistic particles is less than one interaction length for inelastic p + p collisions. In the regions where the column density of matter is greater than one interaction length (in our case for the angles $> \alpha_{out}$), the efficiency of γ-ray emission significantly drops.

The angular and energy dependent spectrum of γ-ray photons from π^0 decay was calculated by integration over the proton spectrum multiplied by the energy and angular distribution of the γ-ray spectrum from a single p + p interaction:

$$\frac{dN}{dE_\gamma d\Omega_\gamma dt} = \int\int \frac{dP}{dE_p d\Omega_c dt} \cdot \frac{dQ_\gamma}{dE_\gamma d\Omega_\gamma} \cdot d\Omega_c dE_p \tag{6.4}$$

where $dP/dE_p d\Omega_c dt$ is the differential proton spectrum and $dQ_\gamma/dE_\gamma d\Omega_\gamma$ is the angular and energy photon spectrum from single p + p collision (see chapter 3 and Bednarek et al. 1990).

The calculated spectra of γ-rays from π^0 decay, produced by a monoenergetic cone beam, can mimic a power law photon spectrum in the energy range between 1-10GeV with spectral index depending on the parameters: γ_p, β, α_{in} and α_{out}. Since we assumed a rather low column density of background matter in the outer parts of the disk (corona), these photons will escape freely.

The angular and energy dependent spectrum of secondary electrons from $\pi^\pm$ decay was calculated by integration over the proton spectrum multiplied by the energy and angular spectrum of secondary electrons from a single p + p interaction:

$$\frac{dN_{e^\pm}}{dE_{e^\pm} d\Omega_{e^\pm} dt} = \int\int \frac{dP}{dE_p d\Omega_c dt} \cdot \frac{dQ_{e^\pm}}{dE_{e^\pm} d\Omega_{e^\pm}} d\Omega_c dE_p \tag{6.5}$$

where $dQ_{e^\pm}/dE_{e^\pm} d\Omega_{e^\pm}$ is the angular and energy spectrum of secondary electrons from a single p + p collision (see chapter 3 and Bednarek & Calvani 1991).

The secondary electrons can interact with the magnetic field, matter and radiation in the funnel of the thick accretion disk and produce γ-rays in bremsstrahlung and ICS processes. The relative importance of these processes can be estimated by comparison of energy losses calculated for presumable parameters of the emitting volume. We accept that the energy losses of secondary electrons are dominated by ICS of UV thermal photons which fills the funnel of the accretion disk with a density of the order of black body distribution. This is true if the magnetic field in the funnel is $B_\perp < 700Gs$ (obtained from a comparison of synchrotron and inverse Compton losses of secondary electrons). The bremsstrahlung losses are negligible in comparison to Compton losses for required parameters of the emitting volume: the estimated height of the thick accretion disk $r_{acc} \sim 10^{16}cm$ (to be consistent with observed 3 day variability in γ-rays) and column density of matter $< 70g/cm^2$ (required for efficient escape of γ-ray photons).

The energy loss time scale of secondary electrons moving in the field of black body UV photons ($T_{bb} = 4.5 \times 10^4$K) is too short to allow escape of electrons from the funnel without significant energy losses. So the steady state distribution of electrons in the funnel should be calculated assuming a thick-target model (Ginzburg & Syrovatskii 1964) and is given by:

$$\frac{dR_{e\pm}}{dE_{e\pm}d\Omega_{e\pm}} = \frac{1}{\varepsilon(E)}\int_{E}^{E_{max}} \frac{dN_{e\pm}}{dE'_{e\pm}d\Omega_{e\pm}dt}dE' \tag{6.6}$$

where $dN_{e\pm}/dE'_{e\pm}d\Omega_{e\pm}dt$ is the spectrum of secondary electrons (given by eq. 6.5); $\varepsilon(E)$ is the energy loss rate of secondary electrons in ICS process.

Now we can calculate the spectrum of γ-ray photons produced in comptonization of black body UV photons by a steady state distribution of electrons. It is expressed by the formula:

$$\frac{dN_{Comp.}}{dE_\gamma d\Omega_\gamma dt} = \int \frac{dR_{e\pm}}{dE_{e\pm}d\Omega_{e\pm}} \cdot \int n(\epsilon) \cdot \frac{dQ(E_{e\pm},\epsilon)}{dE_\gamma dt} d\epsilon dE_{e\pm} \tag{6.7}$$

where $dR/dE_{e\pm}d\Omega_{e\pm}$ is the spectrum of relativistic electrons (given by eq. 6.6);

$dQ(E_{e\pm},\epsilon)/dE_\gamma dt$ is the cross section for ICS of photons with energy ϵ into the energy E_γ by monoenergetic electrons with energy $E_{e\pm}$ (see Blumenthal & Gould 1970) and $n(\epsilon)$ is the differential concentration of UV black body photons.

The combined spectrum of photons, from π^0 decay and ICS of UV photons by secondary electrons, calculated simultaneously, for fixed parameters (γ_p, β, α_{in} and α_{out}), is very nearly fit by a power low shape with spectral index flatter in soft X-rays and steeper in the GeV γ-ray range. The fast cut-off in the photon spectrum in the higher energy range is determined by the value of γ_p and the relative dependence between β, α_{in} and α_{out}.

6.4.3 Comparison with γ-ray spectrum of 3C 279

The γ-ray spectrum of 3C 279 observed by the EGRET detector on Compton GRO (Hartman et al. 1992c) is compared with photon spectra calculated in the previous section. As an example, in Fig. 6.8, we show the fit for $\gamma_p = 30$, $\beta = 2^0$, $\alpha_{in} = 7^0$ and $\alpha_{out} = 12^0$ (for redshift z=0.538). The data in the γ-ray energy range are reasonably well fit by the photon spectrum from π^0 decay (above a few hundred MeV) and by a self-consistently calculated spectra of photons from ICS of UV thermal photons by secondary electrons.

From the fitting presented in Fig. 6.8 we are able to calculate the required total luminosity of the quasar 3C 279 in relativistic protons which is $L_p \cong 2.5\times10^{47} erg/s$ for a mean column density crossed by the relativistic proton beam in the disk corona $\lambda = 30 g/cm^2$ (z=0.538, $H_0 = 75 km/s/Mpc$ and $q_0 = 1/2$). We assumed a column density of this order since it supplies enough target for γ-ray production and still permits free escape of γ-rays from the accretion disk region. In fact L_p is the lower limit on the quasar luminosity in relativistic protons since substantial number of particles may also be emitted at higher angles ($\alpha > \alpha_{out}$). For such angles γ-rays will be absorbed by the optically thick disk and only a strong neutrino signal may be observed.

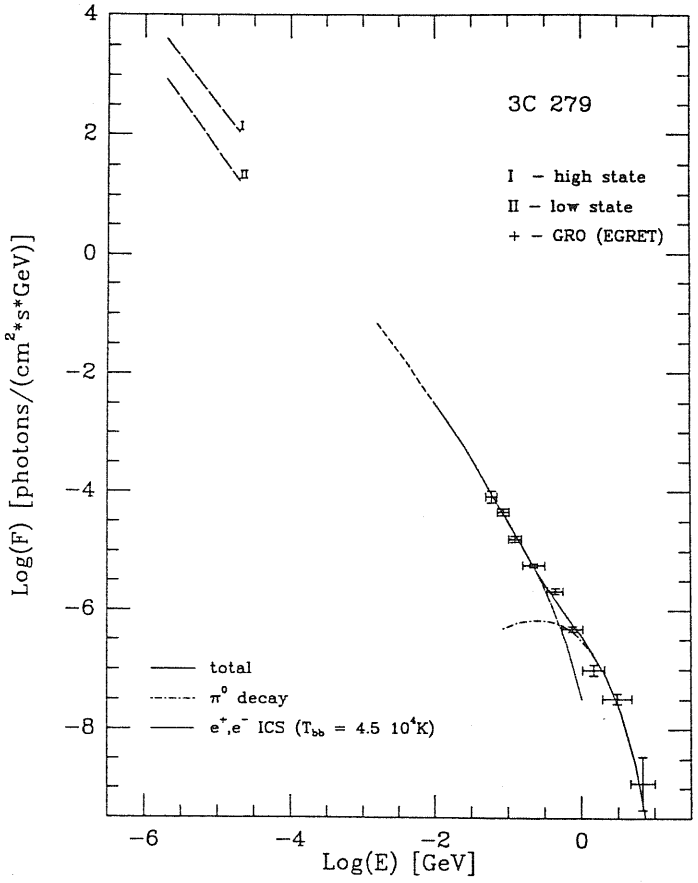

Figure 6.8: The γ-ray spectrum observed by EGRET (error boxes, Hartman et al. 1992c) and soft X-ray spectrum observed by GINGA (long dashed lines - low and high state, Makino et al. 1989) from 3C 279 are shown. The full line is the fit of the data using the calculated photon spectrum for $\gamma_p = 30, \beta = 2^0$, $\alpha_{in} = 7^0$ and $\alpha_{out} = 12^0$. The dot-dashed line is the photon spectrum from π^0 decay. The dotted line is the photon spectrum from ICS of UV photons ($T_{bb} = 4.5 \times 10^4 K$) by secondary electrons. The short dashed line is the part of the calculated photon spectrum which is influenced by transfer processes in the matter of the disk corona (from Bednarek 1992b).

6.4.4 Discussion

We tried to envisage here the physical scenario for the γ-ray production in 3C 279 in terms of the standard model of AGN (thick accretion disk around massive black hole). We assumed that the inner parts of the accretion disk have a dense corona which is illuminated by relativistic protons. The protons are emitted within the angle α_{out} by a blob (or blobs) moving in the disk funnel which has the opening angle α_{in}, less than α_{out} (see Fig. 6.7). The γ-ray photons are produced in the inelastic collisions of relativistic protons with matter in the disk via π^0 decay and in ICS of UV thermal photons by secondary electrons from $\pi^{\pm}$ decay. In order to permit free escape of γ-rays from the production volume, the mean column density of background matter should be essentially less than one interaction length for p + p collisions. We were able to fit reasonably the γ-ray spectrum of 3C 279 (see Fig. 6.8). We note that the parameters of this fitting are not unique. In

order to distinguish between different fits, the simultaneous observations in lower photon energies (X-rays, soft γ-rays) are needed and detailed calculations of the transfer of photons with energies less than 10 MeV in the disk corona should be performed. However we leave these complicated calculations to more detailed studies of this model since we are mainly interested here in the high energy γ-rays. The estimated luminosity of this quasar in relativistic protons should be at least $L_p \cong 2.5 \times 10^{47} erg/s$ for a mean column density of the background matter $\lambda = 30 g/cm^2$. The 3 day variability in γ-ray emission, reported by Hartman et al. (1992c), can be caused by the crossing of a relativistic proton blob in the disk limb.

The low and high states of soft X-ray emission from 3C 279 were reported by Makino et al. (1989). We are not able to calculate detailed spectrum in this energy range because of complicated transfer of X-ray photons through the disk corona (although significant comptonization of thermal radiation may occur also in the central part of the funnel by primary electrons where matter is not present). This emission may be produced as well by Compton scattering of radiation from the disk by secondary or primary electrons in the region farther from the disk (a scenario similar to that one recently studied by Dermer et al. 1992) or in the comptonization of synchrotron radiation by secondary or primary electrons (e.g. Jones, O'Dell & Stein, 1974; Marscher 1980; Ghisellini et al. 1985; see also the model for 3C 273 by Courvoisier & Camenzind 1989). Such a composed model postulates a time delay between soft X-ray and γ-ray emission which can be observationally tested.

One of the consequences of the model is the possibility of induction of a strong wind surrounding the relativistic particle beam since a large amount of energy is transferred to the inner part of the accretion disk. Such a wind may have a direct relation to the broad emission regions of AGNs.

Our model postulates the high collimation of γ-ray emission from AGNs along the axis of the disk funnel. Provided that magnetic fields do not significantly influence the motion of the protons we can conclude: a) AGNs, seen close to face on, may emit γ-rays and neutrinos during the outburst phase when relativistic proton blobs are formed; b) some AGNs may only be strong neutrino sources if observed at large angles to the axis of the disk funnel ($\alpha > \alpha_{out}$) where the column density of matter is greater than one interaction length. The intensity and spectrum of neutrinos in case a) will be similar to the intensity of γ-rays from π^0 decay (see dot-dashed line in Fig. 6.8). In case b), the intensity of neutrinos will be essentially larger and the mean energy of neutrinos smaller (because of the thick target met by the proton beam). Therefore, our model predicts strong, non-isotropic emission of low energy neutrinos by AGNs, contrary to the model by Stecker et al. (1991) which postulates isotropic emission of high energy neutrinos ($\sim 10^4 \div 10^{10}$ GeV).

We consider a relatively mild relativistic proton beam so the absorption of γ-rays by isotropic, thermal UV photons is not important because,

$$\sqrt{0.5 \cdot < \epsilon_{UV} > \cdot E_\gamma \cdot (1 - cos\theta)} < 0.511\ MeV, \tag{6.8}$$

where θ is the incident angle between photons.

Similar strong collimation of radiation from X-ray up to soft γ-ray photons (produced by secondary electrons in ICS process) with γ-ray photons (originated in decay of π^0) permits free escape of γ-ray photons from 3C 279 since the probability of e^+e^- pair production in $\gamma - \gamma$ collision is reduced by a factor $(1 - cos\theta)$.

The physical scenario, discussed by us, can be extended to relativistic proton beams with much higher Lorentz factors. However, in this case the γ-rays would be very efficiently absorbed by UV photons, resulting in multiple e^+e^- pair production. Such e^+e^- pair dominated models (see e.g. Zdziarski et al. 1990) predict the appearance of a strong annihilation line in AGNs spectra and the spectral index of differential photon spectrum in the GeV energy range significantly steeper than that observed from 3C 279.

If really only mildly relativistic protons are present in the central part of 3C 279, we should observe the cut-off in the γ-ray spectrum just above $\sim$ 10 GeV. Recent observations of 3C 279 by the Whipple observatory γ-ray collaboration (Weekes 1992b) shows no significant photon emission above 0.5 TeV during the period 24 March - 8 May 1992. However, they report positive detection of invariable emission above 0.5 TeV from Mkn 421, which is similar to 3C 279. The main problem concerning high energy observations of 3C 279 (from soft X-rays up to TeV γ-rays) is that they are not simultaneous and this fact does not allow final conclusions at this stage.

We would like to note that the relativistic blob (shock) will finally emerge outside the region of the accretion disk but the acceleration of particles by it may continue. Also other mechanisms of γ-ray production may work simultaneously with our scenario, for example, synchrotron self-Compton emission from a relativistic beam (see e.g. Grindlay 1975b; Königl 1981) or proton initiated cascade (Mannheim et al. 1991). They may be responsible for the stable photon emission above 0.5 TeV reported recently from Mkn 421 during the period 24 March - 8 May 1992 (Weekes 1992).

This chapter partially base on two papers: *"X and γ-ray emission from 3C 273"* 1991, A&A 245, 41 by W. Bednarek & M. Calvani (included in an Appendix) and *"On the γ-ray emission from 3C 279"* 1992b, ApJL submitted by W. Bednarek.

References

Abramowicz, M.A., Calvani, M. & Nobili, L. 1980, ApJ 242, 772
Abramowicz, M.A. & Piran, T. 1980, ApJL 241, L7
Altschuler, D.R. 1989, Fund. Cos. Phys. 14, 37
Antonucci, R.R.J. & Miller, J.S. 1985, ApJ 297, 621
Atoyan, A.M. & Nahapetian, A. 1990, A&A 219, 53
Baity, W.A. et al. 1981, ApJ 244, 429
Baity, W.A. et al. 1984, ApJ 279, 555
Bassani, L. & Dean, A.J. 1983, Sp. Sci. Rev. 35, 367
Bassani, L. & Dean, A.J. 1986, A&A 161, 85
Bassani, L. et al. 1986, ApJ 311, 623
Bassani, L. et al. 1985, *Active Galactic Nuclei*, ed. J.E. Dison (Manchester University Press), 252
Bassani, L. et al. 1991, 22nd ICRC (Dublin) 1, 173
Bednarek, W. 1992b, ApJL submitted
Bednarek, W. & Calvani, M. 1991, A&A 245, 41
Bednarek, W., Giovannelli, F., Karakuła, S., Tkaczyk, W. 1990, A&A 236, 268
Begelman, M.C. 1986, *Twelfth Texas Symposium on Relativistic Astrophysics*, eds. M. Livio & G. Shaviv, Annals of the New York Academy of Sciences, v. 470, 51
Begelman, M.C., Blandford, R.D. & Rees, M.J. 1984, Rev.Mod. Phys., 56, 255
Begelman, M.C. & Rees, M.J. 1984, MNRAS 206, 209
Begelman, M.C., Rudak, B., Sikora, M. 1990, ApJ, 362, 38
Bezler, M. et al. 1984, A&A 136, 351
Biermann, P.L. & Stritmatter, P.A. 1987, ApJ 322, 643
Bignami, G.F. et al. 1979, ApJ 232, 649
Bignami, G.F. et al. 1981, A&A 93, 71
Blandford, R.D. & Eichler, D. 1987, Phys. Rep. 154, 1
Blandford, R.D. & Znajek, R. 1977, MNRAS 179, 433
Blandford, R.D. 1985, *Active Galactic Nuclei*, ed. J.E. Dison (Manchester University Press), 281
Blumenthal, G.R. & Gould, R.J. 1970, Rev. Mod. Phys. 42, 237
Bregman, J.N. 1990, Astr. Ap. Rev. 2, 125
Bridle, A.H. & Perly, R.A. 1984, ARAA 22, 319
Calvani, M. & Nobili, L. 1983 *Astrophysical Jets*, eds. Ferrari and Pacholczyk, Reidel
Carraminana, A. et al. 1990, A&A 228, 327
Cavaliere, A.G., Morrison, P. & Pacini, F. 1970, ApJL 162, L133
Clay, R.W. et al. 1984, Aust. J. Phys. 37, 91
Cawley, D.J. et al. 1985, 19th ICRC (La Jolla) 1, 264
Cohen, M.H. 1986, *Highlights of Modern Astrophysics*, eds. S.L. Shapiro & S.A. Teukolsky (A Wiley-Interscience Publication, New York), 299
Colpi, M., Maraschi, L. & Treves, A. 1984, ApJ 280, 319
Colpi, M., Maraschi, L. & Treves, A. 1986, ApJ 311, 150
Cotton, W.D. et al. 1979, ApJL 229, L115
Courvoisier, T.J.-L. et al. 1987, A&A 176, 197
Courvoisier, T.J.-L. & Camenzind, M. 1989, A&A 224, 10
Davis, R.J., Unwin, S.C. & Muxlow, T.W.B. 1991, Nat 354, 374
Dean, A.J. et al. 1990, ApJ 349, 41
De Young, D.S. 1986, ApJ 307, 62
Dermer, C.D., Schlickeiser, R., & Mastichiadis, A. 1992, A&AL 256, L27
Eilek, J.A. 1980, ApJ 236, 664
Eilek, J.A. & Kafatos, M. 1983, ApJ 271, 804
Fernini, I. et al. 1991, ApJ 381, 63
Fichtel, C.E. 1986, *Supermassive Black Holes*, ed. M. Kafatos (Cambridge University Press, New York)
Fichtel, C.E. et al. 1992, IAU Circ. No. 5460
Fraix-Burnet, D. & Nieto, J.-L. 1988, A&A 198, 87
Garrington, S.T. et al. 1988, Nat 331, 147
Gehrels, N. et al. 1984, ApJ 278, 112
Ghisellini, G., Maraschi, L., & Treves, A. 1985, A&A 146, 204

Ginzburg, V.L. & Syrovatskii, S.I. 1964, *The Origin of Cosmic Rays*, (New York: MacMillan)
Giovannelli, F., Karakuła, S. & Tkaczyk, W. 1982, A&A 107, 377
Giovannelli, F., Karakuła, S. & Tkaczyk, W. 1984, Adv. Sp. Res. 3, 335
Giovanoni, P.M. & Kazanas, D. 1990, Nat 345, 319
Greenstein, J.L., & Schmidt, M. 1964, ApJ 140, 1
Grindlay, J.E. et al. 1975a, ApJL 197, L9
Grindlay, J.E. 1975b, ApJ, 199, 49
Guilbert, P.W., Fabian, A.C. & Rees, M. 1983, MNRAS 205, 593
Hall, R.D. et al. 1976, ApJ 210, 631
Harris, D.E. & Stern, C.P. 1987, ApJ 313, 136
Hartman, R.C. et al. 1992a, IAU Circ. No. 5519
Hartman, R.C. et al. 1992b, IAU Circ. No. 5477
Hartman, R.C. et al. 1992c, ApJL 385, L1
Hawking, S.W. 1974, Nat 248, 30
Hermsen, W. et al. 1981, 17th ICRC, 1, 230
Hermsen, W. et al. 1992, A&AS (in press)
Hoyle, F. & Fowler, W.A. 1963, MNRAS 125, 169
Jaroszyński, M., Abramowicz, M.A. & Paczyński, B. 1980 Acta Astr. 30, 1
Jones, T.W. 1979, ApJ 233, 796
Jones, T.W., O'Dell, S.L. & Stein, W.A. 1974, ApJ 188, 353
Jones, T.W. & Stein, W.A. 1990, ApJ 349, 443
Jourdain et al. 1991, 22nd ICRC (Dublin) 1, 177
Kanbach, et al. 1992, IAU Circ. No. 5431
Kazanas, D. & Ellison, D.C. 1986, ApJ 304, 178
Kellerman, K.I. & Pauliny-Toth, I.I.K. 1981, ARAA 19, 373
Kidger, M., Garcia Lano, P. & Antonio de Diego, J. 1992, A&AS 93, 391
Kirk, J.G. & Mastichiadis, A. 1989, A&A 213, 75
Koch, H.W. & Motz, J.W. 1959, Rev. Mod. Phys. 31, 920
Kolykhalov, P.I. & Sunyaev, R.A. 1979, Sov. Astr. 23, 189
Königl, A. 1981, ApJ 243, 700
Krolik, J.H. & London, R.A. 1983, ApJ 267, 18
Kunieda, H. et al. 1991, *Iron line Diagnostics in X-ray Sources*, eds. A. Treves, G.C. Perola & L. Stella, (Springer-Verlag)
Laing, R.A. 1988, Nat 331, 149
Leiter, D. & Kafatos, M. 1978, ApJ 226, 32
Lovelace, R.V.E. 1976, Nat 262, 649
Madau, P. 1988, ApJ 327, 116
Maisack, M. & Yaqoob, T. 1991, A&A 249, 25
Makino, F. et al. 1989, ApJL 347, L9
Makino, F. et al. 1991, *Variability of Active Nuclei*, eds. H.R. Miller & P.J. Witta, Cambridge University Press
Malkan, M.A. & Sargent, W.L. 1982, ApJ 254, 22
Mannheim, K. & Biermann, P.L. 1992, A&AL 253, L21
Mannheim, K., Krülls, W.M. & Biermann, P.L. 1991, A&A 251, 723
Maraschi, L., Roasio, R. & Treves, A. 1982, ApJ 253, 312
Maraschi, L. & Treves, A. 1977, ApJL 218, L113
Marsher, A.P. et al. 1979, ApJ 233, 498
Marscher, A.P. 1980, ApJ, 235, 386
Marshall, N. et al. 1981, MNRAS 194, 987
Mastichiadis, A. & Protheroe, R.J. 1990, MNRAS 246, 279
Meegan, C.A. & Haymes, R.C. 1979, ApJ 233, 510
Meier, D. 1982, ApJ 256, 693
Melia, F. & Königl, A. 1989, ApJ 340, 162
Michelson, P.F. et al. 1992, IAU Circ. No. 5470
Morganti, R. et al. 1992, MNRAS 256, 1p
Morrison, P. 1969, ApJL 157, L73
Morrison, P. et al. 1984, ApJ 280, 483

Novikov, I.D. & Thorne, K.S. 1973, *Black Holes*, eds. C. DeWitt & B. DeWitt, Gordon and Breach, New York
O'Neill, T. et al. 1989, ApJ 339, 78
Osterbrock, D.E. & Mathews, W.G. 1986, ARAA 24, 171
Ozernoy, L.M. & Chertoprid 1966, Sov. Astr. 10, 15
Ozernoy, L.M.& Usov, B.B. 1971, Astr. Ap. Sci. 12, 267
Pacini, F. & Salvati, M. 1978, ApJL 225, L99
Papaloizou, J.C.B. & Pringle, J.E. 1984, MNRAS 208, 721
Park, M.-G. 1990, ApJ 354, 83
Pearson, T.J. et al. 1981, Nat 290, 365
Penrose, R. 1969, Riv. Nuovo Cimento 1 (Numero Speciale), 252
Perotti, F. et al. 1979, Nat 282, 484
Perotti, F. et al. 1981, ApJL 247, L63
Perotti, F. et al. 1991, ApJ 373, 75
Piran, T. & Shaham, J. 1977, Phys. Rev. D16, 1615
Pollock, A.M.T. et al. 1981, A&A 94, 116
Primini, F.A. et al. 1979, Nat 278, 234
Pringle, J.E. & Rees, M.J. 1972, A&A 21, 1
Protheroe, R.J. & Kazanas, D. 1983, ApJ 265, 620
Ramaty, R. & Lingenfelter, R.E. 1982, Ann. Rev. Nucl. Part. Sci. 32, 235
Rees, M.J. 1984, ARAA 22, 471
Rees, M.J. et al. 1982, Nat 295, 17
Roberts, D. 1984, ApJ 285, 64
Röser,H.-J. & Meisenheimer, K. 1986, A&A 154, 15
Saikia, D.J. & Salter, C.J. 1988, ARAA 26, 93
Salpeter, E.E. 1964, ApJ 140, 796
Salvati, M. et al. 1983 *Positron-Electron Pairs in Astrophysics* eds. M.L. Burns, A.K. Harding & R. Ramaty, AIP 101, 332
Schlickeiser, R. 1982, A&A 106, L5
Schmidt, M. 1963, Nat 197, 1040
Seielstad, G.A. et al. 1979, ApJ 229, 53
Shakura, N.I. & Sunyaev, R.A. 1973, A&A 24, 337
Shapiro, S.L. 1973, ApJ 180, 531
Shields, G. 1978, Nat 272, 706
Shvartsman, V. 1971, Sov. Astr. 15, 377
Sikora, M. et al. 1987, ApJL 320, L81
Sikora, M., Begelman, M.C. & Rudak, B. 1989, ApJL 341, L33
Sikora, M. & Wilson, A. 1981 MNRAS 197, 529
Sparks, W.B. et al. 1992, Nat 355, 804
Stecker, F.W. et al. 1991, Phys. Rev. Let. 66, 2697
Stiavelli, M. et al. 1992, Nat 355, 802
Strong, A.W. & Bignami, G.F. 1983, ApJ 274, 549
Svensson, R. 1984, MNRAS 209, 175
Swannenburg, B.N. et al. 1978, Nat 275, 298
Trombka, J.I. & Fichtel, C.E. 1983, Phys. Rev. 97, 173
Turner, M.J.L. et al. 1990, MNRAS 244, 310
Unwin, S.C. et al. 1985, ApJ 289, 109
Unwin, S.C. et al. 1989, ApJ 340, 117
Urry, G.M. 1988, *Multiwavelength Astrophysics*, ed. F.A. Cordova (Cambridge University Press)
Urry, G.M., Maraschi, L. & Phinney, E.S. 1991, Comm. on Astrophys. 3, 111
Vacanti, G. et al. 1990, 21st ICRC (Adelaide) 2, 329
Von Ballmoos, P. et al. 1987, ApJ 312, 134
von Montigny, C. et al. 1992, A&AS (in press)
Wang, J.C.L., Sulkanen, M.E. & Lovelace, R.V.E. 1990, ApJ 355, 38
Webb, J.R. et al. 1990, AJ 100, 1452
Weekes, T.C. 1988, Phys.Rep. 160, 1
Weekes, T.C. 1992, Sp.Sci.Rev. 59, 314
Weekes, T.C. 1992b, IAU Circ. No. 5522

Whitney, B.J. et al. 1971, Science 173, 225
Wiita, P.J. 1985, Phys. Rep. 123, 117
Willingale, R. 1981, MNRAS 194, 359
Worrall, D.M. et al. 1979, ApJ 232, 683
Young, E.C.M. & Yu, K.N. 1988, J. Phys. G: Nucl.Phys. 14, L115
Zamorani, G. et al. 1984, ApJ 278, 28
Zdziarski, A.A. 1985, ApJ 289, 514
Zdziarski, A.A. 1991, *Beams and Jets in Extragalactic Radio Sources*, Paris
Zdziarski, A.A., et al. 1990, ApJL, 363, L1
Zeldowich, Ya.B. 1964, Sov. Phys.-Doklady 9, 195

7 Summary and Conclusion

The amount of our knowledge concerning discrete γ-ray sources suddenly increased during last two years due to the new generation of operating instruments. However detailed analysis of the already collected data (and expected) will take a few years and at present only some preliminary conclusions may be reached. The most important is that the γ-ray sky is highly variable. The strong γ-ray variability was recently reported for e.g., the quasar 3C 279, Galactic center annihilation source, Nova Musca etc... These results connected with previously discovered transient γ-ray sources like: Solar flares, γ-ray bursts or even some transient features observed in the γ-ray light curves of radio pulsars (e.g. Vela pulsar), strongly support the above conclusion. The observations, mentioned here, will surely stimulate the theoretical efforts for the next decade since their present understanding is unsatisfactory.

Another fact, we think important, is that the γ-ray emission from most of the sources (e.g., AGNs, pulsars, X-ray binary systems, Solar flares) is probably strongly anisotropic. This feature is crucial for the construction of models of γ-ray sources since most of the theoretical efforts were concentrated on the isotropic scenarios which are, however, much easier to analyze in detail. In this thesis we calculate the angular and energy dependent γ-ray spectra from the interaction of a relativistic electron beam with radiation (inverse Compton scattering) and from the interaction of a proton beam with background matter (γ-rays created directly from the decay of π^o and in bremsstrahlung and ICS processes of secondary electrons, which, in turn, originate from the decay of $\pi^{\pm}$). We propose that such calculations may play an essential role in the binary systems (the specific case of Cyg X-1 is discussed in sect. 3.3), old accreting neutron stars, and AGNs.

The main result of this thesis is contained in the propositions of physical scenarios, for a few types of discrete sources, in which some aspects of γ-ray production can be envisaged. Our work concerns the γ-ray emission from radio pulsars, X-ray binary sources and AGNs, and is summarized below.

- The nature of the γ-ray production in the radio pulsars in not completely clear. It is now commonly believed that the main role in these sources is played by the leptonic processes of γ-ray production in strong radiation and magnetic fields (see sect. 4.2). The excellent

signature of such processes will be the appearance of the e^+e^- annihilation feature in the pulsar spectrum and, in fact, such a redshifted e^+e^- annihilation line at $\sim$ 440 keV was recently reported from the Crab Nebula pulsar. We propose the picture, based on the pulsar model of Ruderman and collaborators, in which the origin of this line can be envisaged. In our scenario, the positrons are produced by photons of MeV energy hitting the pulsar crust, which, in turn, are generated by inverse Compton scattering of electrons (positrons) accelerated in the inner polar gap of the pulsar. The e^+e^- line should be also accompanied by the emission feature at $\sim$ 150 keV, due to the Compton backscattering of 0.511 MeV photons. The estimated flux of this feature is comparable to the sensitivity of the OSSE detector on Compton GRO, and may be an important test of our proposition. Because of the tuning required by our picture, it is possible that the emission features in the Crab pulsar spectrum are transient and occur only in the region of one polar cap of the neutron star. We suggest, moreover, that these two features may be also physically related to the other transient features, which are sporadically reported in the Crab pulsar γ-ray spectrum (e.g., MeV bump, variability of MeV – GeV pulsar light curve, PeV γ-ray bursts).

- The evidences of an excess of particles with energies $> 10^{11}$ eV from several X-ray binary systems were one of the most fascinating reports of last decade. It is almost certain that the very high energy γ-ray emission from these sources must originate in hadronic collisions. In this thesis, we discuss a few possible mechanisms which may be responsible for such emission, taking into more detailed consideration Cyg X-3. It is concluded that reported neutral emission in the TeV – EeV energy range from Cyg X-3 may be explained in terms of two mechanisms which are not in contradiction with other features of Cyg X-3 (see sect. 4.3). In the first one, the relativistic neutrons emitted by the compact object interact with the matter accumulated in the binary system. In the second one (originally proposed by Hillas), the relativistic nuclei (e.g., He) initiate the cascade in the matter and magnetic field. In both scenarios the TeV – PeV emission observed from Cyg X-3 is interpreted as due to photons and EeV emission as due to extremely relativistic neutrons.

- The γ-ray production in AGNs we discuss in more detail in the case of two sources 3C 273 and 3C 279 (chap. 6). The physical scenarios, proposed by us, apply hadronic interactions as responsible for γ-ray production. It is now too early to definitively answer the question whether the main role in the production of γ-rays in AGNs is played by leptonic interactions (e.g., synchrotron self-Compton mechanism) or hadronic interactions (decay of pions) interactions. The hadrons are favourite candidates, because of fewer problems with their acceleration to very high energies. However, γ-ray production in AGNs may be a more complicated process

than discussed up to now (sect. 6.2). Different ranges of the γ-ray spectrum may originate in different mechanisms which, moreover, may be located in different places of AGNs (e.g., the central core may be responsible for lower energy γ-rays, jets or extended halos for very high energy γ-ray emission).

We propose that the γ-ray emission from 3C 273 may originate in the extended optical jet of this source, in the interactions of relativistic protons with the matter entrained in the jet volume. As a result of these interactions, γ-ray photons are produced via decay of π^o and in the bremsstrahlung and ICS of microwave black body radiation by secondary electrons originated, in turn, in decay of $\pi^{\pm}$. Our model postulates long term stable γ-ray emission from 3C 273. Preliminary results of analysis of the Compton GRO data and earlier data collected by the COS B can not conclusively answer the question whether the γ-ray emission from 3C 273 is time variable. We note also, that postulated, by our model, relativistic motion in the extended optical jet of 3C 273 is supported by recent observations of other (closer) AGNs (see discussion in sect. 6.3). Similar processes of γ-ray production, however in a different physical scenario, have been applied by us to recently discovered γ-ray emission from 3C 279 (sect. 6.4). In our model, the γ-ray emission originates in the funnel of the thick accretion disk, as a result of the interactions of relativistic particles with the matter of the disk walls. The γ-ray spectrum is formated by photons from the decay of π^o and by comptonization of the thermal radiation of the disk by secondary relativistic electrons from $\pi^{\pm}$ decay. The model can fit reasonably well the observed γ-ray spectrum and explain the reported variability of γ-ray emission from 3C 279 as due to the crossing of the disk limb by the relativistic blobs. Note that such model can not explain possible γ-ray emission above $\sim$ 10 GeV (although, not detected up to now from 3C 279), because of the absorption on the thermal UV photons. The possible emission above $\sim$ 10 GeV may be caused by the relativistic blobs which already emerged from the disk funnel. However, in this case the variability time scale of emission should be much longer. The scenario, summarized here, may be in general agreement with observations of the stable TeV γ-ray emission from another active galaxy Mkn 421, which is similar source to 3C 279.

Appendix

Astron. Astrophys. 236, 268–274 (1990)

ASTRONOMY AND ASTROPHYSICS

The photon spectra from beam interactions with matter and radiation

W. Bednarek[1], F. Giovannelli[2], S. Karakula[1], and W. Tkaczyk[1]

[1] Institute of Physics, University of Lodz, Ul. Nowotki 149/153, PL 90-236 Lodz, Poland
[2] Istituto di Astrofisica Spaziale, CNR, C.P. 67, I-00044 Frascati, Italy

Received June 30, 1989; accepted February 2, 1990

Abstract. We study the Inverse Compton Scattering (ICS) of arbitrary background radiation by a relativistic electron beam and the photon production from proton-proton interactions via π° decay of a relativistic proton beam, in order to obtain the photon spectra. The results of the calculations in the case of interactions of the electron-proton beam with the surrounding matter and/or radiation are presented for selected beam Lorentz's factors and selected angles α_1 between the direction of the emitted photons and the beam axis.

The calculations of differential photon spectra due to ICS were performed for isotropic bremsstrahlung and black body background spectra. The shapes of the comptonized bremsstrahlung spectra are similar to that of the background spectrum, while the shapes of the comptonized black body spectra differ. In both cases, the comptonized spectra are determined by the shape of the background spectrum, the electron beam Lorentz's factor and the angle between the direction of the emitted photons and the beam axis.

The photon spectra from π° decay, produced in the interaction of the relativistic proton beam with the matter, show a strong dependence on the beam's Lorentz factor γ and on the angle between the direction of the emitted photons and the beam axis. For small angles α_1 (with respect to $1/\gamma$), the intensities and positions of the maxima of the photon spectra increase proportionally to the beam's Lorentz factor. For large angles α_1 (with respect to $1/\gamma$), the photon intensities are almost independent of the beam's Lorentz factor, while the positions of the maxima are determined by the value of this angle.

Key words: gamma-ray production – Inverse Compton Scattering – π° decay – relativistic beams

1. Introduction

There is a great deal of observational evidence for highly anisotropic emission and nonspherical structure in the case of some astronomical objects. Jet-like features have been detected in more than 100 extragalactic sources (Bridle and Perley, 1984) and for a number of sources within our own Galaxy e.g. SS 433, SCO X-1, CYG X-3 (see review paper by Rees, 1985). Superluminal motion has been discovered in the central regions of 13 extragalactic radio sources (Cohen and Urwin, 1984; Porcas, 1985; Zensus et al., 1987), which suggests that particles are moving with Lorentz factor $\gamma \gg 1$, at small angles, towards the line of sight. Moreover, X-ray and γ-ray emissions have been detected from some sources with jets (e.g. 3C 273, Cen A, M 87).

Relativistic particles emitted by the central engine of such sources should interact with the surrounding radiation and matter. In the case of Active Galactic Nuclei (AGNs), isotropic background radiation can be produced in the surrounding hot plasma (Frank et al., 1985). In the case of Galactic sources, relativistic particles emitted by pulsars or black holes can interact with the radiation and matter of SNR, or in close binary systems with thermal radiation and matter from the stellar companion. In both cases (AGNs and Galactic sources), anisotropic background radiation can be produced from accretion disks or disk coronae.

Several studies have considered specific models for particle acceleration by different objects (e.g. neutron stars, black holes). In some papers, mechanisms either of acceleration of particles in the high electrical potential produced at the surface of pulsars or accretion disks (Goldreich and Julian, 1969; Lovelace, 1976; Blandford, 1976; Chanmugam and Brecher, 1985), or of acceleration by a magnetic dipole in a strong wave (Gunn and Ostriker, 1969) were proposed. Other proposals, concerning either the acceleration by diffusive shock fronts at the outer boundaries of the SNR, or shock acceleration in accretion flows onto massive black holes, have been also discussed (Krymsky, 1977; Axford et al., 1977; Bell, 1978a, b; Blandford and Ostriker, 1978; Protheroe and Kazanas, 1983; Kazanas and Ellison, 1986). Most of these models consider non-isotropic acceleration of the particles.

In this work we derive the differential photon spectra in the case of single interactions of a mono-energetic, one-dimensional electron-proton beam with the surrounding matter and or radiation.

In Sect. 2 we analyze the ICS of the electron beam with the background photons (bremsstrahlung, black body, etc.) in the general case: i.e. for an arbitrary photon spectrum and selected Lorentz factors of the electrons γ.

In Sect. 3 we derive the high energy photon spectra produced in the interactions of a relativistic proton beam with matter via π° decay. Since the observer can see the beam axis under different angles, we calculate the photon spectra for different angles with respect to the beam axis.

In Sect. 4 we discuss some applications of these calculations to explain the emission of high energy photons from point-like sources and AGNs.

Send offprint requests to: F. Giovannelli

2. The photon spectra from ICS of an electron beam with background photons

The comptonization of photons by relativistic electrons has been studied in an astrophysical context by several authors (e.g. Blumenthal and Gould, 1970; Schlickeiser, 1979; Sunyaev and Titarchuk, 1980; Canfield et al., 1987; Begelman and Sikora, 1987). These authors usually introduce some assumptions – such as the Thomson limit, highly relativistic electrons, low optical depth, etc. – since in the general case the solution is very difficult to achieve.

In this paper we analyze the ICS of arbitrary background photons by a relativistic one-dimensional electron beam.

The comptonized photon spectra (Q) were derived for a given electron beam's Lorentz factor and fixed angle α_1 between the direction of the emitted photons and the beam axis. These spectra are described by the formula:

$$\frac{dN}{d\varepsilon_1\, d\Omega\, dt\, dV} = \frac{n_e}{\gamma^2(1-\beta\cos(\alpha_1))} \iiint c\, n'(\varepsilon', \alpha') \frac{d^2\sigma}{d\Omega_1'\, d\Omega_1} \frac{d\Omega_1'}{d\Omega^*} \frac{d\Omega'}{d\Omega_\mu} d\Omega_\mu\, d\varepsilon' \qquad (1)$$

where: $d\Omega_1'/d\Omega^* = 1$, $d\Omega'/d\Omega_\mu = 1$ are the Jacobians (see Appendix A), $1/\gamma^2(1-\beta\cos(\alpha_1))$ the Jacobian of the transformation of the photon spectrum from the electron's rest frame to the observer's frame, $n'(\varepsilon', \alpha')$ the distribution of the background photons in the electron's rest frame, $d^2\sigma/d\Omega_1' d\varepsilon_1'$ Klein-Nishina cross-section, n_e the beam electron density, c velocity of light. For details of this analysis see Appendix A.

The calculations were made for isotropic bremsstrahlung and black body-type background photon spectra normalized to the photon energy density equal to 1 MeV cm^{-3}, and for the electron beam parameters: $n_e = 1$ cm^{-3} and $\gamma \gg 1$.

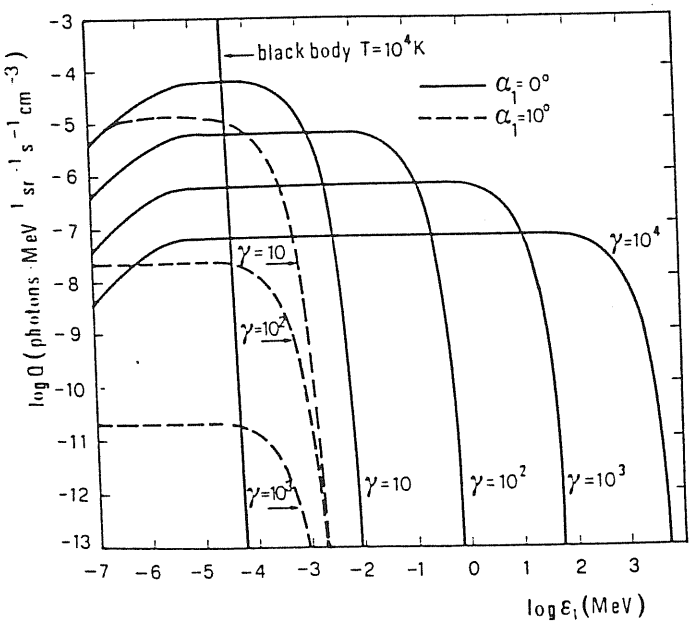

Fig. 1. The comptonized black body spectra ($T = 10^4$ K) for the electron beam Lorentz's factors $\gamma = 10$, 10^2, 10^3, 10^4 and two values of the angles between the direction of the emitted photons and the beam axis: $\alpha_1 = 0°$ (solid line) and 10° (dashed line)

Figures 1 and 2 show the comptonized black body spectra ($T = 10^4$ K and 10^7 K, respectively), for beam's Lorentz factors $\gamma = 10$, 10^2, 10^3, and 10^4, and for two values of the angle between the emitted photon direction and the beam axis ($\alpha_1 = 0°$ and 10°). Figure 3 shows the comptonized black body spectra for $\gamma = 10^3$. $T = 10^7$ K at different angles α_1.

Figures 4a and 4b show the background black body and bremsstrahlung spectra, respectively, for an arbitrary value of the electron beam Lorentz factor γ: (i) in the electron rest frame for

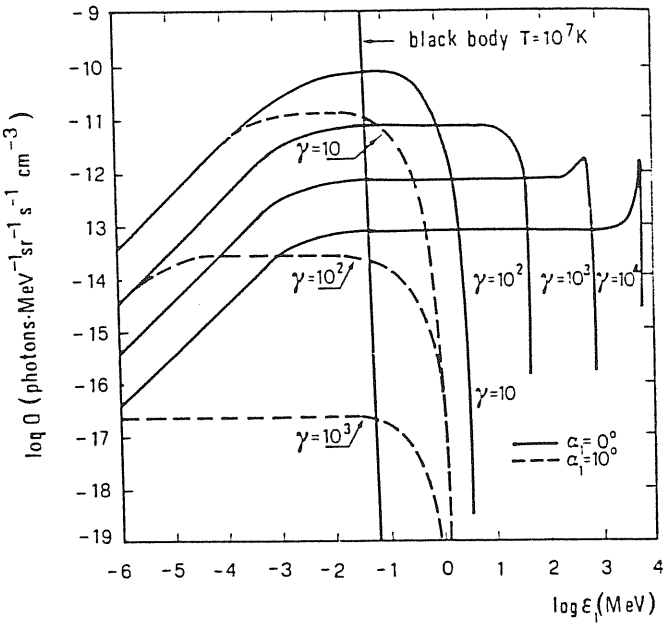

Fig. 2. The comptonized black body spectra ($T = 10^7$ K) for the electron beam Lorentz's factors $\gamma = 10$, 10^2, 10^3, 10^4 and two values of the angles between the direction of the emitted photons and the beam axis $\alpha_1 = 0°$ (solid line) and 10° (dashed line)

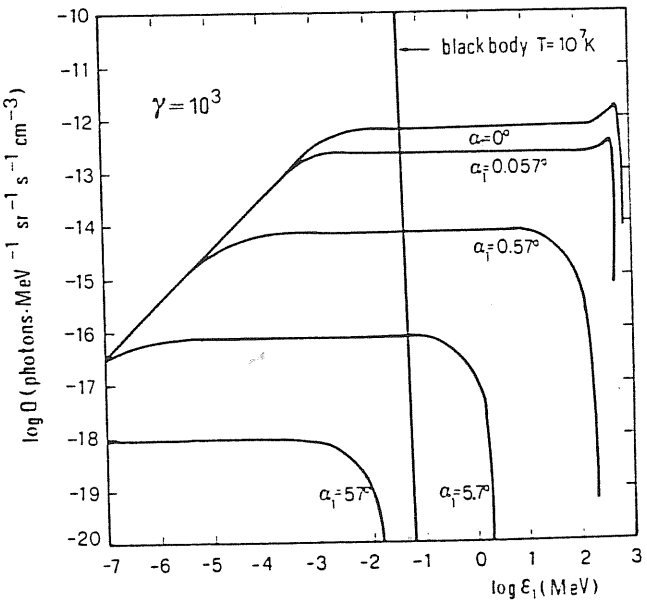

Fig. 3. The comptonized black body spectra ($T = 10^7$ K) for the electron beam Lorentz's factor $\gamma = 10^3$ and selected angles α_1

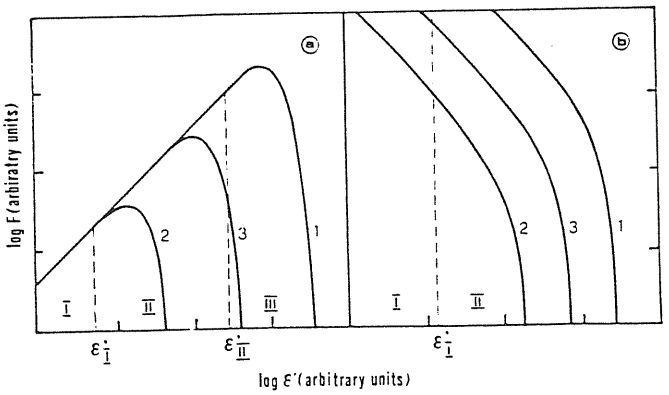

Fig. 4. The background black body (a) and bremsstrahlung (b) spectra in the electron rest frame for an arbitrary value of the electron beam's Lorentz factors γ and selected angles between the direction of the incident photon and the beam axis: $\alpha = 0^\circ$ (curves 1), $\alpha = 180^\circ$ (curves 2) and the photon spectra in the observer frame (curves 3)

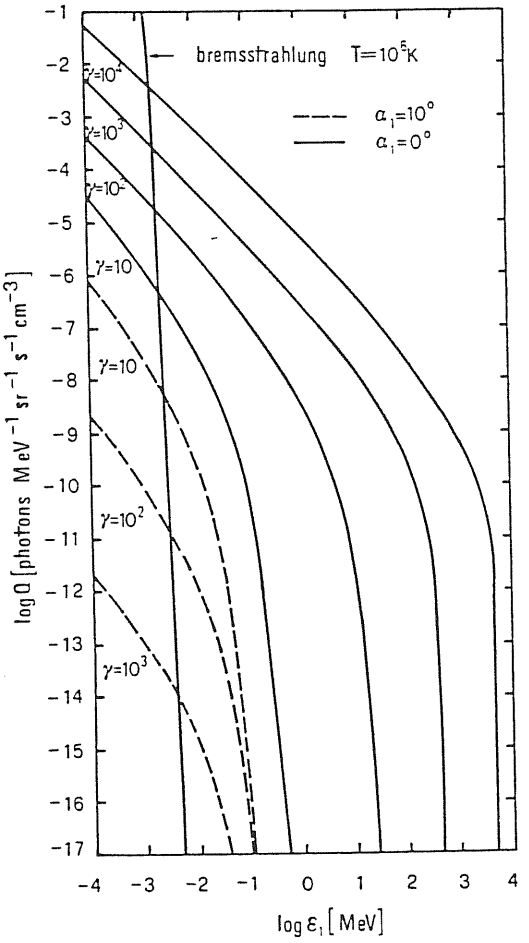

Fig. 5. The comptonized thermal bremsstrahlung spectra ($T = 10^6$ K) for electron beam Lorentz's factor $\gamma = 10$, 10^2, 10^3, and 10^4, and two values of the angles between the directions of emitted photons and the beam axis: $\alpha_1 = 0^\circ$ (solid line) and 10° (dashed line)

two angles between the direction of the incident photons and the beam axis, namely $\alpha = 0^\circ$ (curves 1) and $\alpha = 180^\circ$ (curves 2), respectively; (ii) in the observer frame (curves 3).

In the low energy range (where photon energies in the electron rest frame are $\varepsilon'_1 < \varepsilon'_I$; ε'_I is the photon energy below which all the spectra have a spectral index about 1, see Fig. 4a), the comptonized black body spectra are independent of the angle α_1 and their shapes are the same as that of the low energy part of the black body background spectrum, as also shown in Fig. 3. Analyzing formula 1 for the case of Thomson cross section, one can easily understand such spectral features. For photon energies in the electron rest frame $\varepsilon'_I \leq \varepsilon'_1 \leq \varepsilon'_{II}$ (where ε'_{II} is the photon energy above which all photon spectra have a spectral index essentially different from 1, see Fig. 4a), the spectra become flat showing broad plateaus as is also indicated in Fig. 1. The widths of the plateaus are proportional to γ^2. The flattening of the comptonized spectra in this energy range is clear, since the main contribution to the spectra comes from the area which, in the case of the black body spectrum, is inversely proportional to the photon energy in the electron rest frame. For photon energies in the electron rest frame $\varepsilon'_1 > \varepsilon'_{II}$, the comptonized spectra have an exponential cut-off as is also shown in Fig. 1. From Fig. 2 one can also note that for small angles α_1 (with respect to $1/\gamma$) the cut-off energy in these spectra is determined by γ, while for large angles (i.e. $\alpha_1 = 10^\circ$) the position of the cut-off energy is independent of γ and, on the contrary, is determined by the value of these angles, as more clearly depicted in Fig. 3.

In each case the width of the plateau is determined by the electron energy. For high values of γ (10^3 and 10^4 see Fig. 2) before the sharp cut-off at energies $\varepsilon_1 \cong \gamma m$, the spectra display a characteristic peaked shape. The appearance of these peaks is caused by a rapid extension of the limits of integration (derived from the kinematics of ICS) and by the shape of the black body spectrum.

In general, the intensities of these comptonized black body spectra, for small angles α_1, are inversely proportional to γ (Figs. 1 and 2). For large angles α_1, the intensities are determined by the angle α_1 itself (Fig. 3), and for fixed values of these angles, they are inversely proportional to γ^3 (Figs. 1 and 2). The maximum intensities in the peaks, for fixed angles, are roughly independent of γ as shown in Fig. 2.

Figure 5 shows the comptonized thermal bremsstrahlung photon spectra ($T = 10^6$ K) for $\gamma = 10$, 10^2, 10^3, 10^4 and two angles $\alpha_1 = 0^\circ$ and 10°. In general, these comptonized bremsstrahlung spectra are similar in shape to the background spectrum because the main contribution to the spectra comes from a very small area around the beam axis (curve 1 for $\alpha = 0^\circ$ in Fig. 4b). For photon energies in the electron rest frame $\varepsilon'_1 < \varepsilon'_I$ (see Fig. 4b), all the comptonized spectra are of power law type with power index equal to -1. For photon energies $\varepsilon'_1 > \varepsilon'_I$, the comptonized spectra are characterized by an exponential cut-off. The energy of the cut-off in the comptonized bremsstrahlung spectra is derived as in the case of comptonized black body spectra, because these features are produced by the kinematics of ICS. We note that in the case of comptonized bremsstrahlung spectra the peaked features do not appear at an energy near $\varepsilon_1 \cong \gamma m$ (see the curve for $\gamma = 10^4$ and $\alpha_1 = 0^\circ$ in Fig. 5), while they are present in the comptonized black body spectra (see the curves for $\gamma = 10^3$, 10^4, and $\alpha_1 = 0^\circ$ in Fig. 2). The intensities of the bremsstrahlung comptonized spectra for small angles α_1 are proportional to γ, while for large angles these intensities are inversely proportional to γ^3 (see Fig. 5).

3. The photon spectra from the interaction of a proton beam with matter

The relativistic proton beam passing through a hydrogen cloud loses its energy by proton-proton inelastic interactions. The high energy photons can be produced by the decay of π^0 produced in the reaction $p+p\to\pi^0+$ anything. Analyzing such a process, we have obtained the photon spectra (Q) from a monoenergetic beam and hydrogen cloud interaction for a given angle α_1 between the direction of the emitted photons and the beam axis. These spectra are described by the formula:

$$\frac{dN}{dE_\gamma d\Omega dt dV} = D\iiint \frac{d^3\sigma(p_{\pi^0}, \cos\theta_{\pi^0}, \varphi_{\pi^0})}{dp_{\pi^0} d(\cos\theta_{\pi^0}) d\varphi_{\pi^0}}$$

$$\times P(E_\gamma, \cos\theta, \varphi) dp_{\pi^0} d(\cos\theta_{\pi^0}) d\varphi_{\pi^0}, \qquad (2)$$

where: $D=\beta c n_b n_H$, n_H the hydrogen density in the cloud, n_b the proton density in the beam, βc the proton velocity, p_{π^0} the π^0 momentum in the observer's frame, θ_{π^0}, φ_{π^0} the angles between the direction of the momentum of the emitted π^0 and beam axis in the observer's frame,

$$\frac{d^3\sigma(p_{\pi^0}, \cos\theta_{\pi^0}, \varphi_{\pi^0})}{dp_{\pi^0} d(\cos\theta_{\pi^0}) d\varphi_{\pi^0}} = \frac{p_{\pi^0}^2}{E_{\pi^0}}\left(E_{\pi^0}\frac{d^3\sigma}{dp^3}\right)$$

the cross section in polar coordinates, $E_{\pi^0} d^3\sigma/dp^3$ the invariant cross section (Stephens and Badhwar, 1981), $P(E_\gamma, \cos\theta, \varphi)$ the energy and angular distribution of photons from π^0 decay in the observer's frame, $E_\gamma, \theta, \varphi$ the energy and angles in polar coordinates of the emitted photons in the observer's frame. For the details of this analysis, see Appendix B.

Let us note that in a detailed analysis of models describing the interaction of a proton-beam with matter, Dermer (1986) showed that for a photon energy lower than 3 GeV the characteristics of this interaction are very well described using an isobar model. For a photon energy greater than 12.5 GeV this interaction can be described reasonably well using the scaling model and the approximation of the invariant cross section given by Stephens and Badwar (1981). Since we are interested in the interaction of a high energy proton-beam (Lorentz's factor $\gamma > 10$) with matter, we have used the latter model.

The differential photon spectra from π^0 decay were numerically calculated according to formula (2) in the case of a beam Lorentz factor $\gamma \gg 1$, and for unit density of the proton beam and the hydrogen cloud.

Figure 6 shows the differential photon spectra from π^0 decay for proton beam Lorentz factors $\gamma = 10$, 10^2, 10^3, 10^4 and two values of the angles $\alpha_1 = 0^\circ$ and 10°. In Fig. 7, we illustrate the differential photon spectra from π^0 decay for $\gamma = 10^4$ and selected angles $\alpha_1 = 0^\circ$, 0.057°, 0.57°, 5.7°, and 57°.

In general, the shapes and the intensities of these spectra are very sensitive to γ and/or α_1. For small angles α_1 (with respect to $1/\gamma$), the intensities of the photons' spectra, and the widths and positions of their maxima grow proportionally with γ (Fig. 6), since in this case the momenta of the π^0s, which create these photons, are proportional to γ. For large α_1, the shapes and intensities of the photon spectra are practically independent of γ (see Fig. 6) since the momenta of the π^0s, which create these photons, are roughly the same (see Appendix B). In a certain range of photon energies, the intensities of the spectra, calculated for $\gamma = \text{const}$, are comparable in the rising part for different values of α_1 (e.g. for $\gamma = 10^4$, this is roughly valid in the range $-1 \le \log(E) \le 2$ and for $0^\circ \le \alpha_1 \le 5.7^\circ$). We note that for large angles the positions of the maximum intensities of the photon spectra are determined by the values of the angle α_1 and are independent of γ (see Fig. 6).

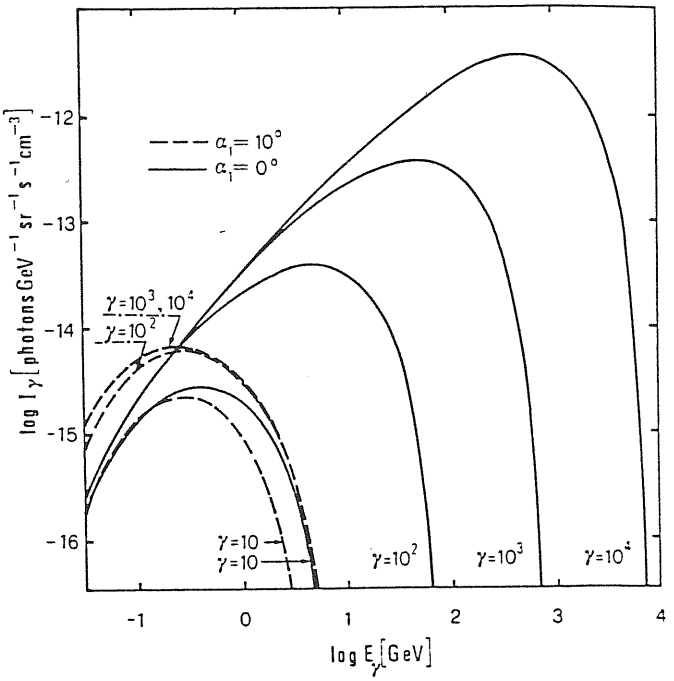

Fig. 6. The photon spectra from π^0 decay for the proton beam Lorentz's factors $\gamma = 10$, 10^2, 10^3, and 10^4 and two values of the angles between the direction of the emitted photons and the beam axis: $\alpha_1 = 0^\circ$ (solid line) and 10° (dashed line), for unit densities ($n_b = n_H = 1\ \text{cm}^{-3}$)

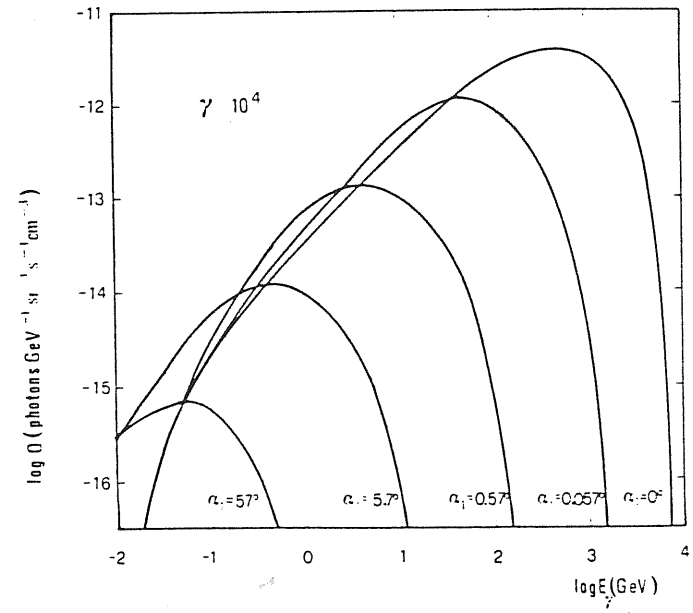

Fig. 7. The photon spectra from π^0 decay for the proton beam Lorentz's factor $\gamma = 10^4$ and selected angles α_1 calculated for unit densities ($n_b = n_H = 1\ \text{cm}^{-3}$)

4. Discussion and conclusions

The interaction of a relativistic electron beam with the background electromagnetic radiation (ICS) and the interaction of a relativistic proton beam with the surrounding matter ($p+p\rightarrow\pi^{\circ}+$ anything, $\pi^{\circ}\rightarrow 2\gamma$) have been analyzed in order to obtain the differential photon spectra.

The production of charged pions which decay into electrons and positrons generates a γ-ray continuum via bremsstrahlung. This continuum dominates the π°-decay component for γ-ray energies $E<50$ MeV independent of the interstellar gas density (Schlickeiser, 1982). In our case, the considered energies of the γ-rays are $E>67.5$ MeV, which is the peak energy coming from π°-decay (Giovannelli et al., 1982a; 1982b). At these energies the π°-decay component dominates.

The expression for the photon spectra from ICS has been derived for an arbitrary distribution of the background photons, various electron beam Lorentz factors γ and selected angles α_1 between the direction of the emitted photons and the beam axis, by using Klein-Nishina cross section. Numerical calculations of the photon spectra have been performed for optically thin thermal bremsstrahlung and black body background radiation in the case of an isotropic distribution of photons, and for $\gamma\gg 1$. Such background photons probably surround AGNs and close binary systems. Bremsstrahlung radiation can be originated from clouds at temperatures of about 10^6 K, surrounding AGNs (Frank et al., 1985); or black body radiation from an accretion disk, at a temperature of about 10^7 K (Shakura and Sunyaev, 1973); and/or from a stellar companion with temperature $\geq 10^4$ K in close binary systems.

In general, for an isotropic distribution of photons, the shapes of the comptonized spectra are determined by the shape of the background spectrum, but the cut-offs of the comptonized spectra strongly depend on the electron beam Lorentz factor and on the angle between the direction to the observer and the beam axis (see Figs. 1, 2, 3, and 5). The main features of these spectra are: for large angles α_1 (with respect to $1/\gamma$), the comptonized spectra are mainly determined by the angle α_1 itself, while for small angles α_1, they are essentially dependent on the electron beam's Lorentz factor γ. We can note that for large γ and small α_1 the comptonized black body spectra show peaks just before the sharp cut-off for an electron energy $\varepsilon_1\cong\gamma m$ (curves for $\gamma=10^3$, 10^4 and $\alpha_1=0^{\circ}$ in Fig. 2). These spectral features should be observed from sources emitting monoenergetic electron beams which propagate in optically thin fields of quasi isotropic background photons.

The expression for the photon spectra from π° decay has been derived for various Lorentz factors of the proton beam γ and selected angles α_1 between the direction of the emitted photons and beam axis. The photon spectra have been calculated in the case of $\gamma\gg 1$ and for unit densities of the proton beam and hydrogen cloud.

In general, the shapes and the intensities of the photon spectra from π° decay are very sensitive to the proton beam's Lorentz factor and/or to the angle α_1. The main features of these spectra are: for small angles α_1 (with respect to $1/\gamma$) the intensities, the widths and positions of the maxima of their spectra grow proportionally with γ, while for large angles α_1 they are determined by the value of this angle, and are practically independent of γ (Fig. 6). The last feature means, that for large angles α_1 in spite of the different shape of the proton spectrum and propagation of the proton beam, the photon spectra should have roughly the same shape.

Up to now, a number of point sources which emit photons in TeV and PeV energy range – e.g. Cyg X-3, the Crab Pulsar, Hercules X-1, Vela X-1, 4U 0115+63 (Hillas, 1985; Hillas, 1987; Lamb, 1987; Lewis et al., 1989) have been discovered. The presence of such high energy photons (if they are produced in the interactions of a proton beam with the background matter via π° decay) means that relativistic particles should move practically in our direction inside a cone $\alpha_1[\text{rad}]<1/(E_{\text{ph}}[\text{GeV}])$, (see Fig. 7). From a statistical point of view, the existence of TeV photon sources suggests that a number of photon sources should be observed at much larger angles α_1. So, if we observe two identical photon sources, the first one at a very small angle α_1, and the second one at a larger angle α_1, both should be observed with comparable intensity in the GeV range, while only the first one should be observed in the TeV range (see Figs. 6 and 7).

In our next paper we shall use these results in order to explain the experimental photon spectrum of Geminga measured by COS B (Masnou et al., 1981) and the experimental photon spectrum of Cyg X-1 in the MeV region (McConnell et al., 1987).

Acknowledgements. We wish to thank the referee, Dr. G. Kanbach, for his valuable suggestions.

Appendix A: the calculation of the photon spectra from ICS

The scattering of a photon with an energy ε' and with an incidence angle α' (with respect to the direction of the electron velocity), and an angle α'_1 and an energy ε'_1 in the electron rest frame and in the observer's frame, are shown in Figs. A1a and A1b, respectively.

We derived the photon spectra in the electron rest frame and then transformed these spectra into the observer's frame.

In the electron rest frame, the distribution of the scattered photons per electron is given by the following formula:

$$\frac{\mathrm{d}N}{\mathrm{d}t'\,\mathrm{d}\Omega'_1\,\mathrm{d}\varepsilon'_1}=n'[\varepsilon(\varepsilon',\alpha')]\,c\,\frac{\mathrm{d}\sigma}{\mathrm{d}\Omega'_1\,\mathrm{d}\varepsilon'_1}\,\mathrm{d}\Omega'\,\mathrm{d}\varepsilon'. \tag{A1}$$

The differential photon density in the electron rest frame $n'[\varepsilon(\varepsilon',\alpha')]$ for isotropic distribution is expressed by:

$$n'[\varepsilon(\varepsilon',\alpha')]=\frac{1}{4\pi}J_1\,n[\varepsilon(\varepsilon')] \tag{A2}$$

where: $J_1=1/\gamma(1-\beta\cos(\alpha'))$ the Jacobian of the transformation, $n[\varepsilon(\varepsilon')]$ the differential photon energy density in the observer's frame.

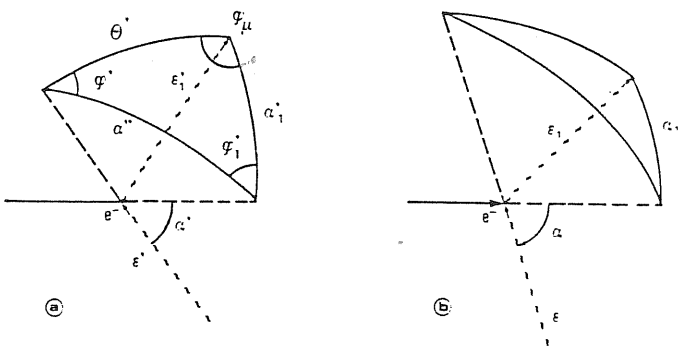

Fig. A1a and b. Kinematics of the ICS in the electron rest frame (a) and in the observer frame (b)

In the electron's rest frame, the Klein-Nishina's cross section is given by:

$$\frac{d^2\sigma}{d\Omega'_1 d\varepsilon'_1}=\frac{1}{2}r_0^2\left(\frac{\varepsilon'_1}{\varepsilon'}\right)^2\left(\frac{\varepsilon'}{\varepsilon'_1}+\frac{\varepsilon'_1}{\varepsilon'}+\cos^2(\theta)-1\right)\times\delta\left(\varepsilon'_1-\frac{\varepsilon'}{1+\frac{\varepsilon'}{m}(1-\cos(\theta'))}\right).$$

So, the photon spectra in the electron's rest frame can be expressed by:

$$\frac{dN}{dt'd\Omega^*d\varepsilon'_1}=\frac{c}{4\pi}\int\int\int\frac{n[\varepsilon(\varepsilon')]}{\gamma(1-\beta\cos(\alpha'))}\frac{d^2\sigma}{d\Omega'_1 d\varepsilon'_1}\frac{d\Omega'_1}{d\Omega^*}\frac{d\Omega'}{d\Omega_\mu}d\Omega_\mu d\varepsilon' \tag{A3}$$

where: $d\Omega^*=d(\cos(\alpha'_1))d\varphi'_1$, $d\Omega'_1=d(\cos(\theta'))d\varphi'$, $d\Omega'=d(\cos(\alpha''))d\varphi'_1$, $d\Omega_\mu=d(\cos(\theta'))d\varphi_\mu$ (see Fig. A1a), $-\cos(\alpha')=\cos(\theta')\cos(\alpha'_1)+\sin(\theta')\sin(\alpha'_1)\cos(\varphi_\mu)$ the relation between the angles derived from spherical trigonometry (see Fig. A1a), $\varepsilon'=\gamma\varepsilon(1+\beta\cos(\alpha))$, $\varepsilon'_1=\gamma\varepsilon_1(1-\beta\cos(\alpha_1))$, $\alpha'_1=\arctan(\sin(\alpha_1)/\gamma[\cos(\alpha_1)-\beta])$.

The integration over $d(\cos(\theta'))$, in the formula (A3), was analytically performed, by using Dirac's δ-function:

$$\frac{dN}{dt'd\Omega^*d\varepsilon'_1}=\frac{1}{2}\frac{c}{4\pi}r_0^2 m\int\int\frac{n[\gamma\varepsilon'(1-\cos(\alpha'(x)))]}{\gamma(1-\beta\cos(\alpha'(x)))}\times\frac{1}{(\varepsilon')^2}\left(\frac{\varepsilon'}{\varepsilon'_1}+\frac{\varepsilon'_1}{\varepsilon'}+x^2-1\right)d\varphi_\mu d\varepsilon' \tag{A4}$$

where, $x=\cos(\theta')=1-m/\varepsilon'_1+m/\varepsilon'$.

The limits of integration in the formula (A4), over φ_μ and ε' are given by:

for $\varepsilon'_1\geq\frac{m}{2}$, $\varepsilon'_1\leq\varepsilon'<\infty$ and $0\leq\varphi_\mu\leq 2\pi$,

for $\varepsilon'_1<\frac{m}{2}$, $\varepsilon'_1\leq\varepsilon'\leq\frac{\varepsilon'_1}{1-2\frac{\varepsilon'_1}{m}}$ and $0\leq\varphi_\mu\leq 2\pi$.

The photon spectra were obtained by the transformation of the formula (A4) into the observer's frame. It is expressed by:

$$\frac{dN}{dt\,d\Omega\,d\varepsilon_1\,dV}=J_2 n_e\frac{dN}{dt'd\Omega^*d\varepsilon'_1} \tag{A5}$$

where, $J_2=1/\gamma^2(1-\beta\cos(\alpha_1))$ is the Jacobian of the transformation.

We note that, for an angle between the photon emission direction and the beam axis $\alpha_1=0°$, and $\alpha_1=180°$, the integration over φ_μ in the formula (A4) can be easily performed, since the function under the integral is independent of φ_μ.

Appendix B: the calculation of the photon spectra from π° decay

We derived the detailed formula for the photon spectra from π° decay which was directly used in the calculations.

The distribution of the photons in the π° rest frame is isotropic and can be described by:

$$P(\cos(\theta'),\varphi',E'_\gamma)\,d(\cos(\theta'))\,d\varphi'\,dE'_\gamma=\frac{2d(\cos(\theta'))\,d\varphi'}{4\pi}\delta\left(E'_\gamma-\frac{m_{\pi^\circ}}{2}\right)dE'_\gamma \tag{B1}$$

and after the transformation into the observer's frame, the distribution of the photons takes the form:

$$P(\cos(\theta),\varphi,E_\gamma)\,d(\cos(\theta))\,d\varphi\,dE_\gamma=J_3\frac{2}{4\pi}\delta\left(\gamma_{\pi^\circ}E_\gamma(1-\beta_{\pi^\circ}\cos(\theta))-\frac{m_{\pi^\circ}}{2}\right)d(\cos(\theta))\,d\varphi\,dE_\gamma \tag{B2}$$

where, $J_3=2E_\gamma/m_{\pi^\circ}$ is the Jacobian of the transformation.

Substituting into formula (2) the photon distribution in the observer's frame (B2), we obtain the expression for the photon production spectrum:

$$\frac{dN}{dE_\gamma d\Omega\,dV\,dt}=\beta c n_b n_H\int\int\int\frac{p_{\pi^\circ}^2}{E_{\pi^\circ}}\left(E_{\pi^\circ}\frac{\hat{c}^3\sigma}{\hat{c}p^3}\right)\frac{2E_\gamma}{m_{\pi^\circ}}\frac{2}{4\pi}\times\delta\left(\gamma_{\pi^\circ}E_\gamma(1-\beta_{\pi^\circ}\cos(\theta))-\frac{m_{\pi^\circ}}{2}\right)d(\cos(\theta_{\pi^\circ}))\,d\varphi_{\pi^\circ}\,dp_{\pi^\circ}, \tag{B3}$$

where the angle θ (between the directions of the π° momentum and the emitted photons) is expressed via spherical trigonometry (see Fig. B1):

$$\cos(\theta)=\cos(\theta_{\pi^\circ})\cos(\alpha_1)+\sin(\theta_{\pi^\circ})\sin(\alpha_1)\cos(\varphi_{\pi^\circ}).$$

In order to perform numerical calculations, we distinguish two cases:

(i) For angles between the direction of the photons emitted and the beam axis, $\alpha_1\neq 0°$ and $\alpha_1\neq 180°$.

The integration over φ_{π° in the formula (B3) was analytically made taking into account the properties of Dirac's δ-function:

$$\frac{dN}{dE_\gamma d\Omega\,dV\,dt}=\beta c n_H n_b\left\{\int_{p_{\min}}^{p_1}\int_{\xi_1}^{\xi_2}A(p_{\pi^\circ},\xi,\alpha,E_\gamma)\,dp_{\pi^\circ}\,d\xi+\int_{p_1}^{p_2}\int_{\xi_3}^{\xi_2}A(p_{\pi^\circ},\xi,\alpha,E_\gamma)\,dp_{\pi^\circ}\,d\xi\right\} \tag{B4}$$

where

$$A(p_{\pi^\circ},\xi,\alpha_1,E_\gamma)=\frac{1}{\pi}\frac{p_{\pi^\circ}^2}{E_{\pi^\circ}}\left(E_\pi\frac{\hat{c}^3\sigma}{\hat{c}p^3}\right)\frac{1}{p_{\pi^\circ}}\left\{\sin^2(\alpha_1)(1-\xi^2)-\left[\frac{1}{\beta_{\pi^\circ}}\left(1-\frac{N}{\gamma_{\pi^\circ}}\right)-\xi\cos(\alpha_1)\right]^2\right\}^{-1/2}$$

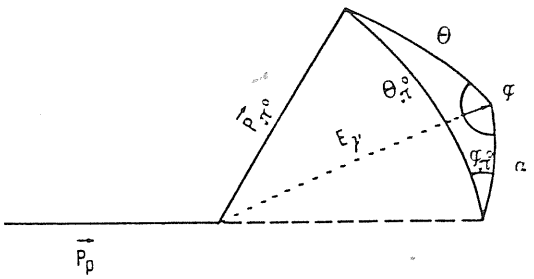

Fig. B1. Geometry of the photon production in the proton-proton interaction via π° decay in the observer frame

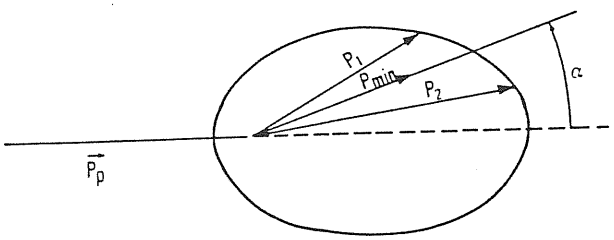

Fig. B2. The limit values of the π° momenta ($p_{\min}, p_1, p_2$) which produce photons with energy E_γ in the direction α_1

$\xi=\cos(\theta_{\pi^\circ})$, $p_{\min}=m_{\pi^\circ}(N^2-1)/2N$, $N=m_{\pi^\circ}/2E_\gamma$, $p_{\min}$ the minimum π° momentum which can produce photons with energy E_γ at an angle α_1 with respect to the beam axis (see Fig. B2).

Transforming the maximum π° momentum in the central mass system into the observer's frame, it is possible to evaluate the limits of integration over the π° momenta (p_1, p_2) for a given proton energy (E_p) (Fig. B2), by solving the equation:

$$\cos(\theta_{\pi^\circ}^{\max})=\cos(\alpha_1\pm\theta), \tag{B5}$$

where:

$$\cos(\theta_{\pi^\circ}^{\max})=\frac{m_{\pi^\circ}\gamma_{\pi^\circ}\gamma_s-(p_{\max}^{*2}+m_{\pi^\circ}^2)^{1/2}}{m_{\pi^\circ}[(\gamma_s^2-1)(\gamma_{\pi^\circ}^2-1)]^{1/2}}$$

is the cosine of maximum angle of π° emission for a given proton energy and fixed π° momentum,

$$s=2m_p(m_p+E_p),\ \gamma_s=E_p+m_p/\sqrt{s},$$

$$p_{\max}^*=\left[\frac{(s-4m_p^2-m_{\pi^\circ}^2)^2-16m_p^2m_{\pi^\circ}^2}{4s}\right]^{1/2},\ \cos(\theta)=\frac{\gamma_{\pi^\circ}-N}{\sqrt{\gamma_{\pi^\circ}^2-1}}.$$

Solving the Eq. (B5), we obtained the limit values of Lorentz factors for the π° and then the π° momenta p_1 and p_2.

The limits of integration over ξ for a given π° momentum are equal to:

$$\xi_1=\cos(\alpha_1+\theta),\quad \xi_2=\cos(\alpha_1-\theta),\quad \xi_3=\frac{\sqrt{p_{\pi^\circ}^2+m_{\pi^\circ}^2}-m_{\pi^\circ}M}{p_{\pi^\circ}\beta_s}$$

where:

$$M=\frac{1}{\gamma_s}\left[\left(\frac{p_{\max}^*}{m_{\pi^\circ}}\right)^2+1\right]^{1/2};$$

(ii) For angles between the direction of the emitted photons and the beam axis $\alpha_1=0^\circ$ and $\alpha_1=180^\circ$.

In this case the function under the integral in the formula (B3) is independent of φ_{π°, so that the integral over φ_{π° can easily be evaluated, and the integral over $\cos(\theta_{\pi^\circ})$ can be analytically performed taking into account the properties of Dirac's δ-function. The final result is expressed by:

$$\frac{dN}{dE_\gamma\,d\Omega\,dV\,dt}=\beta c n_b n_H\int_{p_{\min}}^{p_{\max}}2\frac{p_{\pi^\circ}^2}{E_{\pi^\circ}}\left(E_{\pi^\circ}\frac{\hat{c}^3\sigma}{\hat{c}p^3}\right)\frac{dp_{\pi^\circ}}{p_{\pi^\circ}} \tag{B6}$$

where: $p_{\min}$ defined as in the case (i), $p_{\max}$ derived from Eq. (B5).

References

Axford, W.I., Leer, E., Skadron, G.: 1977, *Proc. 15th Int. Cosmic. Ray Conf.* (Plovdiv) **11**, 132

Begelman, M.C., Sikora, M.: 1987, *Astrophys. J.* **322**, 650

Bell, A.R.: 1978a, *Monthly Notices Roy. Astron. Soc.* **182**, 147

Bell, A.R.: 1978b, *Monthly Notices Roy. Astron. Soc.* **182**, 443

Blandford, R.D., Ostriker, J.P.: 1978, *Astrophys. J. Letters* **221**, L29

Blandford, R.D.: 1976, *Monthly Notices Roy. Astron. Soc.* **176**, 465

Blumenthal, R.G., Gould, R.J.: 1970, *Rev. Mod. Phys.* **42**, 237

Bridle, A.H., Perley, R.A.: 1984, *Ann. Rev. Astron. Astrophys.* **22**, 319

Canfield, E., Howard, W.M., Liang, E.P.: 1987, *Astrophys. J.* **323**, 565

Chanmugam, G., Brecher, K.: 1985, *Nature* **313**, 767

Cohen, M.H., Urwin, S.C.: 1984, *IAU Symp.* **110**, 95

Dermer, C.D.: 1986, *Astron. Astrophys.* **157**, 223

Frank, J., King, A.R., Raine, D.J.: 1985, in *Accretion Power in Astrophysics*, Cambridge University Press, Cambridge

Giovannelli, F., Karakula, S., Tkaczyk, W.: 1982a, *Astron. Astrophys.* **107**, 376

Giovannelli, F., Karakula, S., Tkaczyk, W.: 1982b, *Acta Astron.* **32**, 121

Gluckestern, R.L., Hull, M.H.: 1953, *J. Phys. Rev.* **90**, 1030

Goldreich, P., Julian, W.: 1969, *Astrophys. J.* **157**, 869

Gunn, J.E., Ostriker, J.P.: 1969, *Phys. Rev. Letters* **22**, 728

Hillas, A.: 1985, *Proc. 19th Int. Cos. Ray Conf.* (La Jolla) **9**, 407

Hillas, A.: 1987, in *HE-vHE Behaviour of Accreting X-ray Sources*, eds. F. Giovannelli, G. Mannocchi, Italian Physical Society, Editrice Compositori, Bologna, Italy, p. 235

Kazanas, D., Ellison, D.C.: 1986, *Astrophys. J.* **304**, 178

Krymsky, G.F.: 1977, *Soviet Phys. Dokl.* **23**, 327

Lamb, R.C.: 1987, in *HE-vHE Behaviour of Accreting X-ray Sources*, eds. F. Giovannelli, G. Mannocchi, Italian Physical Society, Editrice Compositori, Bologna, Italy, p. 235

Lewis, D.A., Cawley, M.F., Fegan, D.J., Hillas, A.M., Kwok, W., Lamb, R.C., Macomb, D.J., Porter, N.A., Reynolds, P.T., Vacauti, G., Weekes, C.: 1989, in *Frontier Objects in Astrophysics and Particle Physics*, eds. F. Giovannelli, G. Mannocchi, Italian Physical Society, Editrice Compositori, Bologna, Italy, p. 277

Lovelace, R.V.E.: 1976, *Nature* **262**, 649

Masnou, J.L., Bennett, K., Bignami, G.F., Bloemen, J.B.G.M., Buccheri, R., Caraveo, P.A., Hermsen, W., Kanbach, G., Mayer-Hasselwander, H., Paul, J.A., Wills, R.D.: 1981, *Proc. 17th Int. Cosmic Ray Conf.* (Paris) **1**, 177

McConnell, M.L., Owens, A., Chupp, E.L., Dunphy, P.P., Forest, D.J., Vestrand, W.T.: 1987, *Proc. 20th Int. Cosmic Ray Conf.* (Moscow) **1**, 58

Porcas, R.W.: 1985, in *Active Galactic Nuclei*, ed. J.E. Dyson, Manchester Univ. Press, Manchester, p. 20

Protheroe, R.J., Kazanas, D.: 1983, *Astrophys. J.* **265**, 620

Rees, M.: 1985, *Proc. 19th Int. Cosmic Ray Conf.* (La Jolla) **9**, 1

Schlickeiser, R.: 1979, *Astrophys. J.* **233**, 294

Schlickeiser, R.: 1982, *Astron. Astrophys. Letter* **106**, L5

Shakura, N.I., Sunyaev, R.: 1973, *Astron. Astrophys.* **337**, 24

Stephens, S.A., Badhwar, G.D.: 1981, *Astrophys. Space Sci.* **76**, 213

Sunyaev, R.A., Titarchuk, L.G.: 1980, *Astron. Astrophys.* **86**, 121

Zensus, J.A., Hough, D.H., Porcas, R.W.: 1987, *Nature* **325**, 36

Astron. Astrophys. 236, 175–179 (1990)

ASTRONOMY AND ASTROPHYSICS

Origin of the γ-ray spectra of Cygnus X-1 and Geminga

W. Bednarek[1], F. Giovannelli[2], S. Karakula[1], and W. Tkaczyk[1]

[1] Institute of Physics, University of Lodz, Ul. Nowotki 149/153, PL 90-236 Lodz, Poland
[2] Istituto di Astrofisica Spaziale, CNR, C.P. 67, I-00044 Frascati, Italy

Received May 30, 1989; accepted February 2, 1990

Abstract. The interactions of beamed relativistic particles with matter and/or radiation could be one of the possible mechanisms of high energy γ-ray production in point sources. The shape and the intensity of the photon spectra, produced in such interactions, strongly depend on the beam's Lorentz factor and on the angle between the direction to the observer and the beam axis (Bednarek et al., 1990, hereafter Paper I).

From the calculated photon spectra from Inverse Compton Scattering (ICS) of the background radiation by relativistic electron-beams and photon spectra from proton-proton interaction via π^0 decay for relativistic proton-beams, we search for the best fit between these theoretical spectra and the experimental data from Cyg X-1, at energies above 1 MeV, and from Geminga, in the COS B energy range.

The behaviour of Cyg X-1 at energies greater than 1 MeV can be explained with the comptonized spectrum of the companion star HDE 226868, if the relativistic electrons, with a Lorentz factor equal to about 600, are emitted in our direction. The derived lower limit on the emissivity of relativistic electrons is $N_e \cong 1.5\,10^{38}$ electron s^{-1}, corresponding to the electron luminosity $L_e \cong 7.0\,10^{34}$ erg s^{-1}. If the high energy photons detected from Geminga originate in proton-proton interactions of beamed relativistic particles with surrounding matter, the required beam parameters should be: Lorentz factor greater than 30, the angle between the beam axis and the direction to the observer equal to about 35°. The derived lower limit on the emissivity of the proton-beam, from the COS B data best fit, is $N_p \cong 7.5\,10^{-4}\, d^2/x_p$, d being the distance to Geminga in cm and x_p the column density of the background matter in g cm^{-2}.

Key words: γ-ray spectra – Cyg X-1; Geminga

1. Introduction

The discovery of γ-ray point sources stimulated research on the mechanisms of high energy photon production. It is generally believed that such energetic photons originate either in hot plasma (e^+e^- annihilation, π^0 decay, bremsstrahlung, etc.) or in the interactions of relativistic particles with matter and/or radiation [π^0 decay, Inverse Compton Scattering (ICS), etc.]. Recently, we have studied this second mechanism of photon production (Bednarek et al., 1989, 1990, Paper I). We have obtained the photon spectra from ICS of an arbitrary background radiation by a relativistic electron-beam, and photon spectra from proton-proton interactions via π^0 decay for a relativistic proton beam. The results were given for different beam's Lorentz factors and different angles between the directions of the emitted photons and the beam axis.

In this paper we use these calculated spectra in order to fit the experimental high energy spectra from Cyg X-1 and 2CG 195+04 (Geminga). For this purpose we can briefly summarize the main characteristics of these two sources.

1.1. Cygnus X-1

Cyg X-1 was discovered at the beginning of the X-ray astronomy era as one of the most intense and interesting X-ray sources (Bowyer et al., 1965) and identified as a radio source by Braes and Miley (1971) and by Hjellming and Wade (1971). Since the error box of the radio source was only about 1″, the only star (HDE 226868) contained in it was associated as the optical counterpart of Cyg X-1. HDE 226868 is an 09.7 Iab-5.6 day spectroscopic binary (Webster and Murdin, 1972; Bolton, 1972). For details of the history, the characteristics and multifrequency behaviour of the system Cyg X-1/HDE 226868, see the two review papers by Oda (1977) and by Liang and Nolan (1984) and the references therein.

Briefly, the main parameters of this system are: orbital period $\cong$ 5.6 d; separation of the two components $\cong 3\,10^{12}$ cm; mass function $\cong 0.22\,M_\odot$; distance $\cong$ 2.5 kpc; orbital inclination $\cong 30°$ (Ninkov et al., 1987a).

Since the oldest analysis of the parameters of the system (Webster and Murdin, 1972; Bolton, 1972), the mass of the collapsed object was estimated between 8 and $11\,M_\odot$, also confirmed by the most recent paper by Ninkov et al. (1987a). This suggests that the nature of the collapsed object is very likely a black hole.

The problem of the accretion of matter onto the collapsed companion is not yet definitively solved, even if all the current models for this system assume that the matter flowing from the optical star is responsible for the X-ray emission. But whether matter is accreting via accretion disk or via stellar wind is still an unsettled question. Nevertheless, suggestions that the matter is accreting onto Cyg X-1 via an accretion disk have been given by Bolton et al. (1975) and supported by the observed 294 d X-ray periodicity which can be interpreted as due to the precession of the accretion disk (Priedhorsky et al., 1983). On the contrary, Beall (1984), Ninkov et al. (1987b) found no evidence of the

Send offprint requests to: F. Giovannelli

existence of a large accretion disk around the collapsed object Cyg X-1.

1.2. 2CG 195+04 (Geminga)

The γ-ray source 2CG 195+04 (Geminga) was discovered by the SAS-2 satellite (Kniffen et al., 1975; Thompson et al., 1983) and further detected by the COS B satellite (Hermsen, 1980; 1983) at energies greater than 50 MeV with an integral flux of about $5\,10^{-6}$ photon $cm^{-2}s^{-1}$ at 100 MeV (Masnou et al., 1981). Geminga is one of the 25-γ-ray sources reported in the second COS B catalog (Swanenburg et al., 1981). Among them, only four sources were identified with known astrophysical objects, namely: the Crab pulsar, the Vela pulsar, 3C 273, and the ρ Oph molecular cloud. Up to now, two contradictory suggestions exist about the identification of Geminga with known astrophysical objects in other wavelength regions. The first counterpart candidate of Geminga is the radio source 0630+180, with a flat spectrum, which was optically identified as a quasar with redshift 1.2 (Moffat et al., 1983). The second counterpart candidate is the X-ray source 1 E 0630+178 detected by the Einstein satellite in the range 0.1–4.5 keV, which was claimed to be a neutron star at a distance of about 100 pc (Bignami et al., 1983). Recently two identifications of Geminga with optical objects have been reported:

(i) with a 21st magnitude blue star outside the X-ray error circle of the Einstein observatory (Caraveo et al., 1984).

(ii) with a 25.14 magnitude blue star inside the Einstein error circle of the Einstein observatory (Halpern and Tytler, 1988). They placed this star at a distance of 500–1000 pc.

2. Origin of the high energy photons from Cyg X-1 and 2CG 195+04 (Geminga)

2.1. Origin of the MeV photon spectrum from Cyg X-1

Cyg X-1 is a source with variable radio emission (Hjellming and Wade, 1971; Braes, 1976), and a definitively non-thermal spectrum (Woodsworth et al., 1980). The spectral measurements of Cyg X-1, at energies less than 10 keV, indicate the presence of a time-variable spectrum, which shows essentially two states of emission: low and high. At greater energies, up to 100 keV, the spectrum can be fit with a flat power law (Oda, 1977; Liang and Nolan, 1984; and the references therein). A long term spectral variability in the harder region, up to about 1.5 MeV, shows three different emission states and, in general, the spectrum falls steeply (Liang et al., 1987). From balloon experiments, the spectral measurements, in the range roughly 1–10 MeV, showed a very flat spectrum (Baker et al., 1973; Mandrou et al., 1978; McConnell et al., 1987). Moreover, recent observations of the Moscow State University Group reported a shower excess from the direction of Cyg X-1 (Fomin et al., 1987).

Up to now several suggestions attempting to explain the complex shape and behaviour of the spectrum of Cyg X-1 have been published. At energies below 1 MeV, the spectrum is generally described by a single-temperature inverse Compton model with the electron temperature ranging from 20 to 80 keV and optical depths from 2 to 5 (Sunyaev and Titarchuk, 1980; Nolan et al., 1981; Steinle et al., 1982). At energies above 1 MeV, the nature of the spectrum seems to be different. In order to explain the origin of this spectrum, some proposals concerning thermal mechanisms have been discussed, namely:

(i) annihilation e^-e^+ process in a high temperature plasma (Zdziarski, 1980; Ramaty and Meszaros, 1981);

(ii) two temperature Compton model (Pozdnyakov et al., 1983);

(iii) bremsstrahlung of electrons created by the decay of charged pions (Eilek and Kafatos, 1983).

On the contrary, we suggest that the photon spectrum of Cyg X-1, in the MeV region, is non-thermal. In fact, from the radio measurements performed by Woodsworth et al. (1980), a non-thermal nature of the spectrum was unambiguously derived. They proposed a model in which the radio emission comes from relativistic electrons in a stellar wind. So, following the expression of the photon production spectra derived by us in Paper I, we developed a model in which the MeV photon spectrum originates from ICS of the background photons by relativistic electrons.

The experimental high energy spectrum of Cyg X-1, above 1 MeV (McConnell et al., 1987), can be fitted very well with a comptonized black body spectrum ($T_{bb}=3\,10^4$ K), coming from the supergiant companion HDE 226868, by relativistic electrons with a Lorentz factor 600, emitted in our direction. Figure 1 shows the best fit of the experimental data with our calculated spectrum at energies above 1 MeV, and with the derived spectrum from the single-temperature inverse Compton model (Sunyaev and Titarchuk, 1980) at energies below 1 MeV.

In our model, the observed photon spectrum of Cyg X-1 can be expressed by:

$$I_{obs}=I_{theor}\bar{\rho}_{ph}\frac{1}{d^2}\frac{R}{c}N_e \qquad (2.1)$$

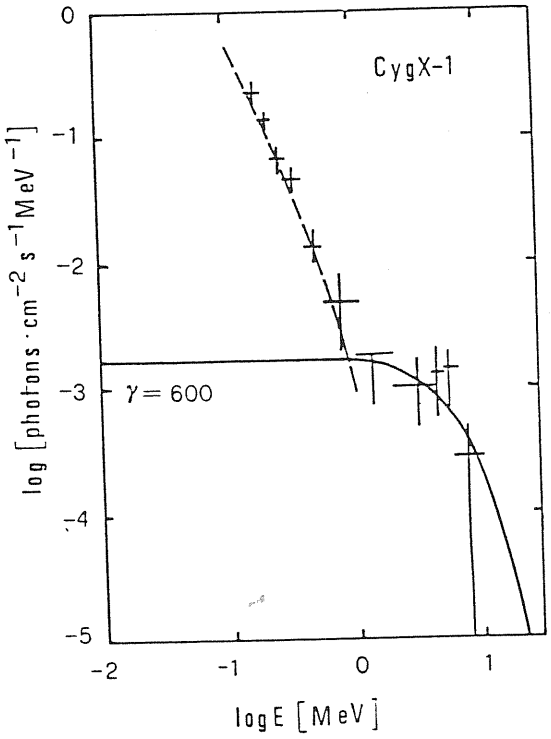

Fig. 1. The differential photon spectrum of Cyg X-1 (McConnell et al., 1987) and the best fitted calculated spectra: dashed line refers to the single-temperature inverse Compton model (Sunyaev and Titarchuk, 1980); full line refers to the comptonized black body spectrum ($T_{bb}=3\,10^4$ K), for the electron-beam's Lorentz factor $\gamma=600$

where:

I_{obs} – the observed photon spectrum, measured by McConnell et al. (1987);

I_{theor} – the comptonized photon spectrum, calculated for a Lorentz factor of electrons equal to 600 and a black body temperature $T_{bb}=3\,10^4$ K (Paper I);

$\bar{\rho}_{ph}$ – the average photon energy density ($\simeq 5\,10^7$ MeV cm^{-3}) along the line of propagation R, calculated from the absolute magnitude of HDE 226868 and the temperature of the radiation: $M_v=-6.5$ and $T=3\,10^4$ K;

d – distance to the binary system Cyg X-1/HDE 226868: 2.5 kpc;

R – the range in which the comptonization of the background photons into the MeV region is important: $4\,10^{12}$ cm, calculated for the orbital inclination angle $i=30^\circ$ and the separation of the two components of the binary system $a=3\,10^{12}$ cm.

All the parameters of the system are from the papers by Ninkov et al. (1987a, b).

N_e – the emissivity of the relativistic electrons;

c – velocity of light.

From the observed intensity of the photons above 1 MeV, we have estimated the lower limit of the emissivity of the relativistic electrons, which is equal to about $1.5\cdot10^{38}$ electron s^{-1}, corresponding to an electron luminosity $7.0\,10^{34}$ erg s^{-1}.

The attenuation length λ in the background photons at $3\,10^4$ K for 0.3 GeV electrons is equal to $1.1\,10^{13}$ cm (Karakuła and Tkaczyk, 1987). So, the electron's Lorentz factor does not change drastically during the propagation, since, in this case, $R/\lambda\cong 0.36$.

We want to remark that the background photon radiation in this system is dominated by HDE 226868, since there is no evidence for the existence of a large accretion disk around the collapsed object Cyg X-1 (Beall, 1984; Ninkov et al., 1987b). A contribution to the photon flux from the system Cyg X-1/HDE 226868 is expected from the bremsstrahlung process occurring because of the interaction of the electron beam with the stellar wind from the supergiant. This contribution is negligible since the directional bremsstrahlung spectra (Gluckstern and Hull, 1953; Dermer and Ramaty, 1986) give the same flux as that from ICS – for an angle between the emitted photon direction and beam axis, $\alpha_1=0^\circ$ – when the density of the stellar wind is about $8\,10^{10}$ H cm^{-3}. An evaluation of the terminal stellar wind velocity of HDE 226868 gives 1500 km s^{-1} (Ninkov et al., 1987b). So, to obtain such a high density in the wind a mass loss rate of about $3.5\,10^5\,M_\odot$ yr^{-1} is required. This value is one order of magnitude greater than the mass loss rate ($3.5\,10^{-6}\,M_\odot$ yr^{-1}) derived by Persi et al. (1980). Moreover, the directional bremsstrahlung spectra are more collimated than the comptonized black body spectra coming from the supergiant. So that in order to have a significant contribution to the emitted photon flux from bremsstrahlung, a mass loss rate much greater than $3.5\,10^5\,M_\odot$ yr^{-1} should be necessary.

2.2. *Origin of the MeV photon spectrum from Geminga*

The differential photon spectrum of Geminga in the energy range 100 MeV–3.2 GeV is consistent with a single power law ($\approx E^{-1.8}$) (Masnou et al., 1981). At energies below 100 MeV, the spectrum flattens significantly. This is also suggested by several observations in the softer regions, such as hard X-ray and soft γ-ray ranges (Haymes et al., 1979; Graser and Schönfelder, 1982; Baker et al., 1983). On the contrary, at energies above 3.2 GeV, the spectrum steepens as suggested by the highest energy point of COS B (Masnou et al., 1981), by the lack of any significant detection above 10^{11} eV (Helmken and Weeks, 1979; Cawley et al., 1985) and by the upper limit of the photon flux from the direction of Geminga at energies 10^{15} eV (Karakuła et al., 1985) derived from the Tien Shan data (Nikolsky et al., 1984). Let us note that the only positive observation in a higher energy range ($\geq 2\,10^{12}$ eV) reported by Zyskin and Mukanov (1985) is in contradiction with the former results.

Several proposals have been made in order to interpret the nature of the spectrum at energies greater than 1 MeV, namely:

(i) inelastic collisions between cosmic-ray particles and the interstellar gas; relativistic electron bremsstrahlung in the interstellar gas (Cesarsky et al., 1976; Bignami et al., 1976; Abdulwahad and Morrison, 1978);

(ii) ICS of background photons by relativistic electrons (e.g. Stecker, 1971; Chupp, 1976).

These two mechanisms have difficulties in explaining the high energy photon emission from Geminga.

In our model, we propose that the high energy photons coming from Geminga originate in the interaction of beamed relativistic particles with the surrounding matter. Such a mechanism of high energy photon production can be realized in close binary systems, where beamed relativistic particles emitted by a collapsed object (e.g. neutron star) interact with the matter from the stellar companion.

In our previous paper (Paper I) we obtained the photon spectra from the interactions of a monoenergetic proton beam with a hydrogen cloud for a given angle α_1 between the direction of the emitted photons and the beam axis. We compare in Fig. 2 the theoretical photon production spectra with the spectral measurements of Geminga from COS B satellite (Masnou et al., 1981). In Fig. 2 one can see that the photon spectrum – calculated for an angle $\alpha_1=35^\circ$ between the direction to the observer and the beam axis and a proton-beam's Lorentz factor $\gamma\geq 30$ – fits very well the COS B data. In order to show how the fit is sensitive to the angle α_1, we have reported in Fig. 2 also the theoretical curves obtained with the same value γ and with the angle α_1 equal to 30° and 40°, respectively.

In this model, which is the best fitting to experimental data, the relationship between the intensities of the theoretical and experimental spectra is given by the formula:

$$I_{obs}=I_{theor}(\gamma\geq 30,\quad \alpha_1=35^\circ)\frac{V}{d^2}. \tag{2.2}$$

where:

I_{obs} – the intensity of the observed spectrum (Masnou et al., 1981);

I_{theor} – the theoretical photons production spectrum (Paper I);

d – the distance to Geminga in cm;

V – the volume in which the proton-beam interacts with the surrounding matter, in cm^3.

From the best fit we obtain the emissivity of the proton-beam, necessary to produce such a spectrum. It is:

$$N_p=7.5\,10^{-4}\cdot\frac{d^2}{x_p}(\text{particle s}^{-1}), \tag{2.3}$$

where x_p is the column density of particles crossed by the proton-beam, in g cm^{-2}.

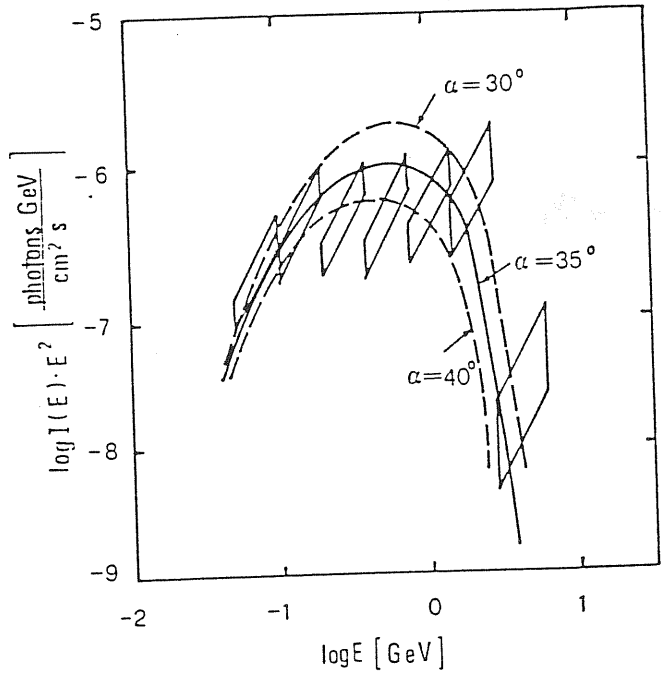

Fig. 2. The differential photon spectrum of Geminga measured by the COS B experiment (Masnou et al., 1981), multiplied by E^2 and the best fitted calculated spectra from the interactions of monoenergetic proton beam with hydrogen cloud for angles between the direction of the emitted photons and the beam axis α_1 equal to 30°, 35°, and 40° and Lorentz's factor γ equal 30

This corresponds to a proton luminosity $L_p = m_p \gamma N_p$, where m_p is the proton rest energy.

We want to comment on the problem connected with the generation of the charged pions which decay into electrons and positrons. These secondary electrons and positrons generate a γ-ray continuum via bremsstrahlung and synchrotron radiation. The energy loss time scale of electrons with energy $E > 400$ MeV can be expressed by (Schlickeiser, 1982):

$$\tau(E) = \frac{E}{dE/dt} \cong \frac{4\,10^7}{n_0} [\mathrm{yr}]$$

where n_0 is the concentration of the ambient matter.

Our proposed model is in favour of a distance to Geminga of order a few hundred parsecs. So, even in the case of very high concentration of the ambient matter such as 10 g cm^{-2}, corresponding to $n_0 \cong 2\,10^4$ H cm^{-3}, the bremsstrahlung loss time scale is greater than the electron propagation time from the source to the observer. Moreover, comparing our spectra from π^0 decay with the directional bremsstrahlung spectra (Gluckstern and Hull, 1953; Dermer and Ramaty, 1986), we have found that the bremsstrahlung spectra are more collimated toward the direction of the beam axis than the former ones. Since the best fitting spectrum from π^0 decay to experimental data gives an angle between the direction of the emitted photons and the beam axis of 35°, the contribution from the bremsstrahlung emission of the secondary electrons and positrons to the photon spectrum is negligible.

3. Discussion and conclusions

In this paper we have examined the possibility of using the electron/proton-beam scenario models for two γ-ray sources: Cyg X-1 and 2 CG 195 + 04 (Geminga). We have used the results of the electron/proton-beam interactions with the surrounding matter and/or radiation, derived in our previous paper (Paper I).

For Cyg X-1 we have shown that its behaviour at energies greater than 1 MeV are compatible with the comptonized spectra (derived in Paper I), if the relativistic electrons with a Lorentz factor of about 600, are emitted in our direction. The hard tail in the MeV region could be caused by comptonization of the black body photons from the supergiant companion HDE 226868. From the observed intensity of the photons above 1 MeV, we have derived the lower limit of the relativistic electron emissivity $N_e \cong 1.5\,10^{38}$ electron s^{-1}, corresponding to an electron luminosity $L_e \cong 7.0\,10^{34}$ erg s^{-1}.

We want to remark that our model expects variations in the intensity of the high energy photons according to the orbital period.

For Geminga, we have shown that the very high energy photons originate in the interaction of beamed relativistic particles with a Lorentz factor equal to 30 (or greater) and the angle α_1 between the beam axis and the direction to the observer equal to 35°. From the best fit of the COS B data, obtained with the calculated photon spectrum from π^0 decay (Paper I) and the former parameters, we have derived the emissivity of the proton-beam of Geminga $N_p \cong 7.5\,10^{-4}\, d^2/x_p$ particle s^{-1}, corresponding to a proton luminosity $L_p = m_p \gamma N_p$.

If Geminga were an extragalactic source, such as the quasar QSO 0630 + 180 placed at $z = 1.2$ as suggested by Moffat et al. (1983), these values would grow drastically and proportionally to d^2. So, from the energetical point of view, our model excludes the identification of Geminga with the QSO 0630 + 180, and favours that one with a galactic source (1 E 0630 + 178) as suggested by Bignami et al. (1983) and recently by Halpern and Tytler (1988).

Our model is definitively valid in the case that Geminga is a binary system, where a density x_p is expected to be several g cm^{-2}. In this case a distance of the order of several hundred parsecs would be acceptable. If Geminga were associated with an isolated neutron star, and then low density in the SN remnant, as suggested by Halpern and Tytler (1988), our model would require a very large proton emissivity ($N_p \cong 10^{40}/x_p$ particle s^{-1} for a distance $\cong 1$ kpc).

Acknowledgements. We wish to thank the referee, Dr. G. Kanbach, for his very useful comments and suggestions.

References

Abdulwahab, M., Morrison, P.: 1978, *Astrophys. J. Lett.* 221, L33
Baker, R.E., Butler, R.C., Dean, A.J., Hayles, R.I., Ramsden, D., Di Cocco, G., Boella, G., Della Ventura, A., Perotti, F., Villa, G.: 1983, *Astron. Astrophys.* 117, 38
Baker, R.E., Lovett, R.R., Orford, K.J., Ramsden, D.: 1973, *Nature Phys. Sci.* 245, 18
Beall, J.H., Knight, F.K., Smith, H.A., Wood, K.S.: 1984, *Astrophys. J.* 284, 745
Bednarek, W., Giovannelli, Karakula, S., Tkaczyk, W.: 1989,

in *Frontier Objects in Astrophysics and Particle Physics*, eds. F. Giovannelli, G. Mannocchi, Italian Physical Society, Editrice Compositori, Bologna, p. 189
Bednarek, W., Giovannelli, Karakula, S., Tkaczyk, W.: 1990, *Astron. Astrophys.* **236**, 268 (Paper I)
Bignami, G.F., Macaccaro, T., Paizis, T.: 1976, *Astron. Astrophys.* **51**, 319
Bignami, G.F., Caraveo, P.A., Lamb, R.C.: 1983, *Astrophys. J. Lett.* **272**, L9
Bolton, C.T.: 1972a, *Nature* **235**, 271
Bolton, C.T.: 1975, *Astrophys. J.* **200**, 269
Bowyer, S., Byram, E.T., Chubb, T.A., Friedman, H: 1965, *Science* **147**, 394
Braes, L.L.E.: 1976, *Nature* **264**, 731
Braes, L.L.E., Miley, G.K.: 1971, *Nature* **232**, 246
Caraveo, P.A., Bignami, G.F., Vigroux, L., Paul, J.A.: 1984, *Astrophys. J. Lett.* **276**, L45
Cawley, M.F., Fegan, D.J., Gibbs, K., Gorham, P.W., Lamb, R.C., Liebing, D.F., MacKeown, P.K., Porter, N.A., Stenger, V.J., Weekes, T.C.: 1985, *Proc. 19th Int. Cosmic Ray Conf.* (La Jolla) **1**, 173
Cesarsky, C.J., Casse, M., Paul, J.: 1976, *Astron. Astrophys.* **48**, 481
Chupp, E.L.: 1976, *Gamma-Ray Astronomy*, Reidel, Dordrecht
Dermer, C.D., Ramaty, R.: 1986, *Astrophys. J.* **301**, 962
Eilek, J.A., Kafatos, M.: 1983, *Astrophys. J.* **271**, 804
Fomin, Yu.A., Kalmykov, N.N., Khrenov, B.A., Khristiansen, G.B., Kulikov, G.V., Pogorely, V.G., Silaev, A.A., Solovyeva, V.I., Sulakov, V.P., Trubitsyn, A.V., Vashkevich, V., Vedeneev, O.V.: 1987, *20th Int. Cosmic Ray Conf.* (Moscow) **1**, 297
Gluckestern, R.L., Hull, M.H.: 1953, *J. Phys. Rev.* **90**, 1030
Graser, V., Schönfelder, V.: 1982, *Astrophys. J.* **263**, 677
Halpern, J.P., Tytler, D.: 1988, *Astrophys. J.* **330**, 201
Haymes, R.C., Meegan, C.A., Fishman, G.J.: 1979, *Astron. Astrophys.* **79**, 88
Helmken, H.F., Weekes, T.: 1979, *Astrophys. J.* **228**, 531
Hermsen, W.: 1980, Ph.D. Thesis, University of Leiden, The Netherlands
Hermsen, W.: 1983, *Space Sci. Rev.* **36**, 61
Hjellming, R.M., Wade, C.M.: 1971, *Astrophys. J. Lett.* **168**, L21
Karakula, S., Stamenov, J.N., Tkaczyk, W.: 1985, *19th Int. Cosmic Ray Conf.* (La Jolla) **1**, 268
Karakula, S., Tkaczyk, W.: 1987, *Acta Universitatis Lodziensis, Folia Physica*, **10**, 127
Kniffen, D.A., Bignami, G.F., Fichtel, C.E., Hartman, R.C., Ogelman, H., Thompson, D.J., Ozel, M.E., Tumer, T.: 1975, *14th Int. Cosmic Ray Conf.* (Munchen) **1**, 100
Liang, E.P., Nolan, P.L: 1984, *Space Sci. Rev.* **38**, 353
Ling, J.C., Mahoney, W.A., Wheaton, W.A., Jacobson, A.S.: 1987, *Astrophys. J. Lett.* **321**, L117
Mandrou, P., Niel, M., Vedrenne, G., Dupont, A., Hurley, K.: 1978, *Astrophys. J.* **219**, 288
Masnou, J.L., Bennett, K., Bignami, G.F., Bioemen, J.B.G.M., Buccheri, R, Caraveo, P.A., Hermsen, W., Kanbach, G., Mayer-Hasselwander, H., Paul, J.A. Wills, R.D.: 1981, *17th Int. Cosmic Ray Conf.* (Paris) **1**, 177
McConnell, M.L., Owens, A., Chupp, E.L., Dunphy, P.P., Forrest, D.J., Vestrand, W.T.: 1987, *20th Int. Cosmic Ray Conf.* (Moscow) **1**, 58
Moffat, A.F.J., Schlickeiser, R., Shara, M.M., Sieber, W., Tuffs, R., Kuhr, M.: 1983, *Astrophys. J. Lett.* **271**, L45
Nikolsky, S.I., Stamenov, J.N., Ushev, S.Z.: 1984, *Adv. Space Res.* **3**, 131
Ninkov, Z., Walker, G.A.H. Yang, S.: 1987a, *Astrophys. J.* **321**, 425
Ninkov, Z., Walker, G.A.H., Yang, S.: 1987b, *Astrophys. J.* **321**, 438
Nolan, P.L., Gruber, D.E., Knight, F.K., Matteson, J.L., Rothschild, R.E., Marshall, F.E., Levine, A.M., Primini, F.A.: 1981a, *Nature* **293**, 275
Oda, M.: 1977, *Space Sci. Rev.* **20**, 757
Persi, P., Ferrari Toniolo, M., Grasdalen, G.L., Spada, G.: 1980, *Astron. Astrophys.* **92**, 238
Pozdnyakov, L.A., Sobol, I.M., Sunyaev, R.A.: 1983, *Soviet Sci. Rev.* (Section E-Astr. Ap. Space Phys. Rev.) **2**, 189
Priedhorsky, W.C., Terrell, J.: 1983, *Astrophys. J.* **270**, 233
Ramaty, R., Meszaros, P.: 1981, *Astrophys. J.* **250**, 384
Schlickeiser, R.: 1982, *Astron. Astophys. Lett.* **106**, L5
Stecker, F.W.: 1971, *Cosmic Gamma Rays*, Mono Book Corp., Baltimore, NASA SP-249
Steinle, H., Voges, W., Pietsch, W., Reppin, C., Trümper, J., Kendziorra, E., Staubert, R.: 1982, *Astron. Astrophys.* **107**, 350
Sunyaev, R.A., Titarchuk, L.G.: 1980, *Astron. Astrophys.* **86**, 121
Swanenburg, B.N., Bennett, K., Bignami, G.F., Buccheri, R., Caraveo, P.A., Hermsem, W., Kanbach, G., Lichti, G.G., Masnou, J.L., Mayer-Hasselwander, H.A., Paul, J.A., Sacco, B., Scarsi, L., Wills, R.D.: 1981, *Astrophys. J. Lett.* **243**, L69
Thompson, D.I., Fichtel, C.E., Hartman, R.C., Kniffen, D.A., Lamb, R.C.: 1977, *Astrophys. J.* **213**, 252
Webster, B.L., Murdin, P.: 1972, *Nature* **235**, 37
Woodsworth, A.W., Higgs, L.A., Gregory, P.C.: 1980, *Astron. Astrophys.* **84**, 379
Zdziarski, A.A.: 1980, *Acta Astron.* **30**, 371
Zyskin, Yu.L., Mukanov, D.B.: 1983, *Soviet Astron. Lett.* **9**, 117

Astron. Astrophys. 245, 41–47 (1991)

ASTRONOMY
AND
ASTROPHYSICS

X- and γ-ray emission from 3C 273

W. Bednarek [1,2] **and M. Calvani** [1,3]

[1] International School for Advanced Studies – Trieste, Strada Costiera 11, I-34014 Trieste, Italy
[2] Institute of Physics, University of Lódź, ul. Nowotki 149/153, PL-90-236 Lódź, Poland
[3] Department of Astronomy, University of Padova, Vicolo dell'Osservatorio, I-35122 Padova, Italy

Received July 2, accepted November 23, 1990

Abstract. In this paper we first investigate the angular dependence of the spectrum of secondary electrons and positrons (differential number of particles vs. energy) which originate in the decay of charged pions that, in turn, are produced in the interaction of a relativistic proton beam with ambient matter. We then apply these results to the quasar 3C 273 and we show that the X-ray emission from the jet and the γ-ray emission from this source can be explained in terms of: 1) bremsstrahlung radiation from secondary electrons and positrons; 2) radiation from Inverse Compton scattering of background microwave photons by secondary electrons and positrons and 3) radiation arising from neutral pions decay. We assume that neutral and charged pions are produced in the interaction of the relativistic proton beam with matter entrained in the jet. We finally deduce, from the fit with the observed spectrum, that the core of 3C 273 must emit a power of $P \approx 2.6\ 10^{47}$ erg/s which corresponds to a mass loss of relativistic protons $\dot{M} \approx 0.7\, M_{\odot}$/yr in the jet.

Key words: active galactic nuclei – jets of – X-rays – γ-rays – quasar 3C 273 – radiation mechanisms

1. Introduction

The spectrum of the quasar 3C 273 extends over several decades in frequency – from radio to γ-rays – being variable and complex with no strong evidence of correlation between different wavelengths (Courvoisier et al. 1987). Soft X-ray emission was detected during several rocket flights and the shape of the spectrum was approximated by a power law with spectral index of 1.5 (Turner et al. 1985; 1990). Hard X-ray emission was first reported by Worrall et al. (1979) and Primini et al. (1979) and subsequently confirmed by balloon flights (e.g. Dean et al. 1990). In this energy range the spectrum is usually described by a power law with index 1.5 (however Bezler et al. 1984 observed a much flatter spectrum with an index of 1.2 up to 200 KeV). A small fraction of the soft X-ray emission is connected with the optical part of the jet of 3C 273 (Willingale 1981; Harris & Stern 1987). γ-ray emission (> 50 MeV) was discovered by the SAS 2 satellite (Swannenburg et al. 1978) and confirmed by COS B (Bignami et al. 1981).

According to Bassani & Dean (1981, 1986), the variability of the X-ray flux implies that X and γ-rays cannot be produced isotropically in the same place because of the large compactness parameter of the X-ray source. They conclude that either X and γ-rays are both beamed or that they are produced in different places. Moreover Bignami et al. (1981) reported the γ-ray emission to be stable during observations with COS B. It seems therefore quite reasonable to locate the production of γ-rays in the jet of 3C 273 and that of hard X-rays in the compact core. Indeed, the presence of relativistic particles in the jet is strongly supported by the discovery of superluminal expansion (Seielstad et al. 1979; Pearson et al. 1981) which, if interpreted in terms of bulk relativistic motion (Rees 1966), implies a Lorentz factor of $\Gamma \approx 6 \times h^{-1}$ ($h = H/100$ km/s/Mpc where H is the Hubble constant) with propagation at an angle $\alpha \leqq 16^{\circ} \times h^{-1}$ to the line of sight (e.g. Unwin et al. 1985).

The above observations led Morrison et al. (1984) to propose a model in which γ-rays are produced by relativistic secondary electrons from p–p collisions in the optical part of the jet, assuming isotropization of relativistic protons by weak magnetic field. However they assumed the jet of 3C 273 to be one-sided in order to avoid difficulties with isotropic production of photons in the outer part of the (possible) counter jet. Although one-sided emission (or flip-flop behaviour) is sometimes invoked in compact sources, there are evidences (e.g. Laing 1988) that the jets are usually two-sided.

In a recent paper Anyakoha et al. (1990) investigated the production of high energy γ-rays from extragalactic jets. However they also assumed isotropization of relativistic protons by random magnetic field, and assumption that is difficult to reconcile with the observed orientation of the magnetic field along the jet axis in 3C 273 (Röser & Meisenheimer 1986) and lack of deceleration of relativistic motion in the inner part of the jet in 3C 273 (Unwin et al. 1985). Moreover Laing (1988) and Garrington et al. (1988) suggest existence of bulk relativistic motion in the outer part of some jets (e.g. Cygnus A) which would be in contradiction with models postulating isotropization of relativistic protons.

In this paper we investigate the possibility that γ-rays from 3C 273 are produced in the jet. In particular, we develop a non-isotropic model according to which γ-rays are produced by secondary electrons and positrons (hereafter we shall use the common name *electrons* for both kind of particles), from the decay of charged pions, in bremsstrahlung process and from the decay of neutral pions. In our scheme moreover soft X-rays from the jet are due to the Inverse Compton scattering of microwave background photons by secondary electrons.

Send offprint requests to: W. Bednarek (italic address)

2. Spectra of secondary electrons

The interaction of the relativistic protons in a jet with the ambient matter gives rise to charged pions which then decay via muons into secondary electrons ($p + p \rightarrow \pi^{\pm} \rightarrow \mu^{\pm} \rightarrow e^{\pm}$). We are here mainly interested in the angular dependence of the spectrum of the secondary electrons with respect to the axis of the proton beam (the jet). Note that similar calculations which assumed however an *isotropic* distribution of protons, were applied by Ramaty (1974) to investigate the spectrum of cosmic electrons and, more recently, by Murphy et al. (1987) to study solar γ-ray flares.

We consider a monoenergetic, one-dimensional proton beam with Lorentz factor Γ. The beam propagates at an angle α to the line of sight. The spectrum of muons from the decay of pions is then described by the formula:

$$\frac{dR}{dE_\mu d\Omega_\mu dt\, dV} = A \iiint \frac{d\sigma(p_\pi, \cos\theta_\pi, \phi_\pi)}{dp_\pi d(\cos\theta_\pi) d\phi_\pi} \cdot P(\gamma_\pi\, E_\mu, \Omega_\mu)\, dp_\pi d\Omega_\pi \qquad (1)$$

where:

$$\frac{d\sigma(p_\pi, \cos\theta_\pi, \phi_\pi)}{dp_\pi d(\cos\theta_\pi) d\phi_\pi} = \frac{p_\pi^2}{E_\pi}\left(E_\pi \frac{d^3\sigma}{dp_\pi^3}\right)$$

and: $E_\pi \times d^3\sigma/dp_\pi^3$ is the invariant cross-section for the production of charged pions, taken from Tan & Ng (1983); $P(\gamma_\pi, E_\mu, \Omega_\mu)$ describes the energy and angular distribution of muons, in the observer's frame, from the decay of pions with momentum p_π and Lorentz factor γ_π; $A = \beta_b c n_b n_H$ with β_b = relative velocity of the beam, c = velocity of light, n_b = concentration of the beam, n_H = concentration of ambient matter. For details of the calculations see Appendix A.

Assuming then that muons decay instantaneously, the angular dependent spectrum of secondary electrons is given by:

$$\frac{dN}{dE_e d\Omega_e dt\, dV} = \iiint \frac{dR}{dE_\mu d\Omega_\mu dt\, dV} Jn^*(E_e^*, \Omega_e^*)\, dE_\mu d\Omega_\mu \qquad (2)$$

where: $dR/(dE_\mu d\Omega_\mu dt\, dV)$ is the angular dependent spectrum of muons from decay of pions expressed by Eq. (1); $J = \gamma_\mu^{-1}(1 - \beta_\mu \cos\theta_e)^{-1}$ is the Jacobian of the transformation of the spectrum of electrons from the muon rest frame to the observer's frame, neglecting the electron rest mass with respect to electron's energy and $n^*(E_e^*, \Omega_e^*)$ is the energy and angular distribution of electrons in the rest frame of polarized muons (Lee & Young 1957). For details of the calculations see Appendix B.

Numerical results for the spectrum of secondary electrons are presented in Figs. 1a, b for Lorentz factors $\Gamma = 10, 10^2, 10^3, 10^4$ of the monoenergetic proton beam and for angles $\alpha = 0°, 10°$. Concentrations of the proton beam n_b and of background matter n_H were taken equal to one particle per cubic centimeter.

The general behaviour of the spectra of secondary electrons is very similar to the spectra of photons from π^0 decay (Bednarek et al. 1990). The shape and maximum intensity of the spectra strongly depend on Γ and α. For small α's (with respect to $1/\Gamma$) and in the relativistic limit $\Gamma \gg 1$, the value and the position of the maxima grow proportionally to Γ (Fig. 1a). The spectra of secondary electrons have smaller intensities and are shifted to lower energies than the spectra of secondary positrons because of the difference in the cross sections for π^- and π^+ production in p+p collisions. For large α's the shape of the spectra and the position of the maxima are practically determined only by the value of α, the intensities for different Γ's in relativistic limit being comparable (Fig. 1b).

3. X- and γ-rays from the jet of 3C 273

In the previous Section we have investigated a simple model in which a monoenergetic, highly collimated proton beam interacts with matter entrained in the jet volume. Turning now to 3C 273, its extended optical jet (in which we locate the production of X- and γ-rays), is elongated at least 22° to the direction of the inner jet observed in radio wavelengths (Greenstein & Schmidt 1964; Unwin et al. 1985). The secondary electrons produced by the decay of charged pions (originated in p–p collisions) can emit observable X- and γ-rays via bremsstrahlung processes, if the column density of matter in the jet is high enough, and Inverse Compton scattering of microwave cosmic background radiation.

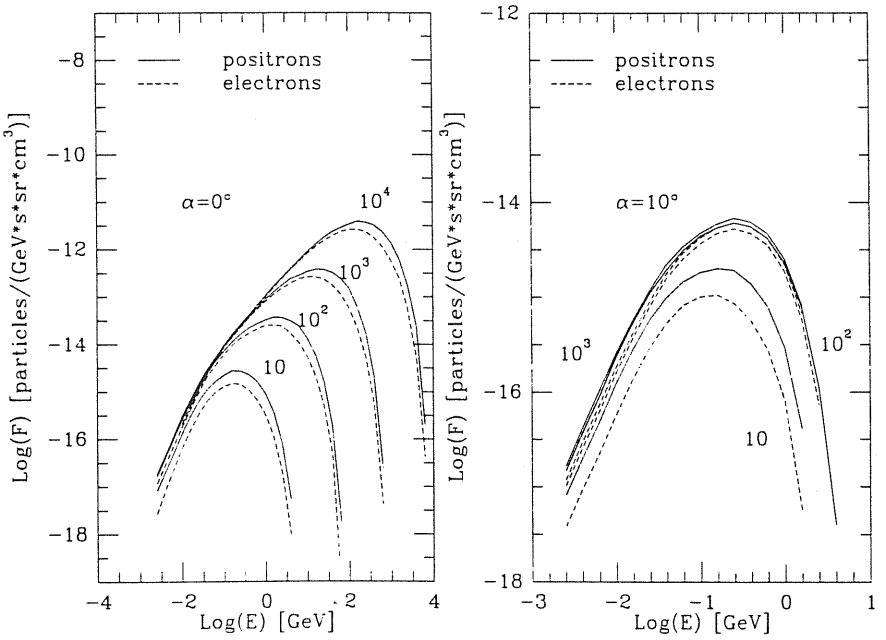

Fig. 1. **a** The spectra of secondary electrons arising from proton-proton interaction ($p+p \rightarrow \pi^{\pm} \rightarrow \mu^{\pm} \rightarrow e^{\pm}$) are shown. The different lines correspond to different values of the Lorentz factors and $\alpha = 0°$. **b** As in **a**, for $\alpha = 10°$

Since secondary electrons are highly relativistic (Lorentz factor up to 10^3), the produced radiation is strongly collimated along the direction of motion of the electrons (Koch & Motz 1959; Bednarek et al. 1990) and we can assume that significant contribution to the bremsstrahlung spectrum emitted at the angle α is given by the secondary electrons moving very close to α.

Under such assumption the spectrum of the bremsstrahlung radiation produced by secondary electrons (calculated according to Eq. 2) is given by:

$$\frac{dN_{\text{brem}}}{dE_\gamma d\Omega dt dV} \simeq \lambda \int \frac{dN}{dE_e d\Omega_e dt dV} \frac{dQ(E_e)}{dE_\gamma} dE_e \qquad (3)$$

where: λ is the mean column density traversed by relativistic electrons in particles/cm^2; $dN/(dE_e d\Omega_e dt dV)$ is the angular dependent spectra of secondary electrons from decay of polarized muons, (see Eq. 2) and $dQ(E_e)/dE_\gamma$ is the bremsstrahlung spectrum produced by monoenergetic electrons with energy E_e (Blumenthal & Gould 1970).

The spectrum of the Comptonized photons produced by secondary electrons (whose spectra were calculated according to Eq. 2) is given by:

$$\frac{dN_{\text{Comp}}}{dE_\gamma d\Omega dt dV} \simeq \frac{l}{c} \int \frac{dN}{dE_e d\Omega_e dt dV} \int n(\varepsilon) \frac{dP(E_e, \varepsilon)}{dE_\gamma dt} d\varepsilon dE_e \qquad (4)$$

where: l is the distance on which Comptonization of photons occurs; c is the velocity of light; $dN/(dE_e d\Omega_e dt dV)$ is the angular dependent spectrum of secondary electrons from decay of polarized muons, (see Eq. 2); $dP(E_e,\varepsilon)/dE_\gamma dt$ is the cross section for Inverse Compton scattering of photon with energy ε into the energy range $E_\gamma : E_\gamma + dE_\gamma$ by monoenergetic electrons with energy E_e (see Blumenthal & Gould 1970; formula 2.42) and $n(\varepsilon)$ is the

In order to apply the above results to 3C 273, we have adopted proton beam parameters: Lorentz factor $\Gamma = 6$ and angle $\alpha = 35°$ (which is reasonable if we take into account possible curvature of the jet, see Unwin et al. 1985). We then compared the photon spectra from bremsstrahlung of secondary electrons (Eq. 3) from Inverse Compton scattering of background microwave photons by secondary electrons and from π^0 decay ($p + p \rightarrow \pi^0 +$ anything: $\pi^0 \rightarrow 2\gamma$, see Bednarek et al. 1990) with the measurements of X-rays from the jet of 3C 273 and γ-rays observed by COS B from direction of this source (Bignami et al. 1981; Hermsen et al. 1981). Fits to observational data are presented in Fig. 2. From the fits we can estimate the total energy in relativistic protons in the jet of 3C 273 using the relation: $E \approx 3\ 10^{17}\, \Gamma d^2\, l/\lambda$ erg where d is the distance to the quasar in cm, $l = d \sin\beta/\sin\alpha$ is the true length of the jet, β is the angular apparent length of the jet. For $\lambda \approx 70$ g/cm^2 (from the fit), $d \approx 860$ Mpc and $\beta \approx 20''$ we find $E \approx 3\ 10^{60}$ erg. The required power emitted in relativistis protons by the core of 3C 273 is the equal to $P = Ec/l \approx 2.6\ 10^{47}$ erg/s, which corresponds to a mass loss in relativistic protons of $M \approx 0.7\, M_\odot$/yr in the jet.

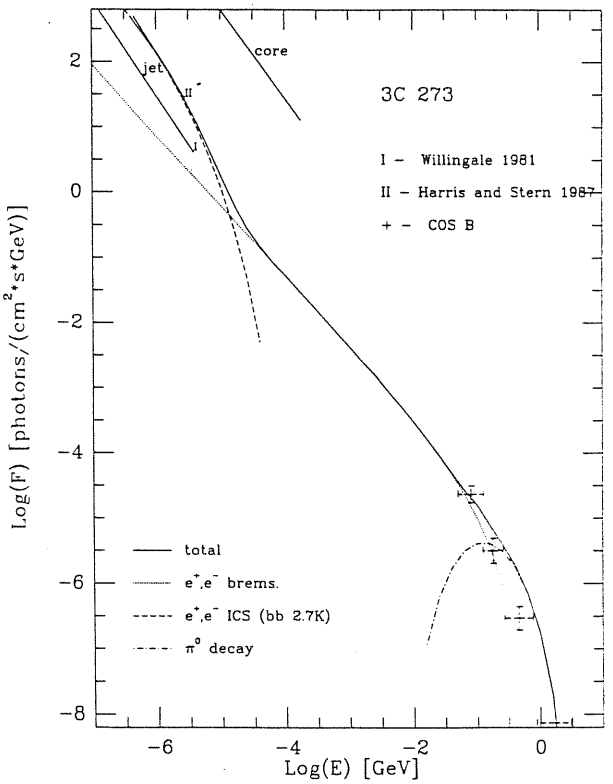

Fig. 2. The observational data of X- and γ-ray emission from 3C 273 are shown. The *full line* is the fit to the data of the calculated photon spectrum (Lorentz factor $\gamma = 6$ and $\alpha = 35°$). The *dot-dashed line* describes the spectrum of γ-rays from π^0 decay; the *dotted line* the spectrum of photons produced by bremsstrahlung of secondary electrons; the *dashed line* the spectrum of photons from Inverse Compton scattering of cosmic microwave background radiation by secondary electrons

4. Discussion

Several models have been suggested in order to explain the X- and γ-ray emission from the quasar 3C 273. However all of them have some difficulties in explaining all current observations. Let us see some of these models in more details:

(1) Synchrotron self-Compton models in which γ-rays are produced by Comptonization of X-ray photons (Jones 1979) or by first order Comptonization of lower energy photons (radio or ultraviolet: Königl 1981; Jones & Stein 1990) have troubles in explaining the observed lack of correlations between different wavelengths (Bignami et al. 1981; Courvoisier et al. 1987; Turner et al. 1990).

(2) Spherically symmetric models in which X- and γ-rays are produced in (p+p) interactions (via pions decay) in the core of 3C 273 have difficulties with the compactness of the central source evaluated from X-ray variability (Marshall et al. 1981; Dean & Bassani 1981), lack of correlation between X- and γ-rays (Bignami et al. 1981) and do not take into account the existence of the jet in 3C 273. In particular Protheroe & Kazanas (1983) assume that protons are accelerated in spherical shocks around the central black hole, while Giovannelli et al. (1984) investigate the γ-ray production in a high temperature electron-proton plasma which forms during accretion onto the black hole.

(3) Models which locate the production of γ-rays in the jet (Morrison et al. 1984; Anyakoha et al. 1990) postulate isotropization of relativistic particles during propagation and one-sideness of the jet. However, as we noted in the Introduction, this assumption is difficult to reconcile with the observed orientation of the magnetic field along the jet axis and with the lack of deceleration of relativistic motion in the inner part of the jet.

We want to stress here that observations of 3C 273 are sometimes scarce and controversial; therefore conclusions based on them may not be confirmed by future observations.

In this paper we have shown that the entire spectrum of 3C 273, X-rays from the jet and γ-rays from the direction of this source, can be explained with a simple model in which these radiations are produced by the interaction of the relativistic proton beam with matter entrained in the jet volume. Our model is similar to the one of Morrison et al. (1984), but it differs in that we assume that a relativistic proton beam propagates along the magnetic field which is parallel to the jet axis. We have considered the angular dependence of the spectrum of secondary electrons produced in the interaction of a relativistic proton beam. In such magnetic field, the trajectory of secondary electrons is a helix along the jet axis. The X (from the jet) and γ-ray spectrum from 3C 273 can be accounted for by bremsstrahlung and Inverse Compton spectra produced by secondary electrons and spectra of photons produced by π^0 decay (assuming a Lorentz factor $\Gamma \approx 6$ for the bulk motion of the proton beam and an angle of $\alpha \approx 35°$ between the jet axis and the line of sight), see Fig. 2. From the fit of the observed spectrum with the theoretical one (bremsstrahlung radiation calculated according to Eq. 3, Inverse Compton spectrum according to Eq. 4 and radiation from π^0 decay calculated in Bednarek et al. 1990), we have found that the total power emitted in relativistic protons by the central core of 3C 273 is equal to $P = 2.6\ 10^{47}$ erg/s which corresponds to a mass loss of $\dot{M} = 0.7\ M_\odot$/yr. However we note that a high column density in the jet of 3C 273 is required: $\lambda \approx 70$ g/cm^2, and accumulation of high amount of matter in the jet volume is possible (see e.g. discussion in Morrison et al. 1984). Numerical simultations of propagation of a jet in the extragalactic medium by De Young (1986) show that a jet can entrain a minimum of $\approx 5\ M_\odot$/yr, which implies a total enrichment as high as $10^9\ M_\odot$ for some jets.

A few different mechanisms of particle acceleration in active galaxies were proposed (see e.g. Wiita 1985). Relativistic particles with power law spectrum can be produced by shocks close to the central engine (see e.g. Blandford & Eichler 1987). Monoenergetic (or close to monoenergetic) relativistic particles can be accelerated in electromagnetic processes (see e.g. Lovelace 1976; Blandford & Znajek 1977) or by radiation pressure (e.g. Abramowicz & Piran 1980; Sikora & Wilson 1981; Calvani & Nobili 1983). In our model we assume that the jet is monoenergetic and made of relativistic protons. Indeed: a) the existence of relativistic knots far away from the central core of 3C 273 suggests such distribution of particles (if not, the knots should be diluted and superluminal motion will not be observed); b) such choice allows us to limit the number of free parameters in the model. In fact we are here mainly interest to investigate the main features of our model to check whether it is in agreement with observations; c) arguments supporting a proton beam are discussed by Roberts (1984).

Our model can work if the energy losses of electrons are not completely dominated by synchrotron processes. This is true if the magnetic field (the perpendicular component to the electron's motion) is $B_\perp\,[\mu\text{G}] \leqq 1.1\ n_H^{1/2}/E$ (from comparison of synchrotron and bremsstrahlung energy losses) and $B_\perp\,[\mu\text{G}] \leqq 14.4\ W_{\text{ph}}$ [eV/cm^3] (from comparison of synchrotron and Inverse Compton energy losses), where E is the energy of electrons in GeV (see Schlickeiser 1982). From polarization measurements. Röser & Meisenheimer (1986) estimate that the magnetic field in the jet of 3C 273 is of the order of 10 μG. If we now compare the synchrotron and bremsstrahlung energy losses, we find that this value is near the acceptable limit for the most energetic secontary electrons (with energy ≈ 1 GeV) but is well acceptable for the lower energy ones. Synchrotron and Inverse Compton energy losses for the above parameters are comparable.

The density of photons with power law spectrum below 10^{15} Hz in the jet volume of 3C 273 (see Fraix-Burnet & Nieto 1988) is about one order of magnitude lower than the density of the microwave background radiation (for the volume of the optical jet and the observed spectrum of photons below 10^{15} Hz from Fraix-Burnet & Nieto 1988). Moreover these photons are probably also collimated along the jet axis of 3C 273 if we keep in mind some observational evidences of their synchrotron origin (Fraix-burnet & Nieto 1988) and the strong collimation of secondary electrons postulated by our model. Therefore Comptonization of these photons (with power law spectrum) to X-ray range is negligible in comparison to Comptonization of cosmic background radiation.

Our model moreover predicts a strong angular dependence of the photon spectrum with respect to the jet direction. The emission of radiation from the counter jet (produced by secondary electrons at an angle $\alpha \approx 145°$ to the line of sight) should be much less than the one from the jet pointing towards us because of much smaller Lorentz factors of secondary electrons produced backwards.

One of the advantages of our model is, we think, its simplicity. Of course, a more realistic model for 3C 273 should take into account propagation effects of relativistic protons and secondary electrons and curvature of the jet. In such case we expect the theoretical photon spectrum to be more steep in the γ-ray range and the deduced parameters of relativistic beam and jet containment less restrictive.

Acknowledgements. We gratefully acknowledge an anonymous referee for having brought to our attention the importance of Inverse Compton scattering of secondary electrons and positrons and for several other useful comments. W.B. would like to thank Drs. F. Giovannelli S. Karakula and W. Tkaczyk for helpful discussions. This work is supported by the Italian Ministero dell'Università e della Ricerce Scientifica e Tecnologica.

Appendix A

In this appendix we derive in details the spectrum of muons produced in the decay of charged pions which in turn are produced in proton-proton collisions.

The kinematics of the production of muons with energy E_μ at an angle α_μ with respect to the direction of motion of the relativistic proton is shown in Fig. 3. The number of muons produced in the above process is given by:

$$dR = \frac{d^3\sigma(p_\pi, \cos\theta_\pi, \phi_\pi)}{dp_\pi\, d(\cos\theta_\pi)\, d\phi_\pi}\, P(\gamma_\pi, E_\mu, \cos\theta_\mu, \phi_\mu) \cdot dp_\pi\, d(\cos\theta_\pi)\, d\phi_\pi\, dE_\mu\, d(\cos\theta_\mu)\, d\phi_\mu \qquad \text{(A1)}$$

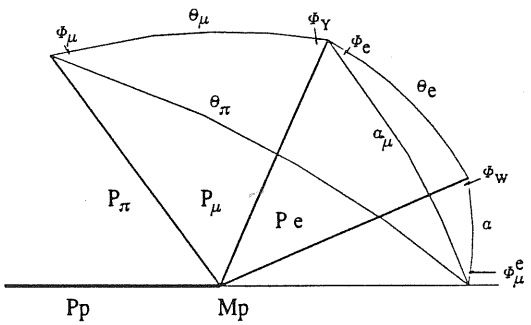

Fig. 3. The kinematics of production of the angular dependent spectra of secondary electrons in proton-proton interaction ($p + p \pi^\pm \to \mu^\pm \to e^\pm$) is here shown

The energy and angular distribution of muons in the observer's frame from the decay of pions with momentum p_π (Lorentz factor γ_π) is described by:

$$P(\gamma_\pi, E_\mu, \cos\theta_\mu, \phi_\mu) = \tfrac{1}{4\pi} J_1 \delta[\gamma_\pi(E_\mu - \beta_\pi p_\pi \cos\theta_\mu) - E_\mu^*] \quad \text{(A2)}$$

where: $J_1 = p_\mu / p_\mu^*$ is the Jacobian of the transformation of distribution of muons from the rest frame of pions to the observer's frame; $E_\mu^* = (m_\mu^2 + m_\pi^2)/2m_\pi$ and $p_\mu^* = (m_\pi^2 - m_\mu^2)/2m_\pi$ are the energy and the momentum of muons in the pion rest frame while E_μ, p_μ are in the observer's frame; β_π is the relative velocity of pions. All angles are defined in Fig. 3.

Substituting A2 into A1, we obtain the angular dependent spectrum of muons (per unit energy, solid angle, volume and time):

$$\frac{dR}{dE_\mu\, d(\cos\alpha_\mu)\, d\phi_\pi\, dV\, dt} = \frac{A p_\mu}{4\pi p_\mu^*} \times \iiint \frac{d^3\sigma(p_\pi, \cos\theta_\pi, \phi_\pi)}{dp_\pi\, d(\cos\theta_\pi)\, d\phi_\pi} \cdot \delta[\gamma_\pi(E_\mu - \beta_\pi p_\mu \cos\theta_\mu) - E_\mu^*]\, J_2\, d(\cos\theta_\mu)\, dp_\pi\, d\phi_Y \quad \text{(A3)}$$

where the angle $\cos\theta_\pi$ is expressed via spherical trigonometry (see Fig. 3) by:

$$\cos\theta_\pi = \cos\theta_\mu \cos\alpha_\mu + \sin\theta_\mu \sin\alpha_\mu \cos\phi_Y$$

and jacobian

$$J_2 = \frac{d(\cos\theta_\pi)\, d\phi_\mu}{d(\cos\alpha)\, d\phi_Y} = 1 .$$

A-described in paper (Eq. 3). The integration over $\cos\theta_\mu$ in A3 is done analytically using the properties of Diracs δ-function. After changing variable of integration from p_π to γ_π we obtain:

$$\frac{dR}{dE_\mu\, d\Omega_\mu\, dV\, dt} = A \frac{m_\pi^2}{2\pi(m_\pi^2 - m_\mu^2)} \cdot \iint \frac{d^3\sigma(p_\pi, \cos\theta_\pi, \phi_\pi)}{dp_\pi\, d(\cos_\pi)\, d\phi_\pi} \frac{1}{\beta_\pi^2 \gamma_\pi}\, d\gamma_\pi\, d\phi_Y \quad \text{(A4)}$$

where:

$$\cos\theta_\mu = \frac{(E_\mu - E_\mu^*/\gamma_\pi)}{\beta_\pi p_\mu} \quad \text{(A5)}$$

from the Lorentz transformation. m_π, m_μ are the masses of the charged pions and muons respectively.

Let us discuss now the integration limits. The minimum and maximum values of the Lorentz factor γ_π of the pions that can produce muons with energy E_μ are calculated for the cases when $\cos\theta_\mu = 1$ (minimum) and $\cos\theta_\mu = -1$ (maximum). They are given by:

$$\gamma_{\min} = \frac{(E_\mu^* E_\mu - p_\mu p_\mu^*)}{m_\mu^2}; \quad \gamma_{\max} = \frac{(E_\mu^* E_\mu + p_\mu p_\mu^*)}{m_\mu^2} \quad \text{(A6)}$$

In order to perform the numerical integrations, we distinguish two cases:

(i) The energy of the muon emitted at the angle α_μ in the observer's frame is less than the energy of the muon in the pion's rest frame ($m_\mu \leqq E_\mu \leqq E_\mu^*$).

Since the cross-section for pions production in p+p interactions is given for $\gamma_p \geqq 2$ (see Tan & Ng 1983), the function W describing possible values of pion Lorentz factors (see A5) which can produce muons with energy $m_\mu < E_\mu \leqq E_\mu^*$ is inside the function V describing the maximal ellipsoid of momentum of pions produced in $p+p$ interactions (see Fig. 4a). The limits of integration (in A4) are given by:

$$\gamma_{\min} \leqq \gamma_\pi \leqq \gamma_{\max} \quad \text{and} \quad -\pi \leqq \phi_Y \leqq \pi .$$

(ii) The energy of the muons emitted at the angle α_μ in the observer's frame is greater than the energy of the muon in the pion rest frame: $E_\mu > E_\mu^*$. This case is shown in Fig. 4b.

Three possibilities arise now depending on the relative values of $\gamma_{\min}$, $\gamma_{\max}$ (A6) with respect to the maximum value of the Lorentz factor of the pions γ_α produced in $p+p$ interaction at the angle α_μ (see Fig. 4b), where:

$$\gamma_\alpha = \frac{M + K\sqrt{M^2 + K^2 - 1}}{1 - K^2} . \quad \text{(A7)}$$

$M = E_{\max}^*/m_\pi \gamma_S$; $K = \beta_S \cos\alpha_\mu$; $E_{\max}^*$ is the maximum energy of pions produced in $p+p$ interaction in the center of mass of the colliding protons (see Tan & Ng 1983); γ_S, β_S are the Lorentz factor and relative velocity of the center of mass of the colliding protons, $\gamma_S = \sqrt{(E_p + m_p)/2m_p}$ (E_p – energy of relativistic protons). The three cases are:

(a) $\gamma_{\min} \geqq \gamma_\alpha$. No muons with energy E_μ at an angle α_μ are produced.

(b) $\gamma_{\min} \leqq \gamma_a < \gamma_{\max}$. The limits of integration (in A4) are: $\gamma_{\min} \leqq \gamma_\pi \leqq \gamma_1$ with $-\pi \leqq \phi_Y \leqq \pi$, and $\gamma_1 \leqq \gamma_\pi \leqq \gamma_2$ with $-\phi_0 \leqq \phi_Y \leqq \phi_0$.

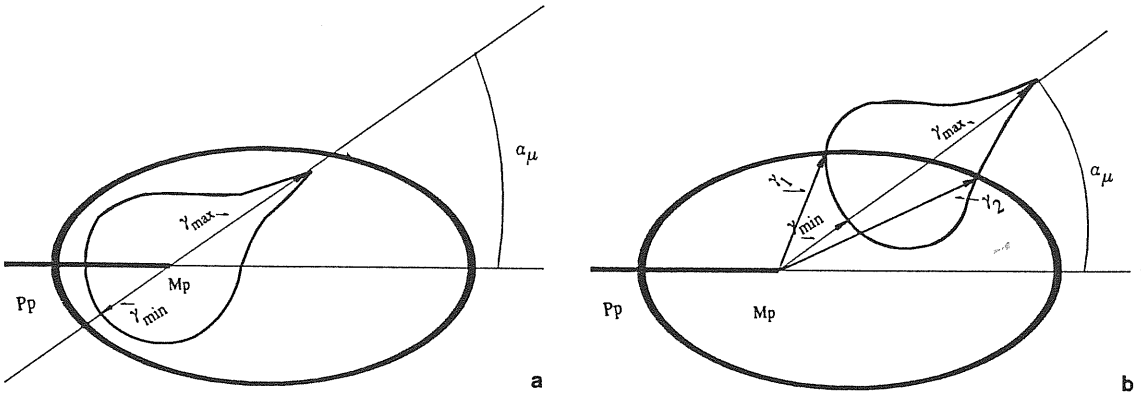

Fig. 4a and b. The maximal ellipsoid of momentum of pions produced in $p+p$ interactions is shown together with the function describing the production of muons with fixed energy in the pion momentum space. Case **a** is for $m_\mu \leqq E_\mu \leqq E_\mu^*$ and case **b** for $E_\mu > E_\mu^*$

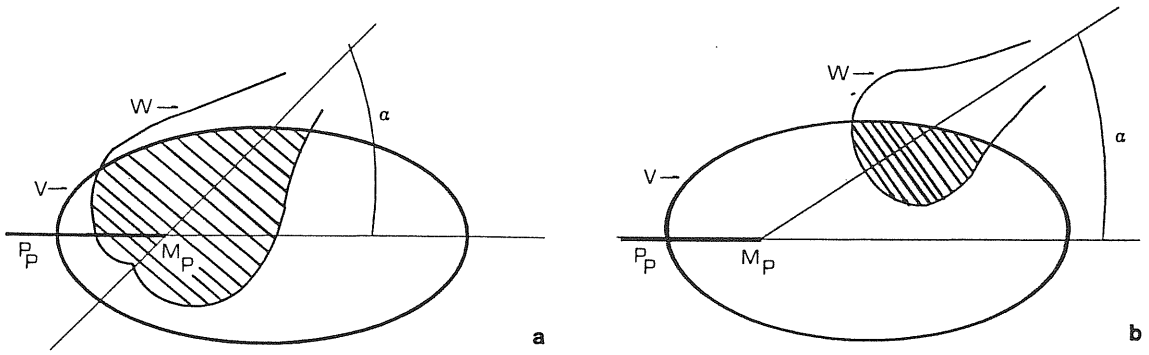

Fig. 5a and b. The maximal ellipsoid of momentum of muons produced from pions decay is shown together with the function describing the production of electrons with fixed energy in the muon momentum space. Case **a** is for $E_e \leqq E_e^*$ and case **b** for $E_e > E_e^*$

The values of pions Lorentz factors γ_1 and γ_2 are obtained by solving w.r.t.γ_π the equation

$$\cos\theta_{\max} = \cos(\theta_\mu \pm \alpha_\mu) \tag{A8}$$

where:

$$\cos\theta_{\max} = \frac{\gamma_\pi\gamma_S - E^*_{\max}/m_\pi}{\gamma_\pi\beta_\pi\gamma_S\beta_S}$$

while $\cos\theta_\mu$ is given by (A5).

The angle ϕ_0 is found from:

$$\cos\phi_0 = \frac{\cos\theta_{\max} - \cos\theta_\mu\cos\alpha_\mu}{\sin\theta_\mu\sin\alpha_\mu}$$

(c) $\gamma_\pi \geqq \gamma_{\max}$. The limits of integration are : $\gamma_{\min} \leqq \gamma_\pi \leqq \gamma_{\max}$ with $-\pi \leqq \phi_Y \leqq \pi$.

For the particular values $\alpha_\mu = 0°$ and $\alpha_\mu = 180°$, the integrand function in A4 does not depend on ϕ_Y and this integration can be performed analytically.

Appendix B

We present here a short description of the calculations needed to obtain the angular dependent spectra of secondary electrons (positrons) from the decay of muons which were produced in the reactions: $p+p \to \pi^\pm +$ anything; $\pi^\pm \to \mu^\pm + \nu_\mu$. The decay of muons in three particles ($\mu^\pm \to e^\pm + \nu_e + \nu_\mu$) was described by Lee & Yang (1957) in the case of negligible electron rest mass w.r.t. the muon rest mass. In the following derivation we assume that $E_e \gg m_e$.

The number of electrons emitted at the angle α per unit energy, solid angle, time and volume is described by:

$$\frac{dP}{dE_e\, d\cos\alpha\, d\phi^e_\mu\, dV\, dt} = \iiint \frac{dR(E_\mu, \cos\alpha_\mu)}{dE_\mu\, d\cos\alpha_\mu\, d\phi^e_\mu\, dV\, dt}\, J_1\, \frac{dN(E_e^*, \cos\theta_e^*)}{dE_e^*\, d\cos\theta_e^*\, d\phi_e^*} \cdot J_2\, dE_\mu\, d\phi_W\, d\cos\theta_e \tag{B1}$$

where the two fractions in the integrals are described in the paper (Eq. 2); $J_1 = p_e/p_e^* = 1/\gamma_\mu(1-\beta_\mu\cos\theta_e)$ is the Jacobian of the transformation from the muon rest frame to the observer's frame of the distribution of secondary electrons; p_e, p_e^* are respectively the momentum of electron in the observer's frame and in the muon rest frame and $J_2 = d\cos\alpha_\mu\, d\phi_e/d\cos\alpha\, d\phi_W = 1$ is the Jacobian of the transformation of the solid angles; $\cos\alpha_\mu$ is given via spherical trigonometry by: $\cos\alpha_\mu = \cos\theta_e\cos\alpha + \sin\theta_e\sin\alpha\cos\phi_W$. All angles are defined in Fig. 3. Substituting then into Eq. (B1) the distribution of secondary electrons in the muon rest frame (Lee & Yang 1957), the Jacobians J_1 and J_2 and changing variable of integration from E_μ to γ_μ, we obtain:

$$\frac{dP}{dE_e\, d\cos\alpha\, d\phi^e_\mu\, dV\, dt} = \frac{2E_e}{\pi m_\mu} \times \iiint \frac{dR(E_\mu, \cos\alpha_\mu)}{dE_\mu\, d\cos\alpha_\mu\, d\phi^e_\mu\, dV\, dt} \cdot \varepsilon[(3-2\varepsilon) + (1-2\varepsilon)\cos\theta_e^*]\, d\gamma_\mu\, d\phi_W\, d\cos\theta_e \tag{B2}$$

where: $\varepsilon = 2E_e\gamma_\mu(1-\beta_\mu\cos\theta_e)/m_\mu$; $\theta_e^* = \arctan\ [\sin\theta_e/\gamma_\mu(\cos\theta_e - \beta_\mu)]$; E_μ, γ_μ, m_μ are the energy, Lorentz factor and rest mass of the muon.

In order to perform the numerical integration, one has first to fix the integration limits. This is straightforward, although quite involved. In general there are two different relevant cases: 1) $E_e \leqq E_e^*$ (see Fig. 5a) and 2) $E_e \geqq E_e^*$, where $E_e^* = m_\mu/2$, see Fig. 5b. In both of them the integration is performed over the common part of the two three-dimensional functions in the momentum space describing respectively, the ellipsoid of maximal muon momentum (function V) and the permitted values for muons momentum which can produce electrons of energy E_e (function W). The relative positions of function V according to fixed function W depends on the electron energy and many different cases are possible. Two of such configurations are shown in Fig. 5a, b where the hatched area denotes the volume of integration.

References

Abramowicz M. A., Piran T., 1980, ApJ 241, L7
Anyakoha M. W., Okoye S. E., Okeke P. N., 1990, Astron. Lett. and Commun. 27, 373
Bassani L., Dean A. J., 1981, Nat 294, 332
Bassani L., Dean A. J., 1986, A&A 161, 85
Bednarek W., Giovannelli F., Karakula S., Tkaczyk W., 1990, A&A 236, 268
Bezler M., Kendziorra E., Staubert R., Hasinger G., Pietsch W., Reppin C., Trumper J., Voges W., 1984, A&A 136, 351
Bignami G. F., Bennett K., Buccheri R., Caraveo P. A., Hermsen W., Kanbach G., Lichti G. G., Masnou J. L., Mayer-

Hasselwander H. A., Paul J. A., Sacco B., Scarsi L., Swannenburg B. N., Wills R. D., 1981, A&A 93, 71
Blandford R. D., Eichler D., 1987, Phys. Rep. 154, 1
Blandford R. D., Znajek R., 1977, MNRAS 179, 433
Blumenthal G. R., Gould R. J., 1970, Rev. Mod. Phys. 42, 237
Calvani M., Nobili L., 1983, in: Astrophysical Jets, eds. A. Ferrari and A. G. Pacholczyk, Reidel, Dordrecht
Courvoisier T. J.-L., Turner M. J. L., Robson E. I., Gear W. K., Staubert R., Blecha A., Bouchet P., Falomo R., Valtonen M., Terasranta H., 1987, A&A 176, 197
Dean A. J., Bazzano A., Court A. J., Dipper N. A., Lewis R. A., Maggioli P., Perotti F., Quadrini M., Stephen J. B., Ubertini P., 1990, ApJ 349, 41
De Young D. S., 1986, ApJ 307, 62
Fraix-Burnet D., Nieto J.-L., 1988, A&A 198, 87
Giovannelli F., Karakula S., Tkaczyk W., 1984, Adv. Space Res. 3, 335
Garrington S. T., Leahy J. P., Conway R. G., Laing R. A., 1988, Nat 331, 147
Greenstein J. L., Schmidt M., 1964, ApJ 140, 1
Harris D. E., Stern C. P., 1987, ApJ 313, 136
Hermsen W., Bennett K., Buccheri R., Caraveo P. A., Kanbach G., Masnou J. L., Mayer-Hasselwander H. A., Paul J. A., Sacco B., Wills R. D., 1981, 17th ICRC 1, 230
Jones T. W., 1979, ApJ 233, 796
Jones T. W., Stein W. A., 1990, ApJ 349, 443
Koch H. W., Motz J. W., 1959, Rev. Mod. Phys. 31, 920
Königl A., 1981, ApJ 243, 700
Laing R. A., 1988, Nat 331, 149
Lee T. P., Young C. N., 1957, Phys. Rev. 105, 1674
Lovelace R. V. E., 1976, Nat 262, 649
Marshall N., Warwick R. S., Pounds K. A., 1981, MNRAS 194, 987
Murphy R. J., Dermer C. D., Ramaty R., 1987, ApJS 63, 721
Morrison P., Roberts D., Sadun A., 1984, ApJ 280, 483
Pearson T. J., Unwin S. C., Cohen M. H., Linfield R. P., Readhead A. C. S., Seielstad G. A., Simon R. S., Walker R. C., 1981, Nat 290, 365
Primini F. A., Cooke B. A., Dobson C. A., Howe S. K., Scheepmaker A., Wheaton W. A., Lewin W. H., Baity W. A., Gruber D. E., Matteson J. L., Peterson L. E., 1979, Nat 278, 234
Protheroe R. J., Kazanas D., 1983, ApJ 265, 620
Ramaty R., 1974, in: High Energy Particles and Quanta in Astrophysics, eds. F. B. McDonald and C. E. Fichtel, MIT Press, Cambridge Mass.
Rees M. J., 1966, Nat 211, 468
Roberts D., 1984, ApJ 285, 64
Röser J.-H., Meisenheimer K., 1986, A&A 154, 15
Schlickeiser R., 1982, A&A 106, L5
Seielstad G. A., Cohen M. H., Linfield R. P., Moffer A. T., Rommey J. D., Schilizzi R. T., Schaffer D. B., 1979, ApJ 229, 53
Sikora M., Wilson A., 1981, MNRAS 197, 529
Swannenburg B. N., Bennett K., Bignami G. F., Caraveo P. A., Hermsen W., Kanbach G., Masnou J. L., Mayer-Hasselwander H. A., Paul J. A., Sacco B., Scarsi L., Wills R. D., 1978, Nat 275, 298
Tan L. C., Ng L. K., 1983, J. Phys. G 9, 1289
Turner M. J. L., Courvoisier T., Staubert R., Molteni D., Trumper J., 1985, Space Sci. Rev. 40, 623
Turner M. J. L., Williams O. R., Courvoisier T. J.-L., Stewart G. C., Nandra K., Pounds K. A., Ohashi T., Makishima K., Inoue H., Kii T., Makino F., Hayashida K., Tanaka Y., Takano S., Koyama K., 1990, MNRAS 244, 310
Unwin S. C., Cohen M. H., Biretta J. A., Pearson T. J., Seielstad G. A., Walker R. C., Simon R. S., Linfield R. P., 1985, ApJ 289, 109
Wiita P. J., 1985, Phys. Rep. 123, 117
Willingale R., 1981, MNRAS 194, 359
Worrall D. M., Mushotzky R. F., Boldt E. A., Holt S. S., Serlemitsos P. J., 1979, ApJ 232, 683

THE ASTROPHYSICAL JOURNAL, 390:489–493, 1992 May 10
© 1992. The American Astronomical Society. All rights reserved. Printed in U.S.A.

ON THE 440 keV LINE IN THE CRAB NEBULA PULSAR

W. BEDNAREK,[1,2] O. CREMONESI,[3] AND A. TREVES[1]

Received 1991 June 17; accepted 1991 October 10

ABSTRACT

We consider the observations of an emission line at 440 keV from the Crab Nebula pulsar. A picture is proposed where the line is due to redshifted positron annihilation in the neutron star crust. The positrons are produced by photons of MeV energy hitting the pulsar cap, which in turn are generated by inverse Compton scattering of electrons in an inner electric gap ($E \cdot B \neq 0$). It is shown that the picture appears in agreement with basic constraints of pulsar electrodynamics and follows the main ideas of the pulsar model of Ruderman and collaborators.

Subject headings: elementary particles — gamma rays: theory — pulsars: individual (Crab Nebula) — radiation mechanisms: miscellaneous

1. INTRODUCTION

The existence of an emission feature at 440 keV associated with the Crab Nebula was suspected since the observations of Leventhal, MacCallum, & Watts (1977). However, the feature was confirmed and disproved by various groups, so that the possibility of an intrinsic variability is seriously considered. For a detailed review on the subject we refer to Owens (1990). Among the most recent and significant observations we quote the ones from the FIGARO II team. The feature was observed in two balloon flights, one in 1986 (Agrinier et al. 1990), and one in 1990 (Massaro et al. 1991), and it appears only in correspondence with the secondary pulsar peak. Its significance, as from the addition of the data from the two flights, is about 3 σ. The line is located between 0.43 and 0.46 MeV, and its width is consistent with the energy resolution of the detector; its intensity is $I \cong 0.86 \pm 0.33 \times 10^{-4}$ photons cm^{-2} s^{-1}. An obvious interpretation of the feature is that it is due to the 511 keV e^+e^- annihilation line redshifted by the gravitational field of the neutron star (see Owens 1990 for references). Although far from being uncontroversial, we accept this interpretation as a valuable working hypothesis.

In this paper we discuss some implications that the observation of the annihilation line may have on the pulsar electrodynamics.

2. CONSTRAINTS ON PULSAR PARAMETERS

Assuming a distance of 2 kpc and a beaming factor k, the observed flux corresponds to a rate of release of annihilation photons

$$R \cong 4 \times 10^{38} k_{100} \text{ photons s}^{-1}, \quad (1)$$

where k_{100} is $k/0.01$.

This corresponds to a line luminosity

$$L_{511} \cong 3 \times 10^{32} k_{100} \text{ ergs s}^{-1}, \quad (2)$$

which is a small fraction of the total pulsar luminosity

$$L_{\text{tot}} \cong 10^{35} k_{100} \text{ ergs s}^{-1} \quad (3)$$

and of the nebula luminosity

$$L_{\text{nebula}} \cong 10^{38} \text{ ergs s}^{-1}. \quad (4)$$

The 511 keV photons are produced by annihilation of positrons, which in turn will be a product of an electromagnetic shower. We now consider that the showers are produced by a flow of particles accelerated toward the neutron star. The picture will be specified in the following text. It seems difficult to us to consider an atmosphere of pairs, since due to the huge fields, it would immediately expand, and the annihilation process, if occurring at all, would take place in a region of low gravitational redshift. In this context the picture may be different from that envisaged for annihilation line production in γ-ray burst sources (see, e.g., the review by Hameury & Lasota 1984).

The flow of particles responsible for the generation of the showers, and therefore ultimately for the annihilation photons, can be expressed as

$$P_{\text{Sh}} \cong 4 \times 10^{38} \xi^{-1} k_{100} \text{ s}^{-1}, \quad (5)$$

where ξ is the number of annihilation photons outgoing from the star for infalling primary particle.

The current associated to the particle flux is

$$I_e = eP_{\text{Sh}} \cong 2 \times 10^{31} \xi^{-1} k_{100} \text{ esu s}^{-1}. \quad (6)$$

The associated magnetic field can be estimated from Ampere's law, if a relevant space dimension l is chosen. Assuming as a scale the radius of the neutron star $l_6 = l/10^6$ cm, we get

$$B_e = 2I_e/(cl) \cong 1.3 \times 10^{13} l_6^{-1} \xi^{-1} k_{100} \text{ G}. \quad (7)$$

If $l = 10^5$ cm which is the dimension of the active polar cap and $k_{100} \approx 1$, one would have

$$B_{\text{pc}} \sim 10^{14}/\xi \text{ G}. \quad (8)$$

The magnetic field on the Crab pulsar surface is estimated to be $\sim 6 \times 10^{12}$ G s. Therefore in order not to destroy the

[1] International School for Advanced Studies, Strada Costiera 11, I-34014 Trieste, Italy.
[2] Institute of Physics, University of Łódź, ul. Pomorska 149/153, PL 90-236 Łódź, Poland.
[3] Università di Milano, Via Celoria 16, I-20133 Milano, Italy.

neutron star magnetic field, the number of annihilation photons ξ produced in cascade which is initiated by single relativistic particle should be

$$\xi \gg 100 . \quad (9)$$

In order to have an estimate of a realistic value ξ, we consider first relativistic electrons hitting the neutron star surface. In particular, we have considered a Monte Carlo simulation of showers produced by electrons impinging perpendicularly onto an iron slab. Based on the EGS4 (electron gamma shower simulation program: Nelson, Hirayama, & Rogers 1985) the code follows the shower development down to energies of a few keV and gives full information for the particles going back from the slab. Possible effects due to strong magnetic fields are not taken into account. A plot of ξ as a function of electron energy is given in Figure 1*a*, while in Figure 1*b* the fractional energy which is released in the form of an outgoing annihilation line is given versus the electron energy. Independently of the energy of the impinging electron, the photon yield is ~ 3, which means that energetically it is much more favorable to hit the surface with low-energy positrons (electrons, photons). Even taking into account effects typical of neutron star matter (see calculations of cascade in the iron crust by Jones 1979; Bogovalov & Kotov 1990), it seems difficult to consider much higher values of ξ. Therefore it appears that condition (9) cannot be fulfilled.

It seems to us that a possibility that remains is that the current is indeed transported by primary relativistic particles, but the shower starts to develop above the crust, because of the interaction of electrons and photons with the magnetic and photon field.

The particles will arrive at the crust with low energy, and the yield of annihilation photons may be reasonably high. If such a situation may be established, the limitation due to the condition of not overcoming the neutron star magnetic field (eq. [7]) may be fulfilled, and the yield of annihilation photons may be still compatible with the observations.

A further constraint to energy $E_{\rm prim}$ of the particle impinging the star crust can be set by the upper limit on the thermal emission from the neutron star which is known to be $L_{\rm th} \sim 5.8 \times 10^{34}$ ergs s^{-1} (Toor & Seward 1977; Harnden & Seward 1984). The shower developing in the crust will heat up the crust at rate

$$L_{\rm Sh} = E_{\rm prim} P_{\rm Sh} \cong 4 \times 10^{38} E_{\rm prim} k_{100} \xi^{-1} \text{ ergs s}^{-1} , \quad (10)$$

where $E_{\rm prim}$ is the energy of primary electron in ergs.

From $L_{\rm Sh} < L_{\rm th}$ and assuming $k_{100} = 1$ and ξ independent of the energy of the primary electron (see Fig. 1), we obtain

$$E_{\rm prim}[\text{MeV}] < 900\xi , \quad (11)$$

which gives immediately $E_{\rm prim} < 100$ MeV for $\xi \approx 0.1$.

The limitations derived in this section from consistency with pulsar electrodynamics put strong constraints on the possible models. In the next section we present a picture which attempts to satisfy these constraints.

3. DESCRIPTION OF THE MODEL

We refer to the model of Ruderman and collaborators where particles are accelerated in an outer gap (far away in the magnetosphere: Cheng, Ho, & Ruderman 1986a, b) and in a second gap close to the polar cap (see Ruderman & Sutherland 1975). The surface of the polar cap is heated to a much higher temperature than the temperature of the neutron star because of the flux of high-energy particles on it. Typical temperatures are supposed to be 10^6–10^7 K (Helfand, Chanan, & Novick 1980). According to Cheng et al. (1986b) for a young pulsar, one would have in the outer gap production of 3×10^{32} electrons s^{-1} with energy $\sim 10^{12}$ eV moving toward the star surface (in fact, in the paper the case of the Vela pulsar was exemplified). The associated magnetic field is negligible (see eq. [7]). Primary electrons with energy $\sim 10^{12}$ eV will produce an electromagnetic cascade via curvature radiation (CR) in the strong magnetic field, inverse Compton scattering (ICS) of thermal photons emitted by the neutron star, and pair production in the strong magnetic field by photons which in turn were produced in CR and ICS (such a cascade, although in an opposite direction, was calculated by Daugherty & Harding 1982).

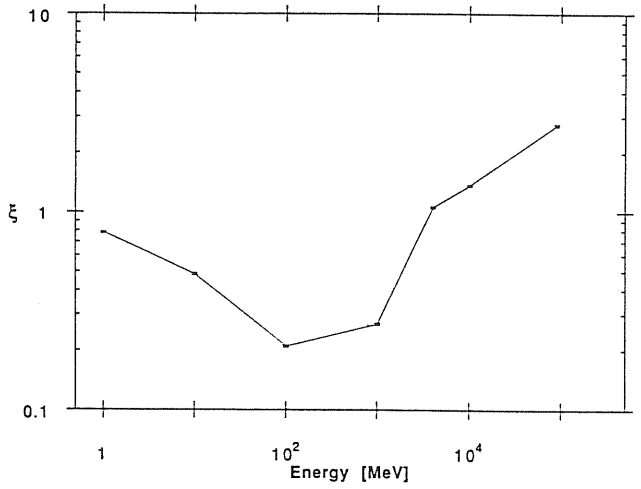

FIG. 1*a*

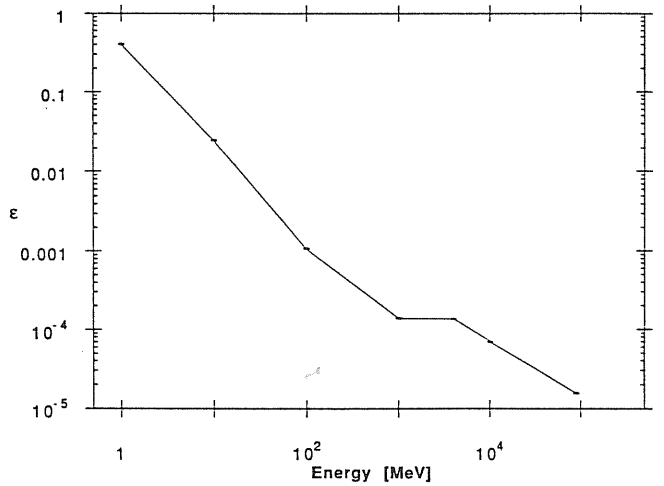

FIG. 1*b*

FIG. 1.—(*a*) Number of outgoing annihilation photons vs. the energy of the electron producing an electromagnetic shower impinging on an iron slab. (*b*) Fraction of energy outgoing in the form of annihilation photons vs. the energy of the electron producing the electromagnetic shower.

From such calculations it is possible to derive that the amplification of the number of particles will be of the order 10^3, yielding a flux moving downward $\sim 10^{35}$ electrons s^{-1}. We suppose that a fraction of particles will enter the inner gap.

The energy of these particles will be strongly influenced by the resonant ICS in strong magnetic field, which in the vicinity of the neutron star is regulated by the surface temperature and strength of the magnetic field. We calculated energy losses of relativistic electrons on the ICS of thermal photons in a strong magnetic field following analytical formulas derived by Dermer (1990) (see also numerical calculations by Xia et al. 1985 and Daugherty & Harding 1989). However, contrary to Dermer (1989), we assumed again that electrons are moving toward the surface of the neutron star. In Figure 2 we report the results of our calculations of the energy loss versus the electron energy for various temperatures and magnetic field 6×10^{12} G. From Figure 2 it is apparent that for temperatures larger than 10^6 K, energy losses are so large that one can assume that the final Lorentz factor of electrons will be small, and therefore its energy just above the polar cap will be of the order of a few MeV. The cascade process in the pulsar magnetosphere will not be modified by the electric field since $\boldsymbol{E} \cdot \boldsymbol{B} = 0$.

The situation is different when electrons are propagating in the polar gap because now $\boldsymbol{E} \cdot \boldsymbol{B} \neq 0$ (see model by Ruderman & Sutherland 1975). In the polar gap there is a competition between electron energy losses and energy gains. In Figure 3 we have calculated such losses and gains versus the energy of electrons entering the polar gap for a magnetic field $B_{pc} = 6 \times 10^{12}$ G, temperature of the polar cap $T_{pc} = 10^7$ K, and a few strengths of the electric field in the gap, which we assumed in the first approximation as homogeneous through the gap. The interesting property is that there are two Lorentz factors of electrons (γ_e) for which energy losses are equal to energy gains γ_1 and γ_2. If $\gamma_e > \gamma_2$, electrons will be accelerated reaching very high energy. If $\gamma_1 < \gamma_e < \gamma_2$, electrons will be quickly decelerated and achieve Lorentz γ_1. If $\gamma_e < \gamma_1$, electrons will be quickly accelerated also to the Lorentz factor γ_1. This means that the electron distribution during their propagation in the polar gap will be strongly peaked in the γ_1.

The characteristic energy of Comptonized photons by electrons crossing the polar gap will be determined by γ_1 and the temperature of the polar cap,

$$\epsilon_{ph} \sim \epsilon_{therm} \gamma_1^2 , \tag{12}$$

where we assumed $\epsilon_{therm} \simeq 3\ kT_{pc}$, and T_{pc} is the surface temperature of the polar cap.

For some parameters of γ_1 and T_{pc}, the energy of Comptonized photons is peaked at about 1 MeV. If the potential drop in the polar gap is of the order of $\sim 10^{11}$–10^{12} eV, which is suggested in the original paper by Ruderman & Sutherland (1975), one obtains that each electron crossing the polar gap will produce about 10^5 photons with energy close to 1 MeV. So, the total number of MeV photons entering the surface of the polar cap is of the order 3×10^{32} (from the outer gap) times 10^3 (multiplication in the magnetosphere) times 10^5 (multiplication in the polar cap in ICS) $= 3 \times 10^{40}$. From comparison of this value with P_{ph} (eq. [5]), we obtain for $k_{100} = 1$ that $\xi_{ph} \sim 10^{-2}$. This value is consistent with the expectations from the Monte Carlo simulations (see Fig. 1 and

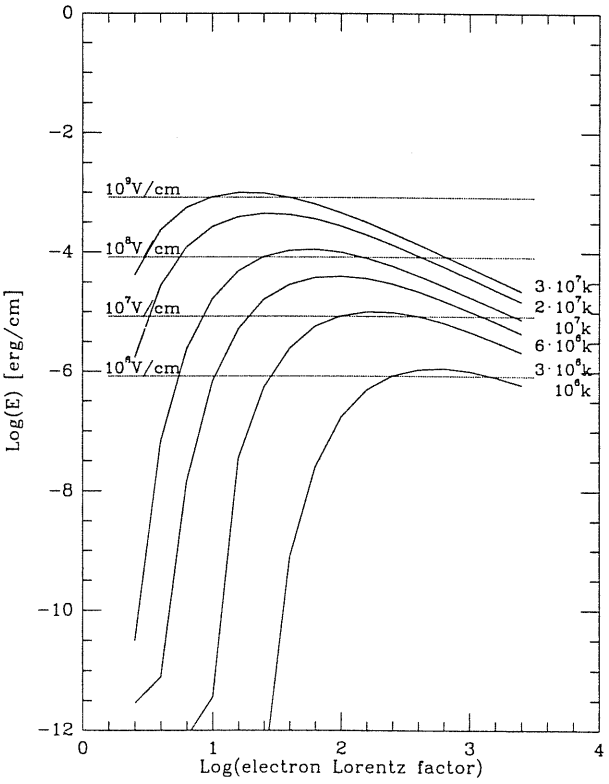

FIG. 2.—Energy losses of electrons by ICS in a strong magnetic field vs. Lorentz factor for a magnetic field strength 6×10^{12} G and different temperatures of blackbody radiation emitted by the polar cap. Dotted lines represent the electron energy gain for various homogenous electric fields.

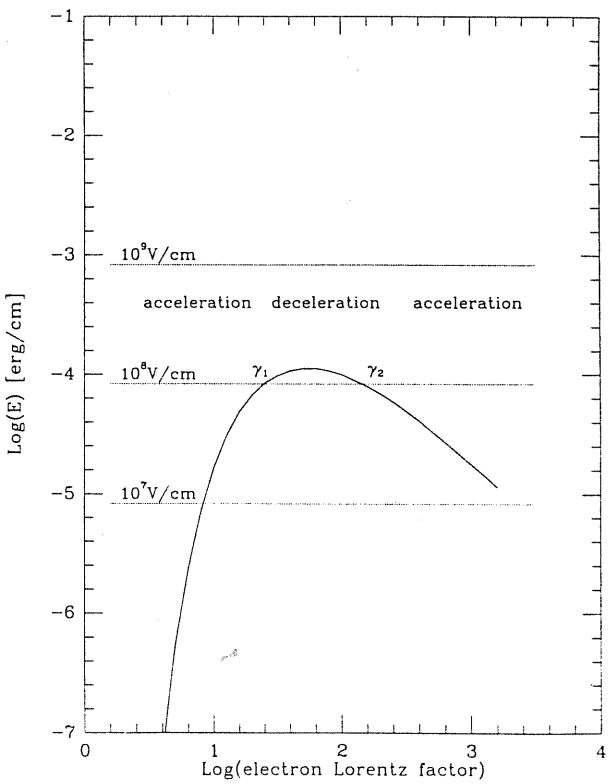

FIG. 3.—Same as Fig. 2. The γ_1 and γ_2 points are indicated for a particular value of energy gain 10^8 V cm^{-1}, and $T = 10^7$ K, and $B = 6 \times 10^{12}$ G. They define regions of acceleration and deceleration of electrons in the inner gap.

calculations by Bogovalov & Kotov 1990). The total energy of MeV photons falling onto the polar cap in the above picture is consistent with the condition of not overheating of the polar cap (eq. [10]). The high collimation of produced annihilation photons along the magnetic field lines, which is inferred from the observed pulsation of the annihilation line, is consistent with calculations of photon spectra from e^+e^- pair annihilation at rest in a strong magnetic field (see Kaminker, Pavlov, Mamradze 1991).

4. DISCUSSION

We considered a picture where the annihilation line is created by positrons interacting with the neutron star surface. The first result is that the required positron current has an associated magnetic field which exceeds the pulsar field; therefore the positrons must hit the neutron star in the form of pairs or showers. However, it is not possible to consider very energetic electrons hitting the surface, because in that case the shower would develop well inside the crust, and the yield of outgoing annihilation photons becomes very small. In that case the neutron star crust could be overheated. The particles hitting the surface must be of energy of about 1 MeV. We have then shown that within the model of Ruderman and collaborators such a situation can be envisaged. The outer gap is used as a source of particles moving downward. They are multiplied and slowed down by the interaction with the magnetic field and the photon atmosphere. In the inner gap the electrons acquire a fixed energy such to radiate downward gamma rays which interact with the surface and produce positrons. Positrons can be produced also by nuclear interaction in the crust (see, e.g., Jones 1978, 1979; Bogovalov & Kotov 1990), but here we have concentrated on the electromagnetic channel.

The positrons in the crust cool very efficiently, losing their energy in synchrotron and bremsstrahlung processes up to energy of the order of 10 keV (Ramaty, Lingenfelter, & Bussard 1981; Lamb, Wang, & Wasserman 1989) and next annihilate with thermal electrons of the crust ($T_{pc} \sim 10^6$–10^7 K). The width of the annihilation line is determined by two processes: broadening in the strong magnetic field and Doppler broadening. These processes are not considered in our Monte Carlo simulation. The broadening in the strong magnetic field is of the order $(\Delta E_\gamma/E_\gamma)_{\rm FWHM} \approx 0.35 B/B_{\rm cr}$ (see Daugherty & Bussard 1980) and for Crab pulsar magnetic field $B \approx 6 \times 10^{12}$ G s is ~ 20 keV. The first-order Doppler broadening in nonrelativistic plasma is $\Delta\omega_{\rm D} = (2kT\, mc^2)^{1/2}$, which for the temperature of the plasma $kT = 1$ keV is ~ 30 keV. While it is fully consistent with the energy resolution of the FIGARO II detector of about 59 keV (Massaro et al. 1991), it may conflict with a line width ~ 3 keV reported by Leventhal et al. (1977) and ~ 15 keV reported by Ayre et al. (1983). However, these two measurements were performed with wide field of view detectors, and no phase analysis were done, so these results may not refer to the Crab pulsar. The FIGARO II experiment did not observe these lines because of automatic subtraction of off-pulse spectrum.

Our model, however, requires that the central energy of the line remains essentially unchanged since annihilation of positrons is proposed to occur in the crust of the star at a well-defined redshift. This is not in contradiction with suggestions of the possibility of variation of the position of the line. As we mentioned above, the positive measurements of the line emission by Leventhal et al. (1977) and Ayre et al. (1983) did not refer to a periodic signal.

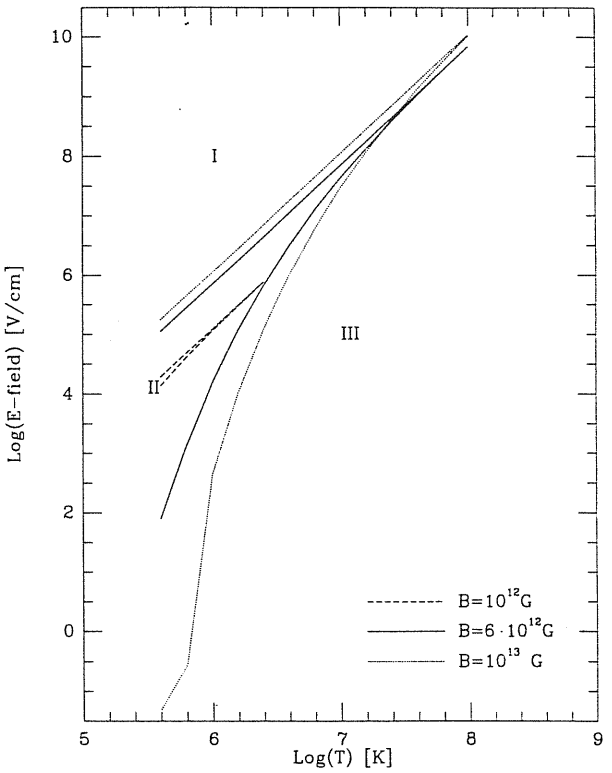

FIG. 4.—The gap electric field–cap temperature plane is divided in three parts. In part I, the electrons are accelerated, in part II they reach steady energy γ_1 which yields Compton photon with an energy above 1 MeV, and in part III the Compton photons have energy below 1 MeV.

Another problem concerns the escape of 0.511 MeV photons from the region of the polar cap and the possibility of Comptonization by impinging electrons. We note that electrons impinge the polar gap only along the magnetic field lines which connect the inner and the outer gap. The 0.511 MeV photons are expected to be emitted from a much bigger area.

Depending on the photon atmosphere (i.e., on the temperature of the polar cap), the magnetic field, and the electric field in the inner gap one may have a situation where the gamma rays produced by the Comptonization are too energetic in the sense that the showers enter too deeply in the crust. Oppositely, it is possible that the photons are below the threshold of pair production. Figure 4 illustrates the parameter space obtained from the calculations. Note that for a magnetic field of the Crab Nebula pulsar $\sim 6 \times 10^{12}$ G and the electric field of the inner gap 10^8 V cm^{-1} we obtained from Figure 4 that the efficient Comptonization of photons into the MeV energy range occurs for a polar cap temperature ~ 3.5–6×10^6 K.

Because of the tuning required to produce photons in the correct energy interval it is possible that the annihilation line occurs only in one polar cap in correspondence with the secondary pulsar peak, as suggested by the observation of line emission. The same argument may also justify the variability of the line intensity.

We are grateful to the FIGARO II team for informing us of their results in advance of publication. This work is supported by the Italian Ministero dell'Università e della Ricerca Scientifica e Tecnologica.

REFERENCES

Agrinier, B., et al. 1990, ApJ, 355, 645
Ayre, C. A., Bhat, P. N., Ma, Y. Q., Myers, R. M., & Thompson, M. G. 1983, MNRAS, 205, 285
Bogovalov, S. V., & Kotov, Yu. D. 1990, Astrophysics, 31, 490
Cheng, K. S., Ho, C., Ruderman, M. 1986a, ApJ, 300, 500
———. 1986b, ApJ, 300, 522
Daugherty, J. K., & Bussard, R. W. 1980, ApJ, 238, 296
Daugherty, J. K., & Harding, A. K. 1982, ApJ, 252, 337
———. 1989, ApJ, 336, 861
Dermer, C. D. 1990, ApJ, 360, 197
Greenstein, G., & Hartke, G. L. 1983, ApJ, 271, 283
Hameury, J. M., & Lasota, J. P. 1984, in AIP Conf. Proc. Gamma-Ray Bursts, ed. E. P. Liang & V. Petrosian (New York: AIP), 141
Harnden, F. R., & Seward, F. D. 1984, ApJ, 283, 279
Helfand, D. J., Chanan, G. A., & Novick, R. 1980, Nature, 283, 337
Jones, P. B. 1978, MNRAS, 184, 807
———. 1979, ApJ, 228, 536
Kaminker, A. D., Pavlov, G. G., & Mamradze, P. G. 1991, Ap&SS, 174, 241
Lamb, D. Q., Wang, J. C. L., & Wasserman, I. 1990, ApJ, 363, 670
Leventhal, M., MacCullum, C., & Watts, A. 1977, ApJ, 216, 491
Massaro, E., et al. 1991, ApJ, 376, L11
Nelson, W. R., Hirayama, H., & Rogers, D. W. O. 1985, SLAC Report 265
Owens, A. 1990, in Proc. International Symp. on Gamma-Ray Line Astronomy, ed. N. Prantzos & P. Durchoux (New York: AIP), 341
Ramaty, R., Lingenfelter, R. E., & Bussard, R. W. 1981, Ap&SS, 75, 193
Ruderman, M. A., & Sutherland, P. G. 1975, ApJ, 196, 51
Toor, A., & Seward, F. D. 1977, ApJ, 216, 560
Xia, X. Y., Qiao, G. J., Wu, X. J., & Hou, Y. Q. 1985, A&A, 152, 93

Astron. Astrophys. 000, 000–000 (1992) 12(02.18.5; 02.14.1; 13.07.3; 08.14.1; 08.09.2 Cyg X-3)

ASTRONOMY AND ASTROPHYSICS

The emission mechanism of neutral particles from discrete sources in the TeV–EeV energy range

W. Bednarek [1,2]

[1] International School for Advanced Studies-Trieste, Strada Costiera 11, I-34014 Trieste, Italy
[2] Institute of Physics, University of Lódź, ul. Pomorska 149/153, 90-236 Lódź, Poland

Received January 2, accepted May 19, 1992

Abstract. We discuss different production mechanisms of very high energy (VHE) photons and neutrons ($\geq 10^{11}$ eV). Our aim is to distinguish which of them, and under what conditions, can be responsible for the VHE emission reported from several discrete sources. We will concentrate on the Cyg X-3 (one of the most frequently mentioned in VHE photon energies) since the recent evidence of an excess of neutral particles above $5\,10^{17}$ eV from the direction of this source. We show that, among the proposed models, only two are able to describe the general shape of the spectrum of Cyg X-3 above 10^{11} eV being not in contradiction with the estimates of the magnetic field strength derived from radio observations. In the first, the VHE neutrons emitted by the compact object interact with low column density of the background matter. In the second, relativistic nuclei (e.g. He) develop an electromagnetic cascade in matter and magnetic field.

Key words: radiation mechanisms – γ-rays – neutrons; discrete sources – Cyg X-3

1. Introduction

During the last 20 years several discrete sources were reported at energies $>10^{11}$ eV, for a review we refer to e.g. Weekes (1988). Most of them are pulsars (or supernova remnants) and X-ray binary systems. Although increasing scepticism concerning these observations, still new positive results appear. In this paper we try to establish which kind of mechanism can be responsible for the VHE emission from these sources using for more detailed considerations the X-ray binary system Cyg X-3.

Cyg X-3, a low mass X-ray binary system with orbital period of 4.8 h (Parsignault et al. 1972; Becklin et al. 1972), shows a variety of peculiar behaviour in all ranges of the observed spectrum. For a review of wide range observations of Cyg X-3 (form radio up to 10^{15} eV), see Bonnet-Bidaud & Chardin (1988). The discovered 12.6 ms period by Chadwick et al. (1985) (see also Brazier et al. 1990), although not confirmed by independent observations (e.g. Fegan et al. 1989), suggests that the Cyg X-3 system consists of a main-sequence star plus a neutron star.

One of the most interesting features of this source is the discovery of very high energy emission in the TeV (10^{12} eV) (Vladimirsky et al. 1973) and PeV (10^{15} eV) (Samorsky & Stamm 1983; Lloyd-Evans et al. 1983) energy ranges. These first positive observations were later confirmed by other experiments (more recently Baltrusaitis et al. 1987; Muraki et al. 1991), although negative results were also reported (see for review et al. Weekes 1988 or Fegan 1990). All positive observations of Cyg X-3 above TeV energies show an excess close to two phases of the 4.8 h orbital period, at ≈ 0.2 and ≈ 0.6 (starting from X-ray minimum). However, recent reports concern only the emission at this second phase. The surprising detection of Cyg X-3 in EeV (10^{18} eV) energy range was reported by the Fly's Eye group (Cassiday et al. 1989, 1990). This excess of particles, although not seen in Haverah Park data (Lawrence et al. 1989), was again confirmed by the Akeno group (Teshima et al. 1990; Hayashida et al. 1991). Also another X-ray binary 2A 1822-37 was recently reported as a source of neutral particles above 10^{17} eV (Clay et al. 1992).

The integral photon spectrum from Cyg X-3 (from MeV up to PeV), summed over different periods of the observations, can be described by a power law with spectral index close to -1.1. The results reported by Lloyd-Evans et al. (1983) suggest the presence of a cut-off at energies 10 PeV. However the neutral emission at energies >0.5 EeV (Cassiday et al. 1989, 1990; Teshima et al. 1990) seems to follow the spectral index -1.1. In Fig. 1 are shown some results of observations of neutral emission from Cyg X-3 in TeV and PeV energies (collected by Watson 1985 plus some most recent) and fluxes in EeV energies observed by Cassiday et al. (1989, 1990) and Teshima et al. (1990).

Cassiday et al. (1989) recently suggested that the excess of the neutral particles from the direction of Cyg X-3 above 0.5 EeV can be caused by relativistic neutrons. Sommers and Elbert (1990) discussed in detail the consequences of the TeV–EeV emission from Cyg X-3 and proposed several different mechanisms of EeV neutron production in this source.

Based on the reported observational parameters of Cyg X-3, we fit the general spectrum in TeV–EeV energy range by the spectra of photons and neutrons calculated selfconsistently according to different production mechanisms. From these fittings, we calculate the required total luminosity of Cyg X-3 in relativistic particles. The model in which the EeV emission from Cyg X-3 is due to neutron flux is favorable from energetical viewpoint

Send offprint requests to: W. Bednarek (Trieste address)

A & A
proofs for correction

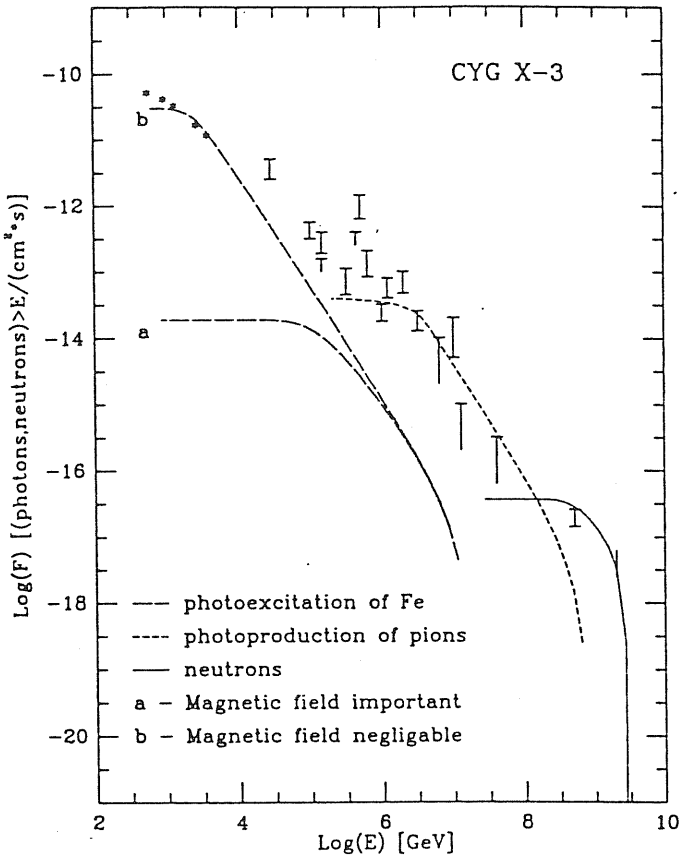

Fig. 1. The observational results of VHE emission from the direction of Cyg X-3 above 10^{11} eV fitted by the γ-ray spectrum from: (1) the photoexcitations of relativistic Fe nuclei (power low, spectral index 2.7) by low energy black body photons with $kT=10$ eV – long dashed line; the photoproduction of neutral pions created in the interactions of nuclei with thermal photons – short dashed line; (2) by the neutron spectra from the photodisintegration of Fe nuclei – dotted line

(acceleration of particles to lower energies is postulated) and avoids difficulties concerning attenuation of VHE photons in the strong magnetic field of the binary system. We show that a model in which relativistic neutrons, emitted by the compact object, interact with the background matter occulting the compact object in the orbital phase period observed in TeV and PeV energy ranges, seems to be the most successful in describing the spectrum of Cyg X-3 and gives reasonable values for the required total particle luminosity. Also a model in which the electromagnetic cascade initiated by nuclei (e.g. He) and developing in the matter and magnetic field surrounding the binary system is consistent with observations.

2. Production of γ-rays and neutrons in Cyg X-3

The VHE observations of Cyg X-3 postulate the acceleration of particles in the source to extremely high energies (at least $\approx 10^{18}$ eV). It is difficult to imagine a model of acceleration of particles up to so high energies if we keep in mind additional radiative processes that take place in strong magnetic and radiation fields. It seems very likely that electrons cannot be responsible for this emission because of the huge synchrotron losses that would result during acceleration processes. Also small rigidity of electrons will not allow them to propagate linearly through the binary system and observed emission close to fixed phase of 4.8 h orbital cycle should be diluted.

The source of energy, required by observations, seems to be problematic in the accretion scenario onto a neutron star if we assume isotropic acceleration of particles. Super-Eddington accretion of matter onto a neutron star, accretion onto a more massive object (e.g. black hole) or highly anisotropic acceleration of particles by neutron star is recommended. For a recent critical discussion on energy generation and particle acceleration in Cyg X-3, we refer to the paper by Mitra (1991).

A few different mechanisms of production of VHE emission by Cyg X-3 were recently discussed by Sommers & Elbert (1989). In general they can be classified depending on the kind of target encountered by the relativistic particles: matter or radiation. The most promising of them are:

(a) Interaction of relativistic nuclei (emitted by the compact object–CO) with background photon field. The VHE photons are produced through de-excitation of relativistic nuclei ($A+\gamma_{ph}\rightarrow A_1^*\rightarrow A_1+\gamma$) and through decay of neutral pions produced in the interaction of nuclei (and their fragments) with low energy photons ($p+\gamma_{ph}\rightarrow\pi^0+\cdots;\ \pi^0\rightarrow 2\gamma$). The neutrons are produced from fragmentation of nuclei ($A+\gamma_{ph}\rightarrow n+\cdots$) and in charge exchange of protons during their interactions with photons ($p+\gamma_{ph}\rightarrow n+\cdots$);

(b) Interaction of relativistic protons (accelerated by CO) with thin column density of matter. The VHE photons are produced through the decay of neutral pions ($p+p\rightarrow\pi^0+\cdots;\ \pi^0\rightarrow 2\gamma$) and the neutrons from charge exchange of proton beam ($p+p\rightarrow n+\cdots$);

(c) Interaction of relativistic neutrons (produced in CO) with thin column density of matter. The VHE photons and neutrons are produced like in item (b) plus neutrons which escape without interaction;

(d) Formation of the VHE neutral spectrum from Cyg X-3 in cascade initiated by monoenergetic particles. TeV and PeV photons are produced in electromagnetic cascade calculated by Hillas (1984). EeV neutrons are produced in fragmentation of nuclei during their interaction with matter.

(e) Interaction of relativistic nuclei (with power law spectrum) with thin column density of matter (<1 interaction length). The VHE photons are produced through the decay of neutral pions ($A+p\rightarrow\pi^0+\cdots;\ \pi^0\rightarrow 2\gamma$) and neutrons mainly from fragmentation of nuclei and charge exchange of relativistic protons.

Of course, in reality several – if not all – of these mechanisms can be important. However, for simplicity we will discuss them separately as a unique explanation of possible VHE emission from Cyg X-3.

3. Interaction of nuclei with the photon field

The production of VHE photons in the interaction of relativistic nuclei with radiation field was firstly investigated in the context of cosmic γ-ray sources by Balashov et al. (1990). The authors described the VHE photon spectra from two sources: Cyg X-3 (10^8–10^{16} eV) and the Crab pulsar (10^{11}–10^{16} eV) by a component model, iron nuclei and protons interacting with radiation field. However, their fitting to Cyg X-3 spectrum is somewhat controversial (spectral indexes of photons seems to be incorrect) and within the model it is impossible to describe the recent observations in the EeV energy range and the spectrum below

10^{11} eV only by photons from p+p interaction. The required amount of energy in relativistic particles would be enormous and EeV photons should be absorbed in magnetic field.

We performed calculations of the photon spectra including also contribution of neutrons from fragmentation of iron nuclei to the total emitted spectrum. It was assumed that the relativistic Fe nuclei (accelerated by e.g. neutron star) with a power law spectrum and high energy cut-off interact with black body radiation ($T_{bb} \approx 10$ eV) emitted by the stellar companion and/or accretion disk around compact object in Cyg X-3 system. The spectra of photons from deexcitation of nuclei were obtained in an approximate way following the calculations of multiplicity and average energy of photons produced during the decay of nuclear giant resonance (Moskalenko & Fotina 1989). The complete disintegration of Fe nuclei was assumed. The spectra of photons from photoproduction of neutral pions in particle–photon collisions were calculated according to resonance approximation (see Stecker 1973). This approximation is good enough since the considered energy range is far away from jet region of particle–photon interaction where the cross section raises again (for detailed results see Mannheim & Biermann 1989). The spectrum of neutrons from fragmentation of nuclei and further interaction of products of fragmentation with background photons were calculated assuming an elasticity coefficient equal to 0.4 and a probability of proton conversion into neutron equal to 0.5 (Kirk & Mastichiadis 1989). The probability of survival of relativistic neutrons against decay on the way from Cyg X-3 to the Earth was included in the calculations by the formula $P = \exp[-0.108 D\,(\mathrm{kpc})\, E(\mathrm{Eev})]$ (Cassiday et al. 1989).

In Fig. 1 are shown some results of observations of VHE neutral emission from Cyg X-3 (fluxes reported from a 4.8 h periodicity search) and the calculated spectra of photons and neutrons according to the above prescription. As we can see, it is possible to achieve a reasonable fit for the following parameters: power law spectrum of the iron nuclei with spectral index 2.7 and cut-off at 10^{11} GeV; temperature of the background photon field $\varepsilon = 10$ eV; column density of background photons equal to one interaction length for pion photoproduction in particle–photon collision.

From the fitting of the observed flux of neutral emission from Cyg X-3 by calculated photon spectrum (deexcitation in TeV range, photoproduction in PeV range) and neutron spectrum (from fragmentation in EeV range) we obtained the required luminosity of Cyg X-3 in the energy range $10^6 - 10^{11}$ GeV in relativistic Fe nuclei:

$$L_{Fe}(\mathrm{erg\ s^{-1}}) = 2.2\, 10^{38}\, \Delta\Omega(\mathrm{sr})/\delta t$$

where: $\Delta\Omega$ is a solid angle in which relativistic nuclei are emitted; δt is duty cycle of photon emission. The distance to Cyg X-3 is taken 10 kpc.

If we assume $\delta t = 1/20$ and $\Delta\Omega = 1$, the calculated luminosity is much higher than the classical Eddington one [$\approx 1.3 \times 10^{38} M/M_\odot$ (erg s^{-1})] for a typical mass of the neutron star. This can be accepted if particles emitted by Cyg X-3 are strongly collimated or if the mass of the compact object is much bigger than $1 M_\odot$ (however a black hole would contradict the reported 12.6 ms periodicity).

The photon flux in TeV energy range is consistent with observations (Fig. 1, curve b), if we assume that the magnetic field in the source volume does not influence the electromagnetic cascade initiated by VHE photon in the background photon field. In such case, the essential part of TeV photons can emerge from the source region if the mean value of the magnetic field in the source region is $\sqrt{B^2}(\mathrm{G}) < 10^{12} \times \varepsilon / E_{ph}$ (see Gould & Rephaeli 1978), which e.g. for photon energies $\approx 10^{16}$ eV yields $\sqrt{B^2} < 4\, 10^{-4}$ G. In the opposite case (important magnetic field – electromagnetic cascade do not develop), a much smaller absorption length must be used (see Gould & Schreder 1967) and the VHE photons are strongly attenuated (see Fig. 1 curve long dashed "a"). Another restriction on the magnetic field in this model is connected with the reported evidence of a periodical emission of photons from Cyg X-3 at certain phases of the 4.8 h orbital period. In order to be self-consistent with this observation, the relativistic particles interacting with the photon field have to propagate almost linearly through the source diameter. This requirement puts an upper limit to the magnetic field of ≈ 1 G for nuclei with energy 10^{16} eV and $Z = 26$ and source diameter $r = 10^{12}$ cm.

From modeling of the quiescent radio emission Cyg X-3, Vestrand (1983) estimated the magnetic field strength of $B_\perp^0 \approx 1000$ G, at distance $r \approx 10^{11}$ cm with linear decrease for farther regions of the binary system. Stephens & Verma (1984) gave the lower limit $B_\perp^0 \approx 100$ G, from the consistency of radio observations with the Razin–Tsytovich effect. These lower limits on the magnetic field in Cyg X-3 are much higher than the above upper limits and therefore make this model inconsistent at TeV energies.

When the optical depth for nuclei in the radiation field is much less than the interaction length on photoproduction process, we can neglect the production of photons through the photoproduction of neutral pions. In such case, it is possible to describe the neutral flux from Cyg X-3 in TeV and PeV energy range by the photon spectrum from deexcitations of nuclei if the spectrum of relativistic nuclei is a power law type with spectral index close to 2. However, the neutron flux in EeV energy range from photodisintegration of nuclei (calculated simultaneously) will be much higher than fluxes reported by Cyg X-3 by Cassiday et al. (1989, 1990) and Teshima et al. (1990). Moreover, the previous problems concerning the limit on the magnetic field strength are still valid and the required luminosity of Cyg X-3 in relativistic nuclei should be even greater.

4. Interaction of relativistic protons with background matter

The mechanism of VHE photon production in p+p collisions (via π^0 decay) as a possible explanation of TeV and PeV emission from Cyg X-3 was first proposed by Vestrand & Eichler (1982). The fittings of the general shape of Cyg X-3 spectrum by the calculated photon spectra from of p+p interaction in thin target model were discussed by e.g. Bednarek et al. (1990) and Piskunova (1990). Here, we developed our previous calculations including simultaneously calculated spectra of neutrons from charge exchange of relativistic protons. In Fig. 2 we show the observational data from Cyg X-3 above 10^{12} eV and the photon and neutron spectra for spectral index of primary proton spectrum equal to 2 and different cut-offs at $E_0 = 10^9$ GeV, $E_1 = 10^{10}$ GeV and $E_2 = 2.5\, 10^{10}$ GeV. As we can see, the fitting to the observational data in broad energy range by calculated photon spectrum is quite good (for cut-off in proton spectrum $\approx 10^{10}$ GeV), although the contribution of neutrons from charge exchange of protons in EeV energy range is negligible. From this

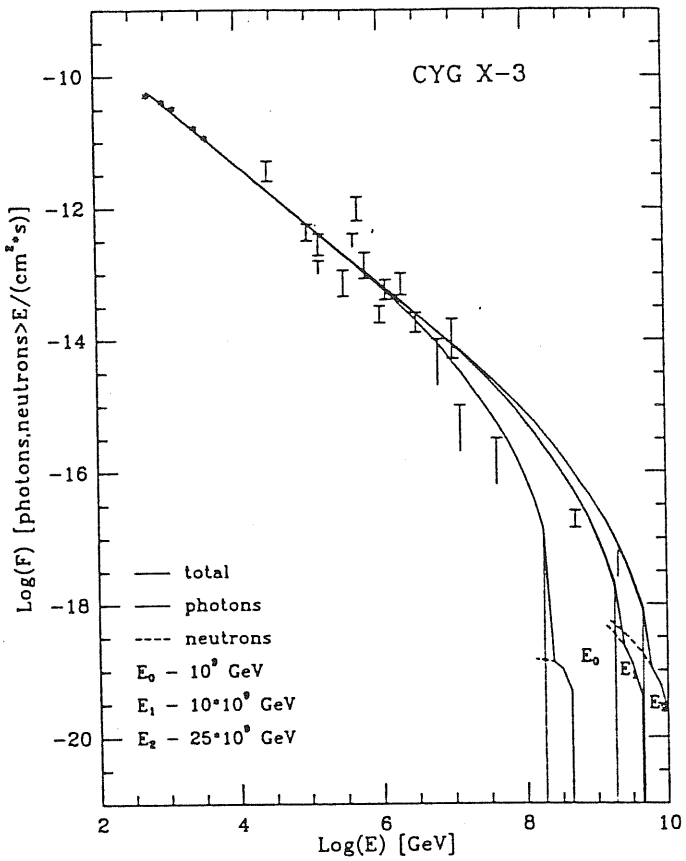

Fig. 2. The observational results as in Fig. 1 fitted by the spectra of photons and neutrons produced in the interaction of relativistic proton beam with background matter: dotted line – γ-ray spectrum from the decay of neutral pions; dashed line – spectrum of neutrons; full line – total spectrum (photons plus neutrons). The spectrum of relativistic protons is a power law type with spectral index 2 and different cut-offs at E_0, E_1, E_2

fit one can compute the proton luminosity in the energy range 10^2–10^{10} GeV for distance to Cyg X-3 equal to 10 kpc

$$L_p(\text{erg s}^{-1}) \approx 5\,10^{38}\Delta\Omega(\text{sr})/\delta t/x_H(\text{g cm}^{-2})$$

where x_H is the column density of background matter in g cm^{-2}.

If we assume $x_H = 30$ g cm^{-2}, $\delta t = 1/20$ and $\delta\Omega = 1$, the proton luminosity is equal to $L_p \approx 3.2\,10^{38}$ erg s^{-1}.

Again, the main trouble of this model concerns the value of the average magnetic field which is required in the Cyg X-3 system in order to avoid strong attenuation of EeV photons in the magnetic field through magnetic pair production processes (Erber 1966). To be consistent with the positive detection of Cyg X-3 at about EeV, the average magnetic field strength up to the distance 10^{13} cm from the center of the binary system should be of the order of ~ 2 G. However, the lower limit on the value of the magnetic field (≈ 100 G, see Sect. a) is much higher. The problems concerning requirements of nearly linear propagation of relativistic protons through source volume in order to guarantee photon emission in fixed phase of 4.8 h orbital period are also still valid.

5. The interaction of relativistic neutrons with matter

The emission of VHE neutrons by compact object is quite probable since it is difficult to imagine the escape of charged relativistic particles from very compact source. During propagation through dense photon field (e.g. from accretion disk or magnetosphere of neutron star) or through the high column density of matter with strong magnetic field (accretion), neutrons from discharge of relativistic protons (and neutrinos) can be the only relativistic particles which escape without troubles (see e.g. the model by Kazanas & Ellison 1986).

Based on such scenario of neutron production, we have calculated the spectra of photons (from $n+p \to \pi^0$; $\pi^0 \to 2\gamma$) and neutrons (from $n+p \to n+\cdots$; plus neutrons which escaped without interaction) for the power law spectrum of neutrons with differential spectral index 2. The cut-off at the neutron spectrum was put at $4\,10^9$ GeV (which is the maximal energy of particles observed from the direction of Cyg X-3, Cassiday et al. 1990). Since we do not know what is the duty cycle for neutron emission, we made calculations for a few different cases, among which: 0.05 – duty cycle observed in TeV and PeV photon energies; 0.3 – suggested by Cassiday et al. (1990) in EeV energies and 1 – suggested by Teshima et al. (1990) also in EeV energies.

The results of these calculations with their fit to the observed flux of particles from Cyg X-3 are shown in Fig. 3. As we can see, the best fit in EeV energies was obtained for neutron duty cycle equal to ~ 0.25 (which is close to value ~ 0.3 suggested by

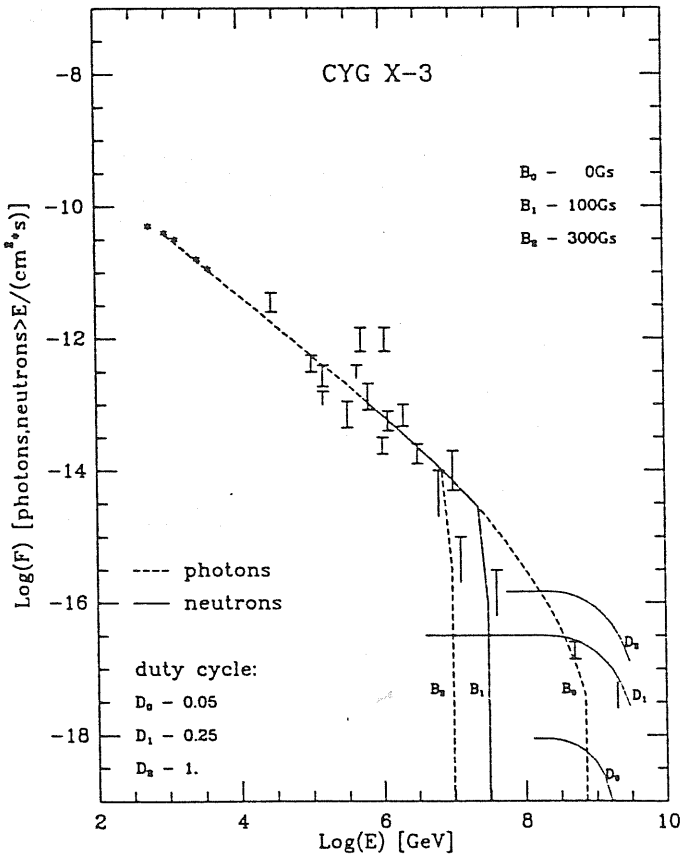

Fig. 3. The observational results as in Fig. 1 fitted by the spectra of photons and neutrons produced in the interaction of relativistic neutron beam with background matter: dashed line – spectra of photons calculated for different values of magnetic field in the source region (B_0, B_1 and B_2); dotted line – spectra of neutrons calculated for different duty cycles of neutron emission D_0, D_1 and D_2. The spectrum of relativistic protons is a power law type with spectral index 2 and cut-off at $4\,10^9$ GeV

Cassiday et al. 1990). We note here that obtained the duty cycle for neutron emission (EeV energy range) is different from the duty cycle for photon emission (TeV and PeV energy range). This can be understood if only a small part of the broad neutron beam emitted by the compact object is obscured by background matter where photons are produced. Such a picture postulates that the photon emission can appear sporadically (when the observer is inside the broad cone of neutron beam) although the 4.8 h modulation during this active period can be observed.

The estimated neutron luminosity of the compact object in the energy range $10^2-4\,10^9$ GeV is equal to

$$L_n(\mathrm{erg\ s^{-1}}) \approx 4.5\,10^{38}\,\Delta\Omega(\mathrm{sr})/\delta t/x_H(\mathrm{g\ cm^{-2}})$$

where δt is the duty cycle for photon emission.

Corresponding to the above value, the luminosity of charged particles emitted by the compact object is about 2–4 times higher (see estimations of the conversion of luminosity from protons to neutrons by Kazanas & Ellison 1986).

This model has two big advantages. First, there is no problem with linear propagation of relativistic neutrons in the Cyg X-3 binary system which allows to observe particle emission concentrated in spatial phases of 4.8 h cycle. Second, the EeV emission is well described by neutrons which contrary to photons, are not attenuated in the magnetic field of the binary system. The cut-off in Cyg X-3 photon spectrum (at first calculated by Stephens & Verma 1984; and shown in Fig. 3) for average magnetic field $\langle B\rangle = 100$ and 300 G for a source radius $R = 10^{13}$ cm, is not restrictive for the model. For such values of magnetic field, this model predicts a big dip in the integral spectrum of Cyg X-3 between 10 and 100 PeV.

6. Electromagnetic cascade initiated by monoenergetic relativistic particles

The mechanism of production of VHE photons in electromagnetic cascade initiated by monoenergetic protons with energy $\sim 10^{17}$ eV was applied to Cyg X-3 by Hillas (1984) in two scenarios:

— when the column density of background matter is very high (~ 16 radiation length) and magnetic field is negligible;

— when the column density of matter is of the order of 1–4 radiation lengths but magnetic field is of the order ~ 500 G (which is the value proposed by Vestrand 1983).

Both models can successfully describe the general shape of the Cyg X-3 spectrum in TeV and PeV energy range if the luminosity of monoenergetic protons is $\sim 10^{39}$ erg s^{-1}.

However the efficiency of energy conversion of relativistic protons into photons with energy above 10^{12} eV is very small in the thick target model (less than 1%) while for thin target models (e.g. $x_H \approx 30$ g cm^{-2}), this value can be of the order of 10% (see e.g. Stanev 1990). That's why from an energetic point of view, the second proposition seems to be more relevant.

In the second proposition, Hillas (1984) showed that if the magnetic field in the matter is >10 G, the electromagnetic cascade develops through synchrotron emission of VHE photons since bremsstrahlung losses are much lower. However if we want to describe observations of EeV neutral emission from Cyg X-3 by this model, the magnetic field should be less than ~ 2 G in order not to attenuate EeV photons on magnetopair production process. This seems in contradiction with the assumption on magnetic field strength >10 G, required by the model.

Moreover in both propositions, the EeV emission from Cyg X-3 cannot be also described by the neutron flux from discharge of relativistic protons, since it is proportional to the photon flux calculated in Sect. 4 (see Fig. 2) and is not able to supply the reported flux at EeV energies.

A much more promising scenario able to explain recent observations also in EeV energies is initialization of the above mentioned cascade by nuclei e.g. helium (a possibility also suggested by Hillas). The energies of nuclei should be ≥ 10 PeV in order to explain TeV–PeV emission but significant number of nuclei should have energy close to ~ 10 EeV in order to produce enough free neutrons (from fragmentation of He) in the EeV energy range.

For simple estimations we can assume that all He nuclei have energy ~ 10 EeV and luminosity of Cyg X-3 in relativistic particles is $\sim 10^{39}$ erg s^{-1} (required to explain flux in TeV–PeV energy range). We can roughly calculate the total number of interacting He nuclei equal to $\sim 6\,10^{31}$ He s^{-1}. For column density of target matter equal to 2 radiation lengths, the number of neutrons produced in fragmentation of He nuclei is equal to $\sim 10^{32}$ neutron s^{-1} which corresponds to a neutron luminosity of $L_n \approx 2\,10^{38}$ erg s^{-1} above 1 EeV. This value is the upper limit since in reality the nuclei with energy greater than ~ 10 PeV take part in the production of the observed flux of photons in TeV–PeV energy range (but on the Earth we can observe only neutrons with energy >0.5 EeV). The derived upper limit is in very good agreement with the estimate of total luminosity from Cyg X-3 above 0.5 EeV equal to $2\,10^{35}$ erg s^{-1} (Cassiday et al. 1989) and allows to explain the EeV emission by neutron flux.

The electromagnetic cascade discussed above cannot be initiated by relativistic neutrons because the time of decay of secondary muons (produced in neutron-proton interaction) with Lorentz factor $\sim 10^9$ into electrons is long enough for them to escape from the binary system.

7. The interaction of relativistic nuclei with matter

The interaction of relativistic nuclei (with a power law spectrum) with matter can be an efficient source of photons from π^0 decay and neutrons from fragmentation of nuclei. In the case of Cyg X-3, the nuclei cannot be very heavy since the data reported by Fly's Eye experiment do not contain cosmic ray background events with energy greater than 80 EeV which for the most energetic particles reported from Cyg X-3 gives an upper limit of $Z \approx 20$ (Sommers & Elbert 1990).

If we take into account the Helium nuclei interacting with background matter, we can assume that very high energy protons and neutrons (bound in helium nuclei) interact with matter as separate particles. So, in rough approximation, the interaction of helium nuclei can be treated as a sum of processes discussed in Sects. 4 and 5. Figures 2 and 3 clearly show that it is impossible to describe the flux from Cyg X-3 in TeV–EeV energy range for low column density of background matter because of too small flux of neutrons in EeV energy range and attenuation of photons with EeV energy in magnetic field.

8. Conclusion

In this paper we discussed the probable emission mechanisms of TeV–EeV neutral particles from discrete sources taking as an example for detailed discussion Cyg X-3. We showed that it is

Cassiday et al. 1990). We note here that obtained the duty cycle for neutron emission (EeV energy range) is different from the duty cycle for photon emission (TeV and PeV energy range). This can be understood if only a small part of the broad neutron beam emitted by the compact object is obscured by background matter where photons are produced. Such a picture postulates that the photon emission can appear sporadically (when the observer is inside the broad cone of neutron beam) although the 4.8 h modulation during this active period can be observed.

The estimated neutron luminosity of the compact object in the energy range $10^2-4\,10^9$ GeV is equal to

$$L_n(\mathrm{erg\ s^{-1}}) \approx 4.5\,10^{38}\,\Delta\Omega(\mathrm{sr})/\delta t/x_H(\mathrm{g\ cm^{-2}})$$

where δt is the duty cycle for photon emission.

Corresponding to the above value, the luminosity of charged particles emitted by the compact object is about 2–4 times higher (see estimations of the conversion of luminosity from protons to neutrons by Kazanas & Ellison 1986).

This model has two big advantages. First, there is no problem with linear propagation of relativistic neutrons in the Cyg X-3 binary system which allows to observe particle emission concentrated in spatial phases of 4.8 h cycle. Second, the EeV emission is well described by neutrons which contrary to photons, are not attenuated in the magnetic field of the binary system. The cut-off in Cyg X-3 photon spectrum (at first calculated by Stephens & Verma 1984; and shown in Fig. 3) for average magnetic field $\langle B\rangle = 100$ and 300 G for a source radius $R = 10^{13}$ cm, is not restrictive for the model. For such values of magnetic field, this model predicts a big dip in the integral spectrum of Cyg X-3 between 10 and 100 PeV.

6. Electromagnetic cascade initiated by monoenergetic relativistic particles

The mechanism of production of VHE photons in electromagnetic cascade initiated by monoenergetic protons with energy $\sim 10^{17}$ eV was applied to Cyg X-3 by Hillas (1984) in two scenarios:

— when the column density of background matter is very high (~ 16 radiation length) and magnetic field is negligible;

— when the column density of matter is of the order of 1–4 radiation lengths but magnetic field is of the order ~ 500 G (which is the value proposed by Vestrand 1983).

Both models can successfully describe the general shape of the Cyg X-3 spectrum in TeV and PeV energy range if the luminosity of monoenergetic protons is $\sim 10^{39}$ erg s^{-1}.

However the efficiency of energy conversion of relativistic protons into photons with energy above 10^{12} eV is very small in the thick target model (less than 1%) while for thin target models (e.g. $x_H \approx 30$ g cm^{-2}), this value can be of the order of 10% (see e.g. Stanev 1990). That's why from an energetic point of view, the second proposition seems to be more relevant.

In the second proposition, Hillas (1984) showed that if the magnetic field in the matter is >10 G, the electromagnetic cascade develops through synchrotron emission of VHE photons since bremsstrahlung losses are much lower. However if we want to describe observations of EeV neutral emission from Cyg X-3 by this model, the magnetic field should be less than ~ 2 G in order not to attenuate EeV photons on magnetopair production process. This seems in contradiction with the assumption on magnetic field strength >10 G, required by the model.

Moreover in both propositions, the EeV emission from Cyg X-3 cannot be also described by the neutron flux from discharge of relativistic protons, since it is proportional to the photon flux calculated in Sect. 4 (see Fig. 2) and is not able to supply the reported flux at EeV energies.

A much more promising scenario able to explain recent observations also in EeV energies is initialization of the above mentioned cascade by nuclei e.g. helium (a possibility also suggested by Hillas). The energies of nuclei should be ≥ 10 PeV in order to explain TeV–PeV emission but significant number of nuclei should have energy close to ~ 10 EeV in order to produce enough free neutrons (from fragmentation of He) in the EeV energy range.

For simple estimations we can assume that all He nuclei have energy ~ 10 EeV and luminosity of Cyg X-3 in relativistic particles is $\sim 10^{39}$ erg s^{-1} (required to explain flux in TeV–PeV energy range). We can roughly calculate the total number of interacting He nuclei equal to $\sim 6\,10^{31}$ He s^{-1}. For column density of target matter equal to 2 radiation lengths, the number of neutrons produced in fragmentation of He nuclei is equal to $\sim 10^{32}$ neutron s^{-1} which corresponds to a neutron luminosity of $L_n \approx 2\,10^{38}$ erg s^{-1} above 1 EeV. This value is the upper limit since in reality the nuclei with energy greater than ~ 10 PeV take part in the production of the observed flux of photons in TeV–PeV energy range (but on the Earth we can observe only neutrons with energy >0.5 EeV). The derived upper limit is in very good agreement with the estimate of total luminosity from Cyg X-3 above 0.5 EeV equal to $2\,10^{35}$ erg s^{-1} (Cassiday et al. 1989) and allows to explain the EeV emission by neutron flux.

The electromagnetic cascade discussed above cannot be initiated by relativistic neutrons because the time of decay of secondary muons (produced in neutron-proton interaction) with Lorentz factor $\sim 10^9$ into electrons is long enough for them to escape from the binary system.

7. The interaction of relativistic nuclei with matter

The interaction of relativistic nuclei (with a power law spectrum) with matter can be an efficient source of photons from π^0 decay and neutrons from fragmentation of nuclei. In the case of Cyg X-3, the nuclei cannot be very heavy since the data reported by Fly's Eye experiment do not contain cosmic ray background events with energy greater than 80 EeV which for the most energetic particles reported from Cyg X-3 gives an upper limit of $Z \approx 20$ (Sommers & Elbert 1990).

If we take into account the Helium nuclei interacting with background matter, we can assume that very high energy protons and neutrons (bound in helium nuclei) interact with matter as separate particles. So, in rough approximation, the interaction of helium nuclei can be treated as a sum of processes discussed in Sects. 4 and 5. Figures 2 and 3 clearly show that it is impossible to describe the flux from Cyg X-3 in TeV–EeV energy range for low column density of background matter because of too small flux of neutrons in EeV energy range and attenuation of photons with EeV energy in magnetic field.

8. Conclusion

In this paper we discussed the probable emission mechanisms of TeV–EeV neutral particles from discrete sources taking as an example for detailed discussion Cyg X-3. We showed that it is

possible to fit the general shape of the spectrum of Cyg X-3 above 10^{11} eV by the spectra of photons and neutrons calculated according to different mechanisms (see Figs. 1, 2 and 3). However, additional features of Cyg X-3 source like: (1) the required luminosity of relativistic particles derived from the above fittings; (2) the value of magnetic field suggested in Cyg X-3 binary system (Vestrand 1983; Stephens & Verma 1984) and (3) the observations of VHE emission in spatial phases of 4.8 h orbital period, allow us to reject the mechanisms of:

(1) interaction of relativistic nuclei with background radiation field (see Sect. 3);

(2) interaction of relativistic protons with matter (see Sects. 4 and 6);

(3) electromagnetic cascade initiated by monoenergetic protons (see Sect. 6);

(4) interaction of relativistic nuclei with matter (see Sect. 7).

Two models are able to describe the VHE neutral emission and they are not in contradiction with the above mentioned features of Cyg X-3 system.

In the first model, the interaction of relativistic neutrons (emitted by compact object) with low column density of background matter is able to describe TeV and PeV emission from Cyg X-3 by photon spectra produced from decay of π^0 and EeV emission by neutrons from $n+p \rightarrow n+\cdots$; plus neutrons which escape without interaction (Fig. 3). The spectrum of neutrons was assumed as a power low E_n^{-2} with cut-off at $4\,10^9$ GeV (which is the maximal energy of particles from Cyg X-3 reported by Cassiday et al. 1990) and duty cycle of neutron emission 0.25 [the value ~ 0.3 was suggested by Cassiday et al. 1990 on the base of observations), the required neutron luminosity $L_n \approx 4.5\,10^{38}$ $\Delta\Omega(\mathrm{sr})/\delta t/x_H$ (g cm^{-2}) above 10^2 GeV] is reasonable if $x_H = 20-30$ g cm^{-2} and duty cycle of photon emission $\delta t = 1/20$. We note that only a part of the broad neutron beam (duty cycle ~ 0.25) emitted by the compact object is obscured by background matter where photons are produced. This conclusion suggests the possibility of long term sporadic appearance of VHE photon emission. During this active phase the emission is modulated according to orbital period 4.8 h.

In the second model (proposed by Hillas 1984), the TeV and PeV emission from Cyg X-3 was successfully described by VHE photons produced in electromagnetic cascade initiated by monoenergetic relativistic particles. However, EeV emission cannot be explained in terms of photon production since photons should be strongly attenuated in magnetic field on magnetopair production process (see, Stephens & Verma 1984 and discussion in Sect. 6). We suggest that if nuclei (e.g. helium) are the primary particles initiating the cascade as calculated by Hillas, then the EeV emission can be caused by neutrons from their fragmentation. The $\sim 10^{39}$ erg s^{-1} (assuming isotropic emission) needed for explanation of TeV–PeV emission from Cyg X-3 can also easily supply the observed luminosity $\gtrsim 2\,10^{35}$ erg s^{-1} above 0.5 EeV, if $\approx 0.5\%$ of luminosity of Cyg X-3 is in the form of relativistic helium nuclei with energy close to ~ 10 EeV.

Acknowledgements. I am very grateful to Prof. A. Treves and Prof. M. Calvani for discussion and to the referee for suggestions and kind corrections of the text. This work is supported by the Italian Ministero dell'Università e della Ricerca Scientifica e Tecnologica.

References

Balashov V.V., Korotkikh V.L., Moskalenko I.V., 1990, Proc. 21st ICRC Adelaide, 2, 416
Baltrusaitis R.M., Cassiday G.L., Cooper R., et al., 1987, ApJ 323, 685
Becklin E.E., Kristian J., Neugebauer G., Wynn-Williams C.G., 1972, Nat. Phys. Sci. 239, 130
Bednarek W., Karakuła S., Tkaczyk W., 1990, 21st ICRC Adelaide, 2, 79
Bonnet-Bidaud J.M., Chardin D., 1988, Phys. Rep. 170, 326
Brazier K.T.S., Carraminana A., Chadwick P.M., et al., 1990, ApJ 350, 745
Cassiday G.L., Cooper R., Corbato S.C., et al., 1989, Phys. Rev. Lett. 62, 383
Cassiday G.L., Cooper R., Elbert J.W., et al., 1990, 21st ICRC Adelaide, 4, 282
Chadwick P.M., Dipper N.A., Dowthwaite J.C., et al., 1985, Nat 318, 642
Clay R.W., Meyhandan R., Horton L., Ulrichs J., Winn M.M., 1992, A&A 255, 167
Erber T., 1966, Rev. Mod. Phys. 38, 626
Fegan D.J., 1990, 21st ICRC Adelaide, 11, 23
Fegan D.J., Cawley M.F., Gibbs K., et al., 1989, A&A 211, L1
Gould R.J., Rephaeli Y., 1978, ApJ 225, 318
Gould R.J., Schreder G.P., 1967, Phys. Rev. 155, 1404
Hayashida N., Honda K., Honda M., et al., 1991, 22nd ICRC Dublin, 1, 309
Hillas A.M., 1984, Nat 312, 48
Kazanas D., Ellison D.C., 1986, Nat 319, 380
Kirk J.G., Mastichiadis A., 1989, A&A 213, 75
Lawrence M.A., Prosser D.C., Watson A.A., 1989, Phys. Rev. Lett. 63, 1121
Lloyd-Evans J., Coy R.N., Lambert A., et al., 1983, Nat 305, 784
Mannheim K., Biermann P.L., 1989, A&A 221, 211
Mitra A., 1991, ApJ 370, 345
Moskalenko I.V., Fotina O.V., 1989, Yad. Fiz. (USSR) 49, 1623
Muraki Y., Shibata S., Aoki T., et al., 1991, ApJ 373, 657
Parsignault D., Gursky E.M., Kellogg T., et al., 1972, Nat. Phys. Sci. 239, 123
Piskunova O.I., 1990, Sov. J. Nucl. Phys. 51, 846
Samorsky M., Stamm W., 1983, ApJL 268, L17
Sommers P., Elbert J.W., 1990, Astron. Lett. Commun. 27, 397
Stanev T., 1990, Nucl. Phys. B. Proc. Suppl. 14A, 17
Stecker F.W., 1973, Ap&SS 20, 47
Stephens S.A., Verma R.P., 1984, Nat 308, 828
Teshima M., Nagano M., Hara T., et al., 1990, Phys. Rev. Lett. 64, 1628
Vestrand W.T., 1983, ApJ 271, 304
Vestrand W.T., Eichler D., 1982, ApJ 261, 251
Vladimirsky B.M., Stepanian A.A., Fomin V.P., 1973, 13th ICRC Denver, 1, 456
Watson A.A., 1985, 19th ICRC La Jolla, 9, 111
Weekes T.C., 1988, Phys. Rep. 160, 1

ref. SISSA 186/A

On the γ-ray emission from 3C 279

W. Bednarek[1]

International School for Advanced Studies,
via Beirut 2-4, I-34014 Trieste, Italy
[1]on leave from University of Łódź, Łódź, Poland

ABSTRACT

Intense γ-ray emission was recently discovered from the direction of the quasar 3C 279 by the Compton GRO. It is proposed here that γ-rays are produced in the inelastic collisions of a mildly relativistic proton beam with matter of a thick accretion disk via decay of neutral pions and as a result of Comptonization of UV thermal photons by secondary electrons from decay of charged pions. The cone proton beam propagates along the axis of the disk funnel and illuminates its walls. From the fit of the observed data by calculated photon spectra we estimate a minimum power of 3C 279 in relativistic protons of $L_p \cong 2.5 \times 10^{47} erg/s$.

Subject headings: galaxies: nuclei: individual (3C 279) – gamma rays: theory

Accepted to Ap. J. Lett. (Oct. 1992)

1. INTRODUCTION

Recent observations by Compton GRO reported several new extragalactic objects as powerful and variable γ-ray emitters above 30 MeV (e.g. Michelson et al. 1992; Fichtel et al. 1992), and now it is clear that high energy processes are common and dominant features of AGNs. One of the objects best studied by GRO is the superluminal quasar 3C 279, which shows outbursts observed from radio (e.g. Unwin et al. 1989) up to X-rays (e.g. Makino et al 1989) with variability time scales from years to hours. Its γ-ray spectrum can be described between 30 MeV to 5 GeV by a simple power law with spectral index 2.02 ± 0.07 and intensity $(2.8 \pm 0.4) \times 10^{-6} ph\ cm^{-2} s^{-1}$ above 100MeV (Hartman et al. 1992), which corresponds to an isotropic emission of $1.1 \times 10^{48} erg/s$ (for z = 0.538 and $H_0 = 75 km/s/Mpc$). Such extremely high photon luminosity strongly suggests the beaming of γ-ray emission which is also supported by the observations of superluminal motion in the central core of 3C 279 (Whitney et al. 1971). Another strong constraint on the model of γ-ray production in 3C 279 is put by a significant variability on the order of 3 days observed by GRO in June 1991 (Kanbach et al. 1992).

In this letter we propose a physical scenario in which γ-ray production and variability in AGNs can be envisaged. In the following sections we describe the main points of this model and calculate the spectra of γ-rays and secondary electrons produced in p + p interactions via pion decay and the spectra of γ-rays produced by secondary electrons in Inverse Compton Scattering (ICS) of UV photons emitted by a thick accretion disk. We then focus on the γ-ray emission from 3C 279. Our model has some points in common with previous works (see mechanisms of γ-ray production discussed by e.g. Begelman et al. (1990); Jones & Stein 1990; Bednarek & Calvani 1991) but contrary to them it is also able to explain the reported variability of γ-ray emission from 3C 279.

2. DESCRIPTION OF THE MODEL

The basic assumption of the model is the existence of the geometrically thick accretion disk (radiation tori) around the central engine of the AGN (see the review by Begelman, Blandford & Rees 1984 and references therein) which is also responsible for production of the UV bump in the AGN spectrum (Shields 1978; Malkan & Sargent 1982). The structure of such radiation supported disks was studied by e.g. Jaroszyński, Abramowicz & Paczynski (1980), and the emission of radiation from the funnels by e.g. Abramowicz, Calvani & Nobili (1980) and Madau (1988).

Moreover, we assume that blobs or shocks containing relativistic particles (e.g. accelerated with one of the mechanisms discussed by Rees 1984) can emerge sporadically from the region close to the central engine. A possible model for the blob

(shock) production may be this one proposed by Protheroe & Kazanas (1983) and Kazanas & Ellison (1986) and may be connected with the rapid change in the accretion scenario in the inner part of AGN or with instabilities of the accretion disk (Papaloizou & Pringle 1984). The blobs are moving inside the narrow funnel of the thick accretion disk (see Fig. 1). If relativistic particles are emitted by such a blob inside a cone with opening angle α_{out} (which is bigger than the disk funnel angle α_{in}) then some of the relativistic particles will interact with matter in the accretion disk. Although this is an *ad hoc* assumption, it may be supported by the existence of viscous forces in the disk funnel. As a result of these forces, the velocity of the relativistic blob (shock) close to the axis of the funnel should be greater than close to the walls. This effect should cause a bending of the shock and permit emission of relativistic particles inside the limiting angle measured from the axis of the funnel.

We assume moreover, that the disk has a dense corona between the angles α_{in} and α_{out}. In the inelastic p + p interactions of relativistic protons with matter of the disk, γ-rays and secondary electrons from pion decay are produced. The γ-rays below $\sim$ 100MeV are produced via ICS of thermal UV photons from the disk by secondary electrons inside the disk funnel. For the shake of simplicity, we assume that the funnel of the optically thick accretion disk emits black body radiation with the temperature $T_{bb} \cong 4.5 \times 10^4$ K. A small gradient of temperature in the narrow funnel of the disk is suspected because of multiple scattering of radiation on the funnel's walls. The thermal emission of the disk funnel is consistent with the upper limit on the disk radiation of 3C 279 equal to $\sim 3 \times 10^{46}$ erg/s (Makino et al. 1991). We note that the radiation of the disk is dominated by the emission from the funnel (Madau 1988).

Under energy release of the relativistic particles, the outer part of the thick disk evaporates producing a strong wind which surrounds the relativistic beam (Fig. 1). The efficient escape of γ-rays from π^0 decay will be possible only in some region close to the limb of the thick disk (disk corona, Fig. 1), where the column density of matter is not extremely high. In the regions where matter is opaque for γ-ray photons ($\alpha > \alpha_{out}$), only high energy neutrinos can escape. We further point out that X- and γ-ray emission from 3C 279 can be described in such a scenario.

3. PRODUCTION OF γ-RAY PHOTONS

As we mentioned above, the main mechanism of the high energy γ-ray production in our model is the interaction between relativistic protons and ambient matter accumulated in the thick accretion disk. In such collisions neutral and charged pions are produced which next decay to γ-ray photons, secondary electrons (electrons and positrons) and neutrinos ($p + p \rightarrow \pi^0 + \pi^{\pm} + ...$; $\pi^0 \rightarrow 2\gamma$; $\pi^{\pm} \rightarrow e^{\pm} + \nu_e + \nu_\mu$). The

application of a power low distribution of relativistic protons seems to be natural, because of their possible acceleration by shocks (see the review by Blandford & Eichler 1987) and the observed power law photon spectrum of 3C 279. However in order to reduce the number of free parameters, we assume instead a monoenergetic proton beam with Lorentz factor γ_p. Since the detailed structure of the thick accretion disk is unknown, we assume for simplicity that the column density of background matter (λ) crossed by relativistic particles is less than one interaction length for inelastic p + p collisions. In the regions where the column density of matter is greater than one interaction length (in our case for the angles $> \alpha_{out}$), the efficiency of γ-ray emission significantly drops.

The angular and energy dependent spectrum of γ-ray photons from π^0 decay was calculated by integration over the proton spectrum multiplied by energy and angular distribution of the γ-ray spectrum from a single p + p interaction:

$$\frac{dN}{dE_\gamma d\Omega_\gamma dt} = \int\int \frac{dP}{dE_p d\Omega_c dt} \cdot \frac{dQ_\gamma}{dE_\gamma d\Omega_\gamma} \cdot d\Omega_c dE_p \qquad (1)$$

where $dP/dE_p d\Omega_c dt$ is the differential proton spectrum and $dQ_\gamma/dE_\gamma d\Omega_\gamma$ is the angular and energy photon spectrum from single p + p collision (see Bednarek et al. 1990).

The calculated spectra of γ-rays from π^0 decay, produced by a monoenergetic cone beam, can mimic a power law photon spectrum in the energy range between 1-10GeV with spectral index depending on the parameters: γ_p, β, α_{in} and α_{out}. Since we assumed a rather low column density of background matter in the outer parts of the disk (corona), these photons will escape freely.

The angular and energy dependent spectrum of secondary electrons from $\pi^\pm$ decay was calculated by integration over the proton spectrum multiplied by the energy and angular spectrum of secondary electrons from a single p + p interaction:

$$\frac{dN_{e^\pm}}{dE_{e^\pm} d\Omega_{e^\pm} dt} = \int\int \frac{dP}{dE_p d\Omega_c dt} \cdot \frac{dQ_{e^\pm}}{dE_{e^\pm} d\Omega_{e^\pm}} d\Omega_c dE_p \qquad (2)$$

where $dQ_{e^\pm}/dE_{e^\pm} d\Omega_{e^\pm} dt$ is the angular and energy spectrum of secondary electrons from a single p + p collision (see Bednarek & Calvani 1991).

The secondary electrons can interact with the magnetic field, matter and radiation in the funnel of the thick accretion disk and produce γ-rays in bremsstrahlung and ICS processes. The relative importance of these processes can be estimated by comparison of energy losses calculated for presumable parameters of the emitting volume. The energy losses of secondary electrons are dominated by ICS of UV thermal photons which fills the funnel of the accretion disk with a density of the order of black body distribution. This is true if the magnetic field in the funnel is $B_\perp << 700 Gs$

(obtained from a comparison of synchrotron and inverse Compton losses of secondary electrons). The bremsstrahlung losses are negligible in comparison to Compton losses for the required parameters of the emitting volume: the estimated height of the thick accretion disk $r_{acc} \sim 10^{16} cm$ (to be consistent with observed 3 day variability in γ-rays) and column density of matter $< 70 g/cm^2$ (required for efficient escape of γ-ray photons).

The energy loss time scale of secondary electrons moving in the field of black body UV photons ($T_{bb} = 4.5 \times 10^4$K) is too short to allow escape of electrons, with Lorentz factor $\gamma_e > 10$, from the funnel without significant energy losses. So the steady state distribution of electrons in the funnel should be calculated assuming a thick-target model (Ginzburg and Syrovatskii 1964) and is given by:

$$\frac{dR_{e^\pm}}{dE_{e^\pm} d\Omega_{e^\pm}} = \frac{1}{\varepsilon(E)} \int_E^{E_{max}} \frac{dN_{e^\pm}}{dE'_{e^\pm} d\Omega_{e^\pm} dt} dE' \qquad (3)$$

where $dN_{e^\pm}/dE'_{e^\pm} d\Omega_{e^\pm} dt$ is the spectrum of secondary electrons (given by eq. 2); $\varepsilon(E)$ is the energy loss rate of secondary electrons in ICS process.

Now we can calculate the spectrum of γ-ray photons produced in comptonization of black body UV photons by a steady state distribution of electrons. It is expressed by the formula:

$$\frac{dN_{Comp.}}{dE_\gamma d\Omega_\gamma dt} = \int \frac{dR_{e^\pm}}{dE_{e^\pm} d\Omega_{e^\pm}} \cdot \int n(\epsilon) \cdot \frac{dQ(E_{e^\pm}, \epsilon)}{dE_\gamma dt} d\epsilon dE_{e^\pm} \qquad (4)$$

where $dR/dE_{e^\pm} d\Omega_{e^\pm}$ is the spectrum of relativistic electrons (given by eq. 3); $dQ(E_{e^\pm}, \epsilon)/dE_\gamma dt$ is the cross section for ICS of photons with energy ϵ into the energy E_γ by monoenergetic electrons with energy $E_{e^\pm}$ (see Blumenthal & Gould 1970) and $n(\epsilon)$ is the differential concentration of UV black body photons.

The combined spectra of photons, from π^0 decay and ICS of UV photons by secondary electrons, calculated simultaneously, for fixed parameters (γ_p, β, α_{in} and α_{out}, T_{bb}), is very nearly fit by a power low with spectral index flatter in soft γ-rays and steeper in GeV γ-ray range. The fast cut-off in the photon spectrum in the higher energy range is determined by the value of γ_p and the relative dependence between β, α_{in} and α_{out}.

4. COMPARISON WITH γ-RAY SPECTRUM OF 3C 279

The γ-ray spectrum of 3C 279 observed with the EGRET detector on Compton GRO (Hartman et al. 1992) is compared with photon spectra calculated in the previous section. As an example, in Fig. 2, we show the fitting for $\gamma_p = 30$, $\beta = 2^0$, $\alpha_{in} = 7^0$, $\alpha_{out} = 12^0$, and $T_{bb} = 4.5 \times 10^4$ K (for redshift z=0.538). The data in the γ-ray energy range are reasonably well fit by the photon spectrum from π^0 decay

(above a few hundred MeV) and by a self-consistently calculated spectra of photons from ICS of UV thermal photons by secondary electrons.

From the fitting presented in Fig. 2 we are able to estimate the required total luminosity of the quasar 3C 279 in relativistic protons which is $L_p \cong 2.5 \times 10^{47} erg/s$ for a mean column density crossed by the relativistic proton beam in the disk corona $\lambda = 30 g/cm^2$ (z=0.538, $H_0 = 75 km/s/Mpc$ and $q_0 = 1/2$). We assumed a column density of this order since it supplies enough target for γ-ray production and still permits free escape of γ-rays from the accretion disk region. In fact L_p is the lower limit on the quasar luminosity in relativistic protons since substantial number of particles may also be emitted at higher angles ($\alpha > \alpha_{out}$). For such angles γ-rays will be absorbed by the optically thick disk and only a strong neutrino signal may be observed.

5. SUMMARY AND DISCUSSION

We tried to envisage here the physical scenario for the γ-ray production in 3C 279 in terms of the standard model of AGN (thick accretion disk around a massive black hole). We assumed that the inner parts of the accretion disk has a dense corona which is illuminated by relativistic protons. The protons are emitted within the angle α_{out} by a blob (or blobs) moving in the disk funnel which has the opening angle α_{in}, less than α_{out} (see Fig. 1). The γ-ray photons are produced in the inelastic collisions of relativistic protons with matter in the disk via π^0 decay and in ICS of UV thermal photons by secondary electrons from $\pi^{\pm}$ decay. In order to permit free escape of γ-rays from the production volume, the mean column density of background matter should be essentially less than one interaction length for p + p collisions. We were able to fit reasonably the γ-ray spectrum of 3C 279 (see Fig. 1). We note that the parameters of this fitting are not unique. In order to distinguish between different fits, the simultaneous observations in lower photon energies (X-rays, soft γ-rays) are needed and detailed calculations of the transfer of photons with energy less than 10 MeV in the disk corona should be performed. The estimated luminosity of this quasar in relativistic protons should be at least $L_p \cong 2.5 \times 10^{47} erg/s$ for a mean column density of the background matter $\lambda = 30 g/cm^2$. The 3 day variability in γ-ray emission, reported by Hartman et al. (1992), can be caused by the crossing of a relativistic proton blob in the disk limb.

The low and high states of soft X-ray emission from 3C 279 were reported by by Makino et al (1988). We are not able to calculate the detailed spectrum in this energy range because of complicated transfer of X-ray photons through the disk corona (although significant comptonization of thermal radiation may occur in the central part of the funnel by primary electrons). This emission may be as well produced by

Compton scattering of radiation from the disk by secondary or primary electrons in the region farther from the disk (a scenario similar to this one was recently studied by Dermer et al. 1992) or in the comptonization of synchrotron radiation by secondary or primary electrons (e.g. Jones, O'Dell & Stein, 1974; Marscher 1980; Ghisellini et al. 1985; see also the model for 3C 273 by Courvoisier & Camenzind 1989). Such composed model postulates a time delay between soft X-ray and γ-ray emission which can be observationally tested.

One of the consequences of the model is the possibility of induction of a strong wind surrounding the relativistic particle beam since a large amount of energy is transferred to the inner part of the accretion disk. Such a wind may have a direct relation to the broad emission regions of AGNs.

Our model predicts high collimation of the γ-ray emission from AGNs along the axis of the disk funnel. Provided that magnetic fields do not influence significantly the motion of the protons we can conclude: a) AGNs, seen close to face on, may emit γ-rays and neutrinos during the outburst phase when relativistic proton blobs are formed; b) some AGNs may only be strong neutrino sources if observed at large angles to the axis of the disk funnel ($\alpha > \alpha_{out}$) where the column density of matter is greater than one interaction length. The intensity and spectrum of neutrinos in case a) will be similar to the intensity of γ-rays from π^0 decay (see dot-dashed line in Fig. 2). In case b), the intensity of neutrinos will be essentially larger and the mean energy of neutrinos smaller (because of the thick target met by the proton beam). So then our model predicts strong, non-isotropic emission of low energy neutrinos by AGNs which is contrary to the model by Stecker et al. (1991) which postulates isotropic emission of high energy neutrinos ($\sim 10^4 \div 10^{10}$ GeV).

We consider a relatively mild relativistic proton beam so that the absorption of γ-rays by isotropic, thermal UV photons is not important because,

$$\sqrt{0.5 \cdot < \epsilon_{UV} > \cdot E_\gamma \cdot (1 - cos\theta)} < 0.511 MeV \qquad (5)$$

where θ is the incident angle between photons.

Similar strong collimation of radiation from X-ray up to soft γ-ray photons (produced by secondary electrons in ICS process) with γ-ray photons (originated in decay of π^0) permits free escape of γ-ray photons from 3C 279 since the probability of e^+e^- pair production in $\gamma - \gamma$ collision is reduced by a factor $(1 - cos\theta)$.

The physical scenario, discussed by us, can be extended to relativistic proton beams with much higher Lorentz factors. However, in this case the γ-rays would be very efficiently absorbed by UV photons, resulting in multiple e^+e^- pair production. Such e^+e^- pair dominated models (see e.g. Zdziarski et al. 1990) predict the appearance of a strong annihilation line in AGNs spectra and the spectral index of

differential photon spectrum in the GeV energy range significantly steeper than that observed from 3C 279.

If really only mildly relativistic protons are present in the central part of 3C 279, we should observe the cut-off in the γ-ray spectrum just above $\sim$ 10 GeV. Recent observations of 3C 279 by the Whipple observatory γ-ray collaboration (Weekes 1992), shows no significant photon emission above 0.5 TeV during the period 24 March - 8 May 1992. However, they report positive detection of invariable emission above 0.5 TeV from Mkn 421, which is similar to 3C 279. The main problem concerning high energy observations of 3C 279 (from soft X-rays up to TeV γ-rays) is that they are not simultaneous and this fact does not allow final conclusions at this stage.

We would like to note that the relativistic blob (shock) will finally emerge outside the region of the accretion disk but the acceleration of particles by it may continue. Also other mechanisms of γ-ray production may work simultaneously with our scenario, for example: synchrotron self-Compton emission from a relativistic beam (see e.g. Grindlay 1975; Konigl 1981) or proton initiated cascade (Mannheim & Biermann 1992). They may be responsible for stable photon emission above 0.5 TeV reported recently from Mkn 421 during the period 24 March - 8 May 1992 (Weekes 1992).

ACKNOWLEDGMENTS

The author is indebted to Prof. A. Treves for several useful discussions and comments, to Prof. M.A. Abramowicz for discussion and to Dr. P. Haines for reading of the manuscript. This work is supported by the Italian Ministero dell'Universita e della Ricerca Scientifica e Tecnologica.

REFERENCES

Abramowicz, M.A., Calvani, M. & Nobili, L. 1980, ApJ 242, 772

Bednarek, W. and Calvani, M. 1991, A&A 245, 41

Bednarek, W., Giovannelli, F., Karakuła, S., Tkaczyk, W. 1990, A&A 236, 268

Begelman, M.C., Blandford, R.D. & Rees, M.J. 1984, Rev.Mod. Phys., 56, 255

Begelman, M.C., Rudak, B., Sikora, M. 1990, ApJ, 362, 38

Blandford, R. & Eichler, D. 1987, Phys. Rep. 154, 1

Blumenthal, G.R. & Gould, R.J. 1970, Rev. Mod. Phys. 42, 237

Courvoisier, T.J.-L. & Camenzind, M. 1989, A&A 224, 10

Dermer, C.D., Schlickeiser, R., & Mastichiadis, A. 1992, A& AL 256, L27

Fichtel, C.E. et al. 1992, IAU Circ. No. 5460

Ghisellini, G., Maraschi, L., & Treves, A. 1985, A&A 146, 204

Ginzburg, V.L. & Syrovatskii, S.I. 1964, *The Origin of Cosmic Rays*, (New York: MacMillan)

Grindlay, J.E. 1975, ApJ, 199, 49

Hartman, R.C. et al. 1992, ApJL 385, L1

Jaroszyński, M., Abramowicz, M.A. & Paczyński, B. 1980 Acta Astr. 30, 1

Jones, T.W., O'Dell, S.L. & Stein, W.A. 1974, ApJ 188, 353

Jones, T.W. & Stein, W.A. 1990, ApJ 349, 443

Kanbach, et al. 1992, IAU Circ. No. 5431

Kazanas, D. & Ellison, D.C. 1986, ApJ 304, 178

Konigl, A. 1981, ApJ 243, 700

Madau, P. 1988, ApJ 327, 116

Makino, F. et.al. 1991, in Variability of Active Nuclei, eds. H.R. Miller & P.J. Witta, Cambridge University Press

Makino, F. et al. 1989, ApJL 347, L9

Malkan, M.A. & Sargent, W.L. 1982, ApJ 254, 22

Mannheim, K. & Biermann, P.L. 1992, A&AL 253, L21

Marscher, A.P. 1980, ApJ, 235, 386

Michelson, P.F. et al. 1992, IAU Circ. No. 5470

Papaloizou, J.C.B. & Pringle, J.E. 1984, MNRAS 208, 721

Protheroe, R.J. & Kazanas, D. 1983, ApJ 265, 620

Rees, M.J. 1984, ARAA 22, 471

Shields, G. 1978, Nat 272, 706

Unwin, S.C. et al. 1989, ApJ 340, 117

Stecker, F.W., Done, C., Salamon, M.H. & Sommers, P. 1991, Phys. Rev. Let. 66, 2697

Weekes, T.C. 1992, IAU Circ. No. 5522

Whitney, B.J. et al. 1971, Science 173, 225

Zdziarski, A.A., Ghisellini, G., George, I.M., Svensson, R., Fabian, A.C., & Done, Ch., 1990, ApJL, 363, L1

FIGURE CAPTIONS

Fig. 1.

Schematic picture of the central part of an AGN (not to scale). The relativistic blob is emerging from the region close to the central black hole and is moving in the funnel. Protons emitted by the blob interact with the matter of the disk in the disk corona (region between angles α_{in} and α_{out}) and produce γ-rays and secondary electrons. The optically thick disk emits UV photons which are comptonized by secondary electrons. The observer is located at the angle β to the disk axis.

Fig. 2.

The γ-ray spectrum observed by EGRET (error boxes, Hartman et al. 1992) and soft X-ray spectrum observed by GINGA (long dashed lines - low and high state, Makino et al. 1989) from 3C 279 are shown. The full line is the fit of the data using the calculated photon spectrum for $\gamma_p = 30$, $\beta = 2^0$, $\alpha_{in} = 7^0$ and $\alpha_{out} = 12^0$. The dot-dashed line is the photon spectrum from π^0 decay. The dotted line is the photon spectrum from ICS of UV photons ($T_{bb} = 4.5 \times 10^4 K$) by secondary electrons. The short dashed line is the part of the calculated photon spectrum which is influenced by transfer processes in the matter of the disk corona.

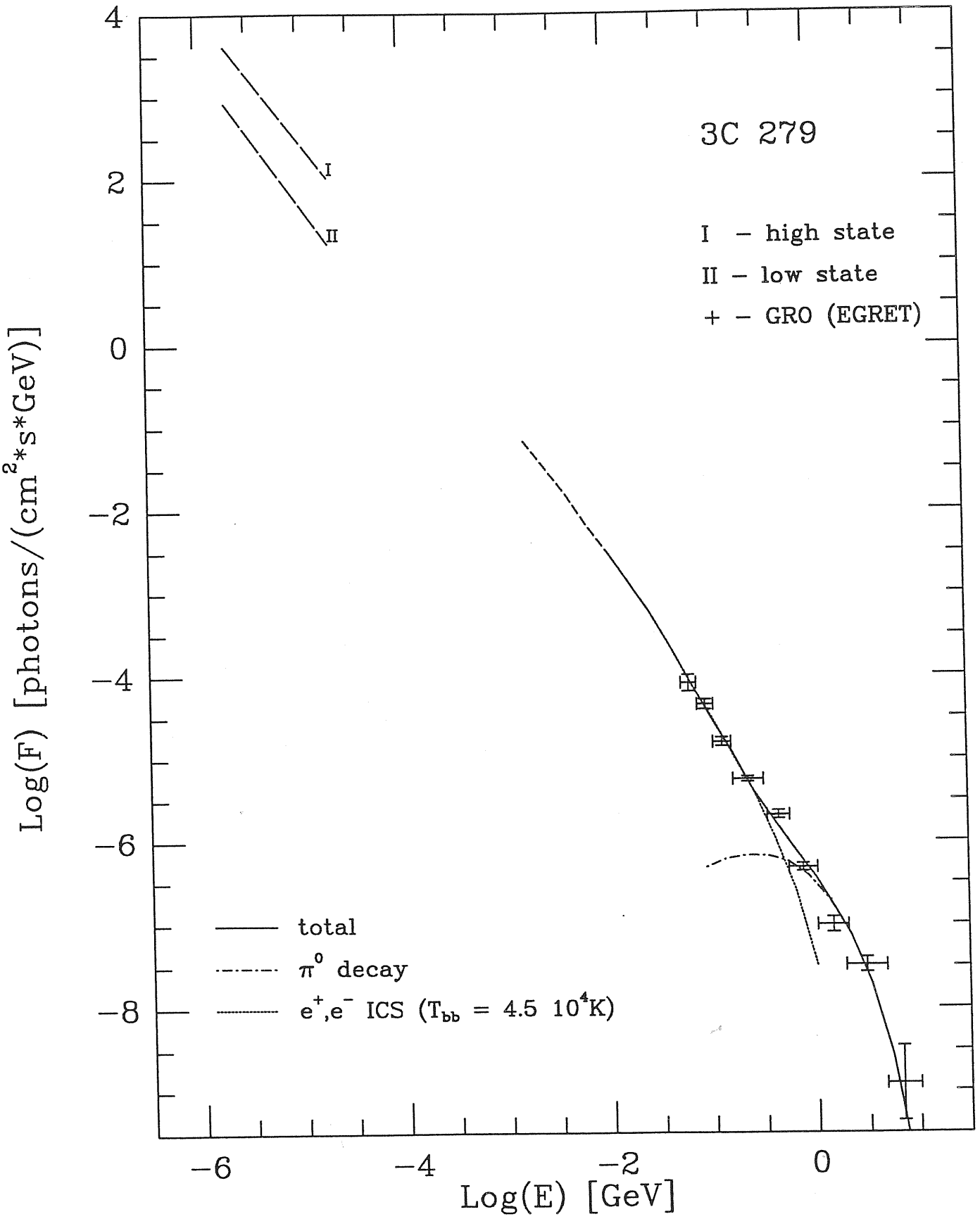
3C 279
I – high state
II – low state
+ – GRO (EGRET)
I
II
total
π^0 decay
e^+,e^- ICS (T_{bb} = 4.5 10^4K)
Log(F) [photons/(cm^2*s*GeV)]
Log(E) [GeV]
4
2
0
−2
−4
−6
−8
−6
−4
−2
0

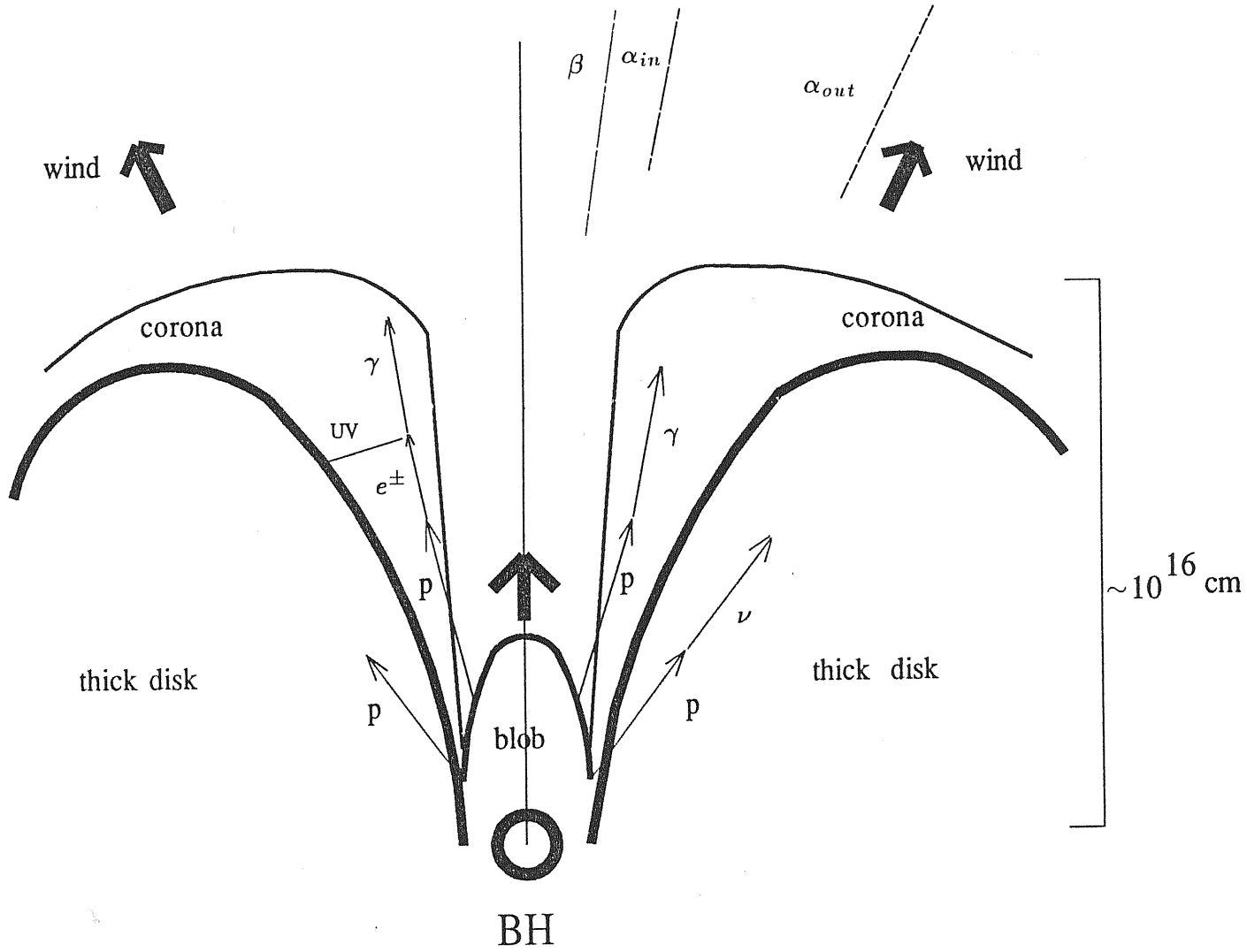
β
α_{in}
α_{out}
wind
wind
corona
corona
γ
UV
$e^{\pm}$
p
p
γ
ν
p
p
thick disk
thick disk
blob
$\sim 10^{16}$ cm
BH